THERMAL AND STRUCTURAL BEHAVIOUR OF BASALT FIBRE REINFORCED GLASS CONCRETE

A thesis submitted to The University of Manchester for the degree of Doctor of Philosophy in the Faculty of Engineering and Physical Sciences

2011

TUMADHIR MERAWI BORHAN

SCHOOL OF MECHANICAL, AEROSPACE AND CIVIL ENGINEERING

ABSTRACT

This study aims to produce a type of concrete with both good thermal and mechanical properties by using environmentally friendly and low cost materials. In addition, the resistance of this concrete to fire conditions was investigated. The experimental work comprises two parts. In the first part, recycled glass was used as a partial replacement for natural sand (at proportions 20%, 40% and 60%) together with basalt fibre having different volume fractions (0.1%, 0.3%, and 0.5%). The results obtained from the experimental work showed that the optimum content is 20% glass and at 28 days, there was a 4.23% and 15% enhancement in the compressive strength and the splitting tensile strength respectively. Above 20% glass there was a slight reduction (6.6% and 22%) in the compressive strength and the splitting tensile strength when 60% glass was used. The results also showed that when glass sand and basalt fibre content increase, there is a decrease in the thermal conductivity range from 4.35% to 50% at temperature levels between 60^{o}C to 600^{o}C.

The structural behaviour of this type of concrete was investigated in the second part of this study by carrying out small-scale slab tests at ambient and elevated temperatures. The results show that there is an increase in the load carrying capacity above the theoretical yield line load, due to membrane action, for all percentages of glass and volume fractions of basalt fibre ranging from 1.35 to 1.68 for the slab tested at ambient temperature and from 3.13 to 3.26 for the slabs tested at elevated temperature. Also the slabs with higher glass sand and basalt fibre content had a higher load enhancement and failed at a higher displacement compared to the control mix.

A comparison between the simplified method and the finite element software package ABAQUS showed that the ABAQUS model gives reasonable predictions for the load–vertical displacement and the temperature–displacement relationships at both ambient and elevated temperature conditions, while the simplified method gives conservative predictions for the maximum allowable vertical displacement for the slab at elevated temperature. A parametric study showed that a 10 mm cover depth is the optimum depth as well as the reinforcement temperature predicted reduced with increasing load ratio (applied load/yield line load).

DECLARATION

No portion of the work referred to in the thesis has been submitted in support of an application for another degree or qualification of this or any other university or other institute of learning

COPYRIGHT STATEMENT

To My Family

ACKNOWLEDGEMENTS

Firstly, I would like to express my gratitude to my supervisor Professor Colin Bailey, for his continued support and guidance throughout this project. Professor Bailey has given me the opportunities to develop on a professional level by being an excellent mentor. I am also very grateful to Dr. Jonathan Dewsbury and Mr. Paul Nedwell for their help and support during my PhD study.

Many thanks also go to the Ministry of Higher Education and scientific Research in Iraq for their funding of the project.

Special thanks go to Mr. John Mason and Mr. Paul Townsend for their help in the experimental work.

I would like to thank my colleagues and friends for their help and kind support. Special mentions to Ahmed Abdullah, Adnan Flayih, Ahmed Majhool, Denise Lee, Mohammed Yaqub, Rao, Emmanuel and many others.

Finally, I am eternally grateful to my family for their endless patience, care, love and encouragement during this project.

LIST OF CONTENT

LIST OF FIGURES

LIST OF TABLES

NOTATION

b = parameter defining magnitude of membrane force

C = *compressive force*

$E_{a,\theta}$ = the slope of linear elastic range

f_1, f_2 = ratio of ultimate strength to yield strength of reinforcement in shorter and longer span

f_{ck} = compressive cylinder strength of concrete

$f_{ctk;0,05}$ = lower bound tensile strength of concrete

$f_{ctk;0,95}$ = upper bound tensile strength of concrete

f_{cu} = compressive cube strength of concrete

$f_{p,\theta}$ = proportional limit

$f_{t,ctm}$ = mean value of axial tensile strength of concrete

f_u = ultimate strength of reinforcement

f_y = yield strength of reinforcement

$f_{y,\theta}$ = the effective yield strength

KT_0 = force in steel per unit width in short span

k = parameter defining magnitude of membrane force

L = longer span of rectangular slab

l = shorter span of rectangular slab

M_0 = moment of resistance when no membrane force is present

n = parameter defining yield-line pattern

S = shear force

T_0 = force in steel per unit width in the longer span

T_1 = tensile force in element 1

T_2 = tensile force in element 2

v = parameter defining extent of central membrane;

φ = angle defining yield-line pattern;

μ = ratio of moment capacity of slab in shorter span to that in longer span.

$\varnothing$ = diameter of reinforcement;

Δ_{Fire} = maximum vertical displacement at failure for elevated temperature tests

$\varepsilon_{p,\theta}$ = the strain at proportional limit

$\varepsilon_{y,\theta}$ =the yield strain

$\varepsilon_{t,\theta}$ =the limiting strain for yield strength

$\varepsilon_{u,\theta}$ =the ultimate strain

θ = temperature

CHAPTER ONE

1 INTRODUCTION

1.1 GENERAL

Sustainable building, sustainable design and green building are recent concepts that explain the efficiency of building in terms of the energy used to reduce the impact of the built environment on human health and the natural environment. These concepts are becoming more prominent in the world due to several reasons such as the environmental damage (pollution caused by the emission of carbon dioxide which causes climate change) and the expected depletion of fossil fuels as well as its cost. According to a data recorded by the World Business Council for Sustainable Development, buildings are responsible for at least 40% of energy use in most countries[1].

Uncontrolled fires can also cause damage to the environment as well as possibility of causing huge injuries, death to people and economic loss. A study found that in a typical year (in Europe, the USA, Canada and Japan) the number of people killed by fires was 1 to 2 per 100,000 inhabitants and the total cost of fire damage amounted to 0.2% to 0.3% of Gross National Product (GNP) [2]. The extent of such damage will depend on a number of factors such as building design and use, structural performance, fire extinguishing devices and evacuation procedures. Thus, the need for the passive control, which refers to fire control by systems that do not need operation by people or automatic controls [3], is required to prevent both spread of fire and structural collapse. The passive control includes the selection of suitable materials for buildings.

The materials used for building can increase its efficiency. The thermal performance of the building's envelop depends on the thermal properties of the material used. In addition, the type of the material used depends on the type of application and the desired properties. For this reason, the production of good insulating load bearing and fire resistance materials is one of the most important issues in the construction materials industry. Many materials

that have good thermal properties have been produced. However, many of these materials have insufficient strength making them unsuitable for load bearing structures.

Concrete is a widely used construction material. Good quality concrete is durable and has sufficient strength. In addition concrete has excellent fire resistance without the need for an additional protective cover. However, its thermal conductivity (*K*) ranges between 1.6 – 2.7 W/m.K for normal weight concrete, depending on its components, which means that concrete is not a very effective insulator compared with other construction materials such as wood (*K* ranges between 0.04-0.4 W/m.K) and gypsum or plaster board (0.17 W/m.K) [4]. The insulation characteristic of concrete is of great importance to control the loss of heat from concrete buildings in winter and the gain of heat in summer. In order to increase the efficiency of concrete structures, different methods have been used to enhance concrete thermal properties. One of these is to use a type of aggregate which has better thermal properties compared to normal aggregates without significantly effecting the mechanical properties of the concrete.

The use of recycled materials, as an aggregate in concrete, has become popular recently in terms of reducing the consumption of natural aggregates and for the environmental advantage of the disposal of waste materials. Examples are recycled glass, plastic, or tyres. Significant research has been carried out on the use of the recycled materials as an aggregate in concrete as reviewed in the following chapter. It was found that among these materials, recycled glass as a partial or totally replacement for natural sand aggregate can produce concrete with sufficient strength, nearer to normal concrete strength, when compared with other types of recycled aggregate [5-7]. Therefore, it is suitable for structural members. Nevertheless, limited research has been carried out to investigate its thermal properties, including its resistance to fire. Previous research has suggested that the use of reprocessed carpet fibres improves this concrete's thermal properties. However, this type of fibre has negative effect on its mechanical properties [8].

In addition, it was found that the main problem of using this type of aggregate in concrete is the expansion due to the alkali silica reaction (ASR) [9]. However, this reaction can be reduced considering many factors such as the particle size of the glass aggregate, the glass content and the glass color [7]. The expansion due to ASR can also be reduced by using metakaolins and other pozzolanic materials with this type of concrete [10, 11]. It was also found that using fibre is effective of reducing the thermal expansion due to the ASR in this type of concrete [12].

Basalt fibre is inorganic fibre produced from basalt rock. It is environmentally friendly, it has no chemical reactions that may damage health or the environment, non-combustible and non-explosive [13, 14]. It has a better resistance to the alkaline solution, even at higher temperature, than glass fibre [15, 16]. The manufacture process of this type of fibre is similar than of glass fibre with less energy consumed and no additives which make it cheaper than glass or carbon fibres [15]. The results obtained in the research carried out by Sim et al. [17], using continuous basalt fibre in concrete, showed an improvement in the thermal and mechanical properties. Limited research has studied the effect of using short basalt fibre on the mechanical properties of concrete [18, 19] and no research has been found on its thermal properties.

Further research is needed to fill the gap in the area of knowledge on the thermal properties and the structural behaviour of concrete, at ambient temperature and in fire, containing waste glass and short basalt fibre. The research presented in this thesis investigates the effect of using glass aggregate as a partial replacement for the natural sand with different volume fractions of basalt fibre in concrete, on its mechanical and thermal properties, together with the structural behaviour when subjected to fire and comparing the results with the other type of concrete.

1.2 OBJECTIVES OF THE RESEARCH

This study aims to produce a type of concrete with good thermal and mechanical properties by using environmentally friendly and low cost

materials. In addition, the structural behaviour at ambient temperature and in fire conditions will be investigated as practical tests for the new concrete.

This study consists of three parts; the first one is to investigate experimentally the thermal and mechanical properties of the concrete produced from glass sand and basalt fibre. To ensure this type of concrete is suitable for structural members the second part of this study investigated its structural behaviour at ambient and elevated temperatures by conducting small-scale slab tests. The slabs were cast using the same mix designs as those investigated in the first part of this research. To investigate the ability of the numerical methods, available in the structural analysis field, to modle the new type of concrete, a numerical analysis was carried out, using the data obtained from the first and second parts of the tests, to model the thermal distribution and structural behaviour of the slabs at ambient and elevated temperatures, which is the third part of this study. The final form of the simplified method proposed by Bailey and Toh [20] to determine the ultimate load carrying capacity of a two-way simply supported horizontally unrestrained slab incorporating the enhancement due to tensile membrane action at ambient and elevated temperatures was used. The finite element software package ABAQUS was also used for this purpose. The results obtained from these methods were compared, discussed and validated against the slab test results.

1.3 THESIS LAYOUT

The outline of each chapter in this thesis is summarised as follows:

Chapter One: Introduction: gives an introduction to the research project and outlines the objective and the scope of the research.

Chapter Two: Materials Properties: This chapter reviews some of the literature about the behaviour of the materials at ambient and elevated temperature relevant to this study.

Chapter Three: Reinforced Concrete Slab: this chapter reviews the concept of tensile membrane action and some of the experimental and theoretical work that has been carried out previously.

Chapter Four: Experimental Work: deals with the methodology of this research and the first part of the experimental work that has been carried out in this study. The results of this work were analysed and discussed. The conclusions and the recommendations as a result of this work were also presented.

Chapter Five: Small-Scale Slab Test: this chapter describes the second part of the experimental work which includes the small-scale slab tests conducted in this study and the results, analysis, discussion and conclusion from this work.

Chapter Six: Methods of Analysis: This chapter presents the methodology of the simplified and advanced analysis of the reinforced concrete slabs. Background information on the simplified method, the finite element method, concrete crack models and its parameters and the ABAQUS package are also presented.

Chapter Seven: Analysis of the Small-Scale Slab: This chapter describes the analysis of the small-scale slabs, conducted in this study, at ambient and elevated temperatures using the simplified method and the finite element software package ABAQUS. The elements and the solution procedure adopted in the thermal and structural models are also described as well as the parametric study to investigate the effect of some parameters on the accuracy of the results and to understand the effect of changing these parameters on the behaviour of the reinforced concrete slab at ambient and elevated temperature.

Chapter Eight: Conclusion and Further Work: The summary of the work carried out in this research project can be found in this chapter along with the conclusions attained and the suggestions for further research.

CHAPTER TWO

2 MATERIAL PROPERTIES

2.1 GENERAL

This chapter reviews some of the literature related to the thermal and mechanical properties of the materials relevant to this study as well as some research that has been carried out on properties of different types of concrete having different ingredients.

2.2 PROPERTIES OF CONCRETE

Concrete is a composite material which consists of two major phases; the paste represents the plastic phase and the aggregate represents the rigid phase. The properties of concrete mostly depend on these phases and the interface zone between them.

2.2.1 Thermal Properties of Concrete

2.2.1.1 Thermal Expansion

The coefficient of the thermal expansion (CTE) is a measure of the material tendency to change in volume or length due to temperature change. It is believed that CTE has an important effect on the concrete building structures depending on many factors as explained later. In fire, the structural elements such as floors, beams, and columns expand significantly which, in turn, induces stress and this can lead to the failure of the element.

The CTE of concrete is a resultant of the CTE of its two components; cement paste and aggregate. If the coefficients of the aggregate and the cement paste differ significantly, a large change in the temperature may induce a break in their bond [21].

It was found experimentally that the higher the CTE of the aggregate the higher the CTE of the concrete and this also depends on the amount of such

aggregate in the mix proportions [22, 23]. A typical range of CTE for different types of aggregate is shown in Table 2-1.

Table 2-1 Typical CTE ranges for different types of aggregate [24]

Aggregate type	Coefficient of thermal expansion
	10^{-6}/℃
Granite	7-9
Basalt	6-8
Limestone	6
Dolomite	7-10
Sandstone	11-12
Quartzite	11-13
Marble	4-7

The effect of moisture content on the CTE of concrete applies to the paste component. For dry or saturated paste the CTE is lower than partially saturated. This is due to the fact that the CTE is made up of two components; the true kinetic coefficient and swelling pressure which increases from the decrease in the capillary tension of water held by the paste with an increase in temperature [21]. For the dry paste the capillaries are unable to supply water to the gel and for the saturated paste, the moisture diffusion from gel to capillary pores is partially eliminated by contraction as the gel loses water so that the apparent CTE is smaller. For partially saturated paste there is not enough water for a free exchange of moisture to occur between the capillary pores and the gel after the temperature change.

Experimental work has shown that the concrete with high CTE is less resistant to the increase in temperature than that with low CTE [25].

According to the experimental test, Takeuchi et al [26] have shown that there is no significant change in the CTE of concrete when the temperature is between ambient and 200°C. However, a rapid increase in the CTE was recorded with temperatures around 600°C due to the transformation of the quartz phase included in the aggregate used. At very high temperatures (700 to 800 °C) most concretes have no, or a reduced, expansion. In some cases the concrete shrinks due to chemical or physical reactions in the aggregates [27, 28].

In the absence of measured values, the data presented in the EC2 [29], for siliceous and calcareous aggregates, can be used to calculate the coefficients of thermal expansion of concrete ($\varepsilon_{c,\theta}$) as follows:

For siliceous aggregates:

$$\varepsilon_{c,\theta}=\begin{cases}-1.8\times10^{-4}+9\times10^{-6}\theta+2.3\times10^{-11}\theta^{3} & 20^{o}C\leq\theta\leq700^{o}C\\ 14\times10^{-3} & 700^{o}C\leq\theta\leq1200^{o}C\end{cases} \quad \text{Equation 1}$$

And for calcareous aggregates:

$$\varepsilon_{c,\theta}=\begin{cases}-1.2\times10^{-4}+6\times10^{-6}\theta+1.4\times10^{-11}\theta^{3} & 20^{o}C\leq\theta\leq805^{o}C\\ 12\times10^{-3} & 700^{o}C\leq\theta\leq1200^{o}C\end{cases} \quad \text{Equation 2}$$

Where θ is the concrete temperature (°C).

However, a sensitivity analysis, using finite element software ABAQUS, carried out by Ellobody and Bailey [30] showed that the EC code coefficients of thermal expansion produced erroneous predictions for the structural behaviour. They compared the results obtained from the experimental work on unbounded post-tensioned one-way concrete slab with that predicted in the ABAQUS model using the measured thermal expansion coefficients given in the literature [31, 32] and in the EC2 [29]. They found that the central

deflection observed experimentally was 62mm at 129 min, compared with 67mm at 130 min and 76mm at 112 min predicted using the measured and the EC code thermal expansion coefficients respectively. Based on this comparison, it can be concluded that the values of the thermal expansion coefficients given in the Euro code are conservative. Therefore, the measured thermal expansion coefficients were used in simulating the slab tests at elevated temperature in the author's study.

2.2.1.2 Thermal Conductivity

Thermal conductivity is a measurement of the ability of the material to conduct heat. The coefficient of thermal conductivity of concrete depends on the moisture content, type of aggregate, porosity, density, presence of fibre and temperature.

Table 2-2 shows the thermal conductivity of concrete and mortar, measured using the transient hot-wire method, in a dry and fully saturated state at normal temperature with different types of coarse aggregate (the rocks were collected from different geological site and crushed in the laboratory). Two types of sand were used type I (reddish land quarried quartz sand) and type II (greyish river sand) [33]. It can be seen from this table that the thermal conductivity of concrete increases with an increase in the moisture content. This is attributed to the changes in voids filled with water, whose thermal conductivity is superior to that of air.

Table 2-2 Thermal conductivity of concrete and mortar with different types of aggregate [33]

Type of concrete	Thermal conductivity (W/mK)			
	Sand type I		Sand type II	
	Dry	Fully saturated	Dry	Fully saturated
Mortar	1.90	2.65	1.37	1.95
Basalt concrete	2.26	3.52	1.97	3.24
Limestone concrete	2.03	2.92	1.60	2.71
Siltstone concrete	2.21	3.61	1.91	2.90
Quartzite concrete	2.77	4.18	2.29	3.49

With increasing temperature, the thermal conductivity of normal weight concrete decreases as shown in Figure 2-1[29] . Kodur and Sultan [28] investigated the effect of temperature on the thermal conductivity of plain and steel fibre reinforced concrete for siliceous and carbonate aggregate. For both concrete types, the thermal conductivity decreases with an increase in temperature. For steel fibre reinforced concrete, the thermal conductivity is almost constant in the temperature range of 400-1000℃. This might be attributed to the presence of the steel fibre-reinforcement in the concrete, which induces multiple cracks in the concrete and limits the crack propagation, and thus decreases the rate of heat transfer in the specimen. The thermal conductivity of siliceous aggregate concrete is higher than that of the carbonate concrete in the temperature range of 200℃ to 800℃ for plain concrete and in the entire temperature range of 20℃ to 1000℃ for fibre reinforced concrete. This is due to the higher crystallinity of the siliceous aggregates as compared to that of the carbonate aggregate. The higher the crystallinity, the higher the thermal conductivity [28].

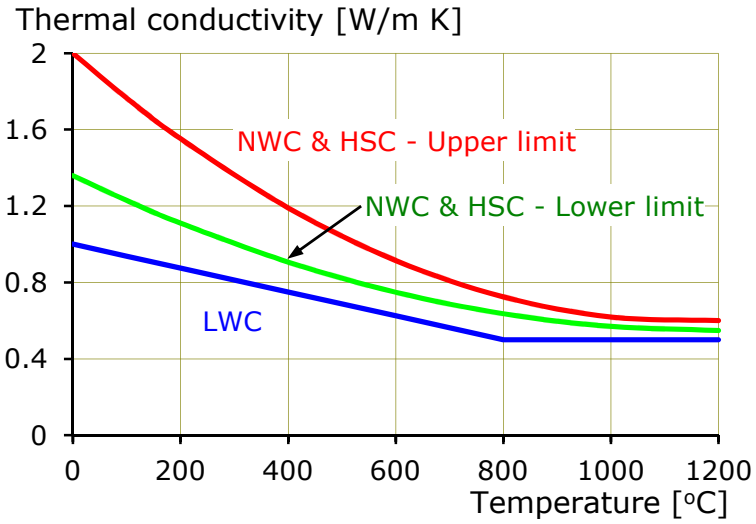

Figure 2-1 Thermal conductivity of concrete versus temperature [29]

2.2.1.3 Methods for Measuring Thermal Conductivity

Two techniques are used to measure the thermal properties of concrete; these are the steady state method and the transient method. The principles of the steady technique are based on creating a steady temperature gradient across a known thickness specimen by controlling the heat flow from one side to another. The determination of the thermal conductivity can be obtained by applying Fourier's law in one dimension. The most common methods used are the guarded hot plate and the heat flow meter method (Figure 2-2) [34]. These methods, however, require a long time to establish the steady state temperature gradient across the specimen where the gradient is required to be large. The size of the specimen is also required to be large. Another problem related to this method is a potentially great influence of thermal contact resistances between the sample and other elements of the measurement system on the results. This problem is particularly significant if the contact surfaces are rough and filled with air [35].

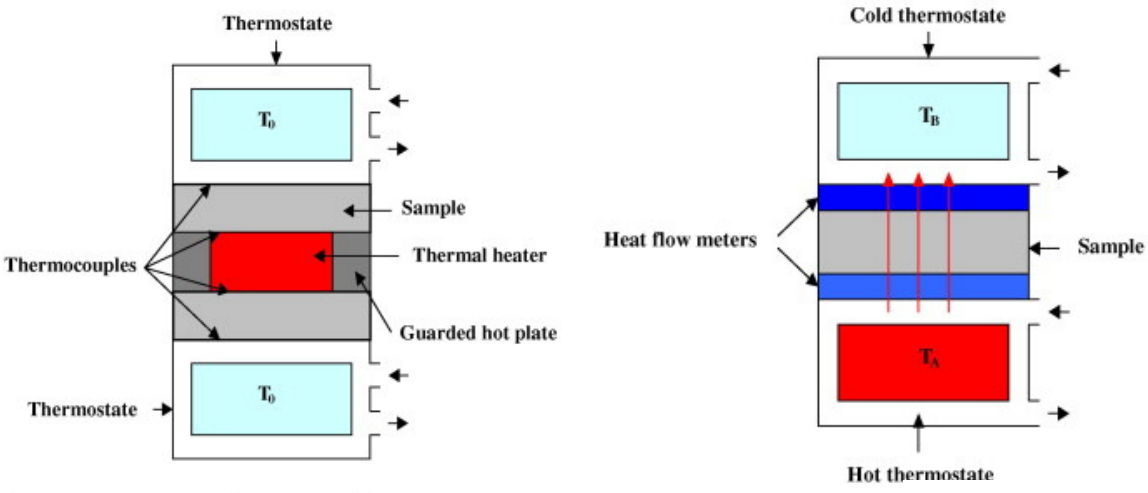

a b

Figure 2-2 Steady state method for measuring the thermal conductivity (a) guarded hot plate (b) heat flow meter [34]

On the other hand transient techniques perform a measurement during the process of heating. The advantage is that these may be made relatively quickly. The most common method used is the transient plane source method which is also called the hot disk method. A plane sensor, a special mathematical model describing the heat conductivity, combined with precise electronics, enables the method to be used to measure thermal transport properties. The disadvantage is that the mathematical analysis of the data is in general more difficult than the steady state methods.

A comparison study showed that over a large range of conductivities (1.4 to ~5 W/ m. K) and rock types there is almost no difference between the results obtained from using both method [36].

A number of researchers have attempted to predict the thermal conductivity of concrete using theoretical models [33, 37, 38]. These models take into consideration the thermal conductivity of each ingredient of concrete, the moisture content, porosity, and other factors. However, they are not suitable for some types of concrete, such as fibre reinforced concrete, nor for all

environment conditions such as fire condition. An easy and accurate method to determine the thermal conductivity of concrete still needs further research.

2.2.1.4 Specific Heat

The specific heat is the heat energy required to raise one gram of material through one degree centigrade, J/kg.^{o}C. For concrete this depends on the moisture content and the temperature. It increases with increasing moisture content [39], which is mainly due to the high specific heat of water.

Toman and Cerney [39] found that the specific heat increases with temperature up to 400^{o}C. For temperatures above 400°C, it slows down its increase with temperature, and for temperatures higher than 600°C it starts to decrease. These changes in the character of the specific heat vs. temperature relation can be explained by structural changes of the material in this temperature range, which are due to the loss of crystallically bonded water and dehydration of some components (C-S-H).

The specific heat of normal weight concrete varies only slightly from different aggregate types used, as most of the rocks have the similar mineralogical content [40].

2.2.1.5 Thermal Diffusivity

Thermal diffusivity (α) is the rate of temperature change in a material and is used to calculate temperature distribution under transient conditions. The thermal diffusivity can be given by:

$$\alpha = k/\rho c \qquad \text{Equation 3}$$

in which k is the thermal conductivity and ρ is the density and c is the specific heat [41].

Since both thermal conductivity and specific heat are significantly affected by presence of moisture, and as the thermal diffusivity is a function of the thermal conductivity and specific heat, its behaviour, in different temperature

level, depends on the same factors, stated in Sections 2.2.1.22.2.1.4, that influencing these properties.

2.2.2 Mechanical Properties of Concrete

2.2.2.1 Strength of Concrete

Concrete exhibits good compressive strength which depends upon many factors, including the quality and proportions of the ingredients and the curing environment.

Strength of concrete is a function of temperature. Takeuchi et al. [26] stated that compressive strength at first decreases with rise in temperature until 120^{o}C then it increases with temperature around 200^{o}C and then decreases with a following increase in temperature. Experimental results obtained by Chan et al [42] showed that compressive strength can be maintained or even slightly increased within a range of temperature from 20 to 400℃. Considerable loss in compressive strength occurs between 400 and 600℃, and most of the original compressive strength before heating may be lost from 600 to 800℃. The variation of concrete strength when subjected to elevated temperature was explained by Dais et al [43] as follows; the first decrease of the compressive strength is due to the swelling of water layer which causes the so - called '' disjoining pressures'' in the cement paste which leads to weakening of bonds. The regaining of the strength would be due to the relief of these pressures caused by drying and densification of the gel. The subsequent deterioration is due to the dehydration of C-S-H gel, and the thermal incompatibility between the aggregate and the cement paste.

Generally, the critical temperature for concrete related to its compressive strength is around 600^{o}C when the strength will rapidly drop off. This is a little higher than the critical temperatures for steel, however, the heat tends not to penetrate very far into the depth of concrete due to its lower thermal conductivity, compared to steel, this allows the structure as a whole to retain much of its strength [44].

Schneider [45] has shown that unstressed concrete with siliceous aggregate exhibited the greatest reduction in strength compared with that of calcareous or lightweight aggregates. This is attributed to the higher thermal expansion of siliceous aggregates and to the volume increase due to chemical instability when temperature increases [46]. This trend was also observed when the concrete was stressed to 40% of the ultimate compressive strength and tested hot. The reduction factors of concrete compressive strength at different temperature levels and different concrete type is shown in Figure 2-3, according to BSEN 1992-1-2 [29].

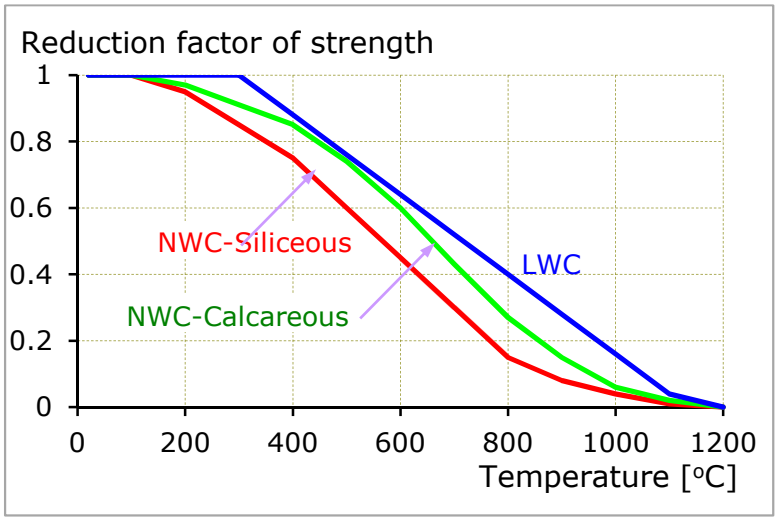

Figure 2-3 Reduction factors of compressive strength [29]

The tensile strength of concrete is relatively much lower than its compressive strength. It can be developed more quickly with crack propagation. It has a fundamental role in the fracture mechanism of hardened concrete. It will often develop cracks, even before being subjected to load, due to shrinkage and volume change at high temperature due to the thermal effects. For this reason it is almost never used without some form of reinforcement. The purpose of this is to accommodate the resulting tensile stresses and control the width of the cracks that develop.

BSEN 1992-1-2 [29] defines the range of tensile strength of concrete based on its compressive strength. The mean, upper bound and lower bound values

are defined as, $f_{t,ctm} = 0.3\ f_{ck}^{2/3}$, $f_{ctk;0,95} = 1.3\ f_{t,ctm}$ and $f_{ctk;0,05} = 0.7\ f_{t,ctm}$ respectively.

The tensile strength of concrete rapidly decreases with increasing temperature. In BSEN 1992-1-2 [29] the relative tensile strength decreases from around 100 ^{o}C and reaches zero at 600^{o}C (Figure 2-4).

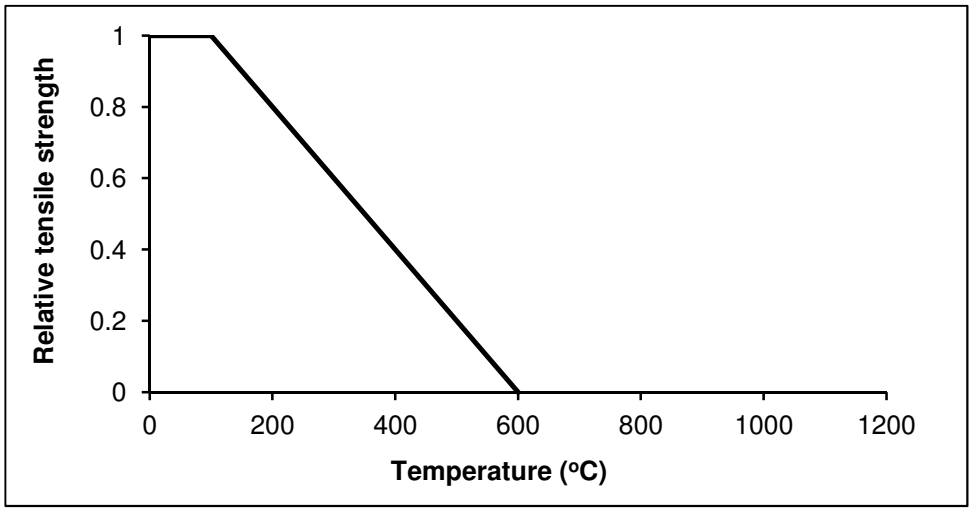

Figure 2-4 Relative tensile strength at elevated temperature [29]

The decrease in the strength at high temperature is mainly due to the bond deterioration and differences of the thermal expansion of the cement paste and the aggregate.

2.2.2.2 Stress-Strain Relationship

The stress-strain relationship of concrete is affected by two main factors; the current temperature and the prehistory of the stress. The stress-strain curve for concrete in compression and tension at ambient and elevated temperatures are shown in Figure 2-5 (A and B). It can be seen that there is a reduction in the strength and modulus of elasticity when heated.

When concrete is subjected to stress during the period of heating, the deformability will be smaller and a slight increase in strength is observed. This is due to the reduction of the thermal expansion under stress and for a

stress equal to about 40% of the ambient temperature strength, the thermal expansion is fully compensated by the stress induced deformation [47].

As the type of the aggregate and the amount of crystallinity in it play an important role in the thermal properties of concrete as mentioned previously, it thus affects the overall stress-strain behaviour of concrete at elevated temperature. The influence of the temperature on the stress-strain curve with siliceous aggregate is greater than that of concrete with calcareous and lightweight aggregate [45].

Anderberg et al. [47] carried out an experimental investigation on the behaviour of loaded concrete under transient high temperature conditions and proposed a constitutive law. They concluded that the total strain is the summation of four terms of strain; elastic strain, unrestrained thermal strain, creep strain and transient strain. The elastic strain is the instantaneous response on the applied load at a constant temperature. The unrestrained thermal strain is the free thermal expansion explained previously. The creep strain is the time - dependent strain which takes place under constant load and constant temperature. The transient strain is also time- dependent and takes into account the temperature change (increase) in concrete under stress.

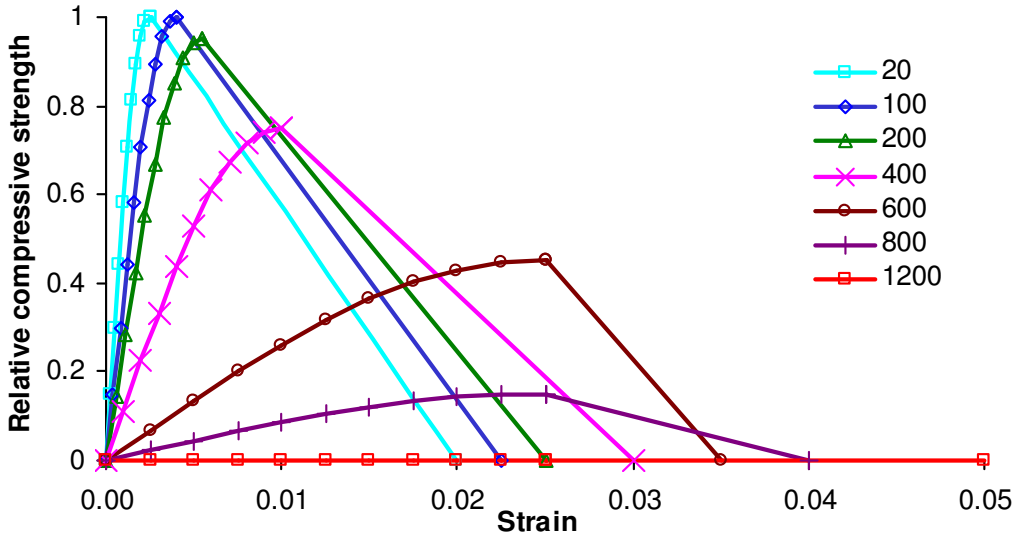

A) Concrete in compression at different temperature.

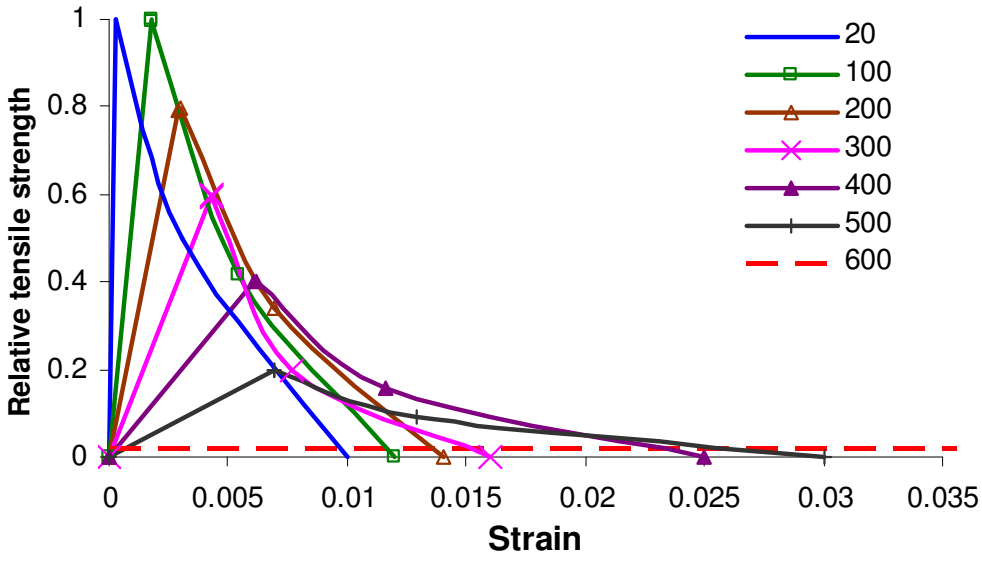

B) Concrete in tension at different temperature.

Figure 2-5 Uniaxial stress-strain relationships of concrete A) compression at different temperature level B) tension at different temperature level [48].

2.3 CONCRETE IN FIRE

Three components are required for fires to take place; fuel, oxygen and heat source. Once a fire starts and the contents and (or) materials in a building are burning, then the fire spreads via radiation, convection or conduction with flames reaching temperatures of between 600℃ and 1200℃. Harm is caused by a combination of the effects of smoke and gases, which are emitted from burning materials, and the effects of flames and high air temperatures [2].

Concrete is a non – combustible material (i.e. it does not burn) and it does not emit any toxic fumes when affected by fire. It has a relatively low thermal conductivity compared to steel (50 times lower) which enables concrete to act as an effective fire shield not only between adjacent spaces, but also to protect itself from fire damage. Therefore, concrete is considered as a high fire resistance material and it has been described as ‘’fireproof’’.

The response of concrete in fire is complex due to the non – uniformity of the material as concrete contains both cement and aggregate elements, and these may react in a variety of ways at high temperature. It experiences a number of physical changes, such as volume change, as explained previously, which leads to cracks as well as spalling, and also chemical changes. Some of these changes are reversible upon cooling but others are non- reversible and may significantly weaken the concrete structure.

Spalling has been observed in concrete at temperatures slightly above 200^{o}C [44]. When surface spalling of fire-exposed concrete structures occurs, smaller or greater parts disappear. The reinforcement cover becomes lower than the value calculated in designing the structure which leads to direct heating of the reinforcement and a rapid decrease of load-bearing capacity for the structure.

Many factors have been identified in the literature review that influence explosive spalling in concrete, such as the following [49, 50]:

- Heating rate and heating profile: increasing the heating rate results in increase in the probability and severity of explosive spalling. In addition.
- Section size: explosive spalling is most likely to occur in medium size sections. The build up pressure is prevented in thin section as the moisture can escape more readily. In the section greater than about 200-300mm, the expulsions are less likely to occur according to experimental evidence.
- Permeability of concrete: the low permeability of concrete accelerates the pore pressure development leading to spalling.
- Moisture content: Spalling can occur if the moisture content of ordinary strength concrete is more than 2% to 3% by weight.
- Strength of concrete: high strength concrete can experience spalling in fire. This is due to the low porosity and permeability of such concrete, whereby even the release of chemically bound water can contribute significantly to pore pressures.
- Compressive stress and restraint: High compressive stress, caused by restraint of thermal expansion, increases the probability of spalling and promotes explosive spalling. It develops when the rate of heating is such that the stresses cannot be relieved by creep quickly enough.
- Reinforcement: the presence of the reinforcement, the cover to the reinforcement not exceeding 40 mm for dense or 50 mm for lightweight aggregate concrete could prevent spalling or limit the extent of spalling.
- Cracking due to aggregate expansion, internal cracks or reinforcement expansion can also cause spalling.

Spalling can be prevented by;

- Reducing the moisture content.
- Reducing the compressive strength.
- Constructing with lightweight concrete.
- Providing additional reinforcement.
- Incorporating fibres into the concrete such as polypropylene, steel, glass and carbon fibre [51, 52].

2.4 CONCRETE WITH DIFFERENT MATERIALS

2.4.1 General Introduction

The ingredients of concrete have a significant effect on its properties as mentioned previously in Section 2.2. The aggregate plays an important part in defining the concrete properties due to its high content (it occupies between 65%-80% of total weight of concrete). Concrete with different types of aggregate possesses different thermal and mechanical properties. Many researchers have studied the effect of using different types of aggregate, admixtures, additives, and fibre to produce concrete with specific properties.

2.4.2 Use of Natural and Artificial Aggregate

Pumice is a natural volcanic sponge – like material. Experimental results have shown that concrete made using volcanic pumice as coarse aggregate (particle size 3-10mm), has good insulation properties, good structural strength characteristics and is 30 to 40% lighter than normal concrete [53, 54].

Demirboa et al. [55, 56] investigated the effect of this type of aggregate (fine and coarse) on the compressive strength of concrete and its thermal conductivity using the hot-wire ASTM C-1113 standard test [57]. The results showed that the 7 and 28 day compressive strengths are about 4.35 and 6.07 MPa respectively and the thermal conductivity is about 0.318 W/m.K. Using expanded perlite in place of pumice (20, 40, 60% by weight) showed an increase in the 7 day compressive strength by up to 52%, 85%, 55% and in the 28 day compressive strength to 80%, 84%, 108% respectively. There

was a less of an increase in the 7-day compressive strength when 60% of pumice aggregate was replaced by expanded perlite. This is explained due to the effect of the high manufacturing temperature for expanded perlite which influences the pozzolanic reactivity of the aggregate – cement past interface, [58]. This is also due to the water absorption of expanded perlite which is twice the amount of the pumice aggregate which might result in less water available for cement past hydration [59].

The expanded perlite aggregate replacement of pumice aggregate (20%, 40%, 80% and 100%) was effective in decreasing the thermal conductivity of lightweight aggregate concrete by up to 43.5%. This is mainly due to the relatively low conductivity of expanded perlite compared to pumice aggregate. [60].

Another type of natural lightweight aggregate is diatomite. Analysis, including compressive strength and thermal conductivity, has been carried out by Unal et al. [61] on block elements with diatomite aggregate (coarse and fine). According to their experimental results, compressive strength of 7-56 day specimens ranged from 2.5 to 8 MPa whilst the thermal conductivity (hot-wire ASTM C-1113 standard test [57]) was around 0.23 W/m.K. From these results it can be concluded that lightweight concrete with diatomite can be used to obtain high insulation but in low compressive strength structures.

Polystyrene is the most well-known artificial lightweight aggregate due to its good thermal properties. In the experimental work conducted by Babu et al. [62, 63] two types of expanded polystyrene spheres (EPS) were used. Type A (4.75-8 mm) with mostly 6.3 mm size beads and type B (1-4.75 mm) with mostly 4.75 mm size, with replacements of the total aggregate ranging from 0-95%. The results indicated that concrete with small expanded polystyrene aggregates size showed higher compressive strength (up to 33%). Also it was observed that the compressive strength decreases with the increase of EPS content and with increase in water / cement ratio similar to normal concrete. Therefore the benefit obtained with the use of small size aggregate was significant. These results were confirmed by Bouvard et al. [64] when the

effect of using EPS as an aggregate on the thermal and mechanical properties of the concrete manufactured by high performance cement was investigated. Two size distributions of fine aggregate were used in this study. In the first, 100% spheres had a diameter in the range of 0.75-1.1 mm (average 1mm) whilst in the second, 30% of spheres had a diameter in the range of 0.75-1.1 mm and 70% were diameter range 1.5-2.6 (average 2.2 mm) to obtain lower concrete density. It was found that with a concrete density of about 492 kg/m^3, the thermal conductivity is 0.164 W/m.K (using the hot wire test method) and the compressive strength is 0.8 MPa. These values increase with increasing density of concrete to reach 0.314 W/m.K for thermal conductivity and 11.4 MPa for compressive strength when the density is 861 kg/m^3 (less voids).

2.4.3 Using Recycled Materials as an Aggregate

Granulated fly ash (an industrial by product from coal based thermal power plants) has been used as a lightweight fine aggregate in concrete. The results obtained have shown the suitability of using fly ash to produce concrete with good mechanical properties as described in the following paragraphs.

Behera et al [65] studied the effect of using sintered fly ash as a partial replacement (20, 30, 40%) by volume of coarse aggregate (size range 3-20mm) on the compressive strength and young's modulus of elasticity of concrete. The results showed that there is a 14% reduction in the weight compared with normal concrete with no significant difference in strength or modulus of elasticity (the differences is less than 1%).

Kayali [66] used sintered fly ash for both fine and coarse aggregate (size range 3-12 mm) to produce high performance concrete. The results showed that the fly ash concrete is 22% lighter and 20% stronger than normal aggregate concrete, moreover, the drying shrinkage is 33% less than the normal aggregate concrete.

Many research studied the thermal properties of concrete containing fly ash as a partial replacement of cement [56, 67-70]. However, the thermal properties of concrete with fly ash as an aggregate have been paid less attention.

Recycled tyres (shredded, ground, or chipped) have become a raw material for many applications such as playground surfaces, lightweight fill or as fuel during the manufacture of other products. Eldin and Senouci [71] studied the effect on concrete mechanical properties by using chipped tyres as fine and coarse aggregate in concrete (rubberized concrete). The results showed a significant reduction in compressive and splitting tensile strengths (up to 85% and 50% respectively) depending on the percentage of the rubber in the mix. The reduction in these properties is lesser (30% to 60%) in the case of sand replacement when compared with coarse aggregate. Nevertheless, rubberized concrete is lighter than normal concrete (up to 25%) and exhibits the ability to absorb large amounts of plastic energy and did not show brittle failure under compression or split tension. These results are confirmed by a number of other researchers [72-75]. This behaviour was explained by Khatip and Bayomy [76] who noted that the rubber particles are much softer (elastically deformable) than the surrounding cement paste. On loading, cracks are initiated quickly around the rubber particles in the mix, which accelerates the failure of the rubber cement matrix. In addition, there was a lack of adhesion between the rubber particles and the paste. It was considered that the soft rubber particles may behave as voids in the concrete matrix. Guneyisi et al. [77] found that the addition of silica fume into the matrix improved the mechanical properties of concretes having up to 25% rubber content by total aggregate volume and might be practically used to produce rubberized concretes with compressive strength of 16–32 MPa.

The results obtained by Sukontasukkul [78] showed that when crumb rubber is used as a fine aggregate, this produces concrete with lower thermal conductivity by about 20 – 50% and in range of 0.241-0.443 W/m.K compared with plain concrete.

Aggregates produced by recycling old glass are being used as a lightweight filling material and protective thermal insulation layer in roads. The use of recycled glass as a lightweight aggregate in concrete is also being investigated [5, 6, 79-81].

An experimental investigation for compressive and tensile strength and workability of concrete manufactured using waste glass (mixed colour glass) with various particle sizes and content was conducted by Polley et al [79]. It was found that concrete with waste glass aggregate up to 20% and particle sizes range between 0.75μm to 150mm performed as well as or better than concrete with no glass (45-50 MPa at 365 days the compressive strength of glass concrete compared to 41-56 MPa for normal concrete)

Topcu and Canbaz [80] investigated the effect of using waste glass (green soda glass) as a replacement for coarse aggregate, particle sizes 4-16mm in proportions of 0-60%, on the workability, compressive, tensile and flexural strengths of concrete. It was found that there is no significant effect upon the workability of the concrete. The compressive, tensile and flexural strengths and the dynamic modulus of elasticity all decrease with increase the glass content. These results are similar with those obtained by Park et al. [5] when waste glass was used as a partial replacement for fine aggregate. This behaviour may be due to the smooth surface of the waste glass which leads to poorer adhesion at the glass and cement paste interface. However, the decrease in strength is less when using glass as a fine aggregate when compared to its use as coarse aggregate (small smooth surface for sand particle). In addition, Park et al. [5] concluded that the addition of pozzolanic material is most effective in enhancing the mechanical properties of glass concrete when up to 30% glass content is used.

Petrella et al. [6] studied the thermal insulation and compressive strength of concrete containing recycled waste glass (mixed colour glass) as an aggregate. According to the experimental results, the thermal conductivity of concrete made from waste glass, as a replacement for fine and coarse aggregate (particle sizes 0.5 -16 mm), was 0.158 W/m.K with a compressive

strength of 4.2 MPa. When waste glass was used as a replacement for fine aggregate only (particle sizes 0.5-2mm) with normal coarse aggregate (particle sizes 2-16mm), the thermal conductivity and the compressive strength were 0.843 W/m.K and 17.9 MPa respectively.

A wide study has been conducted at the University of Colombia into the use of crushed waste glass as an aggregate for concrete by Meyer et al. [81]. They found that the main problem when using glass aggregate is the alkali silica reaction (ASR). This reaction occurs between the reactive silica in the glass aggregate and the salt ions (Na+ and K+) in the cement paste. This reaction results in an increase in volume and thus induces internal stresses which affect the structure of concrete. This phenomenon has been confirmed by many researchers, as explain in the following paragraphs.

The effect of glass particles size, colour and glass content on the expansion caused by alkali silica reaction was investigated by Jin et al. [7] using ASTM accelerated test method (Standard Test Method for Potential Alkali Reactivity of Aggregates) [82]. According to this method, expansion of less than 0.10% at 14 days of age indicates acceptable performance, and expansion of greater than 0.20% indicates unacceptable performance. The results showed that the expansion of the mortar with glass particle size 300μm is the same as the expansion in the mortar with no glass (0.10%). The expansion then increases with increase the particle size of glass aggregate and maximum expansion was occurs for sieve size No.16 (1.18-2.36 mm) and it was approximately 0.4%. The results also showed that green glass has no significant expansion. The colour of glass is normally obtained by adding certain oxides to the glass melt, such as Cr_2O_3 for green colour. The addition of Cr_2O_3 straight to the concrete mixture, was found to increase the expansion considerably. However, if it is added as chemically bounded, it can serve as an ASR inhibitor [83].

Jin et al. [7] also observed that the expansion increases with increasing the glass aggregate content. For 100% glass content, the expansion was 35%

compared to 10% for mortar with no glass. This is in agreement with the results obtained by other researchers [12, 79, 80, 84].

Diamond [85] and Helmuth et al [9] studied the mechanism of ASR. It is believed that the ASR occurs only in the presence of Ca+ ions and water, so, to prevent ASR expansion, the use of pozzolana in the concrete mixture can remove $Ca(OH)_2$ from the solution. Furthermore using the minimum water content possible is favourable in preventing this reaction from occurring. Also another factor that influences the ASR is the permeability of the hydrated cement paste because this controls the movement of water and various ions as well as the silica gel [21].

2.4.4 Using Pozzolana in Concrete

A pozzolanic material which is a reactive silica or silica and alumina has been used for many purposes as a partial replacement of cement. The reaction between SiO_2 from pozzolana and $Ca(OH)_2$ from the hydration of Portland cement, in the presence of water, produces materials that have cementitious properties, which leads to an increase in compressive strength of cement paste materials.

Pozzolana was used in lightweight aggregate concrete to enhance its compressive strength and durability. Demirboa et al [55] reported that 10%, 20% and 30% of silica fume as a partial replacement for cement increases the 28 days compressive strength of concrete (produced by using expanded perlite and pumice as an aggregates) by 29%, 69% and 13% respectively. Similar results were obtained by Babu et al [63, 86] regarding the compressive strength of concrete made with expanded polystyrene aggregate.

Demirboga and Gul [55] studied the effect of using silica fume and fly ash as a partial replacement for cement on the thermal conductivity of concrete produced by using expanded perlite and pumice as aggregates. The results showed that 10, 20 and 30% silica fume reduce the thermal conductivity by 2.5, 6 and 10% respectively compared to the control mix. Concrete with 10,

20 and 30% fly ash reduces the thermal conductivity by 10, 11 and 12% respectively.

Good performance was observed for concrete which has metakaolin compared with silica fume [10, 11, 87]. It was shown that the optimum content of metakaolin is 10% as autogeneses shrinkage increase with increasing metakaolin content [10, 11], the use of metakaolin which partially replaced the cement by 10% results in an increase in compressive up to 30%, at 90 days [10]. Experimental study carried out by Justice et al.[11], using ASTM accelerated test method mentioned previously, showed that the expansion due to the ASR were also reduced by adding 8-15% metakaolin [10, 11]. For this reason, 10% metakaolin as a partial replacement of cement was used in this research.

2.4.5 Use of Fibre

Different types of fibre are widely used to improve the performance of the concrete and to enhance properties like tensile strength, flexural strength, and resistance to impact load, crack resistance, toughness, fire resistance and thermal insulation. Different types of fibre were used in concrete and their effect on the mechanical and thermal properties of concrete were studied.

Duzgun et al. [88] in their study on the effect of steel fibres ratio on the properties of lightweight concrete made with pumice aggregate showed that the unit weight and the mechanical properties decrease with increasing the pumice content in samples containing no steel fibres. Increasing the steel fibre ratio in the mixture results in increasing the unit weight, compressive strength, splitting-tensile strength, flexural strength, and the modulus of elasticity up to 8.5%, 21.1%, 61.2%, and 120.2% respectively. The deformation capability was decreased with increasing pumice aggregate content and steel fibre ratio in the mixture. This is probably due to the delay in the growth of micro cracks by fibres which leads to an increase in strength and strains at peak load. [89].

The presence of steel-fibres increases the thermal conductivity of concrete at temperatures up to about 700℃. This increase in thermal conductivity can be attributed to the fact that the thermal conductivity of steel is about 50 times higher than that of concrete [90, 91]. The thermal expansion also increases up to 600^{o}C then remains constant.

Song et al.[92] observed that the compressive strength, splitting tensile strength and modulus of rupture of nylon fibre concrete improved by 6.3%, 6.7%, and 4.35% respectively, over those of polypropylene fibre concrete. In addition, the impact resistance, the first crack and failure strengths and the shrinkage crack reduction potential also improved more for the nylon fibre mortar.

Park and Lee [12] found experimentally that both steel fibres and polypropylene fibres have a positive effect on the reduction of the expansion due to ASR in waste glass aggregate concrete. In particular, adding 1.5% volume of steel fibres to concrete containing 20% waste glass reduces the expansion ratio by 40% and increases flexural strength by up to 110%.

It was found that using polypropylene fibre can prevent spalling of concrete at fire condition. When concrete is subjected to heat, the polypropylene will melt, creating pathways within the concrete for the exhaust of water vapour and any other gaseous product, which will thereby reduce the building up of pressure within the concrete [51].

The use of short and continuous carbon fibre has been investigated by many researchers. It was found that the increase in carbon fibre content results in an increase in flexural strengths by 85%, the flexural toughness by 205% and the compressive strength by 22% as well as the material price increase of 39% [93]. In addition, the thermal conductivity of concrete contain 1%carbon fibre was 20% lower than the thermal conductivity value for concrete without fibre [94]. This is attributed to the increase in air void content when increasing the fibre content. .

Toutanji et al. [95] investigated the effect of carbon fibres on the tensile strength of concrete. It was observed that the addition of 1,1.5,2, and 3% of volume of polyacrylonitrite-based carbon fibre to a concrete results in an increase in the tensile strength of 32, 42, 48, and 56%, respectively.

Basalt rock is a volcanic rock and can be divided into small particles then formed into continuous or chopped fibres. Basalt fibre has a higher working temperature and has a good resistance to chemical attack, impact load, and fire with less poisonous fumes compared to glass fibre [96]. A previous experimental study on the chemical durability of basalt fibre indicated that this type of fibre has an excellent resistance to alkaline attack, better than glass fibre, however, it has poor resistance to acids [16].

Dias and Thaumaturgo [19] have introduced basalt fibre into concrete composites. They investigated experimentally the influence of the volumetric fraction of chopped basalt fibre on the fracture toughness of geopolymetric cement concrete (PSS) (inorganic cement) reinforced with this type of fibre. They compared it with ordinary Portland cement concrete (PC) also reinforced with basalt fibre. The results showed that there was a gain in splitting tensile strength (up to 34%) for PSS specimens. For PC specimens, there is no significant difference compared to the control mix. This difference in behaviour is probably related to the nature of the bond between the fibre and matrix. However, the volume fractions that been used were considerably high for this type of fibre (0.5 and 1%).

Sim et al [17] investigate the effect of using continuous basalt fibres in concrete subjected to high temperature and compared the results with that obtained using glass and carbon fibre. The results showed that basalt fibre kept about 90% of the normal temperature strength for 2hrs after exposure at 600^{o}C whereas the carbon and the glass fibres not maintain their volumetric integrity. Figure 2-6 shows the variation of the strength of concrete with temperature for different type of fibre.

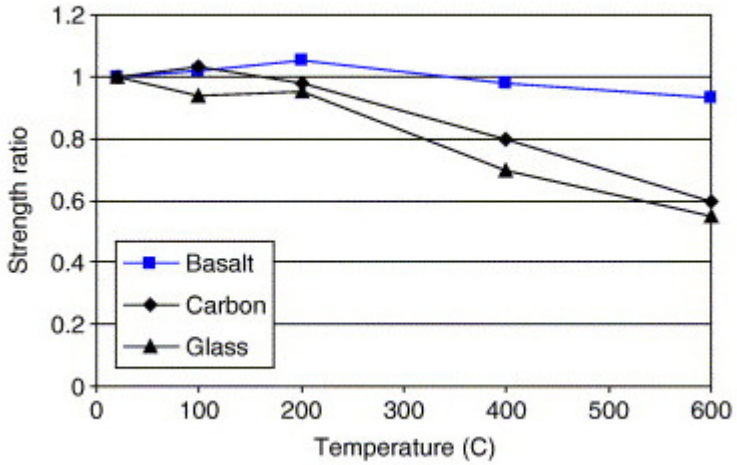

Figure 2-6 Strength variation with respect to heat exposure [17]

Experimental results have shown that the workability of fresh concrete is decreased with the addition of fibre. Fibres hinder the flowability of fresh concrete and this results in a decrease in workability [97-100].

2.4.6 Use of Superplacticizer

Superplasticizer is a water reducing admixture used in concrete to improve its workability at a given water /cement ratio or to reduce the water/ cement ratio at a constant slump. Water reducing admixtures increases the surface area of cement by dispersing the cement particles due to the electrostatic charge. This can undergo initial hydration and also increase the amount of water available for hydration (increase in the hydration area) which leads to an increase in compressive strength [21].

Sari and Pasamehmetoglu [101] concluded that the addition of superplasticizer improves the strength to density ratio of the hardened concrete and the workability of fresh concrete. Similar results were obtained by Aruntas et al [102] who found that higher compressive and flexural strength fibre reinforced concrete can be produced with the addition of superplasticizer.

However, the effect of superplasticizer on compressive strength depends on the cement constituents, the silica reactivity of aggregate and the type of superplasticizer used [21].

2.5 PROPERTIES OF REINFORCING STEEL

2.5.1 Thermal Properties

2.5.1.1 Thermal Expansion

The thermal expansion of various carbon and low – alloy steels depends on the carbon content and the heat treatment. The coefficient of thermal expansion for steel is usually taken to be $11.4\text{x}10^{-6}\text{m}^{-1}\text{°C}^{-1}$ at room temperature[103]. EC3 gives equations to define the thermal strain for mild steel at different temperature, as shown in Table 2-3 [104].

Table 2-3 Equations of thermal strain for mild steel

$-2.416\times10^{-4}+1.2\times10^{-5}\theta+0.4\times10^{-8}\theta^2$	for $20^{o}C\le\theta\le750^{o}C$
11×10^{-3}	for $750^{o}C\le\theta\le860^{o}C$
$-6.2\times10^{-3}+2\times10^{-5}\theta$	for $860^{o}C\le\theta\le1200^{o}C$

The coefficient of thermal expansion increases when the temperature increases and the discontinuity occurs between 700 and 800 °C due to the phase change (Figure 2-7)

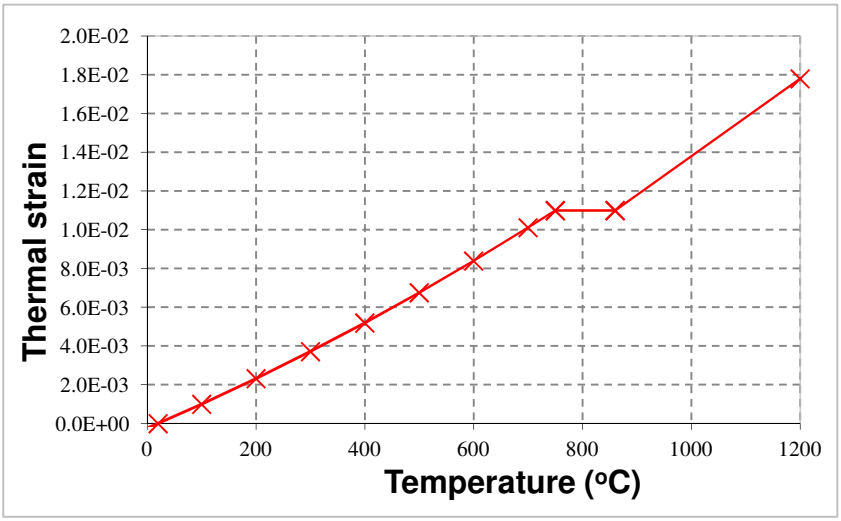

Figure 2-7 Thermal strain of mild reinforcing steel [104]

2.5.1.2 Thermal Conductivity and Specific Heat

The thermal conductivity of steel (λa) depends mainly on the steel type and the temperature. It reduces linearly from 54 W/m.K at 20oC to 27.3 W/m.K at 800oC [104]. It can be determined (in W/m.K) by Equation 4[104]:

$\lambda_{a=}\begin{cases}54-3.33\times10^{-2}\theta_a\\27.3\end{cases}$	For 20°C≤θ_a≤800°C For 800°C≤θ_a≤1200°C

The specific heat ca varies with temperature and can be determined (in J/kg.K) by using Equation 5:

$C_a\begin{cases}425-7.73\times10^{-1}\theta_a-1.69\times10^{-3}\theta_a^2+2.22\times10^{-6}\theta_a^3\\666+\frac{13002}{738-\theta_a}\\545+\frac{17820}{\theta_a-731}\\650\end{cases}$	For 20°C≤θ_a≤600°C For 600°C≤θ_a≤735°C For 735°C≤θ_a≤900°C For 900°C≤θ_a≤1200°C

2.5.2 Mechanical Properties

2.5.2.1 Ultimate and yield Strength

Steel has the same compression and tension with elastic behaviour to a well - defined yield point at normal temperature, and then it shows very ductile behaviour until the ultimate strength is reached, however, this yield point disappears at elevated temperature [3].

Figure 2-8 shows the reduction factors of the yield strength (maximum stress level), $K_{y,\theta}$, and for yield strength (proportional limit), $K_{p,\theta}$, for mild steel at elevated temperature according to EC3 [105].

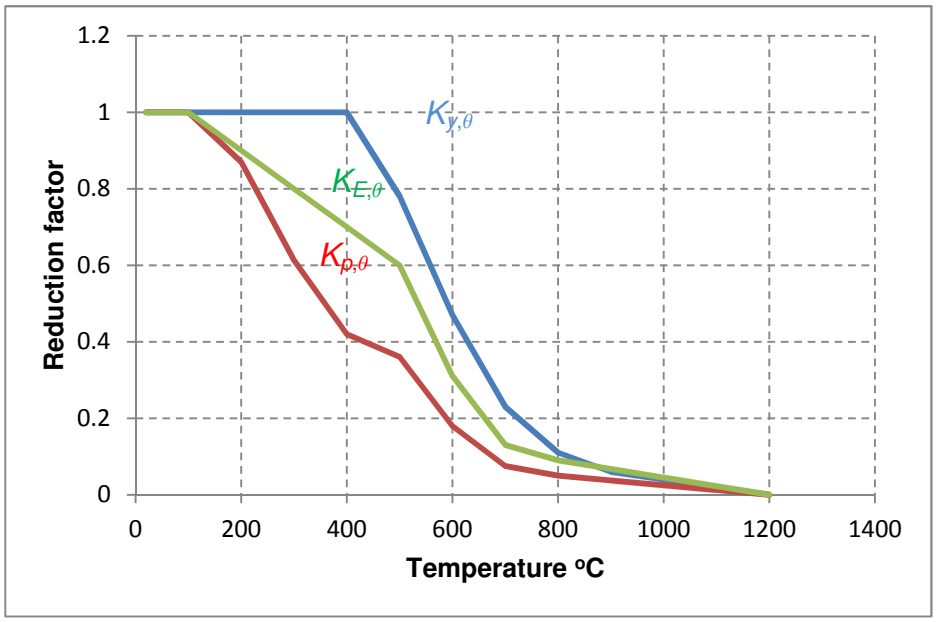

Figure 2-8 Reduction factors for reinforcing mild steel at elevated temperatures [105]

2.5.2.2 Component of Strain

The total strain at elevated temperature for steel is a sum of three components; thermal strain, stress related strain and creep strain.

The thermal strain is the thermal expansion explained before. Creep strain only becomes significant at temperature over 400^{o}C [3]. Previous research has shown that creep is highly dependent on the temperature and stress level of steel (Figure 2-9) [106]. When the steel at a particular stress level reaches a certain temperature, it becomes plastic and, at this stage, the stress – strain relationship is dependent on creep strain.

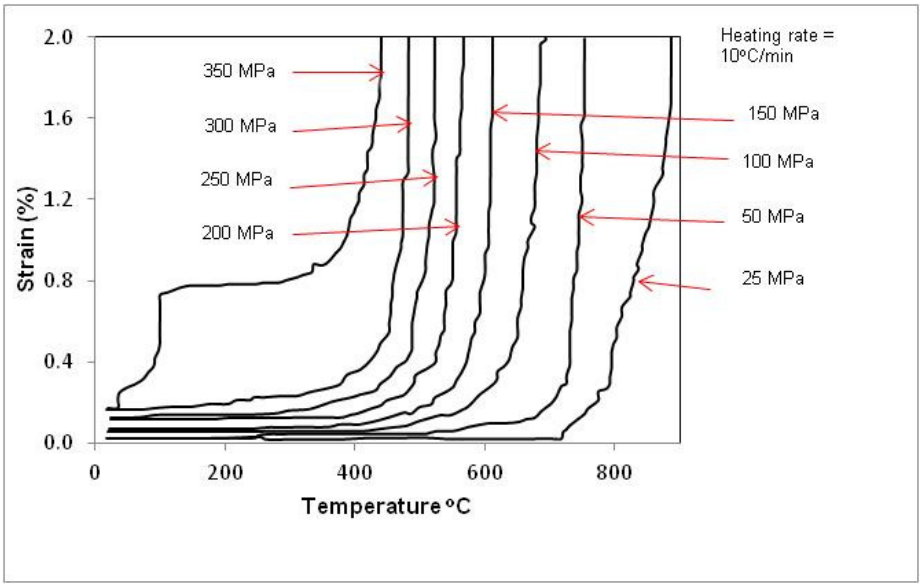

Figure 2-9 Creep of steel in tension [106]

It was assumed that the stress – strain relationships used for design are effective and implicitly include the deformation due to creep [104].

The yield strength and modulus of elasticity decrease with increasing temperature, however, the ultimate tensile strength increases slightly at moderate temperature and then decreases at high temperature. The stress – strain curve of steel according to EC3 at a given temperature is defined by three parameters; the slope of the linear elastic range, the proportional limit and the maximum stress level [104]. The equations that define the stress – strain relationship of reinforcing mild steel can be found in EC3 [104]

CHAPTER THREE

3 REINFORCED CONCRETE SLAB

3.1 GENERAL INTRODUCTION

The structural design for a building must ensure that the structure is safe under the worst load conditions, and able to function without excessive deflections or movements which may cause failure of structural elements, cracking, or discomfort for occupants.

A reinforced concrete slab is a common structural element in a building. It is used as a floor or roof and designed to carry the vertical applied load as well as the fire load. It can be constructed in different forms such as a solid flat slab, waffle slab, or composite slab with steel decking. Apart from resisting the load there are another important factors that have to be taken into consideration in the slab design for fire resistance, they are insulation, integrity and stability.

Currently, the majority of reinforced concrete slab design is based on ultimate limit state principles. Johansen's yield-line analysis [107] is also permitted by many codes to determine the collapse load. These methods are based on flexural behaviour and give an indication of the ultimate load without the development of in plane forces (membrane).

Following full-scale tests carried out at Cardington and real fires in steel framed buildings with composite floors [108, 109], it has been found that concrete slabs experience tensile membrane action under large displacements. The tensile membrane action enables concrete slabs to support loads much greater than those calculated using the yield line method which has proved a positive behaviour for the structure in the event of fire.

3.2 MEMBRANE ACTION IN FLOOR SLAB

At initial deflection and rotation, the slab pushes against the boundaries and large compressive forces are developed through the slab. Increasing the deflection allows for the reduction of these compressive forces starting in the middle of the slab, and leading to areas of tension and cracking in the centre of the slab. With further increase in deflection, these cracks develop further outward, and the slab develops tensile membrane action anchored at or supported by the boundary [110].

At ambient temperature tests, the transition from compressive membrane action to tensile membrane action is likely to be accompanied by a rapid increase in the central deflection of the floor system [111]. The ambient load deflection behaviour of reinforced concrete slabs is summarised schematically in Figure 3-1.

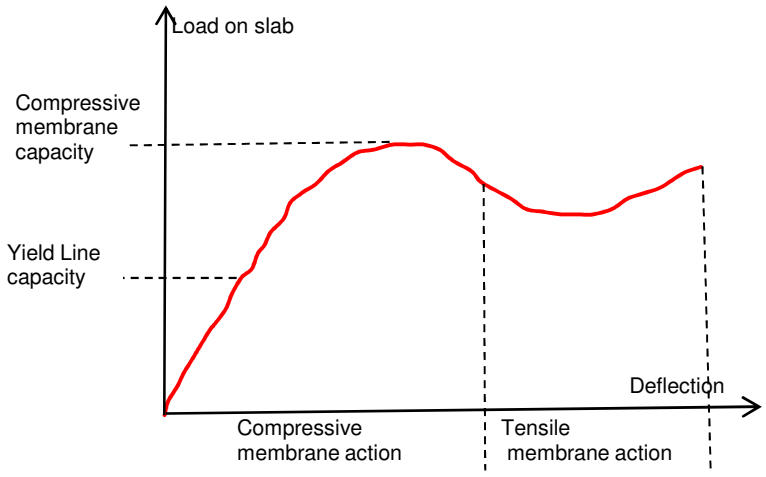

Figure 3-1 Ambient load deflection behaviour of a concrete slab [112]

In fire, the increased temperature and thermal gradient induced in the slab allows large deflections to develop due to thermal strains without the extensive cracking as observed at ambient temperature. These large thermal strains are unaccompanied by corresponding mechanical strains and therefore result in an increase in tensile membrane capacity (Figure 3-2).

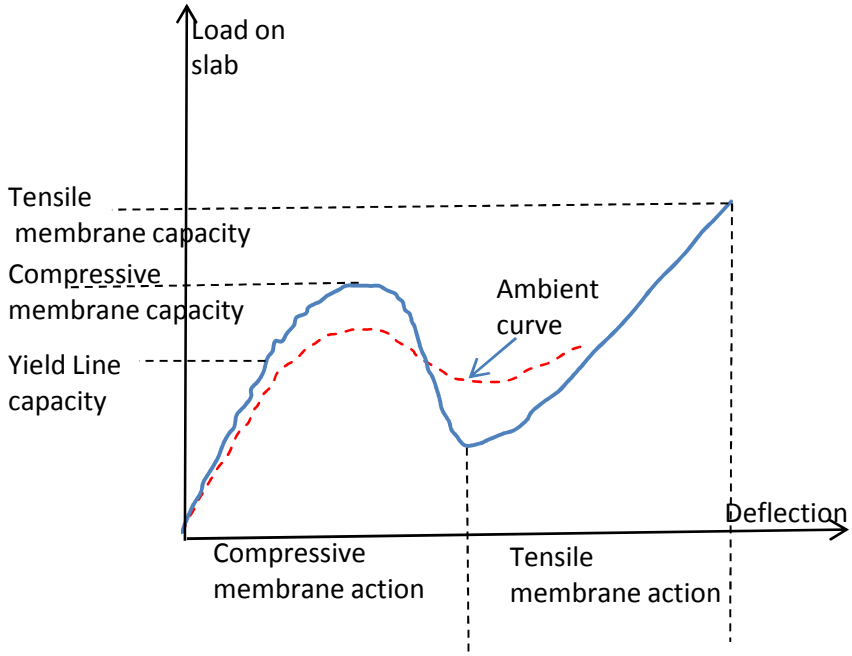

Figure 3-2 Load deflection behaviour of a concrete slab at elevated temperature [112]

3.2.1 Compressive Membrane Action

When the edges of a reinforced concrete slab, subjected to vertical loads, are restraint against horizontal translation, in-plane compressive forces are induces within the slab. The presence of these forces results in increases the stiffness and load-carrying capacity of the slab. This is referred to as compressive membrane action (or arching action). To develop compressive membrane action in a slab, there are two requirements have to be provided. Firstly, the horizontal translational restrained and secondly, the total strain

along longitudinal rebar at the depth of the horizontal restraint must be non-zero if the restraint did not exist [113].

Full scale slab and beam-floor tests were carried out by Ockleston [114]. The results showed that the enhancement due to compressive membrane action (the ratios of experimental ultimate load to predicted Johansen load) were greater than 2.5. These results encourage many researchers to study, both experimentally and theoretically, the phenomenon of membrane action in reinforced concrete slabs.

Small scale rectangular slabs tests, with different reinforcement ratio, were conducted by Powell [115]. The results showed enhancement factors between 1.61 (for 1.53% reinforcement) to 8.25 (for .25% reinforcement).

Wood [116] tested square panels monolithically within a stiff reinforced concrete surround and obtained enhancement factors up to 10.9.

Parak [117] developed a yield-line theory to determine the ultimate strength of uniformly loaded rectangular concrete slabs which have either all or three edges restrained against lateral movement. The theory considers the benefit of the presence of compressive membrane stresses and uses a rigid-plastic strip approximation. The results obtained from this theory was validated against experimental results obtained from tests conducted on thirty-five slabs with various long span to short span ratios, span to depth ratios, and reinforcement contents. The theory shows that Johansen's yield-line theory under-estimates the ultimate strength of restraint slabs and a good correlation was found, on the basis of an empirical value for the deflection at ultimate load, between the theory and the test results.

Compressive membrane action behaviour is unstable, transfers to tensile membrane action at large displacement (Figure 3-1Figure 3-2), and extremely sensitive to the edge restraints. For these reasons, many designers did not consider the presence of the compressive membrane action in the design of the reinforced concrete structures [118].

3.2.2 Tensile Membrane Action

For unrestrained slab, the ability to develop compressive membrane action is very limited. However, at large deflection, an in-plane ring beam in compression can be developed to support the development of tensile membrane action in the central region of the slab [118]. The large deflection is a problem when structures subjected to the accidental loads such as fire. For this reason, the tensile membrane action is important to design structures subjected to fire.

Significant theoretical and experimental research have been carried out investigating tensile membrane action since 1960's, as describe in the following section.

3.2.2.1 Experimental and Theoretical Research on Unrestrained Slabs

Theoretical work on circular slabs has been carried out by Wood [116]. In this work it was assumed that the energy dissipated by the stretching of reinforcement is equal to the energy assumed at the fracture lines. Under radially symmetrical loading, the relationship of the enhancement of the applied load with the normalised deflection was provided with different reinforcement ratio. This was achieved by considering the equilibrium of the internal force and moment of a small element of a circular plate. Wood's analysis was limited to circular slabs.

Taylor [119] proposed a method for unrestrained uniformly loaded square slabs under large deflections with a yield line pattern dividing the slab into four segments. The lower central region of the slab is in tension and the upper outer region is in compression. He assumed the equilibrium of the moment from the loads about the axis of rotation with the moment of internal forces along the yield-line of the slab. As a result of this assumption, a simple method of calculating the load-deflection relationship of the slab was developed. The maximum deflection was assumed to be limited by the serviceability requirement. The limitation of this method is that it ignored the formation of a crack across the shorter span of the slab, which overestimated the load-carrying capacity.

Sawczuk et al. and Hayes[120, 121] have developed analytical methods for considering membrane action in unrestrained slabs. The method by Sawczuk et al [120] was based on an energy method while Hayes developed an equilibrium method based on the failure mode proposed by Sawczuk et al. Their design methods assumed that the critical mode of failure was by cracks forming across the short span of the slab, intersecting the yield lines (Figure 3-3). Its results contradict the tests results conducted at the BRE [122]. This assumption is based on small-scale slab tests conducted at ambient temperature and may not apply to the slab tested in fire condition.

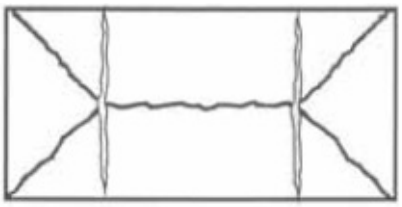

Figure 3-3 Critical mode of failure in the slabs assumed by Ref. [120, 121]

Bailey et al [109, 122] and Bailey [123] have developed a method for determining the ultimate load carrying capacity of two-way slabs incorporating the effects of tensile membrane enhancement at ambient and under elevated temperatures. The method considers the failure mode shown in Figure 3-4 which differs from the failure mode presented by Sawczuk et al and Hayes mentioned before. The design method estimates the load capacity of a two-way slab at a given displacement, based on the membrane forces in the slab. The design method calculates an enhancement factor, due to the effect of the membrane forces on the flexural strength, for the yield line load capacity. This method has shown a good agreement with published data of the fire tests at the Cardington Large Building Test Facility [122]. The design method also includes a check on the ultimate failure of the system based on the maximum permissible deflections due to the mechanical strains of the reinforcement and the thermal bowing deflections.

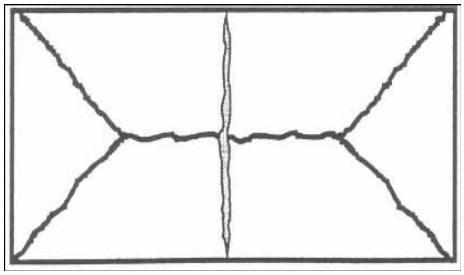

Figure 3-4 Assumed failure mode of the slab by Ref. [123]

Fire tests of two-way concrete slabs were conducted to investigate the behaviour of unrestrained simply supported slabs in a controlled furnace environment [124]. The six slabs were tested. Each slab measured 3.3m wide by 4.3m long, comprising three reinforced concrete flat slabs and three composite steel-concrete slabs with different thickness (90, 100 and 130mm). Different quantities of reinforcing steel were used to investigate their effect on controlling crack widths to prevent integrity failure. The slabs were simply supported on all four sides over the furnace with no horizontal restraint. The slabs performed very well in the fire tests, supporting the loads for the full duration of three hours without collapse. All the slabs suffered extensive surface cracking and loss of moisture. Some of the slabs suffered large midspan deflections (up to 270mm) and full depth cracks which were associated with the yield line crack pattern. The slabs with higher steel content and closer bar spacing suffered only surface cracking, while the slabs with lower steel content suffered full-depth cracks. The tests illustrated the significant influence of tensile membrane action on maintaining the structural stability of the floor slabs under fire conditions, by supporting loads significantly in excess of their predicted yield line capacities. The failure mode was not observed in this test as no slab reached failure.

Foster et al [125, 126] present a series of experiments on the slabs which were horizontally unrestrained and subjected to vertical load. This work was conducted to investigate the influence of isotropic and orthotropic reinforcement. The influence of the bond strength between the reinforcement bars and concrete was also considered by comparing results from smooth

and deformed reinforced bars. For the isotropic reinforced slab at ambient temperature tests, the slab with deformed reinforcing wires supported greater load at a larger deflection than the slabs with smooth reinforcement. The orthotropic reinforced slab results showed that In the case of smooth reinforcement, the load capacity of the slab continued to increase with increase in displacement, beyond the initial peaks, whereas for deformed reinforcement, the load capacity of the slab decreased consistently with increasing displacement in the same range.

The elevated temperatures tests were concentrated on the isotropic reinforcement only. All the test results showed the enhancement of the load carrying capacity due to tensile membrane action. The slabs reinforced with smooth bars performed better than those reinforced with deformed bars. The difference of the load deflection response of the deformed bar slabs to the smooth bar reinforced slabs was due to the effect of progressive fracture of deformed bars across the tension cracks. As the bonding between the smooth bar concrete was poor, the smooth wire did not extensively fracture in the test. However, in the fire test, the slabs were loaded significantly above the yield line load forcing them into membrane action before the slabs were subjected to heating which resulted in unrealistic behaviour and low reinforcement failure temperatures.

Small-scale horizontally unrestrained two-way slab tests were conducted by Bailey and Toh [127] at ambient and elevated temperatures. Two types of reinforcement were used in these tests; mild steel and stainless-steel welded smooth wire meshes with varying bar diameters and spacing. The tests results at ambient temperature showed that slabs with a low reinforcement ratio failed by fracture of reinforcement at the centre of the slab either across the shorter span for the rectangular slabs or across one of the spans for the square slabs. It was found that increasing the reinforcement ratio leads to compressive failure of concrete at the corners of the slabs. The test at elevated temperatures showed that all the slabs failed by fracture of the reinforcement, with displacements ranging from span/12 to span/6. The

results clearly showed that membrane action occurred at both ambient and elevated temperatures.

The previous research stated in this chapter concentrated on the effect of the reinforcement quantity, arrangement or types, the boundary conditions and slab geometry on the failure mode and membrane action of concrete slabs. In this study, the effect of the new type of concrete on the structural behaviour of the floor slabs was investigated at ambient and elevated temperatures.

CHAPTER FOUR

4 EXPERIMENTAL WORK

4.1 METHODOLOGY

It can be concluded from the previous research stated in Chapters 1, 2 and 3 that the type of aggregate used and the environment temperature are important parameters that influence the mechanical and thermal properties of concrete. Also it was found that recycled sand glass concrete has good strength when compared with other types of recycled aggregate concrete strength [5-7] . Furthermore, this type of aggregate has a major problem which is the expansion due to ASR as mentioned in Chapters 1 and 2. However, experimental results, using ASTM accelerated test method (Standard Test Method for Potential Alkali Reactivity of Aggregates), showed that it is possible to reduce this type of expansion by controlling the range of the particle size of glass, glass color, and glass content as well as using fibre and pozzolanic materials in concrete [5-7, 11, 12, 79, 82].

Limited research has been carried out to investigate the effect of glass sand on the concrete thermal properties, including its structural behaviour at fire condition. Previous research suggested using of reprocessed carpet fibres to improve this concrete's thermal properties. However, this type of fibre effects its mechanical properties negatively [8].research is needed to fill the gap in the area of knowledge on the thermal properties of concrete containing waste glass as a partial replacement of the natural sand.

The use of continuous basalt fibre, produced from volcanic rock, in concrete was investigated previously and this results in improving the thermal and mechanical properties [17]. It was also found that basalt fibre has a better resistance to the alkaline solution, even at higher temperature, than glass fibre [15, 16]. As srated in Chapter 1, the manufacture process of this type of fibre need less energy consumed and no additives compared with glass fibre which make it cheaper than glass or carbon fibres [15].Nevertheless, limited

research has studied the effect of using short basalt fibre on the mechanical properties of concrete [18, 19] and no research has been found on its thermal properties.

This research is looking to develop environmentally friendly and low cost materials suitable for enhancing the thermal properties of concrete with no significant reduction in its load bearing capacity. To achieve this objective, experimental work has been carried out in the concrete laboratory in the University of Manchester between November 2009 and September 2010. The experimental work consisted of two parts; the first part was to investigate the thermal and mechanical properties of the new concrete with different percentages of waste glass, as a partial replacement of the natural sand, and chopped basalt fibre. The second part was to investigate the structural behaviour of this type of concrete by conducting small-scale slab tests as a structural application. The content of the suggested materials in this part were selected depending on the results from the first part. Figure 4-1 shows the programme of the experimental work which was conducted during this research

The first part of the experimental work is presented in this chapter while the second part is presented in Chapter 5.

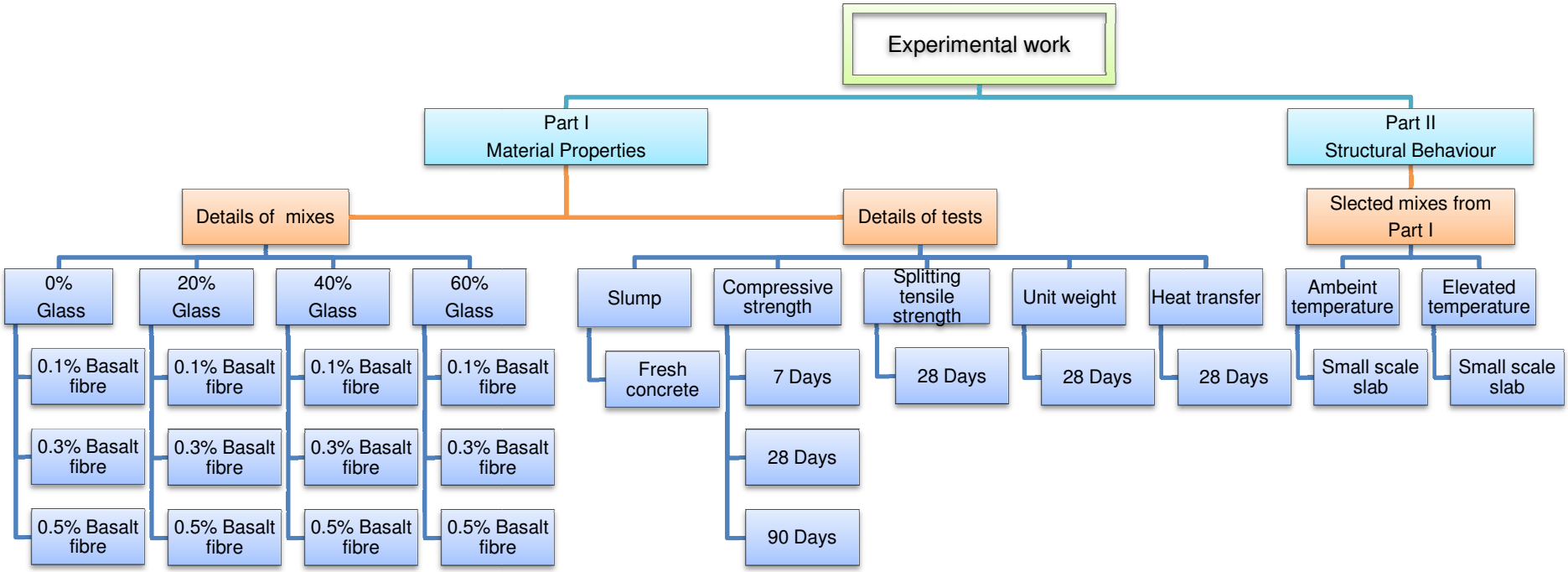

Figure 4-1 Experimental work programme

4.2 MATERIALS USED

The following materials were used in this study;

4.2.1 Cement

Ordinary Portland cement was used as the main binder throughout this research

4.2.2 Pozzolana

China clay (metakaoline) was used to enhance the strength at later ages, avoid segregation and to reduce the expansion due to alkali silica reaction. The percentage used in all mixtures was 10% by weight of cement, which is the optimum content used in the literature as mentioned in Section 2.4.4 [10, 11, 87].

4.2.3 Fine Aggregate

Recycled waste mixed colour glass (Figure 4-2) was used as a partial replacement for natural fine aggregate. The glass percentages of (0%, 20%, 40%, and 60%) by weight were used in this study. The glass was brought from Specialist Aggregates Ltd and manufactured from glass recycled from bottle-bank arisings. The glass has been washed, crushed and screened to remove virtually all particles less than 200 microns in diameter. The glass sieve analysis is shown in Table 4-1

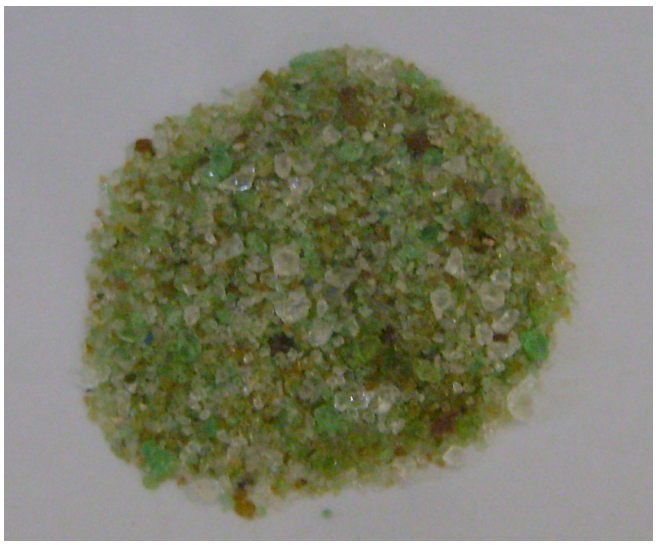

Figure 4-2 Recycled glass aggregate

Table 4-1 Sieve analysis of glass aggregate used in this study

Sieve Size mm	% Passing
4.76	100
2.36	91.1
1.18	70
0.6	5
0.3	0.2
0.15	0.2
Pan	0

4.2.4 Coarse Aggregate

Limestone coarse aggregate with a maximum size of 10mm was used in all mixtures.

4.2.5 Water

Manchester Tap Water was used throughout this study.

4.2.6 Fibre

Chopped Basalt fibres from BASALTEX Ltd in Belgium with volume fraction (0%, 0.1%, 0.3%, and 0.5%) by volume were used to investigate its influence on mechanical and thermal properties of concrete. The fibres are bundles so they do not have uniform diameter as shown in Figure 4-3. The length of the individual fibre is 25.4mm and 13μm in diameter.

Figure 4-3 Basalt fibre

4.2.7 Superplasticizer

The superplasticizer used was a sulphonated formaldehyde condensate (Daracem SP6) supplied by GRACE construction products (UK). The optimum dosage was chosen by carrying out trial mixes for concrete with highest percentage of fibre and no glass. It was used to reduce the water / cement ratio which leads to an increase in the compressive strength with the same workability.

4.3 MIX DESIGN AND PREPARATION

Sixteen concrete mixes were cast with a different percentage of sand glass aggregate and basalt fibre (Table 4-2).

The control mix was designed to achieve a design strength of 35 MPa. The cement, coarse aggregate, water/ binder ratio, the total weight of the fine aggregate and the dosage of the superplasticizer were kept constant for all mixtures to show the effect of the glass aggregate on the strength. The basalt fibre was added as a percentage of the total volume of the mixture. The mix proportion for all mixes was 1:1.75:3.5 (cement: sand: coarse aggregate) by weight and the water/binder ratio was 0.55.

For mixes containing basalt fibre, after adding all the materials into the mixer, the desired volume of fibre were gradually added into the mix while mixing continued in order to achieve good fibre distribution. All the specimens were placed in a water tank until the time of the test.

Table 4-2 Concrete mix details

Specimen mark.	Basalt Ffbre%	Fine glass%
G0F0	0	0
G0F1	0.1	0
G0F3	0.3	0
G0F5	0.5	0
G2F0	0	20
G2F1	0.1	20
G2F3	0.3	20
G2F5	0.5	20
G4F0	0	40
G4F1	0.1	40
G4F3	0.3	40
G4F5	0.5	40
G6F0	0	60
G6F1	0.1	60
G6F3	0.3	60
G6F5	0.5	60

4.4 TESTS AND METHODS

For these tests British (BS), Euro (EN) and ASTM standard tests were adopted.

4.4.1 Slump Test

BS EN 12350-2:2009 [128] slump test was followed to evaluate the workability of fresh concrete.

4.4.2 Density and Compressive Strength Test

The compressive strength test was conducted according to BS EN 12390-3:2002 [129]. Cubic samples (100×100×100) mm were used for these tests, the specimens were tested at three ages; 7days, 28days, and 90 days. The average of three specimens was recorded as a test result.

4.4.3 Splitting Tensile Strength Test

BS EN 12390-6:2000 [130] was followed to conduct the splitting tensile strength. Three cylinder samples (100 mm in diameter and 200 mm high) were tested for this purpose at 28 days and the average was recorded.

4.4.4 Heat Transfer

A simple test was developed by Meyer et al[8], as an alternative to the standard test, to measure the thermal conductivity of concrete by measuring the thermal resistivity. The test procedure utilizes a standard oven with a removable door and automatic temperature control. By replacing the door with a test sample and measuring the temperature on both faces of the sample, the temperature differential between the outside and the inside specimen surfaces is obtained. By plotting the temperature time histories and integrating the area between the curves for the inside and the outside temperature, they obtained a value referred to thermal resistivity. This method is not applicable unless the value of heat flux is known which is not available in the laboratory kiln used in this study. Therefore, the heat transfer through the concrete specimen was measured instead of the thermal resistivity. Small specimens (100x100x25) mm were placed on the top of the kiln and insulated from the other direction (Figure 4-4).

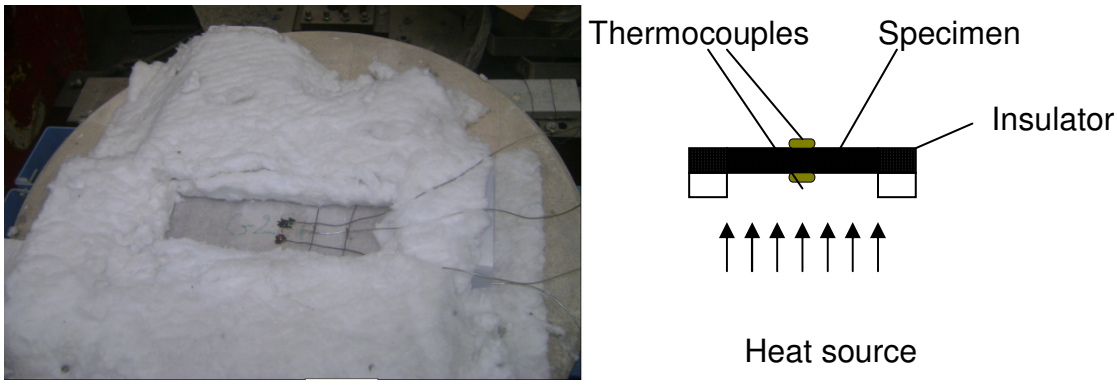

Figure 4-4 Heat transfer test

The temperature was raised to 600°C at a rate of 5°C/min. The outside and the inside surfaces of the specimens centre temperatures were measured using thermocouples (type k) adhered to the surfaces using a special type of glue named "thermo–glue" which is a metal oxide loaded two part epoxy bonding system (APPENDIX –A). The readings of the thermocouples were checked using a thermal imaging camera and surface probe (Figure 4-5). The differential temperature between the outside and the inside faces of the specimen was determined. The comparison between the mixtures was carried out by plotting the temperature difference- time histories.

To ensure the accuracy of this test a number of trial tests were carried out using different methods of adhesion and number of thermocouples, as shown in Figure 4-5 (a and b). The first method is to drill a small hole (3mm depth) and put the thermocouple directly in this hole without using any glue and check the readings, at different temperature levels, with that appearing in the thermal imaging camera and surface probe. The second one is to make two holes for two thermocouples, one of them adhered to it using glue and the other kept without glue and compare the readings with that from the thermal imaging camera and surface probe (Figure 4-6). It was found that the glued thermocouple gave more accurate reading (± 2°C) than the non-glued one. Therefore, the thermo – glue readings were adopted in all tests.

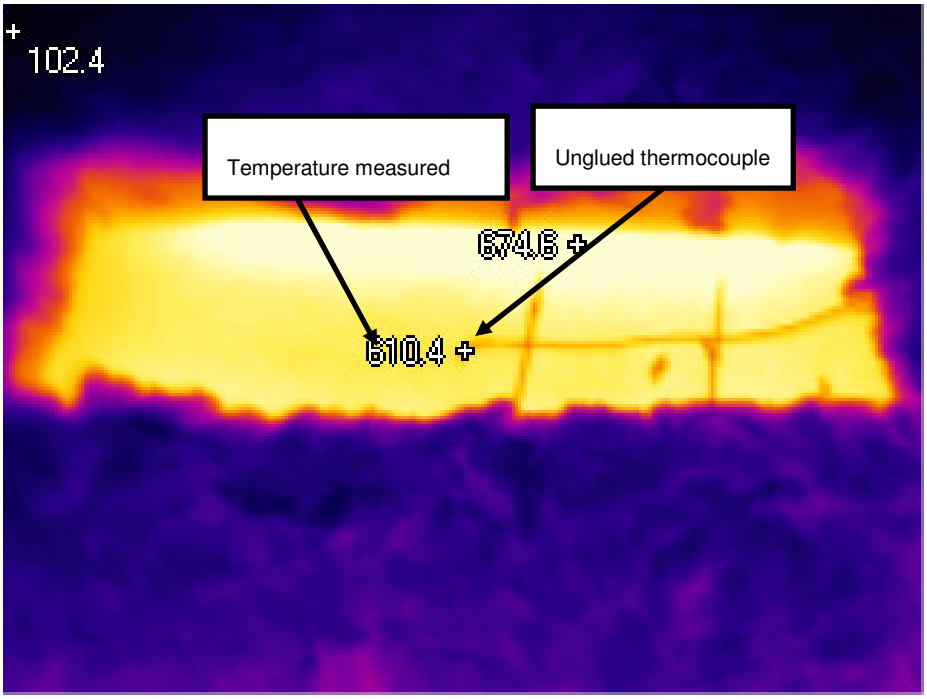

a) One unglued thermocouple on top

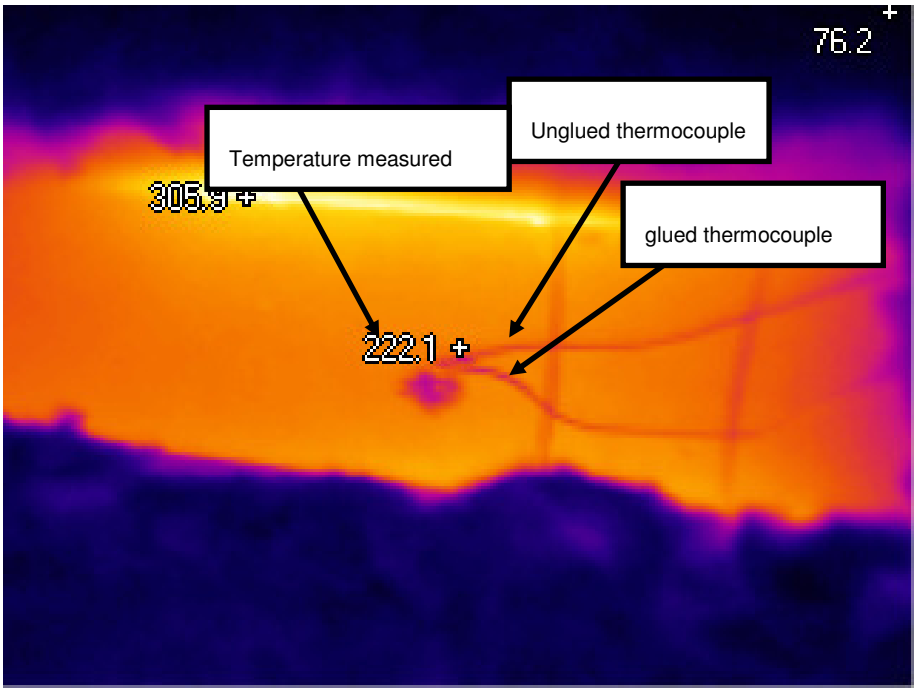

b) One glued thermocouple and one unglued on top

Figure 4-5 Heat transfer test methods with different methods of adhesion and number of thermocouples

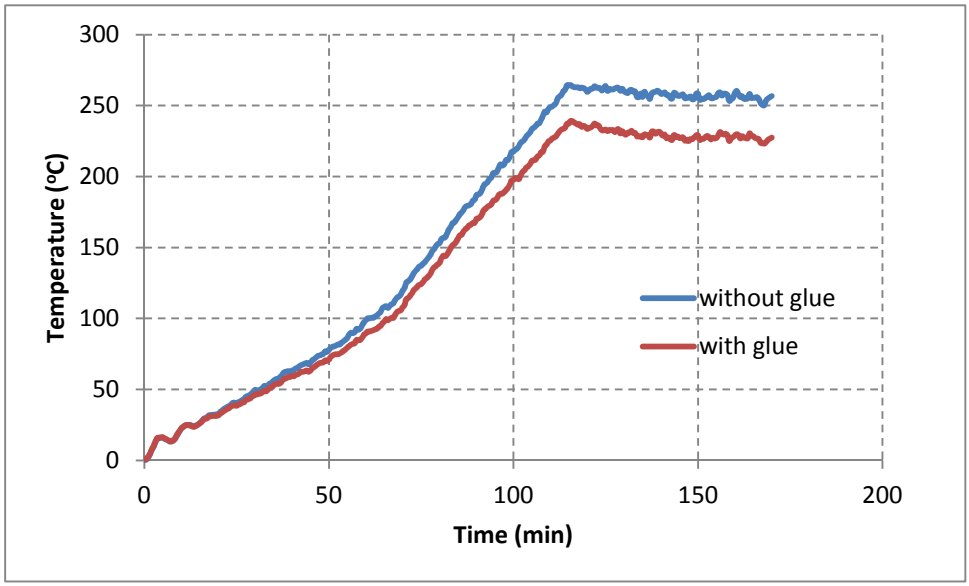

Figure 4-6 Comparison between the reading from unglued and glued thermocouples

4.5 RESULTS AND DISCUSSIONS

4.5.1 Slump of the Fresh Concrete

Figure 4-7 and Table 4-3 show the slump results for different glass sand and fibre contents. The slump results for 0.3% and 0.5% volume fraction of fibre show that for the same volume fraction there is an increase in the slump of the fresh concrete when increasing the glass sand content. The results obtained by Alhumoud et al [131] show that there is a slight increase in the slump with increase in the glass sand content, as shown in Figure 4-7. However, results from Park et al [5] show a contradictory effect of increasing the sand glass content on the slump of the fresh concrete. The variations in the results may be due to the effect of the particle shape and texture and also the fineness modulus of the glass sand used. The sharper the edges, harsher texture and larger particle size results in more cohesion between the cement paste and the aggregate which leads to a decrease in the flowability of the fresh concrete and vice versa.

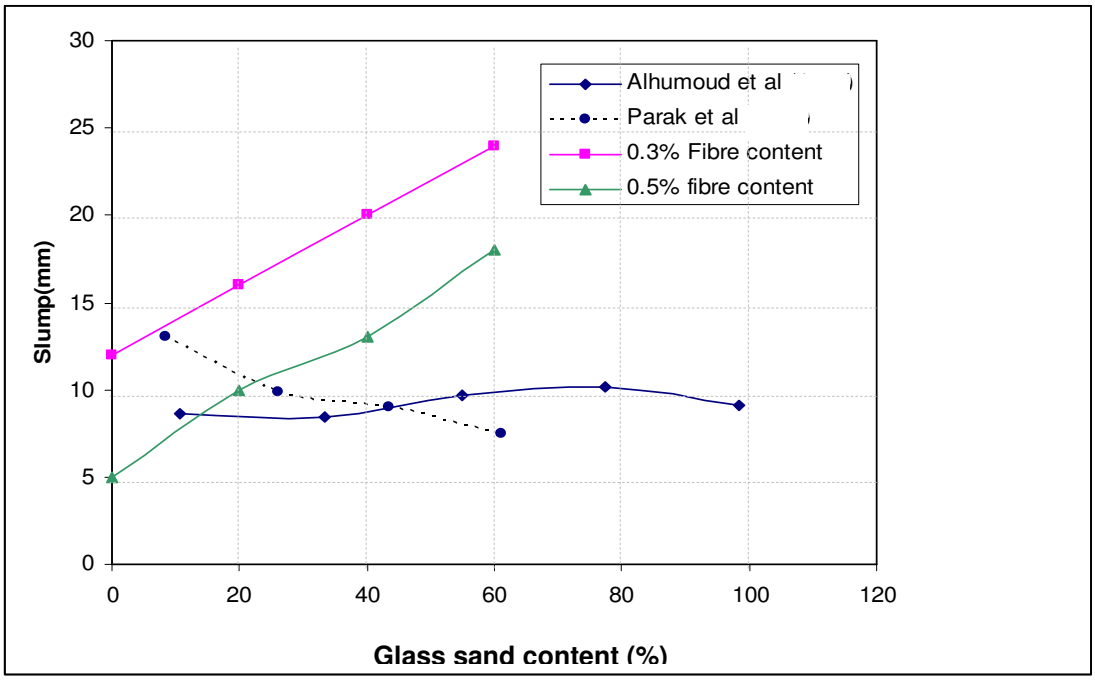

Figure 4-7 Comparison of the slump test results for the author's study with the previous studies

Increasing the percentage volume of fibres leads to a decrease in the slump, as expected. The reduction in the slump when 0.5% basalt fibre is added for different glass content is between 25%-59% compared with 0.3% basalt fibre for the same mix. This is mainly due to the fact that fibres hinder the flowability of fresh concrete and this results in a decrease in workability.

Table 4-3 Slump and unit weight results

Specimen mark.	Slump (mm)	Unit weight (kg/m^3)
G0F0	C*	2418
G0F1	C	2415
G0F3	12	2412
G0F5	5	2410
G20F0	C	2415
G20F1	C	2412
G20F3	16	2410
G20F5	10	2400
G40F0	C	2405
G40F1	C	2386
G40F3	20	2395
G40F5	13	2380
G60F0	C	2373
G60F1	C	2400
G60F3	24	2392
G60F5	18	2380

* C: Collapse

4.5.2 Unit Weight Results

Table 4-3 shows that there is a slight decrease in the unit weight when the glass sand content increases due to the glass sand density which is lower than that of natural sand. This is similar to the results obtained by Ismail and Al-Hashmi and Kou and Poon [132, 133] (Figure 4-8). The differences in the unit weight values between the author's study and the previous studies are due to the differences in the particle size of the glass sand aggregate.

The unit weight is not sensitive to increasing the volume percentage of basalt fibre (Table 4-3) as its content is low in all mixes (equal or less than 0.5% by total volume).

According to reference [134], many codes define lightweight concrete as that of dry density less than 2000 Kg/m^3, while the dry density range for structural lightweight concrete is from 1800 to 2200 Kg/m^3. Based on this definition, this type of concrete is classified as a normal weight concrete.

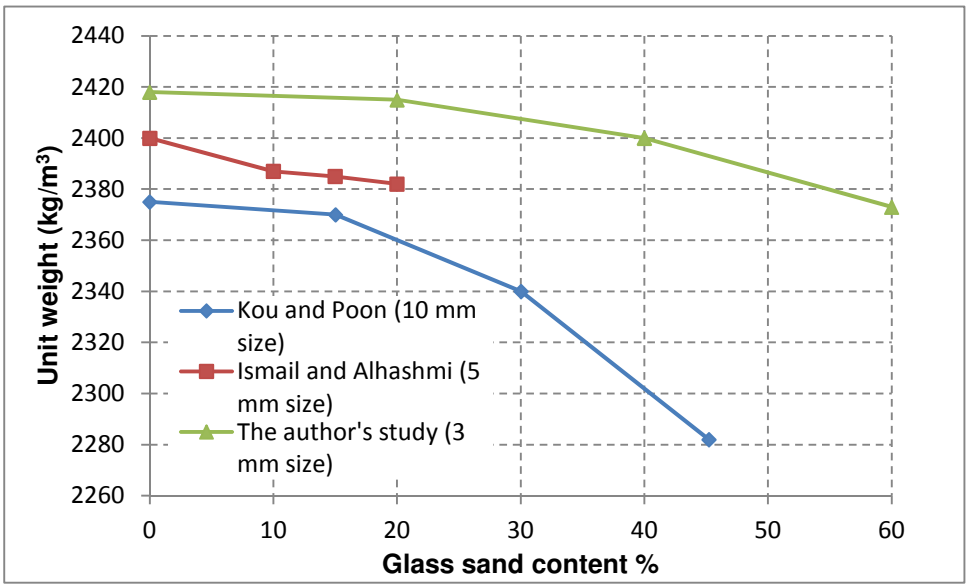

Figure 4-8 Comparison of the unit weight test results for the author's study with the previous studies

4.5.3 Strength of Concrete

A statistical analysis (ANOVA) using the null hypothesis at α equals to 0.05 (i.e., the confidence interval is 95%) was carried out to investigate the variance of the data for each mix. This gives a measure of how the data distributes itself about the mean, and the difference between mixes. The individual data and ANOVA results are shown in Appendix-B and summarize in (Table 4-4). The null hypothesis assumes that there is no difference between the test data (not significant), whereas the alternative hypothesis assumes that there is a difference between them.

Table 4-4 Summary of ANOVA results

Description	ANOVA result
Splitting tensile strength	
0% glass / variation in fibre content	A*
20% glass / variation in fibre content	A
40% glass / variation in fibre content	A
60% glass / variation in fibre content	A
0% fibre/ variation in glass content	R**
Compressive tensile strength (7days)	
0% glass / variation in fibre content	R
20% glass / variation in fibre content	R
40% glass / variation in fibre content	R
60% glass / variation in fibre content	R
0% fibre/ variation in glass content	A
Compressive tensile strength (28days)	
0% glass / variation in fibre content	R
20% glass / variation in fibre content	R
40% glass / variation in fibre content	R
60% glass / variation in fibre content	R
0% fibre/ variation in glass content	R
Compressive tensile strength (90days)	
0% glass / variation in fibre content	R
20% glass / variation in fibre content	R
40% glass / variation in fibre content	R
60% glass / variation in fibre content	R
0% fibre/ variation in glass content	R

*A Accept the null hypothesis

**R Reject the null hypothesis

The variances in tensile strength results for three specimens are small which means we can adopt the mean for each mix as a result for this test. With variation of glass content the null hypothesis is rejected which means that there is a difference between the means while the variation in basalt fibre content leads to accept the null hypothesis (the means are approximately equal).

The statistical analysis for the compressive strength results show that both glass sand and basalt fibre variations lead to reject the null hypothesis, with different curing time, except for 7 days which shows that there is no difference between the means with varying the glass content.

Figure 4-9 (A&B) shows the results of the splitting tensile strength tests (with the standard deviation (SD) for each mix). Based on the statistical analysis stated earlier, there is a 15% enhancement in the splitting tensile strength of concrete when 20% glass was used. Above 20% glass there was a slight reduction (22%) when 60% glass was used. Tensile strength results obtained by Park et al [5] show the same trend with glass percentages start above the optimum percentage of glass in the author's study which is 20%, as shown in Figure 4-9 (A). The enhancement in the splitting tensile strength of concrete when 20% glass was used may be attributed the positive effect of the pozzolanic reactivity of the glass, on the bond properties, more than the negative effect of the ARS. Topcu and Canbaz's experimental work results showed that the expansion due to ARS slow down with deceasing the glass content [98].

Adding basalt fibre to the mixtures remedies this reduction (Figure 4-9 (B)) and results in no significant differences between the control mix and the mixes with glass and basalt fibre as explained in the statistical analysis.

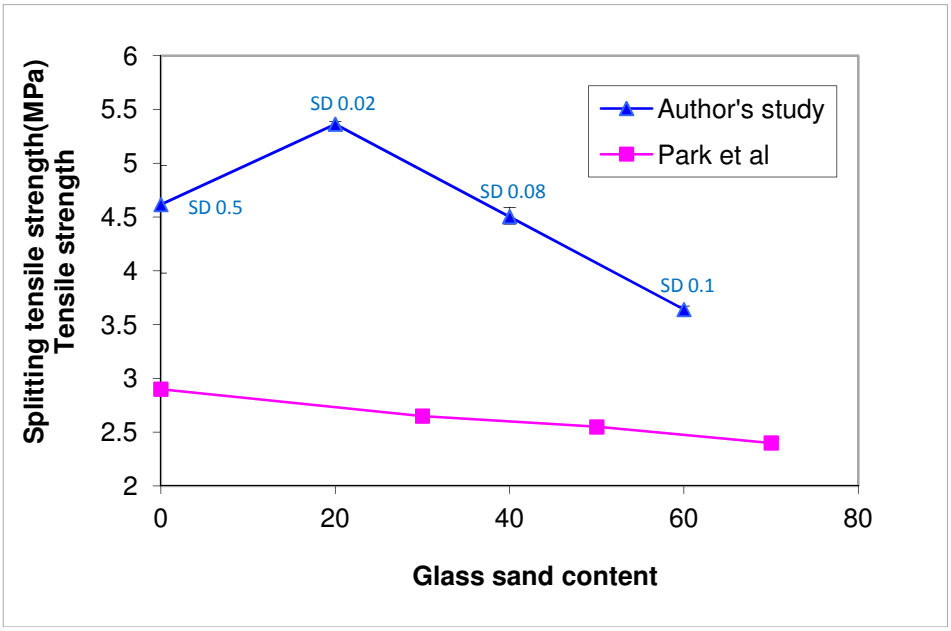

A) Different glass sand

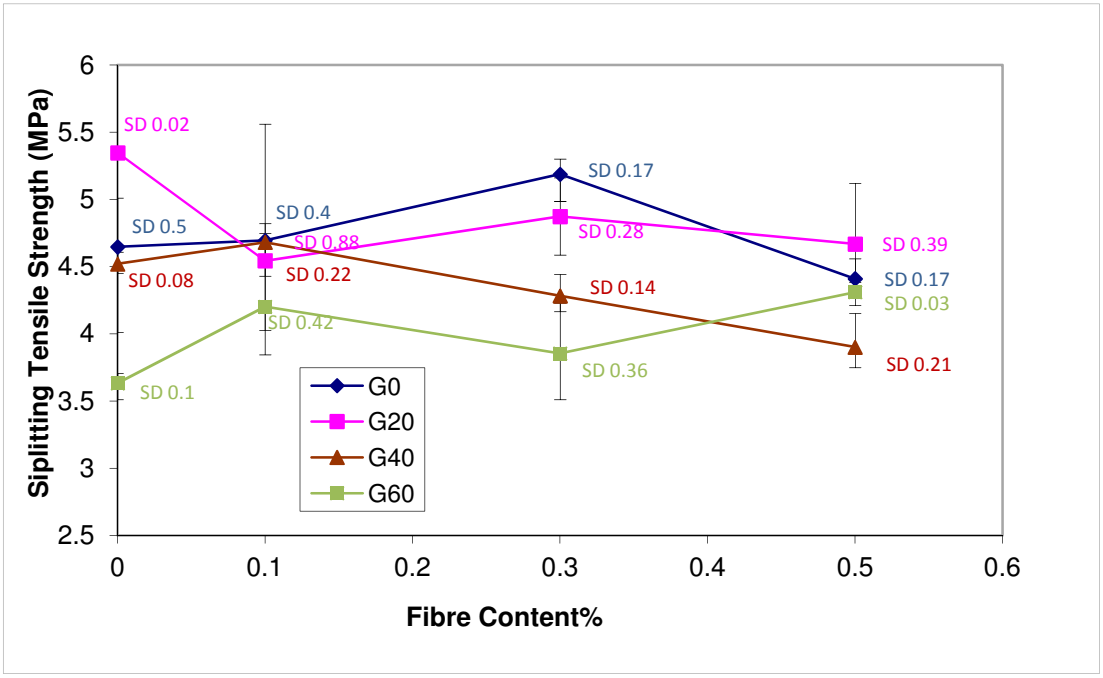

B) Basalt fibre contents

Figure 4-9 Splitting tensile strength of concrete

Figure 4-10 shows the effect of the glass content on the compressive strength of concrete.

The statistical analysis results have shown that there is no significant difference between the compressive strength results for mixes with glass aggregate only with 7 days curing while there is a slight reduction in it with increasing the percentage of glass sand above 20% in 28 and 90 days (up to 6.6%). Ismail and Al-Hashimi [132] results also showed that the optimum content is 20% glass and there was a 4.23% enhancement in the compressive strength at 28 days. This may be attributed to the advantage of the pozzolanic effect of the low percentages glass sand, which becomes significant at a 28 days age, more than the disadvantage of the alkali silica reaction caused by this type of sand.

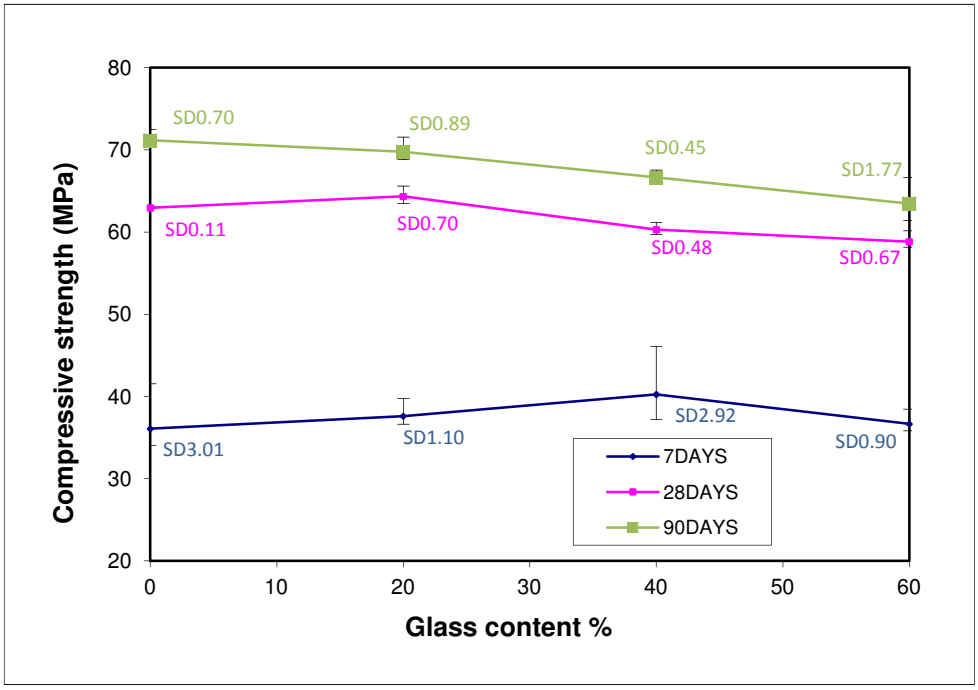

Figure 4-10 Compressive strength of concrete with different glass content

Using basalt fibre leads to an enhancement in the compressive strength of concrete for all mixes (Figure 4-11). Dias and Thaumaturgo's [19] results have shown a 25% and 3.8% decrease in compressive strength when 1% and 0.5% of basalt fibre were used respectively. However, the range of the fibre contents in their study is higher than the author's study. From Figure 4-11 for concrete without glass the strength increases with increase in the fibre content until 0.3% then there is a reduction of 12% when 0.5% fibre was used. The higher the percentage of fibre, the higher the absorption of water and the lower water available for cement hydration. It was found that basalt fibre absorbed CaO from $Ca(OH)_2$ produced by the hydrating Portland cement [135] which means less CaO available for metakaolin to produce materials that have cementitious properties. This may explain the higher reduction in the author's study result when 0.5% was used compared with Dias and Thaumaturgo results. However, this is a benefit when a higher percentage of glass sand is used to add resistance against the ASR as this reaction will not occur without the availability of this ion which explains the enhancement in the compressive strength of the high percentage of glass sand when 0.5% fibre content was used.

The aggregate – cement interface zone plays a major role in the compressive and tensile strengths results obtained in this study. The surface texture of glass sand and also the chemical reaction between the glass and cement may cause a weakness in the bond between the sand and the cement paste which leads to initiation of cracks at this zone more than that in natural aggregate concrete. Tasong et al [136] in their experimental study on the influence of aggregate physical properties on the aggregate-cement paste interface concluded that interfacial bond strength increases with increasing surface area available for bonding (i.e. increasing roughness). The smooth surface of the glass leads to weaker bonding with the cement paste. Adding basalt fibre improves the tensile and compressive strength of glass sand concrete. This is mainly due to the effectiveness of fibre in suppressing the growth of the cracks in the concrete structure which suppresses the reduction in concrete strength (i.e., the fibre enables stress to be transferred across cracked sections allowing concrete to retain some post-crack strength and to

withstand deformations much greater than concrete without fibre). Dias and Thaumaturgo [19] have shown in their experimental results that increasing basalt fibre results in significant improvement in fracture toughness. After the ultimate load was reached the specimens with fibre still deformed and the rupture was more ductile.

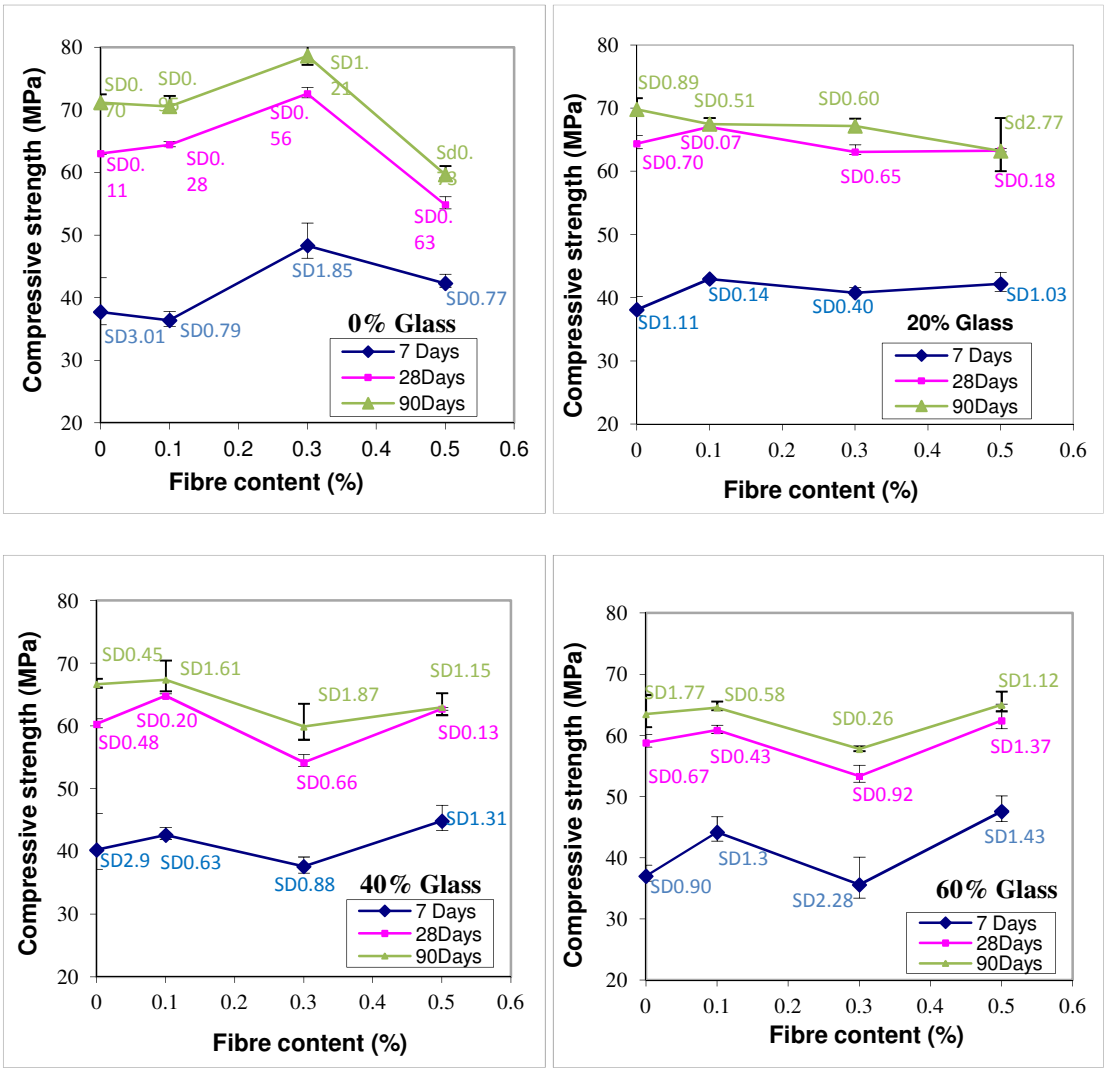

Figure 4-11 Compressive strength of concrete with different glass and basalt fibre content

4.5.4 Heat Transfer

Heat transfer tests for different glass and basalt fibre content results are shown in Figure 4-12 to

Figure 4-14. All tests were conducted at the same condition and using the same kiln, as mentioned previously in Section 4.4.4, to ensure the same thermal exposure. The cyclic behaviour of the temperature profile in these Figures is due to the heating procedure inside the kiln (heating up period followed by rest and so on).

it can be seen that when glass sand and basalt fibre content increases there is a slight decrease in the amount of heat conducted through the thickness of concrete specimens (i.e. decrease in the thermal conductivity) at temperatures below 100^{o}C. The reduction then becomes clearer with high percentage glass sand and basalt fibre and at all temperature levels. Using basalt fibre decreases the thermal conductivity of glass sand concrete significantly, as shown in

Figure 4-14. Sim et al. [17] concluded that the volumetric stability of basalt fibres confirms higher resistance against high temperature exposure. This due to the nature of the basalt rocks, which nucleates at high temperature. Li [137] investigated experimentally the thermal resistance of basalt filament yarns. The results showed that the resistance is constant up to 350^{o}C and is followed by a small decrease until 500^{o}C. At 700^{o}C, fracture of basalt filament occurred and almost all basalt filament were broken when the temperature rised to 800^{o}C.

Limited research has been carried out on the thermal properties of using waste glass sand and short basalt fibre in concrete. Petrella et al. [6] studied the effect of using glass aggregate as a fine and coarse aggregate, glass sand with different types of coarse aggregate and as a coarse aggregate with different types of sand. They found that when using glass as a sand with natural gravel, the thermal conductivity (*K*) was equal to 0.843 W/m k for normal temperature (20-100^{o}C) which is lower than the value for natural sand concrete stated in the literature (K ranges between 1.6 – 2.7 W/m K) [33].

The difference is mainly due to the high porosity and thermal stability of the recycled waste glass compared to the natural aggregate [6].

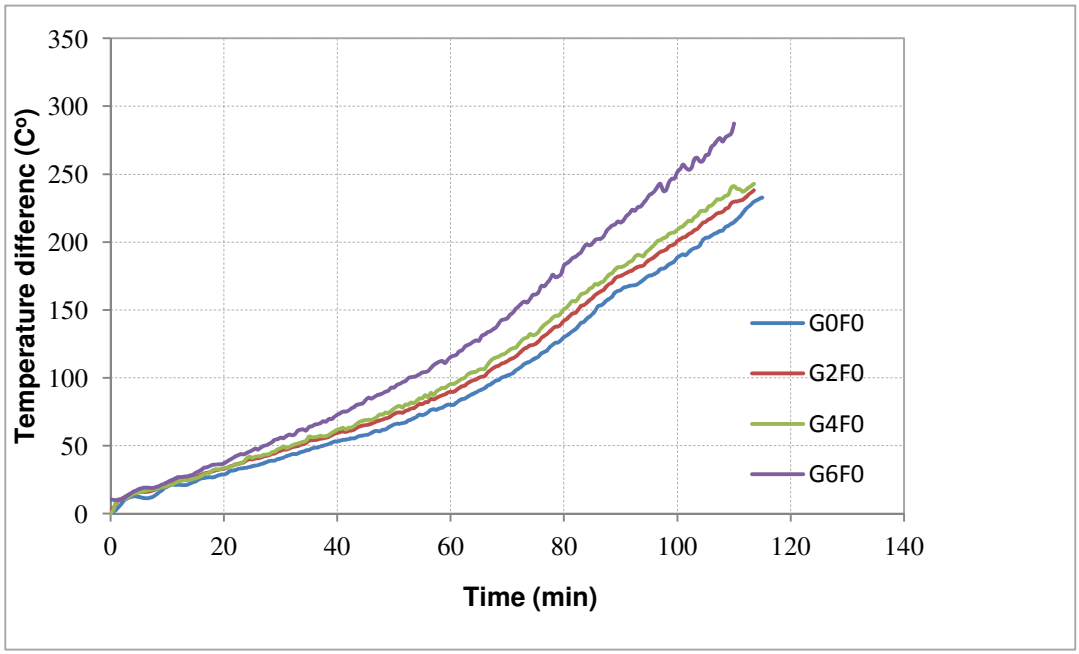

Figure 4-12 Heat transfer through concrete with different glass content

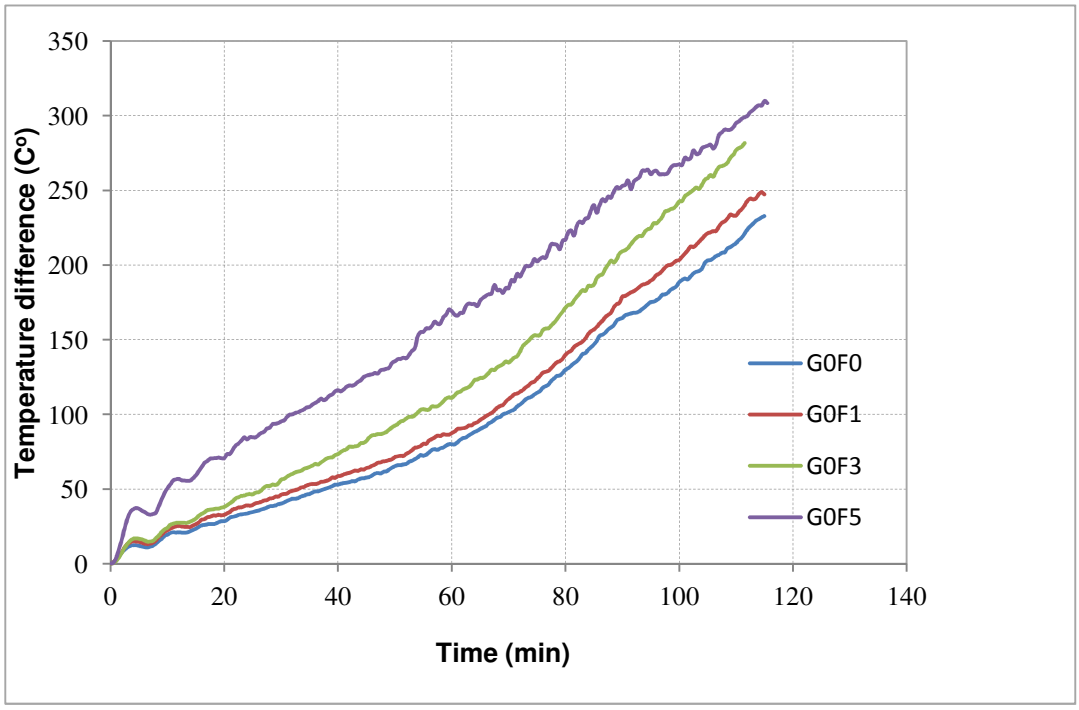

Figure 4-13 Heat transfer through concrete with different fibre content

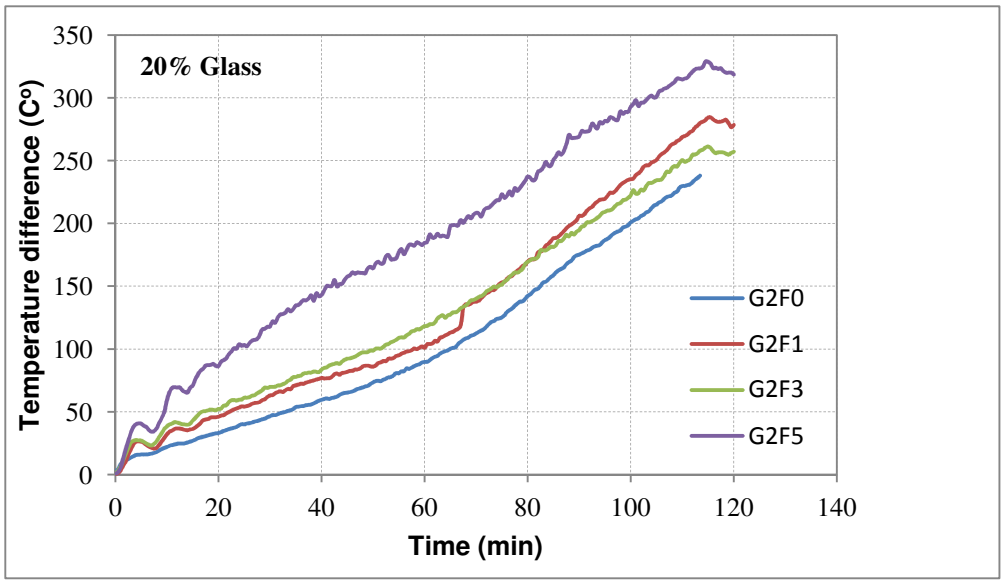

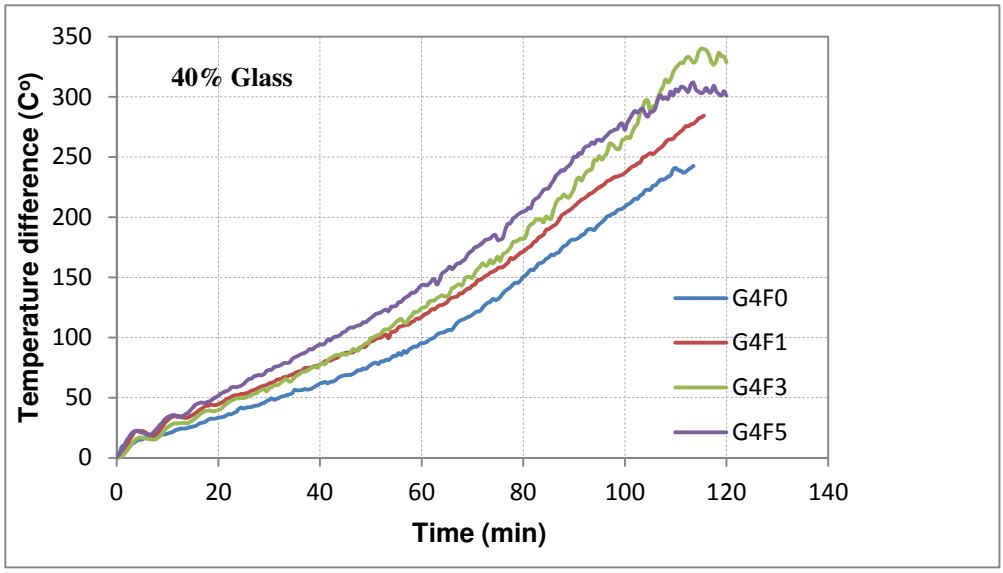

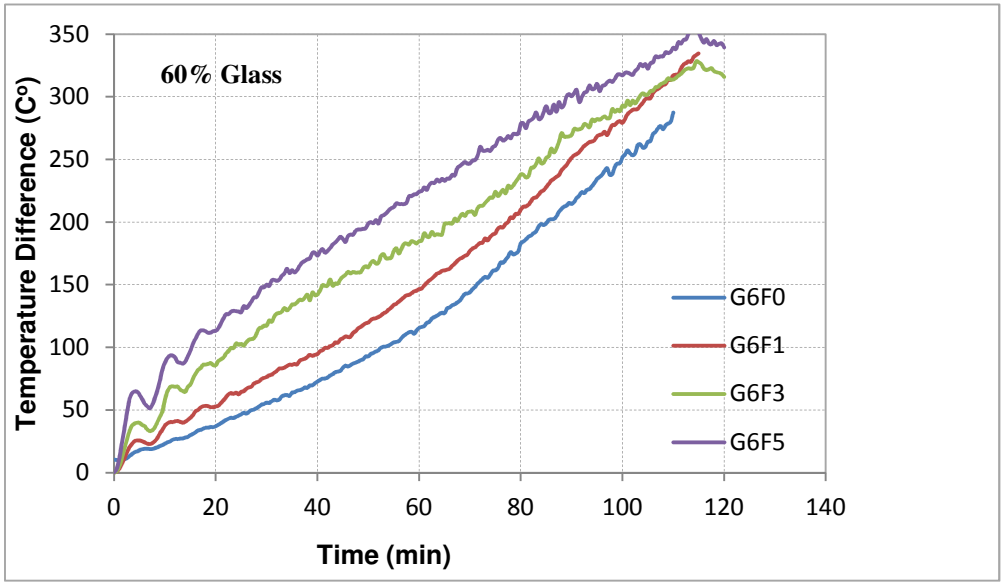

Figure 4-14 Heat transfer through concrete with different glass and fibre content

4.5.5 Prediction of the Thermal Conductivity

The heat transfer test gives an indication about the benefit of using glass sand and basalt fibre on the thermal properties of concrete. However, the values for these properties are needed to compare this type with the other types of concrete. For this purpose, the finite element programme ABAQUS was adopted to predict an approximate value for the thermal conductivity (TC) together with the heat transfer test. The geometry of the specimen for the heat transfer test was modelled. 20-node quadratic heat transfer brick elements (DC3D20) were used. The boundary condition for this model was the temperature profile for the exposed side of the specimen taken from the heat transfer test. The density for each mix was taken from the unit weight test results. The data of the specific heat (SH) was used according to BSEN1992-1-2 [29]. The moisture content of the specimens recorded was between 3 to 5%.

By ‘’trial and error’’, following the heat transfer test results indication as a guide, the values of TC that give the best curve for the unexposed surface temperature profile were recorded for a different temperature and for nearest 0.05 W/m.K (Figure 4-17). The values show that using basalt fibre with glass sand concrete has a benefit of decreasing the thermal conductivity.

Figure 4-16 shows the differences in the results for mix G0F0 when the values of the thermal conductivity and the specific heat changed above or below the recorded values by 0.1 and 0.2 W/m.K, 100 J/kg.^{o}C respectively. Although this method did not give accurate values for the thermal conductivity due to different reasons, such as error possibility of the test and assumed specific heat values, this method can be adopted to compare the value of the thermal conductivity of this type of concrete with other concrete instead of heat transfer test results.

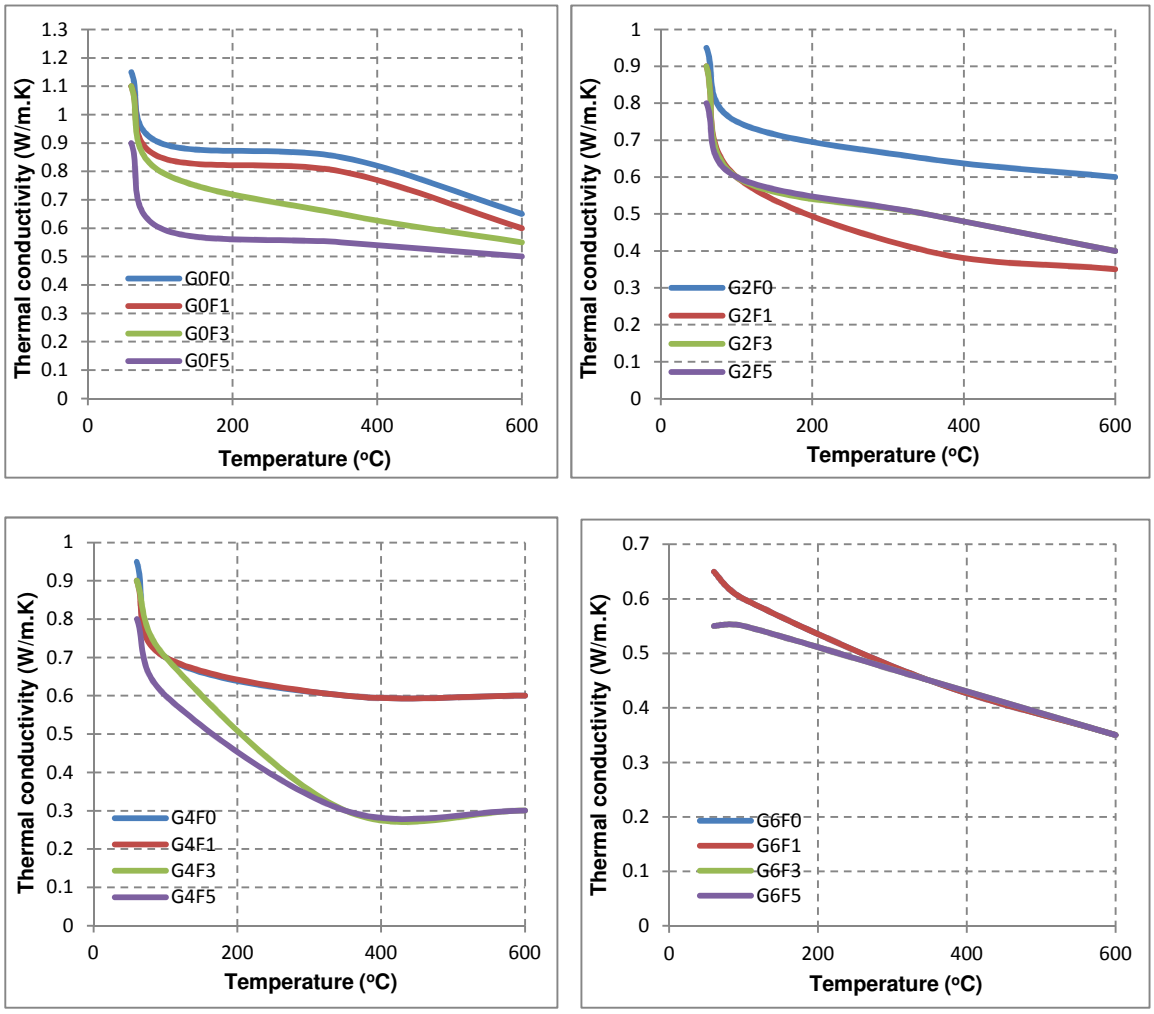

Figure 4-15 Thermal conductivity vs. temperature (ABAQUS)

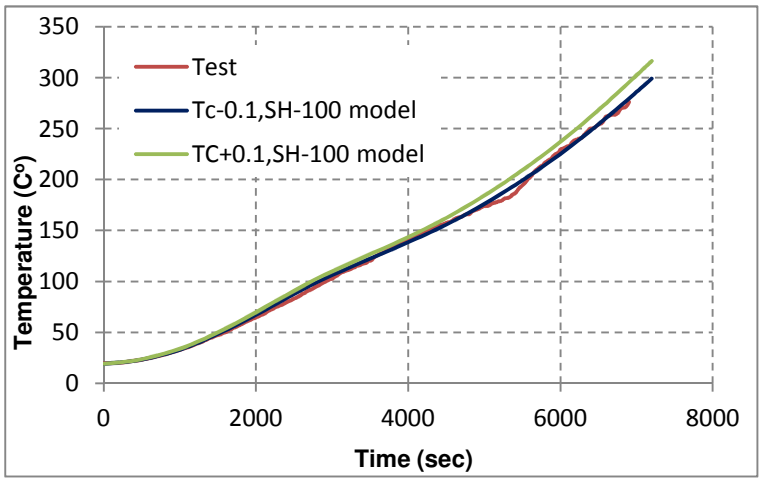

a) Increasing and decreasing TC with increasing and decreasing SH

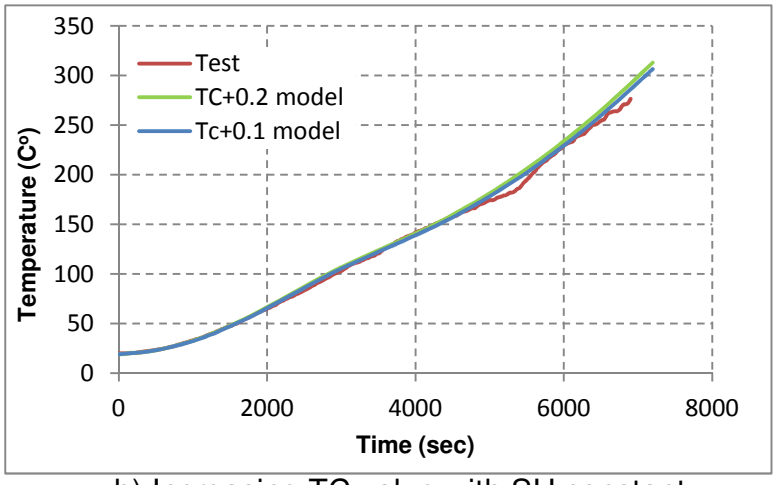

b) Increasing TC value with SH constant

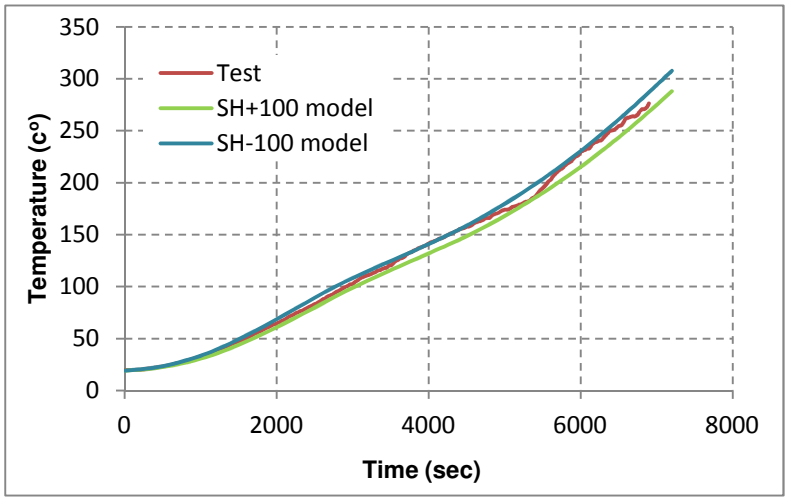

c) Increasing and decreasing SH value with TC constant

Figure 4-16 Prediction of TC and SH different cases

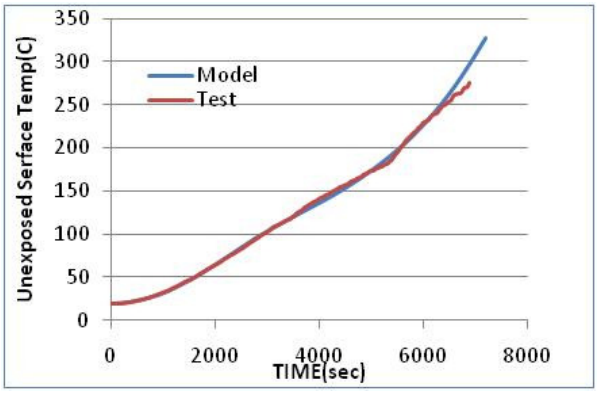

G0F0

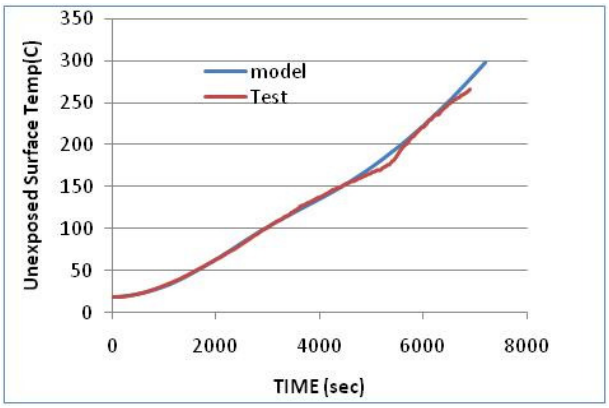

G0F1

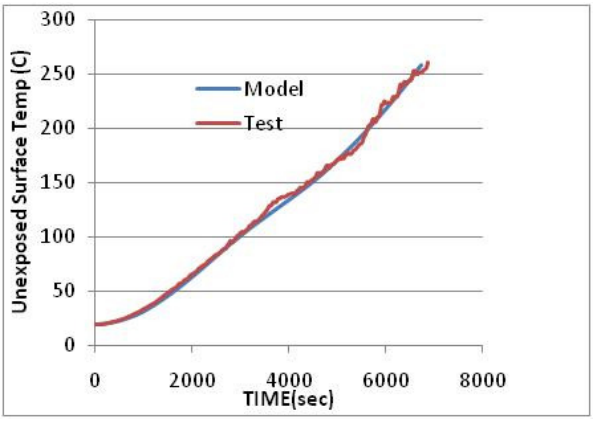

G0F3

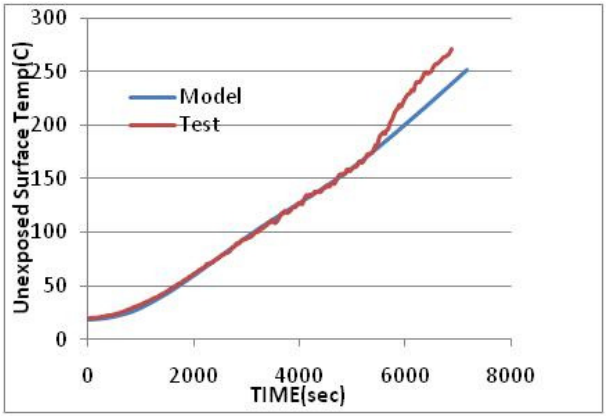

G0F5

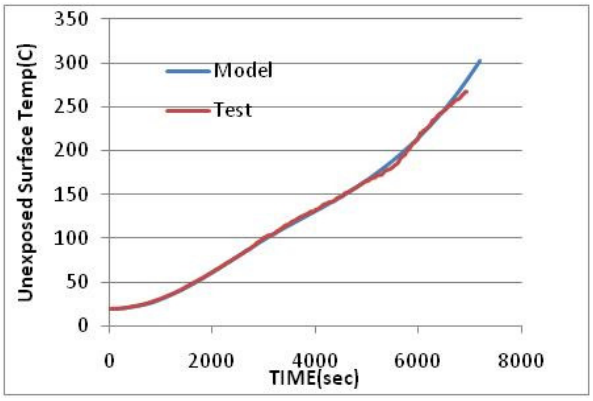

G2F0

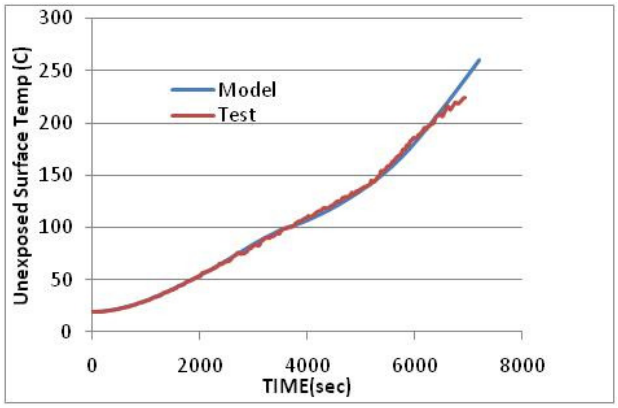

G2F1

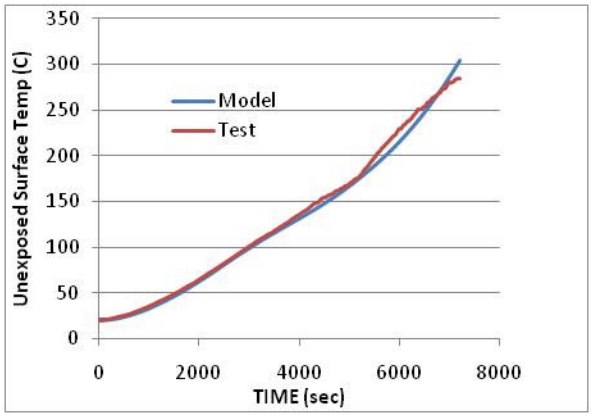

G2F3

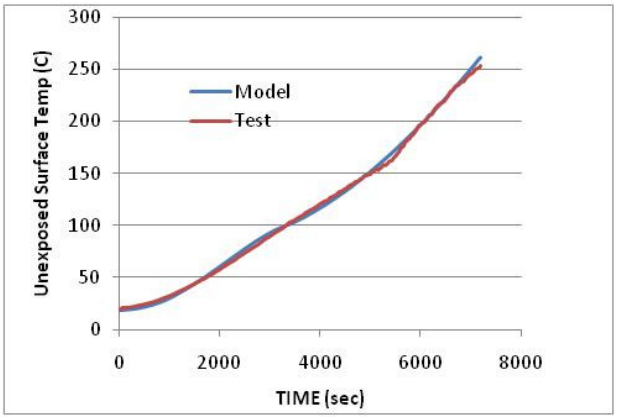

G2F5

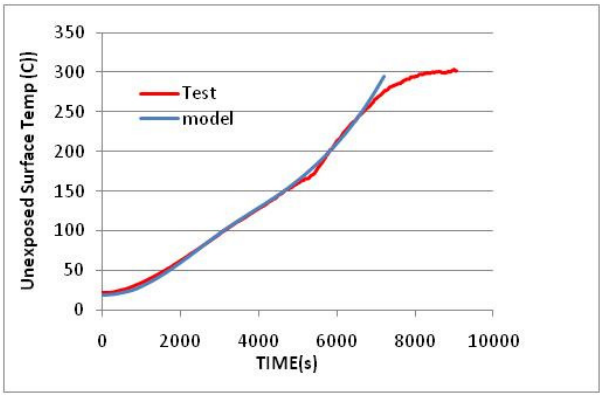

G4F0

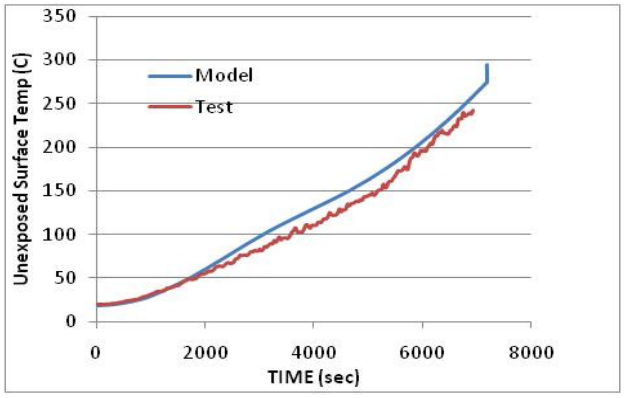

G4F1

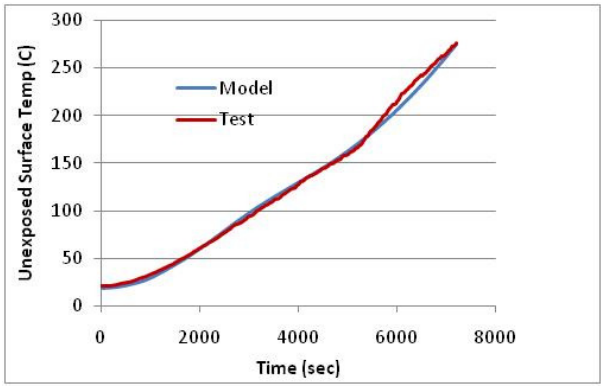

G4F3

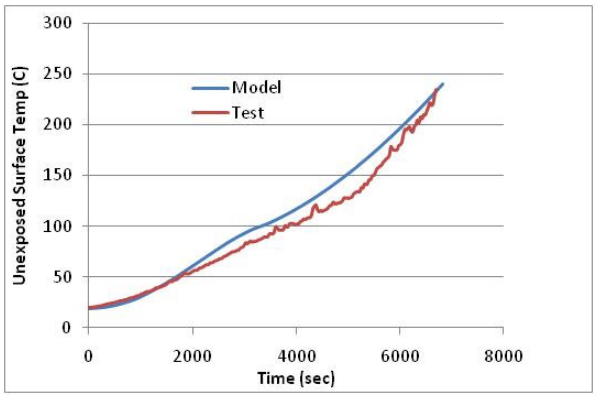

G4F5

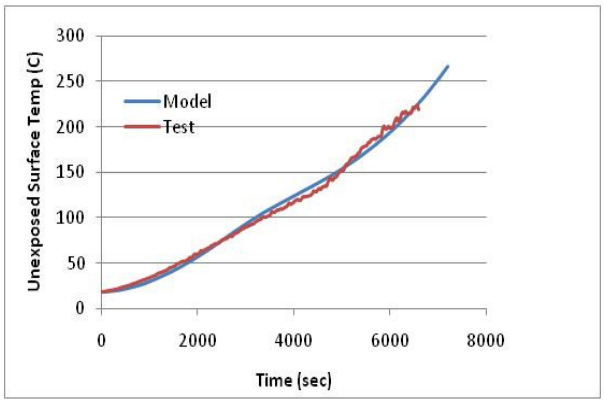

G6F0

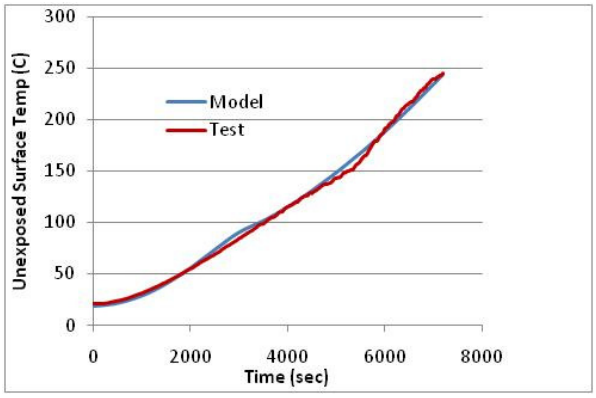

G6F1

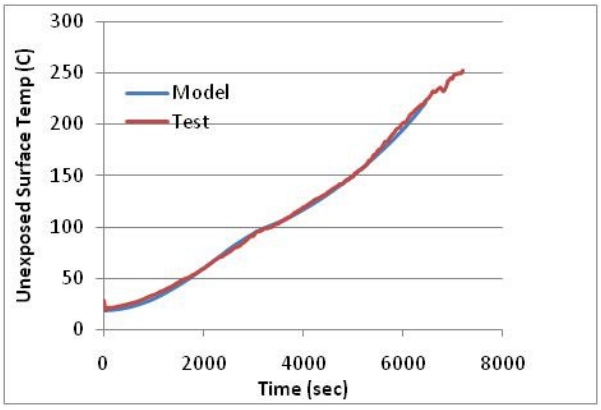

G6F3

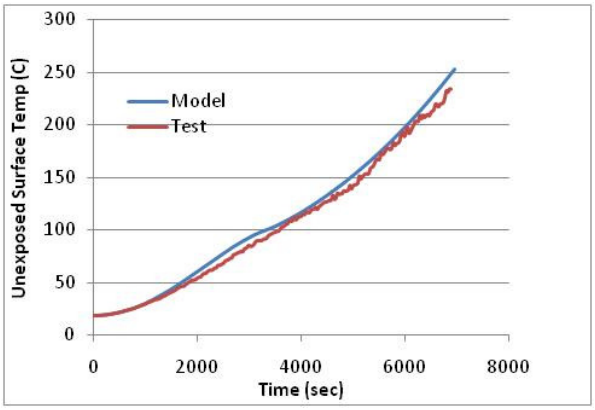

G6F5

Figure 4-17 Prediction of TC (best curve value) for different mixes

4.6 COMPARISION WITH OTHER TYPES OF CONCRETE

As stated previously the aim of this research is to produce an insulating concrete with good mechanical properties using environmentally friendly materials. Some research produced good insulating concrete with low strength as shown in Table 4-5 which shows the comparison between the new concrete with normal concrete and recycled aggregate concrete. It can be seen that sand rubber concrete has a lower thermal conductivity; however, its strength is not sufficient for the structural members. Replacing the natural sand with glass sand without using pozzolana reduces the compressive strength due to ASR. Using pozzolana in concrete reduces the value of the thermal conductivity and increase the compressive strength. Glass sand basalt fibre reinforced concrete gives good strength and low thermal conductivity.

Table 4-5 Comparison between the new concrete with normal concrete and recycled aggregate concrete

Material	Thermal conductivity W/m K 20-100C^{o}	28days compressive strength (MPa)	Reference
Normal concrete +pozzolana	1.057-1.230	51-59	Demirboga [69]
Glass sand+ pozzolana	0.95-0.60	60-64	Author's study
Basalt fibre with pozzolana	1.1-0.6	54-72	Author's study
Glass sand+basalt fibre +pozzolana	0.9-0.55	53-67	Author's study
Glass sand	0.843	20	Petrella et al. [6]
Sand rubber	0.443-0.296	5.4-19.96	Sukontasukkul [78]& Sukontasukkul et al [138]

4.7 SUMMARY

Experimental work was carried out to develop information about the mechanical and thermal properties of basalt fibre reinforced glass aggregate concrete. Recycled waste mixed colour glass (size 0.5-3mm) was used as a partial replacement (20%, 40%, and 60% by weight) for the natural fine aggregates. The volume fractions of basalt fibre (0.1, 0.3, and 0.5% by total mix volume) were used. The effect of the glass content and basalt fibre on the compressive and splitting tensile strength as well as the heat transfer was investigated. The results showed that the optimum content is 20% glass and at 28 days, there was a 4.23% and 15% enhancement in the compressive strength and the splitting tensile strength respectively. Above 20% glass there was a slight reduction (6.6% and 22%) in the compressive strength and the splitting tensile strength when 60% glass was used. Using basalt fibre remedies this reduction and results in no significant differences between the control mix and the mixes with glass and basalt fibre.

A slight decrease in the amount of heat conducted through the thickness of concrete specimens was also observed at temperatures below 100^{o}C. The reduction then becomes clearer at temperature above 100^{o}C. With a high percentage of glass and basalt fibre there is a high reduction in heat transfer for all temperature levels.

ABAQUS with heat transfer tests were used to predict an approximate value for the thermal conductivity. Although this method cannot give accurate values due to different reasons, such as error possibility of the test and assumed specific heat values, this method can be adopted to compare the value of the thermal conductivity of this type of concrete with other concrete instead of heat transfer test results.

From the results obtained, it can be pointed out that concrete with sand glass aggregate in all percentages can give good results, compared with other type of concrete, regarding the mechanical and thermal properties. The use of basalt is recommended with this type of concrete to enhance its thermal and mechanical properties.

CHAPTER FIVE

5 SMALL-SCALE SLAB TESTS

5.1 GENERAL

In fire safety design for building, the structure must fulfil the three requirements; resistance to collapse (stability), prevent spread of the flame (integrity) and resistance to the transfer of excessive heat (insulation). In the event of a fire, the structure must perform at least to the level that maintaining the stability of the structure for as long as possible and provide safe escape and safe firefighting.

In this chapter, the suggested concrete was tested for its functionality, as a structural member, in fire and compared it with normal concrete. The comparison is based on the enhancement, due to membrane action, in the load bearing capacity as well as the resistance to the heat transfer. For this reason, experimental work was conducted for small-scale slabs, having different percentages of basalt fibre and glass sand, at ambient temperature and in fire.

5.2 TEST CONFIGRATION

5.2.1 General

Small-scale slab tests, similar to previous research [127], have been conducted. The slabs were cast, stored, and tested in the concrete laboratory in the University of Manchester between February and September 2010.

The slab mixes were chosen depending on the results of the first part of the experimental work carried out in this study with different percentages of glass sand and different volume fractions of basalt fibre. This section describes the dimensions of the specimens, test rig details, loading conditions, mix proportions and reinforcement details.

5.2.2 Preparing the Specimens

Twelve two-way reinforced concrete slabs were constructed by using a wooden mould. Half of the specimens were stored for the ambient temperature test and the other specimens were stored for the fire test. The slabs measured 1.2m wide by 1.2m long with 35 mm target thickness (Figure 5-1). The thickness of each slab was measured and the recorded value was the average of three positions (in the middle and at 30cm from the right and the left edges) in each side of the slab.

Two of the thermocouples (type k) were placed near the centre of the slab (bottom surface and reinforcement) before casting, the third one was inserted in the small hole (3 mm height approximately) on the centre of the top surface of the slab prior to the test and glued by using special thermal glue similar to that used in the heat transfer test described in Section (4.4.4)

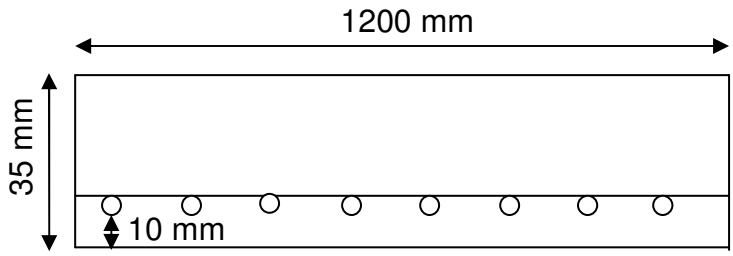

Figure 5-1 Slab dimensions

The concrete cover was 10 mm from the bottom surface of the slab, this was achieved by placing a small plastic rings, with 10mm height, under reinforcement mesh.

The slabs were cast between February and July 2010 and stored at laboratory temperature until the testing date.

5.2.3 The Test Rig

All the slabs were simply supported on all four edges by steel angles that provided line support at a distance of 50 mm from each of the slab edges (Figure 5-2). The slabs were free to move horizontally and the edges of the

slabs were free to rotate upwards along the perimeter supports. The corners of the slabs were lightly clamped with rollers between the clamp and the slab to allow free horizontal movement but restrain the vertical movement in the corners. The span of the slab assumed to be the clear span as the slabs were supported off the edge of the steel angles due to the large displacement.

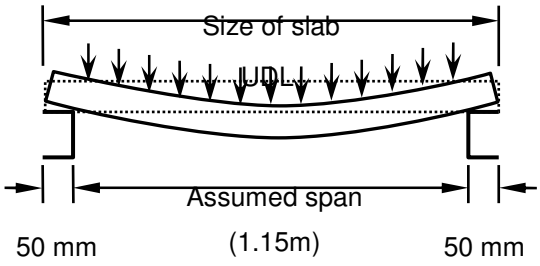

Figure 5-2 Proposed span of the slab

5.2.3.1 Ambient Temperature Test

For the ambient temperature test the slab was sat on the steel frame as shown in Figure 5-3. The frame was supported by four load cells to monitor the total vertical load applied on the slab. The tested slab was subjected to uniformly distributed vertical load over the slab which was provided by using an airbag. The bag was connected to a compressor and the air was pumped slowly during the test until the slab collapsed. The bag was embedded in a wooden frame which represents the reaction frame. The central vertical deflection was monitored using a draw wire displacement transducer placed at the centre of the bottom surface of the slab (Figure 5-4).

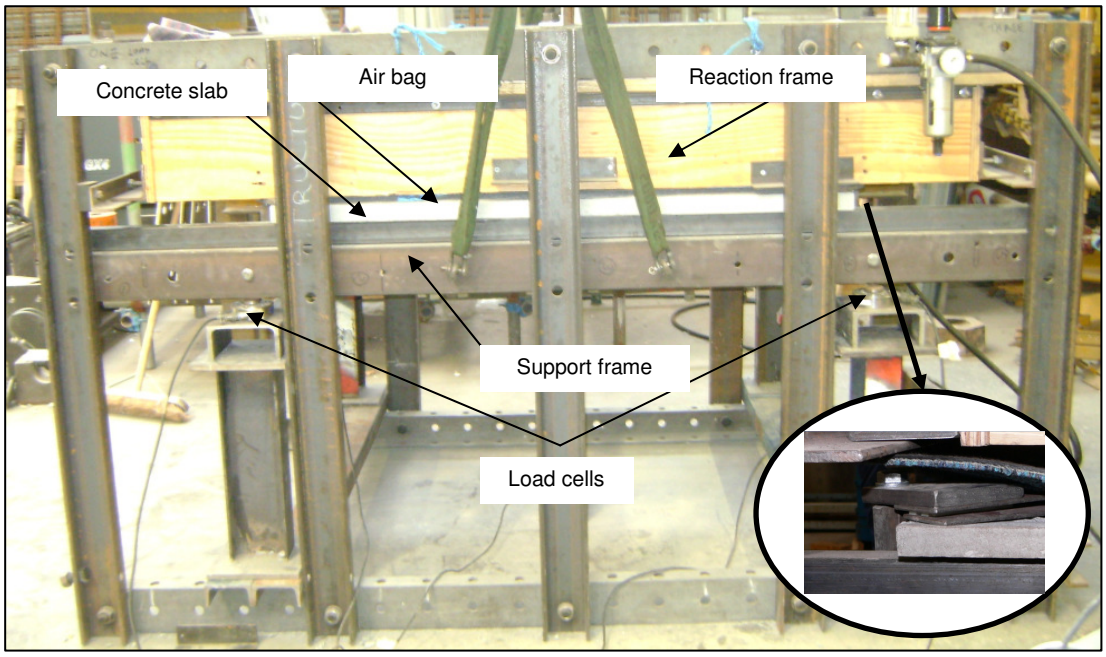

Figure 5-3 Small-scale slab test at ambient temperature

Figure 5-4 Wire displacement transducer

5.2.3.2 Fire Test

An electric kiln was used to carry out the fire test providing a heating rate of 300^{o}C/hr (Figure 5-5). The same slab geometry as the ambient temperature test and similar support conditions were used. All the fire tests were carried out under a transient heating state, with predefined working load uniformly applied on the top surface of the tested slab using dead weights (0.25 kN each weight) (Figure 5-6). However, due to the physical size of the slab's footprint and the weight's size, the use of this dead weight was quite restrictive (limited load can be applied due to limited space). The applied load was (8.41 kN/m^2) for the slabs and it remained constant during the test and the failure was due to heating. The temperatures of the kiln, top surface, bottom surface of the slab, and the reinforcement were recorded during the test using thermocouples (type K). The slab was insulated by using a ceramic blanket placed on the top of the slab in order to reduce the heating loss and allow the kiln and the slab to reach the required temperature (as it is difficult to raise the temperature in the kiln without this insulation). The central vertical deflection was monitored using a draw wire displacement transducer placed on the top of the slab (Figure 5-6).

Figure 5-5 The electric kiln used to carry out the fire test

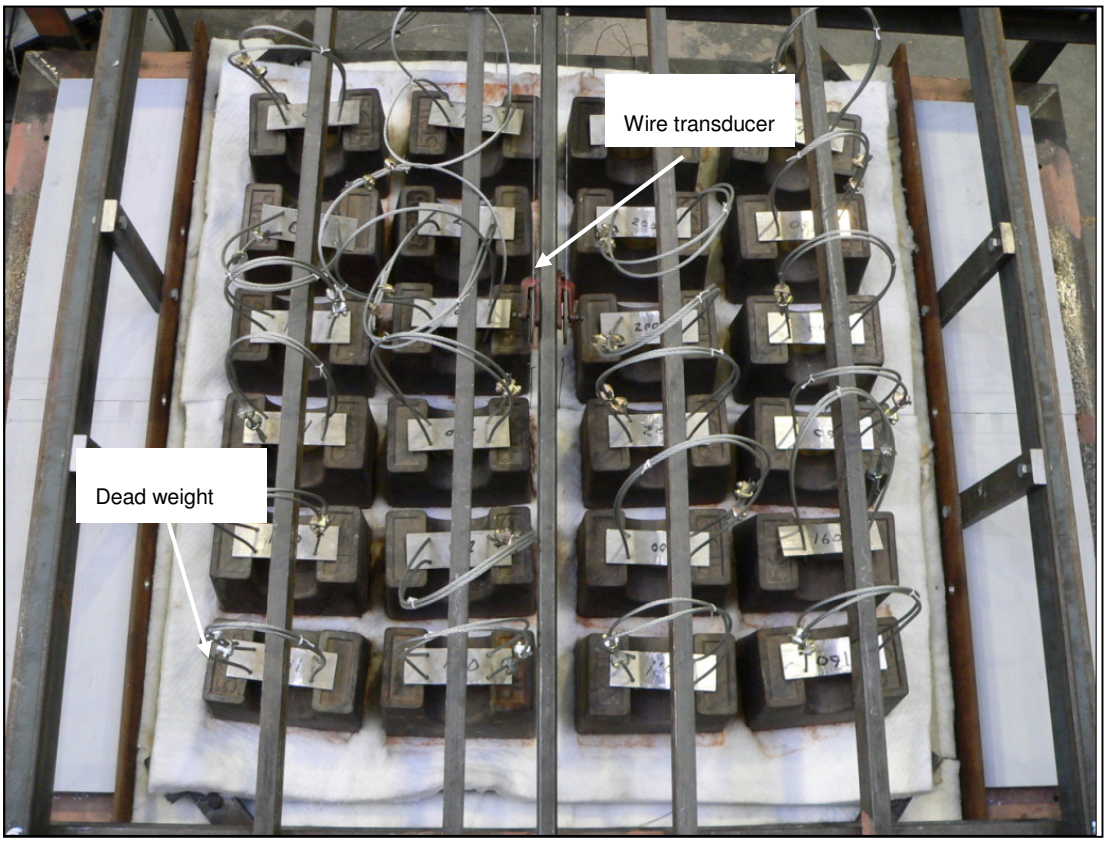

Figure 5-6 Predefined working load using the dead weights

5.2.4 Materials Used

5.2.4.1 Concrete

Concrete with different percentages of glass sand and basalt fibre were used. The mix proportions (1:1.5:2.1) cement: sand: gravel by weight of concrete were adopted to achieve compressive strength of 35 MPa. 6 mm maximum size granite aggregate (grano) was used in this part as a coarse aggregate (Figure 5-7). The other materials are similar to the materials used in the first part of the experimental work.

Figure 5-7. 6mm maximum size grano aggregate

The percentages of the glass sand and basalt fibre were chosen depending on the results of the first part of the experimental work of this study. The results showed that 20% glass sand gave higher compressive and tensile strength compared to the other percentages of glass while 40% and 60% gave better insulation at elevated temperature. 0.1% basalt fibre increased the strength for all mixes and there was an insulation enhancement compared with the plain concrete. According to these results the mixes shown in Table 5-1 were chosen to cast the slabs.

Table 5-1 Slab mix details

Slab	Glass sand %	Basalt fibre %
G0F1	0	0.1
G2F1	20	0.1
G2F3	20	0.3
G2F5	20	0.5
G4F1	40	0.1
G6F1	60	0.1

The compressive strength, modulus of elasticity, and Poisson's ratio were calculated from the stress – strain curve (presented in APPENDIX –C) obtained from the compressive strength test (cylinder specimens) with strain gauges used to monitor the strain laterally and vertically. The averages of the three specimens are shown in Table 5-2. The tests were conducted at the date of the slab tests (different curing time). The compressive strength and the moisture content tests were also conducted at the date of the slab test in fire.

Table 5-2 Properties of concrete for the selected mixes

Mix	Compressive strength (Ambient) (MPa)	Modulus of elasticity (GPa)	Possion's ratio	Compressive strength (Fire) (MPa)	Moisture content %
G0F1	44.42	24.8	0.21	44.3	4.6
G2F1	38.8	29.34	0.22	45.2	5.06
G2F3	44.32	32.11	0.20	38.6	3.7
G2F5	36.90	23.84	0.22	38.6	5.25
G4F1	43.7	34.38	0.21	45.3	3.35
G6F1	35.3	20.5	0.23	41.3	2.6

5.2.4.2 Reinforcement

Mild steel self colour welded smooth wire mesh 2.35 mm in diameter with 50 mm spacing between the bars was used as reinforcement for all the slabs. The properties in each direction of the mesh were determined from the tensile test carried out by the author. the strain – stress results obtained from this test for both short and long direction for three specimens (S1, S2, and S3) are presented in APPENDIX –C. The average of the three specimens was recorded in Table 5-3.

Table 5-3 Reinforcement properties

Direction	Modulus of elasticity (GPa)	Ultimate stress (MPa)	Strain at Max. Load %	Yield stress (MPa)
Long	214	776	2.56	688
Short	206	845	1.28	764

5.3 RESULTS AND DISCUSSION

In this section the results of the experimental work carried out in the laboratory are presented, discussed, and compared with the other experimental work that have been carried out by other researchers.

5.3.1 Ambient Test

Six slab tests at ambient temperature were conducted between May and June 2010. Figure 5-8 shows that the fracture of the reinforcement is the mode of failure for all the slabs and the fracture was along various yield lines, approximately in a diagonal pattern, which confirms the assumptions made by Kemp [139] who assumed that the yield mechanism is the simple diagonal pattern. The results obtained by Bailey and Toh [127] for the square slab reinforced by mild steel (approximately has the same properties), which has the same width and length as the slabs in the author's study with 35.9 mm in thickness, showed the same behaviour while there was two distinct modes of failure for the other slabs with thickness less than 35 mm. These modes comprise fracture of reinforcement along one span or crushing of concrete at the corners of the slabs. This probably depends on the reinforcement ratio, the higher ratio leads the slabs to fail by crushing of concrete rather than the fracture of reinforcement [127].

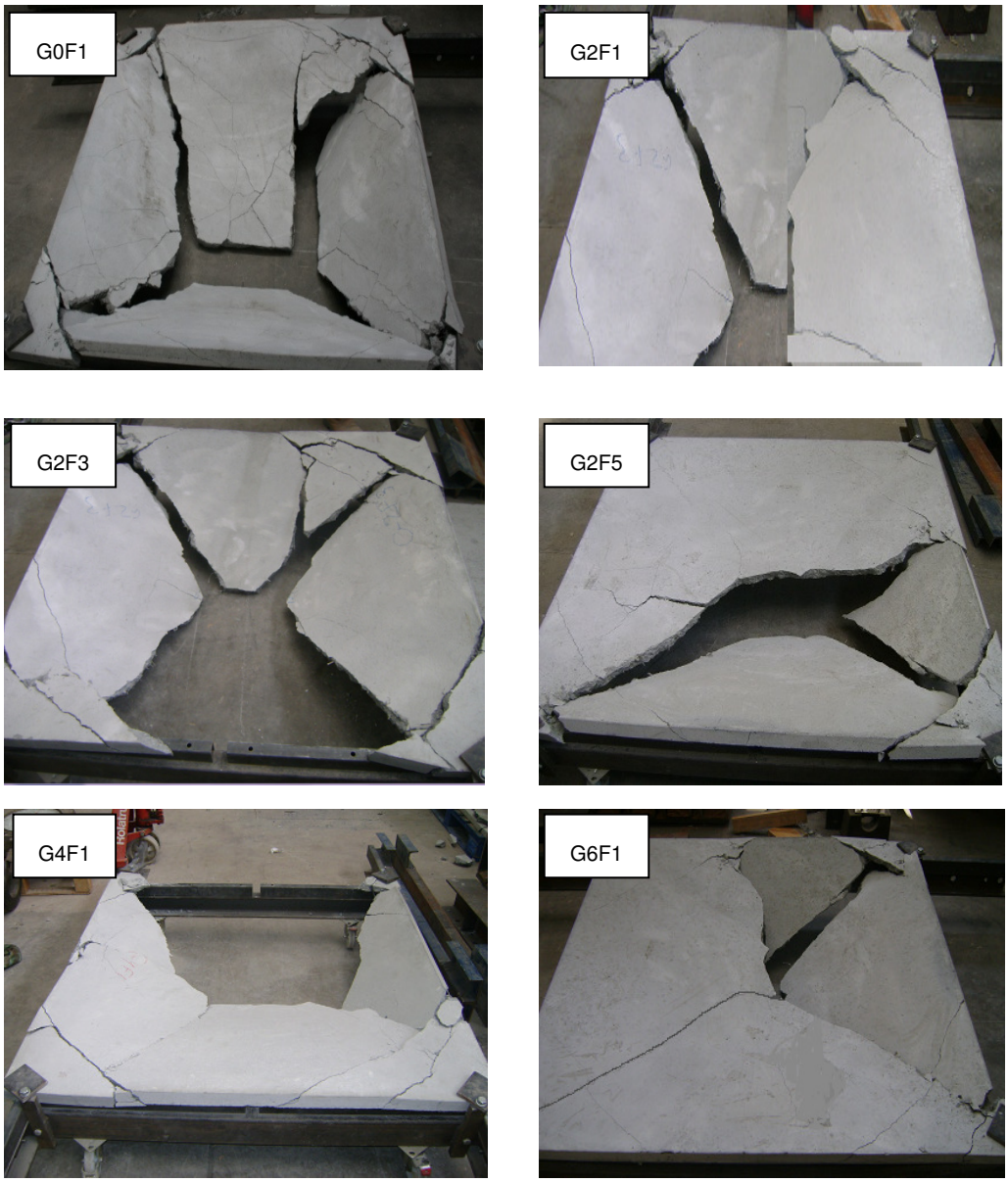

Figure 5-8 The mode of failure for the slabs tested at ambient temperature

Figure 5-9 shows the load – displacement relationship for the tested slabs with different percentages of glass sand and different volume fractions of basalt fibre.

The results are summarized in Table 5-4 and it also shows the comparison between the test load and the theoretical yield line load for each slab.

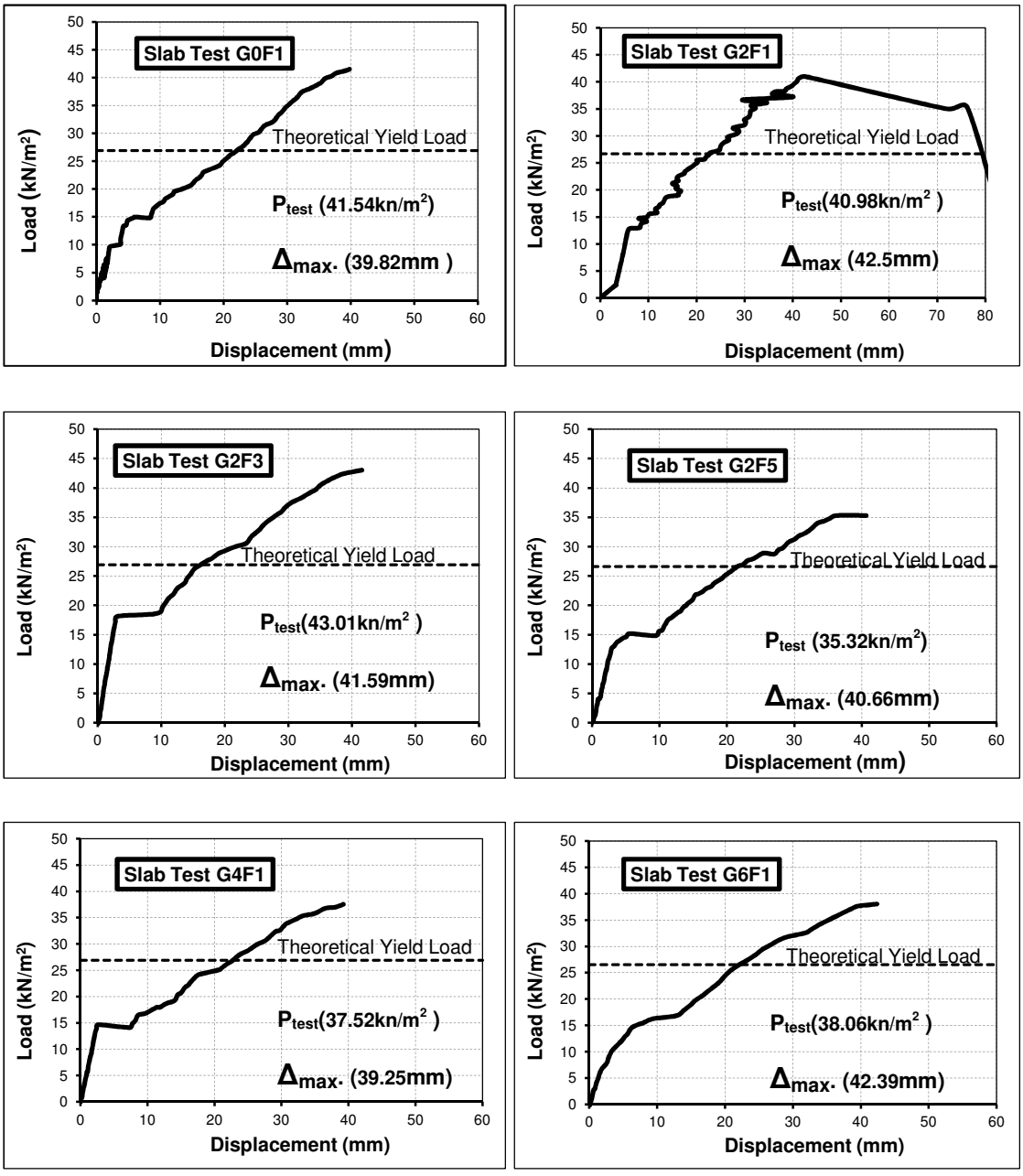

Figure 5-9 Load-Displacement results for the small-scale slab tests

Table 5-4 Details of slab tests at ambient temperature

Test	Thickness (mm)	f_{cu} (MPa)	ρ (%)	P (kN/m^2)	P_{test} (kN/m^2)	e	Δ_{max} (mm)
G0F1	34.80	44.4	0.079	26.64	41.54	1.56	39.82
G2F1	34.30	38.8	0.092	25.82	40.98	1.59	42.50
G2F3	34.00	44.2	0.082	25.64	43.01	1.68	41.59
G2F5	34.70	36.9	0.095	26.25	35.32	1.35	40.66
G4F1	34.10	43.7	0.083	25.75	37.52	1.46	39.25
G6F1	34.80	35.3	0.099	26.30	38.06	1.45	42.39

Where:

P_{test} is the maximum sustained load from the test

Δ_{max} is the maximum displacement

P is the theoretical yield line load obtained from the equation given by [116];

$$\boldsymbol{P = \frac{24\mu M}{l^2}\left[\sqrt{3 + \frac{1}{(a')^2}} - \frac{1}{a'}\right]^{-2}} \qquad \text{Equation 6}$$

M is the moment capacity of the slab in longer span.

μ is the coefficient of orthotropy

$a' = \sqrt{\mu}a$

l is length of the shorter span

e is the enhancement due to membrane action = P_{test} / P

ρ is the reinforcement ratio = $0.5\left[\left(\frac{f_{u,1}\,A_{a,1}}{0.8 f_{cu} d_1}\right)_{long\ span} + \left(\frac{f_{u,2}\,A_{a,2}}{0.8 f_{cu} d_2}\right)_{short\ span}\right]$

It can be seen that all the slabs can carry a load higher than the theoretical yield line load which highlights the presence of the membrane action. The enhancement (*e*) due to membrane action is ranging from 1.35 for G2F5 to 1.68 for G2F3.

Although the slabs did not tested at the same time which results in the variability of the concrete properties and have different recorded thickness, the comparison between the slabs is in term of the enhancement which considers these variations as Equation 6 (to calculate the theoretical yield line load) considers it.

For all the slabs, the enhancement is up to 26% higher than that for the square slab (35.9 mm thick), produced from natural sand and contain no fibre [127] which was equal to (1.33) (Figure 5-10). As the only difference between the slab in reference [127] and the slabs in the author's study is the type of concrete, these results support the recommendation of using the glass aggregate as a partial replacement of the natural sand in concrete with basalt fibre.

The increase in glass content with 0.1% basalt fibre results in a slight increase (3%) in the enhancement when 20% glass aggregate was used then there is a slight reduction with 40% and 60% glass contents (10% and 11% respectively) compared to the slab with no glass and the same percentage of basalt fibre. Those results confirmed the results obtained in the first part of the experimental work carried out in this study that highlighted the slight reduction of the strength with increasing the glass content above 20% due to the alkali silica reaction.

For the slabs with 20% glass sand, increasing the volume fraction of basalt fibre to 0.3% (G2F3) results in increasing the enhancement by 9% compared to G2F1 and 12% compared to G0F1. The effect of using basalt fibre on the glass aggregate concrete strength was explained in Section 4.5.3.

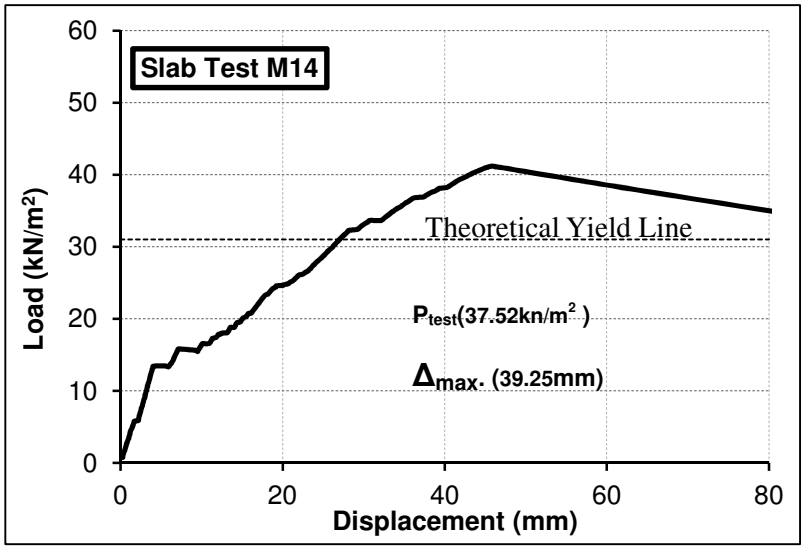

Figure 5-10 Test results for slab with natural sand and no fibre [81]

For a given displacement (39.3 mm) the enhancement with increasing the glass content from 0% to 20%, 40%, and 60% is 1.54 to 1.55, 1.45, and 1.41 respectively, which leads to the same conclusion for the results when the maximum displacement was adopted for comparison. However, they remain higher than the enhancement for the slab with 0% glass and 0% fibre, mentioned before [127], for the same displacement which was 1.22. For G2F3 and G2F5 for the given displacement the enhancement is 1.65 and 1.34 respectively.

Wood and Kemp [116, 139] have concluded that the enhancement above the theoretical yield line load is dependent on the reinforcement ratio. The effect of reinforcement ratio is not clear in this type of concrete, as shown in Table 5-4. This leads to the conclusion that further research might be needed to investigate the effect of reinforcement ratio on the enhancement due to membrane action for fibre reinforced concrete.

5.3.2 Fire Test

Six slab tests in fire were conducted between July and September 2010. The mode of failure for all the slabs was the fracture of the reinforcement with a full-depth crack forming across various yield lines as shown in Figure 5-11 and Figure 5-13. The temperature at the top(T_{top}), reinforcement (T_{Mesh}) and bottom (T_{Bot}) surfaces of the slab are shown in Figure 5-14 and Table 5-5 (which also shows the other details of the tests).

Figure 5-11 The fracture of the reinforcement with full -depth crack (G0F1)

Table 5-5 Details of slab tests in fire

Test	Thickness (mm)	ρ (-)	P (kN/m^2)	$LR = P_{test}/P$	Failure temperature(℃)			P_{Tc} (kN/m^2)	P_{test}/P_{Tc}	Δ_{Fire} (mm)
					(T_{top})	(T_{Mesh})	(T_{Bot})			
G0F1	34.5	0.079	26.26	0.32	745	840.4	871.4	2.69	3.13	85.1
G2F1	34.2	0.079	25.92	0.32	731	843.7	890.5	2.63	3.20	86.3
G2F3	34.3	0.094	25.82	0.33	676.1	846.6	892.6	2.61	3.22	84.2
G2F5	34.2	0.091	25.69	0.33	735.7	849.2	895.3	2.58	3.26	91.8
G4F1	34.1	0.080	25.79	0.33	678.4	844.3	898.5	2.61	3.22	110.4
G6F1	34.2	0.085	25.79	0.33	656.3	846.8	896.4	2.60	3.23	105.7

Figure 5-12 shows that the failure mode for the slabs with higher fibre content (G2F3 and G2F5) was the fracture of the reinforcement forming across the span of the slab while the failure mode for the other slabs was across various yield lines. The temperatures at failure and the displacement are almost the same, for slabs with 20% glass content, considering the experimental error possibility. This may attributed to the presence of fibre which induces multiple interior small cracks and suppresses the growth of a single crack in the concrete structure.

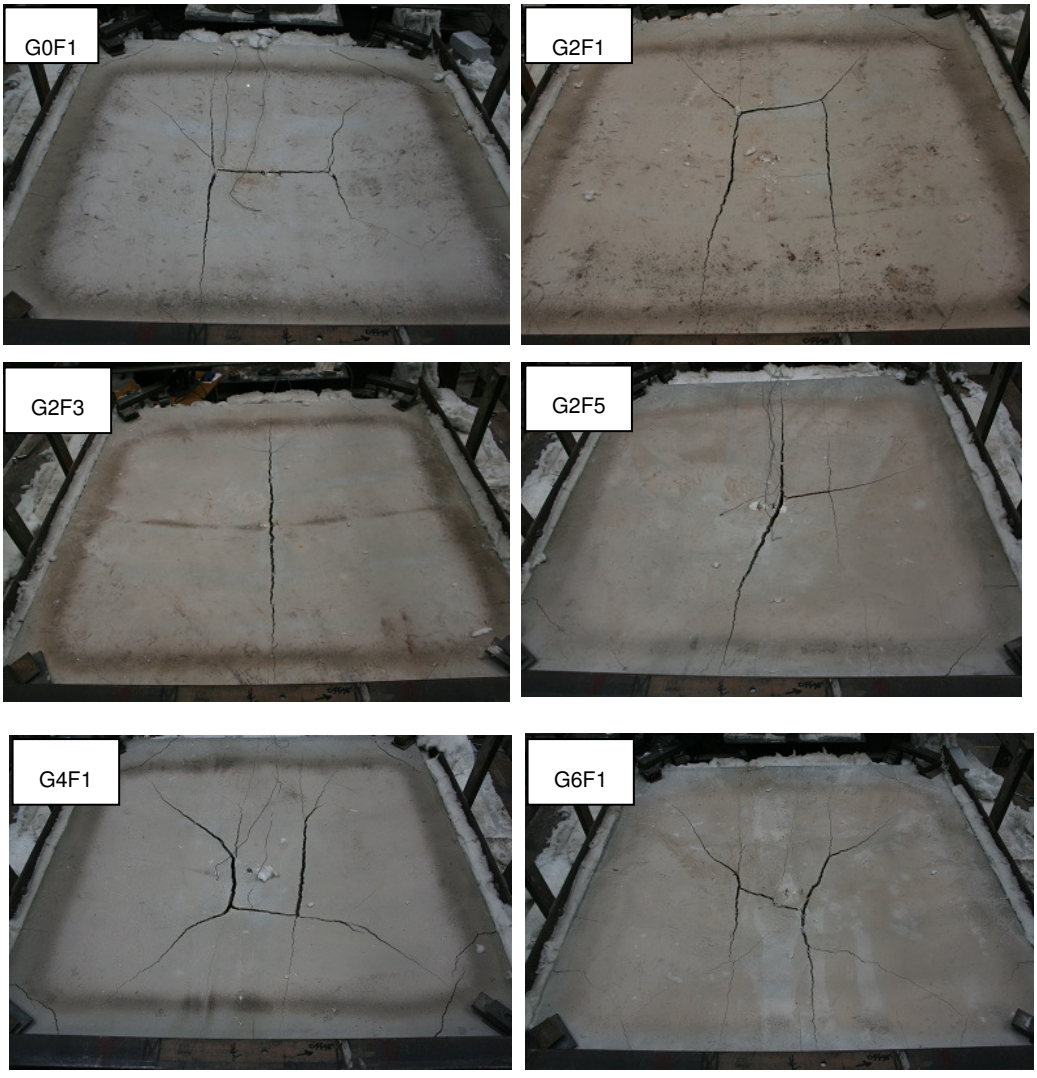

Figure 5-13 The mode of failure for the slabs tested in fire

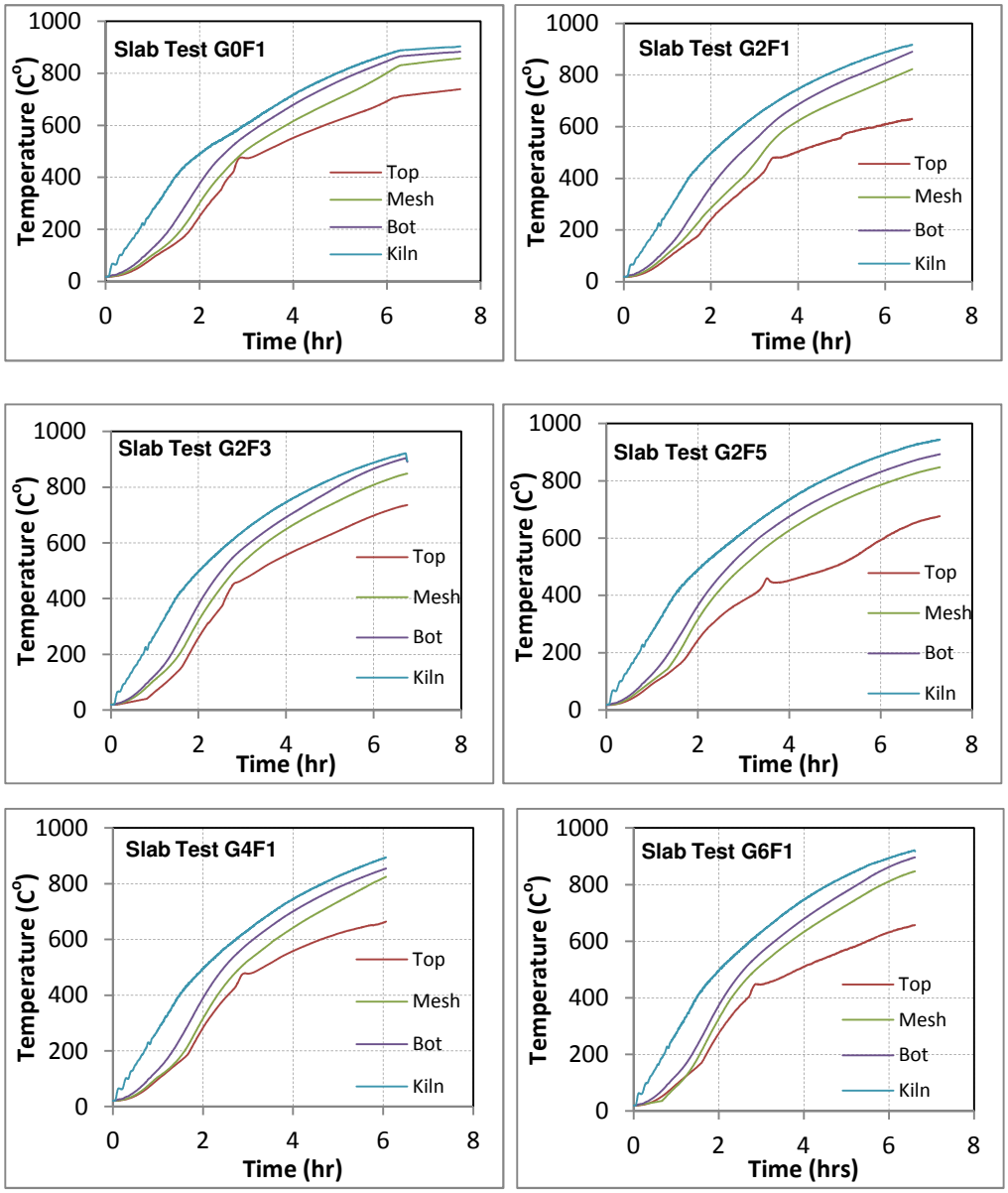

Figure 5-14 Temperature profile of the slabs at different positions

From Table 5-6 and Figure 5-15 it can be seen that the temperature differences between the bottom and the top surfaces increases with increasing glass and basalt fibre content (from 126°C for G0F1 to 240°C for G6F1), which is the same results obtained in Section 4.5.4., providing the resistance to the heat transfer.

The theoretical yield line load at any temperature can be calculated using the strength reduction factors for the reinforcement and concrete given by EN 1994-1-2 [140].

From Table 5-5 it can be seen that the theoretical yield line load at the maximum reinforcement temperature (P_{Tc}) is lower than the applied load (P_{test}) for all the slabs. The enhancement due to membrane action is at least twice higher than that recorded at ambient temperature tests. Previous research's result, for the square slab reinforced by mild steel (approximately has the same properties), the enhancement was 2.38 which is lower than the enhancement when using the new type of concrete by at least 31%.

Again, the effect of reinforcement ratio is not clear in this type of concrete for the slab tested at elevated temperature , as shown in Table 5-5

The displacement-reinforcement temperature relationship is presented in Figure 5-16

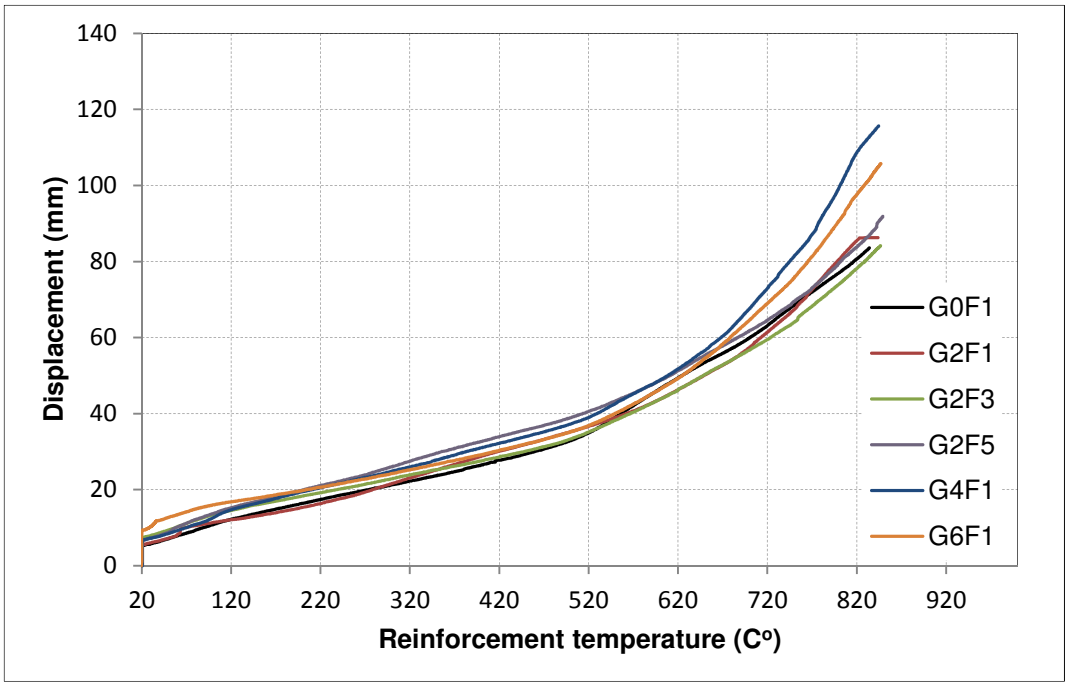

Figure 5-17 Displacement - Reinforcement temperature relaitionship

5.4 SUMMARY

Small-scale slab tests at ambient and elevated temperatures have been conducted between February and September 2010 to investigate the structural behaviour of the new concrete. The slab mixes were chosen depending on the results of the first part of the experimental work carried out in this study with different percentages of glass sand and different volume fractions of basalt fibre. The results show, for ambient temperature tests, that the fracture of the reinforcement is the mode of failure for all the slabs and the fracture was along various yield lines. For the elevated temperature tests the fracture of the reinforcement was across various yield lines. The results also show that there is an increase in load carrying capacity above the theoretical yield line load which highlights the presence of membrane action. For the ambient temperature test, the increase in glass results in a slight increase (3%) in the enhancement when 20% glass aggregate is used then there is a slight reduction with 40% and 60% glass contents (10% and 11% respectively) compared to the slab with no glass and the same percentage of basalt fibre. For the slabs with 20% glass sand, increasing the volume fraction of basalt fibre to 0.3% (G2F3) results in increasing the enhancement by 9% compared to G2F1 and 12% compared to G0F1.

For the elevated temperature test, the enhancement due to membrane action is at least twice higher than that recorded in the ambient temperature tests. Furthermore, the temperature differences between the bottom and the top surfaces increases with increasing glass and basalt fibre content (from 126^{o}C for G0F1 to 240^{o}C for G6F1) providing the resistance to the heat transfer.

From the results presented in this chapter it can be concluded that basalt fibre reinforced glass concrete fulfil the requirements for fire protection.

CHAPTER SIX

6 METHODS OF ANALYSIS

6.1 GENERAL

A numerical analysis was carried out to investigate the ability of the numerical methods, available in the structural analysis field, to predict the structural behaviour of the new type of concrete. The data obtained from the experimental work, carried out in this study, were used to model the thermal distribution and the structural behaviour of the slabs at ambient and elevated temperatures. Background information of the finite element model, concrete crack model and its parameters are presented in this chapter. The methodology of the advanced analysis of the slabs and simplified method introduced by previous work and was adopted in this study are presented. In addition, details of the ABAQUS model and some parameters that effect the analysis are also represented.

6.2 SIMPLIFIED ANALYSIS

A simple analytical method was developed by Bailey and Toh [20] to determine the ultimate load carrying capacity of two-way simply supported horizontally unrestrained slab incorporating the enhancement due to tensile membrane action at ambient and elevated temperatures.

The method based on rigid – plastic behaviour with change of geometry, an increase in vertical displacement results in an increase in the load carrying capacity. For horizontally unrestrained slabs, the slab supports the load by tensile membrane action in the central area of the slab and a ring of compressive membrane action around the perimeter (Figure 6-1).

The method has been developed gradually and reduced the assumptions until it reached the final form. The original design approach was first published in 2000 [141] and presented in more detail in 2001 [142].

The method then was updated in 2006 to include the use of the most efficient reinforcement pattern and the practical use of natural fire [143]. The final form of this method was presented in 2007 which included the refinement of the assumed in-plane stress pattern and prediction of when concrete crushing occurs in the proximity of the corners of the slab [20].

The simplified method at ambient and elevated temperatures in its final form was used in this study.

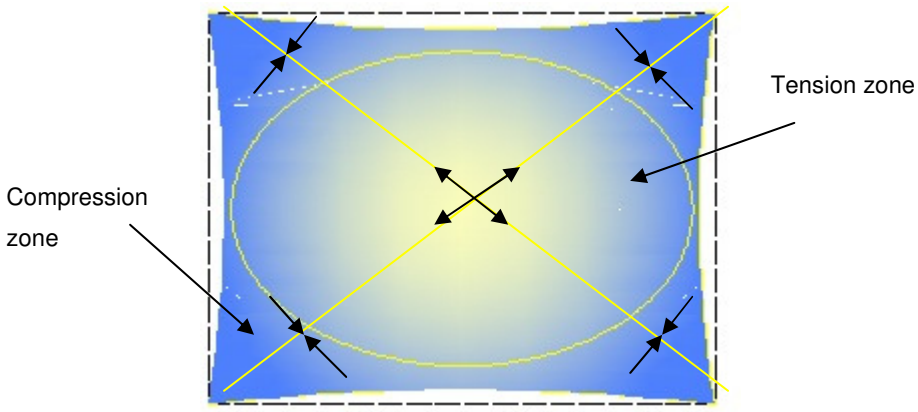

Figure 6-1 Membrane action of horizontally unrestrained slabs[144]

6.2.1 Simplified Method at Ambient Temperature

This section presents a summary of the simplified method at ambient temperature in its final form. The method calculates the increase in the load carrying capacity (the enhancement) above the theoretical yield line load. This enhancement is due to the in-plain tensile stresses developing at the centre of the slab and the increase in yield moment in the outer regions of the slab. The calculation of the enhancement (e*)* assumed the self-equilibrium in-plane forces comprise tensile membrane action in the central area of the slab and compressive membrane action around the perimeter.

The in-plane stress distribution and the in-plane forces along the rigid plates, defined by the constant (*k*, *b*, and *v*), for the 1st Stress Pattern and the 2nd Stress Pattern are shown in Figure 6-2 and Figure 6-3 respectively.

For the 1st Stress Pattern it can be seen that the maximum value of the constant (*b*) (i.e. the maximum stress in the reinforcement in the shorter span = bKT_0) is less than (f_1), where (f_1) defines the ultimate stress (i.e. $f_1 = f_u / f_y$). When the constant (*b*) is found to be greater than f_1, the in-plane stress distribution pattern should change to 2nd Stress Pattern.

The design procedure, based on the stress pattern, is to calculate the enhancement due to membrane action forces for each element and the enhancement due to the effect of in-plane forces on the bending capacity separately and then the overall enhancement for a given displacement is obtained by combining them. The equations used to calculate the enhancement at ambient temperature for the slabs in this study are given by references [20, 123, 145] .

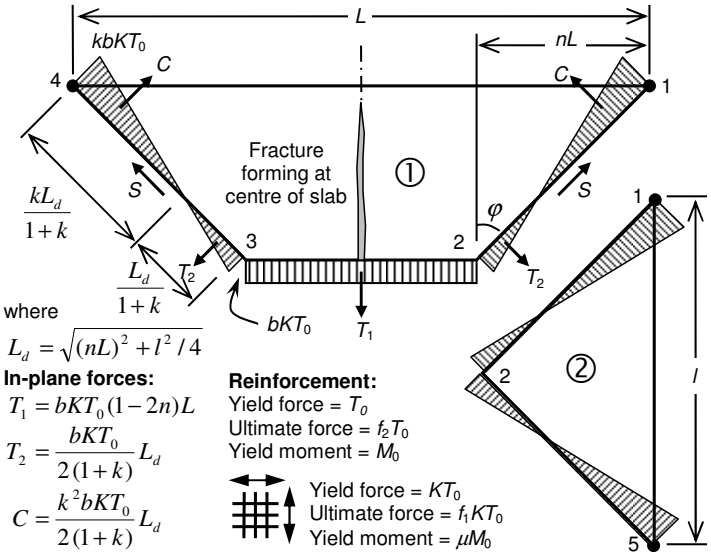

Figure 6-2 The in-plane stress distribution and the in-plane forces for the 1st stress pattern [20]

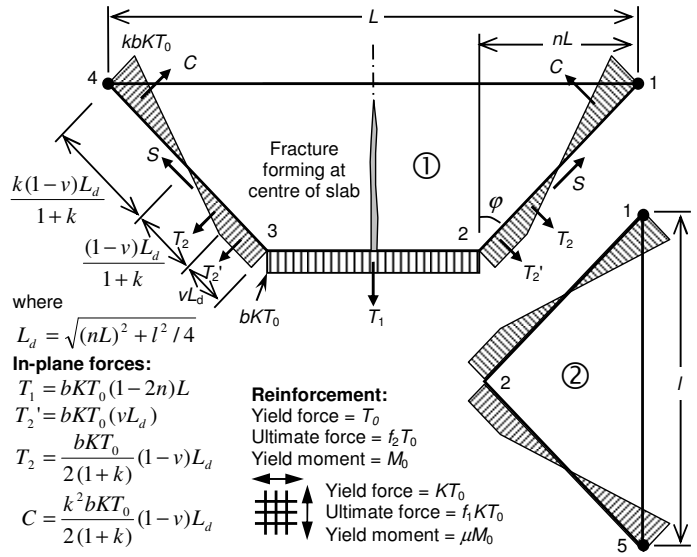

Figure 6-3 The in-plane stress distribution and the in-plane forces for the 2nd stress pattern [20]

6.2.2 Simplified Method at Elevated Temperature

For the slab at elevated temperature, the same equations used to calculate the enhancement at ambient temperature can be applied incorporating the thermal effects on the material properties. The reduction factors at elevated temperatures for the mechanical properties of the mesh reinforcement and concrete were taken from EN1992-1-2 [29].

The design procedure to calculate the enhancement for the slab at elevated temperature can be summarised, as explained in reference [20]:

1- The temperature of the reinforcement is assumed to increase monotonically from 20 to 1000°C and the temperature of concrete is lower than the reinforcement temperature by 20%.
2- Yield line load corresponding to each reinforcement temperature were determined and plotted verses the reinforcement temperature as shown in Figure 6-4 for slab G0F1.
3- The enhancement factors for a series of vertical deflections (*w*) were determined over the range of temperatures specified in step 1.
4- The load carrying capacity was computed by multiplying the yield line loads from step 2 by the enhancement factors from step 3. The

obtained load for each value of *w* was plotted versus the temperatures.

5- For a given constant working load, the corresponding temperatures were extracted for the yield line load and various value of *w*.

As this method is based on rigid plastic behaviour with change of geometry, the method does not predict any displacement until the theoretical yield – line load is reached. For slab G0F1 the theoretical yield – line load is reached at 631°C (Figure 6-4).

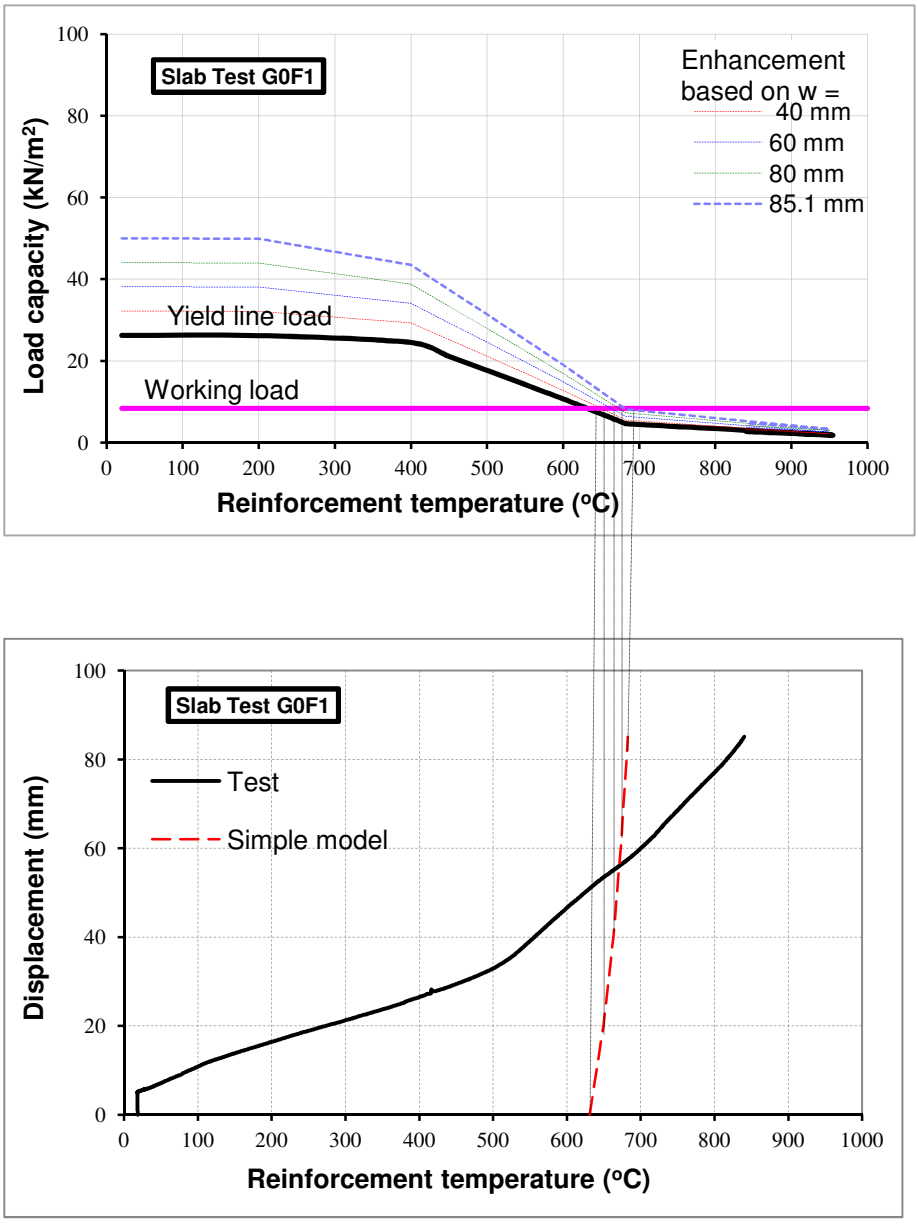

Figure 6-4 Prediction of deflection - temperature relationship using the simplified method

6.3 ADVANCED ANALYSIS

The finite element method (FEM) of modelling concrete at failure has experienced significant progress in the past decades. This method has helped to understand the behaviour of structures and analyse complex cases without the need to carry out extensive tests, which leads to cost and time consumption. Different approaches have been adopted and different models have been developed such as fracture energy models, smeared crack models, plasticity models and others whereby concrete is considered as a quasi-brittle material in which strain softening plays a dominant role.

6.3.1 The Fundamental Principles of the FEM

The finite element method is comprised of three major phases [146, 147]:

(1) ***Pre-processing***, in which the mesh can be created by dividing the structure into small elements with nodes for mathematical analysis, assign the material properties and applying the boundary conditions in the form of restraints and loads. The nodes are generally located at the element corners and perhaps near each midside. Each node has a degree of freedom (e.g. temperature, displacement, rotational). These variables are defined by a suitable shape function from which the stiffness matrix [K] is developed.

(2) ***Solution***, the governing matrix equations are assembled into the global stiffness matrix and solved for the primary quantities (e.g. strain and stress). For example, the applied load matrix [F] can be expressed as follows:

$$[F] = \sum[K][u] \qquad \text{Equation 7}$$

The displacement [u] at every nodal point is calculated and then the element strains and stresses are calculated.

The assembly process depends on the type of the analysis (e.g. static or dynamic), model's element types and properties, material properties and boundary conditions.

(3) ***Post-processing***, investigation of the results of the analysis which comprise checking the validity of the solution, examining the values of primary quantities (such as displacements and stresses), and deriving and examining additional quantities (such as specialized stresses and error indicators).

6.3.2 Types of the Element

The design of a comprehensive set of element test problems should take into account the parameters which affect accuracy. These parameters can be classified under the headings of loading, element geometry, problem geometry, and material properties.

The types of the element most commonly used by structural engineers in many finite element programmes are shell, continuum (solid), beam, and truss elements [146]. The selection of the most suitable type of element for any structure depends on the type of structure being analysed and a balance between computational time and accuracy. For slab concrete, the elements most commonly used to represent concrete are shell and continuum (solid) (Figure 6-5)

Continuum solid is a three dimensional extensional element and can model full three dimensional stress state. It can be used for both linear and complex nonlinear analysis. Solid structures usually lead to large meshes when modelled with solid elements and therefore need large computational time.

Shell elements are used to model structures where one dimension (thickness) is relatively small. It is commonly used for plane stress and plain strain models. Shell elements are the most common type of element used to represent slabs, where the loads act perpendicular to its surface. Compared

to the modelling with solid elements, using shell elements is more comfortable regarding computational time.

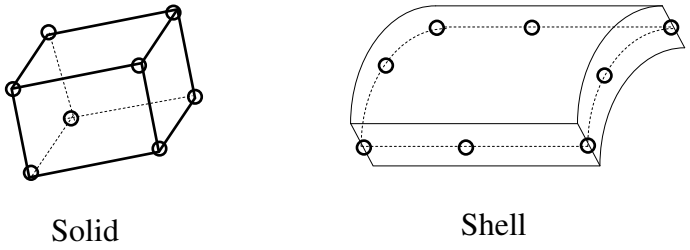

Figure 6-5 The type of the element commonly used in finite element for concrete

6.3.3 Concrete Modelling

As mentioned previously, concrete is poor in tension and prone to develop a number of microcracks, especially at the interface between the aggregate and the cement paste, prior to load. Some of microcracks may develop during loading due to the differences in stiffness between the aggregate and mortar. The propagation of these microcracks during loading contributes to the nonlinear behaviour of concrete and then results in localized failure.

When the tensile strength of concrete is exceeded, the member will crack and then the steel reinforcement will carry the tension. Between two cracks, some tension is transferred from the steel to the concrete through bond and thus tensile stresses are present in the concrete between these cracks. The value and the distribution of bond stress between the cracks determines the distribution of the tensile stress in the concrete and the reinforcing steel. The final cracking state is reached when a tensile force of sufficient magnitude to form an additional crack between two existing cracks can no longer be transferred by bond from the steel to the concrete (Figure 6-6).

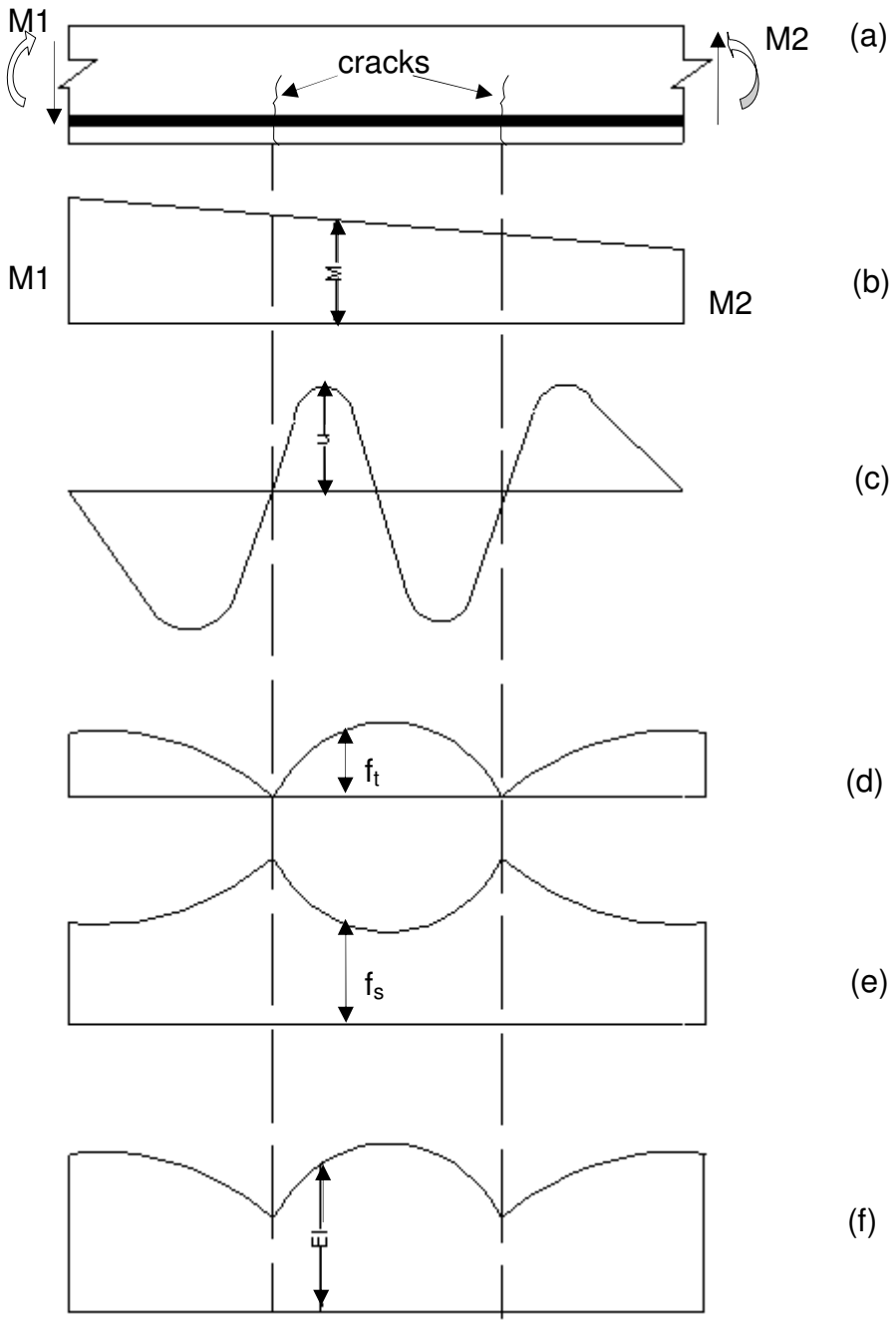

Figure 6-6 Effect of cracking in a reinforced concrete slab or beam [148]

a) Portion of the member
b) Bending moment distribution
c) Bond stress distribution
d) Concrete tensile stress distribution
e) Steel tensile stress distribution
f) Flexural stiffness distribution in elastic range

6.3.3.1 Fracture Mechanics

Fracture mechanics is a set of theories describing the behaviour of solids or structures with geometrical discontinuity at the scale of the structure [149]. It is a combination of the mechanics of cracked bodies and mechanical properties.

It was assumed that all engineering materials contain cracks in which the failure can start. These cracks lead to high stresses near the tip of the crack and the further crack growth can take place from this point [150]. Loading of a cracked body is usually accompanied by inelastic deformation and other nonlinear effects near the crack tip, except for ideally brittle materials. This inelastic zone is usually referred to as the fracture process zone (FPZ).

Linear Elastic Fracture Model (LEFM) is one of the fracture mechanics theories which gives good results for brittle-elastic materials. However, for ductile materials, plasticity will always precede fracture. It cannot be applied to structures when the crack is perfectly sharp in which the stress approaches infinity at the crack tip and using such an approach would predict that materials would have near – zero strength even for a very small applied load. The stress near crack tips would become infinite and the bonds there would rupture. In addition, LEFM cannot be applied when the length of the crack is less than the ultimate crack length when the tensile strength exceeds the ultimate tensile strength.

On the other hand, the nonlinear fracture theory which is applied to metals cannot be directly transplanted to concrete. The difference is that the FPZ is small in the ductile fracture of metals while in concrete is often very large, compared to the cross section of the structure, due to the large size of aggregate. Also, since the plastic deformation of concrete in tension is negligible, the boundary of the FPZ may be considered to be nearly identical to the boundary of nonlinear zone, whereas in metals these boundaries are far apart (Figure 6-7) [151].

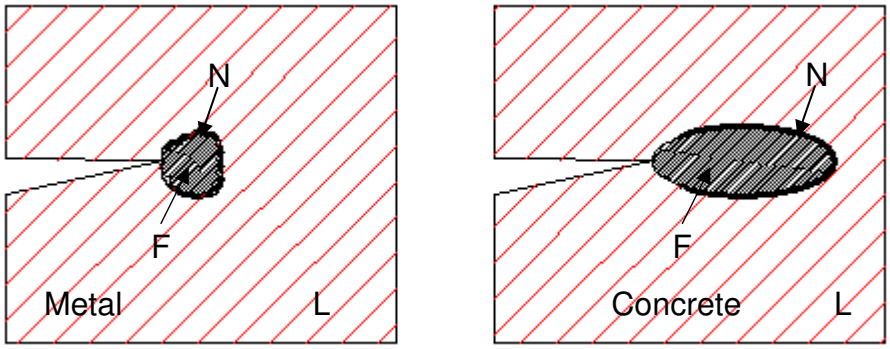

Figure 6-7 The FPZ in metal and concrete

To model the propagation of the crack in quasi-brittle material like concrete alternative approaches were suggested by many researchers such as; stress intensity approach, energy balance approach, strip – yield model by Dugdale, cohesive force model by Barenblatt , Hillerborg et al. fictitious crack model and Bažant concrete fracture model [151-153]. Hillerborg et al. model and Bažant introduced two methods to combine the fracture mechanics and the finite element analysis [151, 152]. In the fictitious crack model, Hillerborg introduced the line – type FPZ labelled as fictitious crack; the formation of this zone involves damage of the material in the zone, which results in a decrease in stress transfer. This decrease in stress causes unloading of the material outside the fracture zone, with a corresponding decrease in strain [153]. The tensile strength (f_t) and the fracture energy (G_f) are the model parameters in the fictitious crack model. The G_f is the amount of energy required to create one unit area of crack surface. The two parameters (f_t and G_f) are also included in the crack band theory, in addition to a third parameter, termed the crack band width (w_c).

6.3.3.2 Concrete Crack models

Concrete cracking can be modelled in finite element analysis by using one of the two methods; discrete or smeared crack.

The discrete crack model was introduced first by Ngo and Scordelis [154] and used in the earlier finite element models. This approach assumes that the cracks were modelled by separating the nodal point of the finite element mesh with a pre – defined path (Figure 6-8a). It involves continuous change in mesh topology and therefore the computational effort for meshing is high. Moreover, the lack of generality in crack orientation has made the discrete crack model unpopular. However, this approach is useful to investigate the local behaviour in the vicinity of a crack and thus plays an important role in the residual strength assessment of concrete structures [155].

The smeared crack approach represents many fine cracks normal to the principal stress direction (Figure 6-8b). This approach can offer automatic generation of cracks and complete generality in crack orientation, without the need of redefining the finite element topology [148]. However, the results of this approach depend on the size of the finite element mesh used in the analysis. When large elements are used, each element has a large effect on the structural stiffness. When the single element cracks, the stiffness of the entire structure is greatly reduced. Therefore, it cannot simulate the actual behaviour if the case is dominated by a crack. In this case the discrete crack model can provide a realistic description of the dominate crack due to its strain discontinuity.

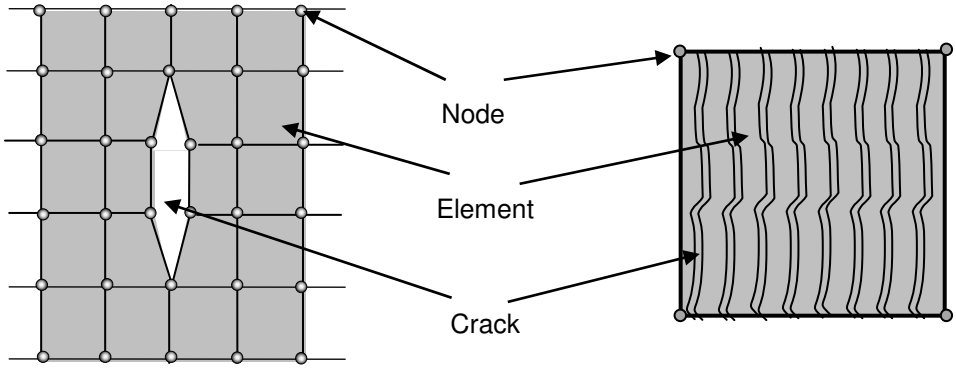

Figure 6-8 Discrete and smeared crack models

It has been found that the smeared crack model can be sufficient to model the overall behaviour of reinforced concrete floor slabs at ambient and elevated temperatures [156, 157].

6.3.3.3 Crack Band Width

In the smeared crack model, it was assumed that the crack strain acts over a certain width within the finite element called the crack band width w_c. Bazant and Oh [151] introduced the crack band theory in the analysis of plain concrete panels. The two basic assumptions of the model are that the crack band width is equal to three times the maximum aggregate size and that the concrete strains are uniform within the band.

When the crack band width is related to the adopted finite element mesh size, the spurious mesh dependency on the structural load-deformation response can be eliminated. Previous research has been conducted to calculate the crack band width.

It was found that the relation between w_c and the finite element size can be determined by trial-and-error fitting of some reliable results (e.g. experimental results or selected discrete crack results) [158].

Oliver [159] has analyzed a singular band in a two-dimensional (2D) domain, in which a crack can be related to the crack orientation and the characteristics of the finite element interpolation functions. However, this approach renders the estimated value of the crack band width constant throughout the entire loading history[160].

According to the CEB [161] the crack band width can be calculated from the square root of the area governed by each individual integration point (I.P) for a two dimensional element (Figure 6-9). This method was adopted in this project.

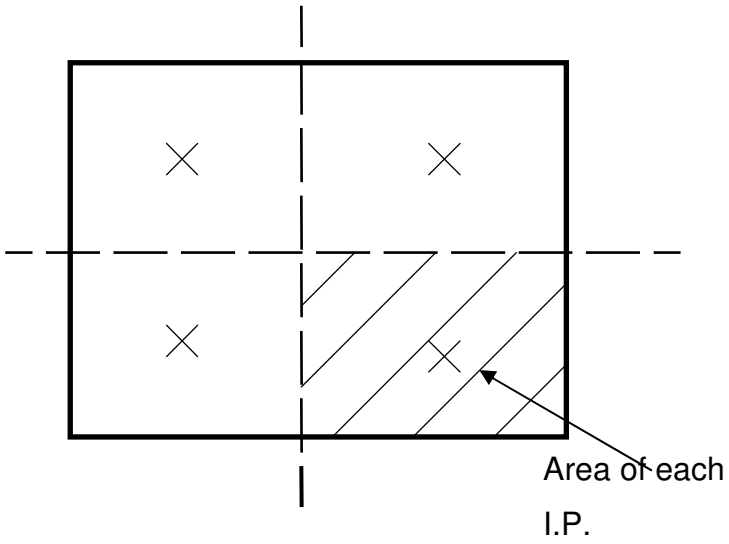

Figure 6-9 Integration point for two dimensional element

6.3.3.4 Fracture Energy and Tension Softening

Knowledge of the tension softening process of concrete and the fracture energy is essential to understand fracture mechanisms, to analyze fracture behavior and to evaluate the properties of concrete. It can be defined as the relationship between tensile stress and crack width (or tensile strain) in the fracture zone (a decrease of stress at increasing strain). The tension softening diagram can describe the post-cracking behavior and express the resistance of concrete against crack development. This diagram can be obtained by applying tension directly to a concrete specimen. The area under the tension softening diagram is the fracture energy which, as defined previously, is the energy required to propagate one unit area of mode I crack surface.

Many formulae have been introduced to describe the tension softening curves; Linear Tension Softening, Multi-linear Tension Softening, Nonlinear Tension Softening (Moelands and Reinhardt) [162]. Nonlinear Tension Softening (Hordijk et al.)[163, 164] (Figure 6-10).

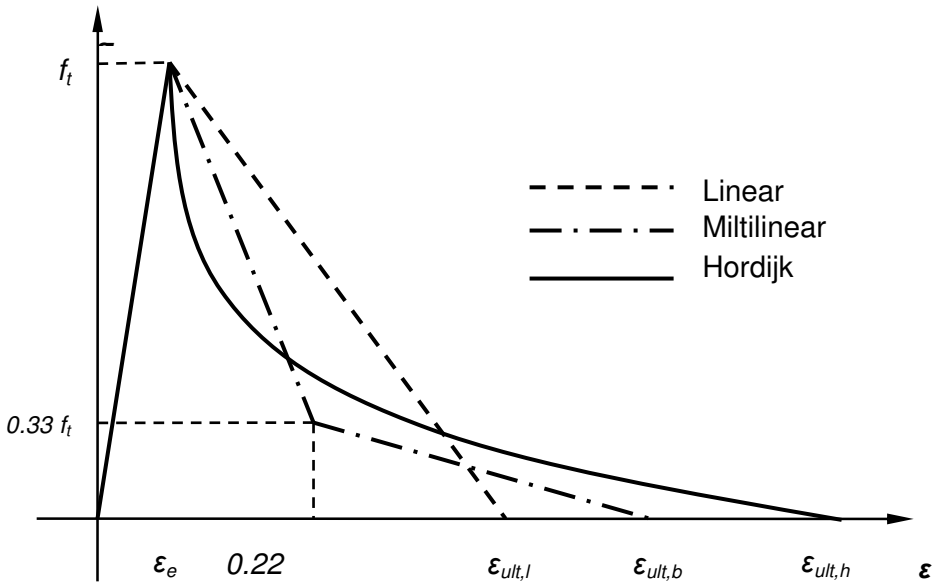

Figure 6-10 The tension softening curves

For linear, multi-linear, and Hordijik softening curve, it was assumed that the area under the fracture energy remains constant within the crack band width so, the ultimate strains can be defined as follows;

- Hordijk: $\varepsilon_{ult,h} = 5.136 G_f / w_c f_t$; Equation 8
- Linear: $\varepsilon_{ult,l} = 2 G_f / w_c f_t$; Equation 9
- Miltilinear: $\varepsilon_{ult,b} = 25 \varepsilon_e$. Equation 10

where;

$\varepsilon_{ult,h}$ is the ultimate strain of concrete in tension (Hordijk softening curve).

$\varepsilon_{ult,l}$ is the ultimate strain of concrete in tension (Linear softening curve).

$\varepsilon_{ult,b}$ is the ultimate strain of concrete in tension(Multi-linear softening curve).

ε_e is the elastic strain of concrete in tension.

G_f is the fracture energy of concrete.

f_t is the concrete strength

w_c is crack band width

Fracture energy and strain softening depends on the composite structure of the material. It is essentially governed by the mechanical interaction of the aggregates with the cement-based matrix. CEB [165] recommend the value of the fracture energy depending on the maximum size of aggregate and the compressive strength of concrete. The equation used to calculate the fracture energy of concrete is described as follows;

$$G_f = G_{F0}\left(f_{cem}/f_{cmo}\right)^{0.7} \quad \text{Equation 11}$$

Where;

G_{Fo} is the base value of fracture energy

f_{cem} is the concrete strength

f_{cmo} is the based value of concrete strength (equal to 10MPa)

Previous experimental work has been conducted on the effect of high temperature on fracture energy of concrete [166]. It was found that the damage introduced by a maximum temperature of 300 to 400^{o}C increases the fracture energy by 50% compared with the reference tests at room temperature. It was also observed that the specimens subjected to high temperatures often show numerous micro cracks within the cement paste. In each of these cracks energy is dissipated, competing to form the final fracture. Furthermore, the fractured surfaces on the heated specimens tend to be more tortuous, going around the aggregates rather than through them, compared to those observed on the specimens at room temperature. Beyond 400^{o}C the trend seems to be that the fracture energy starts decreasing due to the excessive thermal damage within the concrete specimens.

6.3.3.5 Tension Stiffening

As stated previously, concrete contributes to carry tensile stress between the cracks due to the stress transformation from the reinforcement to the concrete through the bond. This contribution of the tensile concrete is known as tension stiffening and it contributes to the overall stiffness of the structure (Figure 6-11). Its magnitude depends on many factors such as the size of aggregate, the bond between the reinforcement and concrete, rebar spacing and diameter, dowel action, and concrete cover. [148]

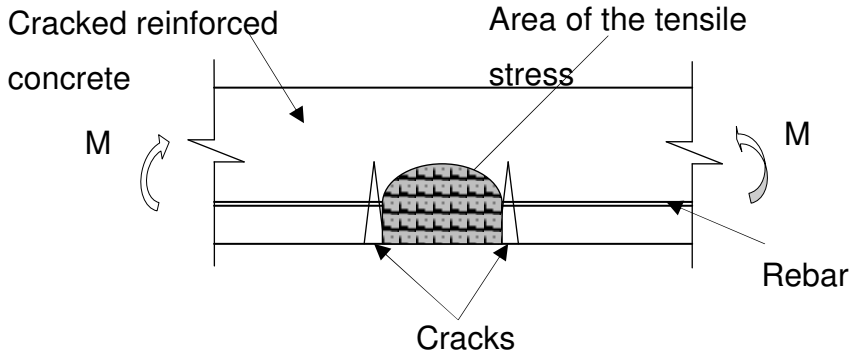

Figure 6-11 the stress transformation from the reinforcement to concrete through bond

Ignoring the effect of tension stiffening results in overestimating the deflection value, maybe by as high as 100% [167].

Many model approaches have been introduced to incorporate the tension stiffening in the analysis, [168-171]. However, many factors which affect the tension stiffening of the concrete are unpredictable such as the bond between the concrete and the rebar. Thus, many researchers have just simply applied a factor to the elastic tensile strain of the concrete corresponding to the maximum tensile stress to attain an ultimate tensile strain.

For structures such as reinforced concrete slabs and pre-stressed concrete slabs the dominating factor in the uniaxial tensile stress-strain behaviour of the concrete should be based on tension softening as tension stiffening is only considered when the concrete structure is densely reinforced.

6.3.4 Modelling Using ABAQUS

6.3.4.1 General

ABAQUS is a suite of general-purpose, advanced nonlinear finite element analysis programs. It is used throughout the world for stress, heat transfer, and other types of analysis in mechanical, structural, and related engineering applications. It consists of three core products: ABAQUS/Standard, ABAQUS/Explicit, and ABAQUS/implicit. Each of these packages offers additional optional modules that address specialized capabilities [146]. Since this study ultimately requires both thermal and structural analysis, the software package ABAQUS version 6.10 was used to perform the structural and thermal model of the reinforced concrete slabs. This section provides a brief description of modelling reinforced concrete slabs in ABAQUS and the approaches adopted in this study.

6.3.4.2 Mesh Element

The linear, 4-node, reduced-integration, quadrilateral shell element (S4R) is robust and is suitable for a wide range of applications, therefore, it was chosen to model the slabs at both ambient and elevated temperatures. ABAQUS uses numerical integration to calculate the stresses and strains independently at each section point through the thickness of the shell to allow nonlinear material behaviour. Also in thermal analysis, the temperature gradient can be provided through the thickness of the shell by these section points [146] .

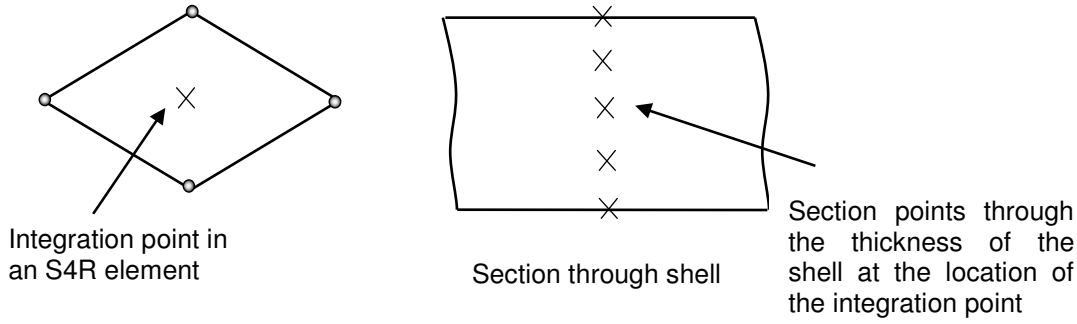

Figure 6-12 Configuration of section points in a numerically integrated shell [146]

6.3.4.3 Material Library

For reinforced concrete, ABAQUS provides two constitutive models to deal with concrete post-cracking behaviour: the smeared crack concrete model in ABAQUS/Standard, and the concrete damaged plasticity model in both ABAQUS/Standard and ABAQUS/Explicit.

The smeared crack concrete model uses the oriented damaged elasticity concept to represent the post cracking stage. Once crack occurs at a point, the subsequent cracks can form in the directions orthogonal of any existing crack surface normal at the same point [146].

The concrete damaged plasticity model in ABAQUS/Standard and ABAQUS/Explicit uses the concept of isotropic damaged elasticity in combination with isotropic tensile and compressive plasticity to represent the inelastic behaviour of concrete. It assumes a non-associated flow rule to determine the flow potential which is based on the Drucker- Prager hyperbolic plastic potential function [146].

$$G = \sqrt{(\in \sigma_{t0} \tan\psi)^2 + \overline{q}^2} - \overline{p} \tan\psi \qquad \text{Equation 12}$$

Where,

$\psi(\theta, f_i)$ is the dilation angle measured in the p–q plane at high confining pressure;

$\sigma_{t0}(\theta, f_i)$ is the ultimate tensile strength, taken from the user-specified tension stiffening data; and

$\in (\theta, f_i)$ is an eccentricity of the plastic potential surface which determine the shape of the flow potential surface together with the dilation angle.

The dilation angle measures the inclination of the plastic stain at high confining pressure. Low value of this angle results in brittle material behaviour while high values will produce more ductile behaviour. A sensitivity test carried out by Malm [172] ,on reinforced beam, shows that the difference in ductile behaviour is rather small between 20^o to 40^o. A sensitivity test carried out by the author for dilation angle ranging from 10 to 30 showed similar results (Figure 6-13). For this reason 20^o dilation angle was adopted in the damage plasticity model conducted in this study. The default value for the eccentricity is 0.1 which implies that the material has almost the same dilation angle over a wide range of confining pressure stress values and it was adopted in this study. The ratio of biaxial to uniaxial compression failure stress in the ABAQUS model was taken 1.16 as there is no experimental data available. The ratio of the second stress invariant on the tensile

meridian to that on the compressive meridian of (K) 0.667 was adopted in this model [173].

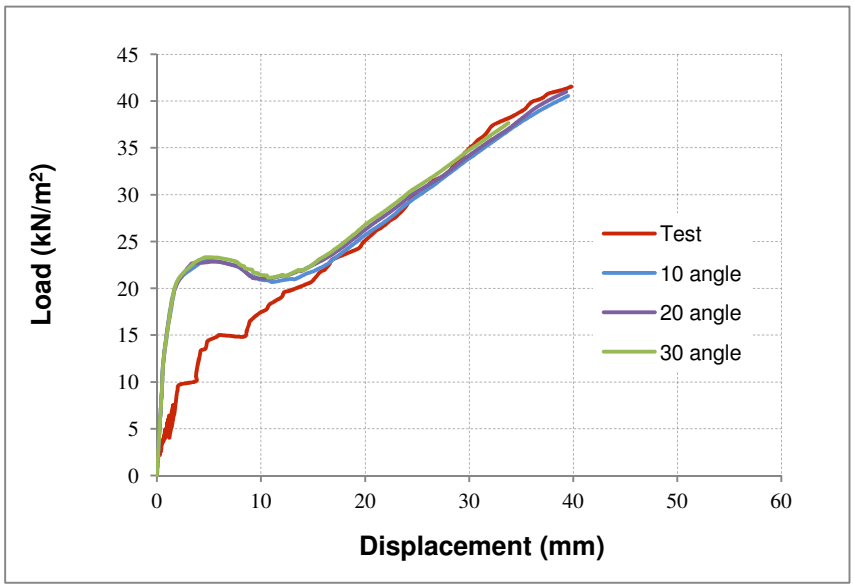

A) Slab at ambient temperature

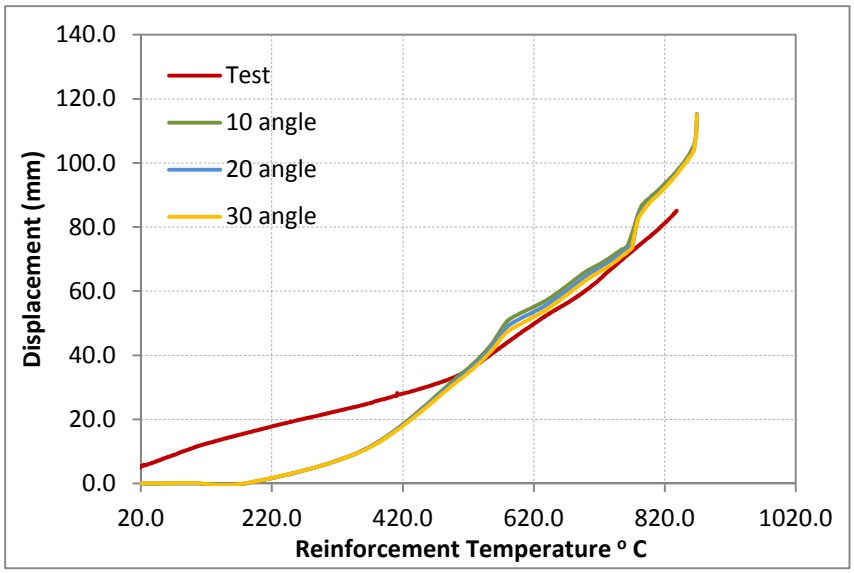

B) Slab at elevated temperature

Figure 6-13 Effect of dilation angle

A comparison between the smeared crack model and the damage plasticity model was carried out using the same material properties. Shell elements (S4R) with 4 nodes doubly curved linear reduced integration scheme was adopted in both models with M6X6 mesh size. Slab G0F1 was taken as an example.

Figure 6-14 shows the result of the slab at ambient temperature and it can be seen that the smeared crack model overestimates the ultimate load and the maximum displacement while the damage plasticity model result appears close to the test result.

For the slabs at elevated temperature the maximum displacement is the same in both models, however, it underestimates the displacement from 200^{o}C up to 800^{o}C while the displacement in damage plasticity model is close to the test data at the same temperature (Figure 6-15). The smeared crack model seems to underestimate the effect of the temperature on the structural behaviour of the slab.

The differences in the results between two models might be attributed to the differences in the assumptions between two models. In the smeared crack model, concrete becomes anisotropic once cracks are formed in one-principle axes, which reduces the strength of the concrete in that principle direction, without impacting the strength of the concrete in the other direction. The allowable value of the tensile stress in the third direction is high compared to the actual tensile strength of concrete. This implies that the third direction will never crack due to the high allowable tensile stress. In the damage plasticity model, the damage caused by the cracking or the crushing not only effects the strength of the concrete in that principle axis, but the reduction in the strength is experienced in all three axis due to the concrete being treated as isotropic, with a different damage parameter for compression and tension.

It can be concluded that the damage plasticity model is more accurate to pridict the ultimate load and displacement for the concrete slab and was adopted in this study.

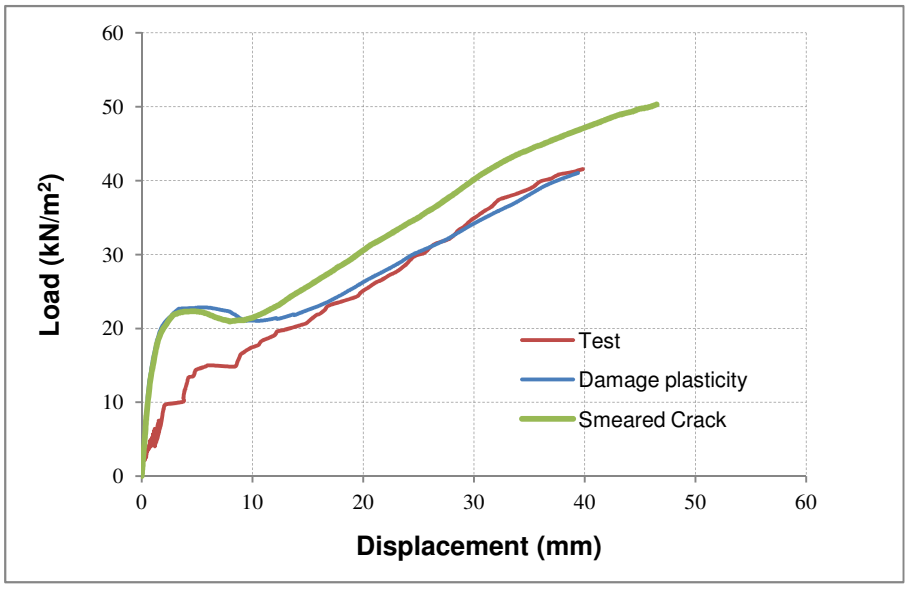

Figure 6-14 Crack models comparison; slab at ambient temperature

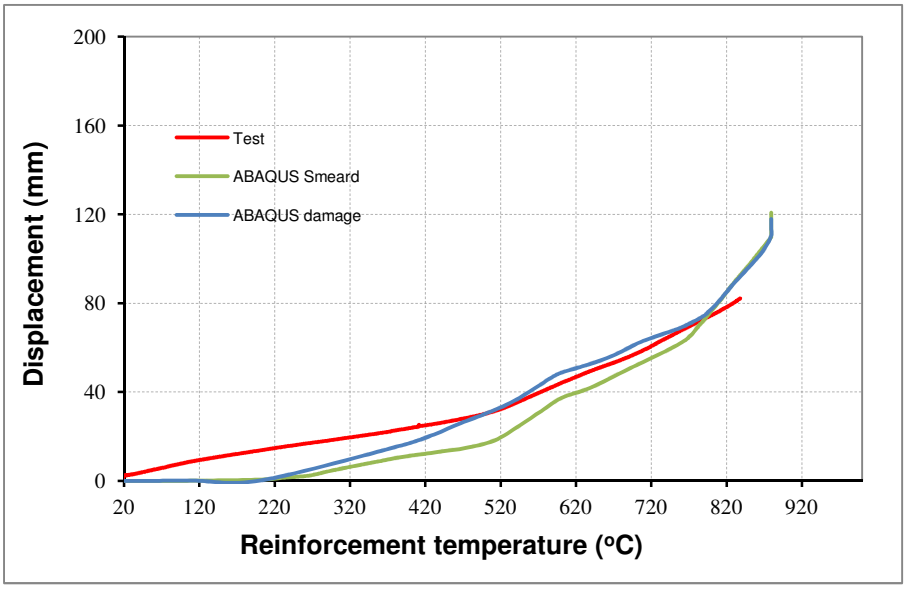

Figure 6-15 Crack models comparison; slab at elevated temperature

6.3.4.4 Analysis procedure

The finite element models generated in ABAQUS are usually nonlinear [146]. Many of the problems are history-dependent, therefore; the solution must be developed by a series of small increments. ABAQUS/Standard generally uses Newton's method as a numerical technique for solving the nonlinear equilibrium equations.

ABAQUS offers two numerical methods to deal with unstable nonlinear problems: the STABILIZE algorithm which is used along with general static analysis procedure and the modified RIKS algorithm.

The STABILIZE algorithm in static general analysis algorithm is suitable for cases where the instabilities are local, in which case global load control becomes inappropriate. In this method ABAQUS apply damping to stabilize the iterations such that the dumping forces are sufficiently large to prevent instantaneous buckling or collapse, but small enough so as not to affect stable behaviour [174]. This method adopts the Newton's method to determine the size of each load step based on the stability of the previous step. Therefore the solution of the static general analysis is obtained as a series of increments with iterations to obtain equilibrium within each increment.

The RIKS method is designed for geometrically nonlinear collapse and global post-buckling analysis, but can include nonlinear materials. It also adopts the Newton method to solve the nonlinear equilibrium equations; in addition it considers the load magnitude as an additional unknown, and the solution is carried out for the load and displacement simultaneously. The progress and increment of the solution is measured by using an arc-length along the static equilibrium path in load-displacement space [175].

Both methods were compared for slab GoF1 modelled at ambient temperature as shown in Figure 6-16 . They nearly yield the same results, however, the ultimate load and displacement in the STABILIZE method is

more accurate, compared to the test results, therefore, it was decided to use the STABILIZE algorithm for the whole study.

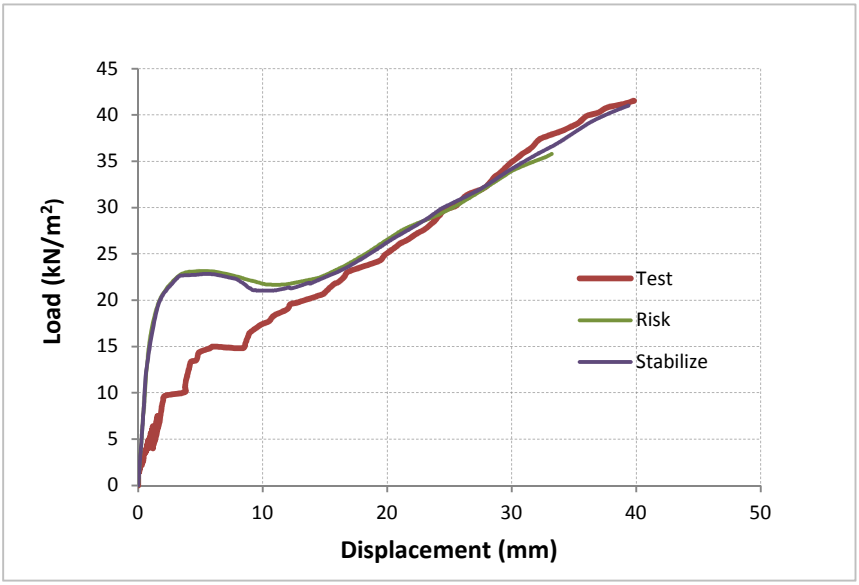

Figure 6-16 Comparison between the RIKS algorithm and STABILIZE algorithm methods

6.4 SUMMARY

The simplified and advanced methods of analysis for reinforced concrete slabs that are adopted in this study were described. Cracking models for reinforced concrete were also explained. ABAQUS version 6.10 is capable to perform the structural and thermal model of the reinforced concrete slabs. A comparison between the smeared crack model and the damage plasticity model, provided by ABAQUS, was carried out using the same materials properties. The results showed that the damage plasticity model is more accurate to pridict the ultimate load and displacement for the concrete slab and it was adopted in this study. A comparition between using the RIKS algorethm and STABILIZE algorthem methods was also carried out and according to the results, the STABILIZE method was adopted in this study.

CHAPTER SEVEN

7 ANALYSIS OF THE SMALL-SCALE SLABS

7.1 GENERAL

This chapter describes the analysis of the small-scale slabs at ambient and elevated temperatures, conducted in this study, using the simplified method stated previously and the finite element software package ABAQUS. Shell elements were adopted in both the thermal and structural models as ABAQUS can provide the thermal distribution through the thickness of the shell by defining the number of the section points.

The simplified and finite element methods results were compared, discussed and validated against the slab test results. Some of the material properties for the mild steel and for concrete (that are not provided from the experimental work) were taken according to BSEN 1992-1-2, BSEN 1993-1-2 and CEB [29, 104, 165].

The ABAQUS input files for modelling slab G0F1 at ambient and elevated temperature are shown in APPENDIX –B.

7.2 SLABS AT AMBIENT TEMPERATURE

Only quarter of the slab was modelled due to double symmetry of the support and loading conditions (Figure 7-1). The slab was assumed to be simply supported with free horizontal movement and ignoring the effect of the corners clamps. The axes of the slab were assumed to be restrained horizontally and rationally in order to represent the continued slab. The span of the slab was assumed to be 1.1x1.1 m.

Shell elements (S4R) with 4 nodes doubly curved linear reduced integration scheme were adopted in the structural model

The reinforcement was modelled in the concrete by means of rebars, which are one-dimensional strain theory elements (rods) that can be defined singly

or embedded in oriented surfaces. According to the data input in the rebar section, ABAQUS will automatically take the total area of the reinforcement and determine an equivalent thickness for a layer of reinforcement.

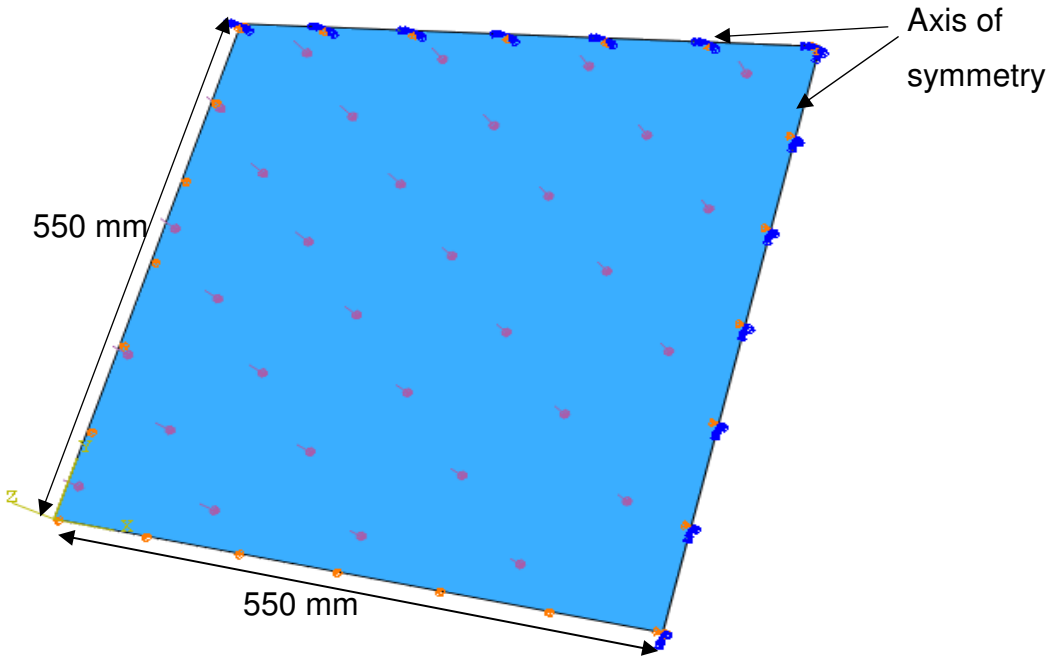

Figure 7-1 Slab model geometry

The key features of the model were as follows:

1- Damage plasticity model was used to model concrete cracking.
2- The STABILIZE algorithm method was adopted as it can predict the nonlinear behaviour of the concrete slab.
3- The reinforcement was assumed to be perfectly bonded to concrete.
4- The crack band width was assumed to be the square root of the area between each integration points.
5- The analysis was terminated once the total step time reached 1.0 or the maximum number of iterations exceeded 1000.

7.2.1 Sensitivity Analysis of ABAQUS Model

This section presents a study on the sensitivity of ABAQUS model, of the slab at ambient temperature, to some parameters to ensure more accurate results and also to understand the effect of changing these parameters on the results of the model. The parameters are:-

- Mesh size.
- Tensile strength.
- Fracture energy.
- Tension softening.

Slab G0F1 was taken as an example for the sensitivity tests carried out in this section.

7.2.1.1 Mesh Size

A number of analyses using different mesh densities were carried out to assess the sensitivity of the results to mesh refinement and to assign the most computationally efficient size of the mesh without affecting the accuracy of the results. The lower bound limit of the tensile strength was assumed and (G_f) was 0.065 N/mm.

The load-deflection relationships obtained from these analyses are compared (Figure 7-2). It can be seen that the maximum deflection and the ultimate failure load gradually decrease and become closer to the test load – displacement curve when the number of the elements increases. The most efficient mesh is M6X6 and it was used to model the structural behaviour of all the slabs at ambient temperature.

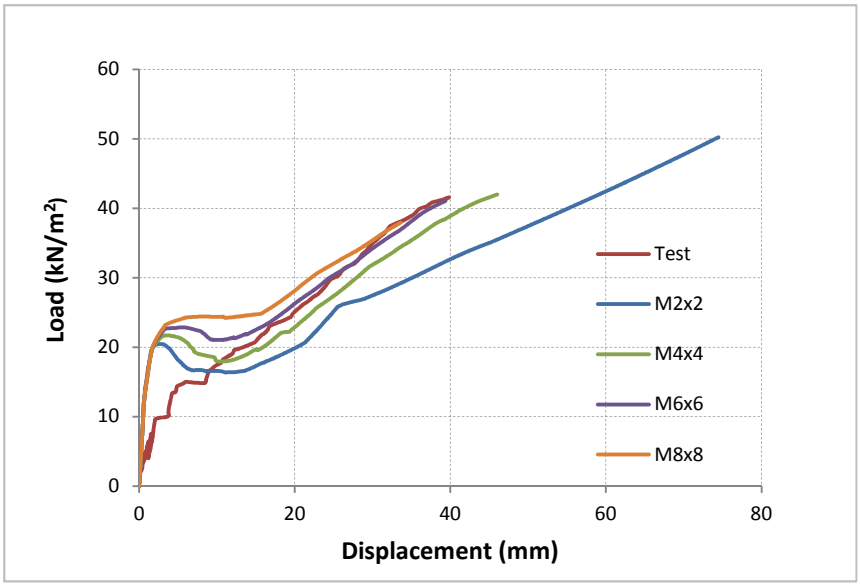

Figure 7-2 Sensitivity of the slab model at ambient temperature to the element size

7.2.1.2 Effect of Tensile Strength

The lower bound, mean and upper bound tensile strength (f_t) were determined according to BSEN 1992-1-2 [29]. The equations for calculating the tensile strength were stated previously in Section (2.2.2.1). The fracture energy value (0.065 N/mm) and M6x6 mesh size were kept constant for all models to show the effect of the tensile strength only.

Figure 7-3 and Table 7-1 show that there is no significant difference in the predicted load carrying capacity when the tensile strength is within the range of the lower bound and the upper bound. The difference is only in the hardening part of the curve as it depends on the f_t value, the peak point in the hardening part increases with increasing the f_t value.

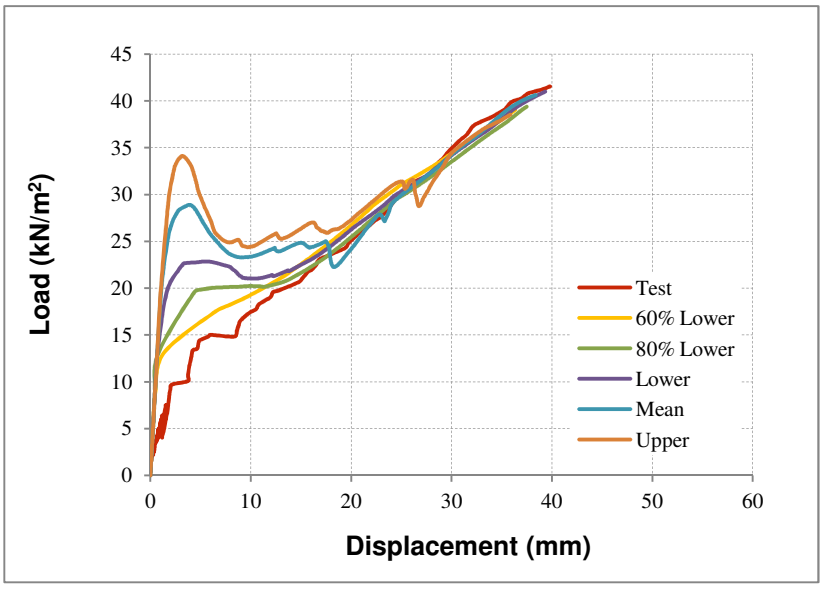

Figure 7-3 Sensitivity of the slab model at ambient temperature to the tensile strength

Table 7-1 Sensitivity of the slab model at ambient temperature to the tensile strength

f_t Value	Predicted Load (kN/m^2)	Predicted Displacement (mm)
Upper bound	38.53	35.84
Mean	40.62	38.38
Lower bound	41.04	39.39
80% Lower bound	39.38	37.48
60% Lower bound	39.04	36.38

7.2.1.3 Effect of Fracture Energy

The assumed fracture energy (G_f) was 0.065 N/mm according to CEB [165]. Figure 7-4 and Table 7-2 show that increasing the G_f to 0.080 N/mm there is a slight increase in the load carrying capacity and the vertical displacement while there is a slight reduction when the G_f reduced to 0.05 N/mm. However, increasing G_f to 1.2 N/mm results in over-predicting the load carrying capacity of the slab.

Table 7-2 Sensitivity of the slab model at ambient temperature to the fracture energy

G_f Value (N/mm)	Predicted Load (kN/m^2)	Predicted Displacement (mm)
0.050	38.89	37.52
0.065	41.04	39.40
0.080	42.42	40.48
0.120	45.55	41.03

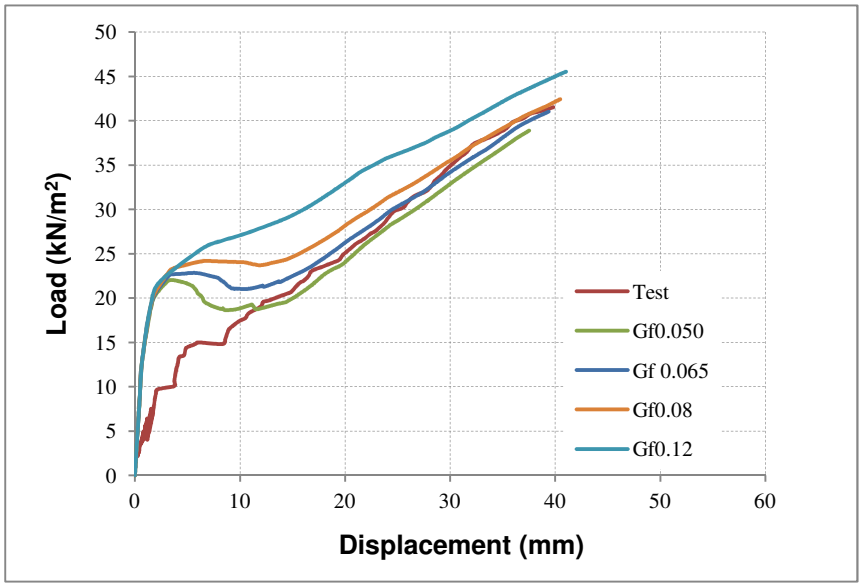

Figure 7-4 Sensitivity of the slab model at ambient temperature to the fracture energy

7.2.1.4 Effect of Tension Softening Curve

As explained in Section (6.3.3.4) many formulae have been introduced to describe the tension softening curve, in this section the following approaches were studied to see their effect on the reinforced concrete slab model:-

- Linear Tension Softening.
- Multi-linear Tension Softening.
- Hordijk Nonlinear Tension Softening

Figure 7-5 shows that the Hordijik approach provides realistic tension softening behaviour compared to the other two approaches and was adopted in modelling the slab at ambient temperature.

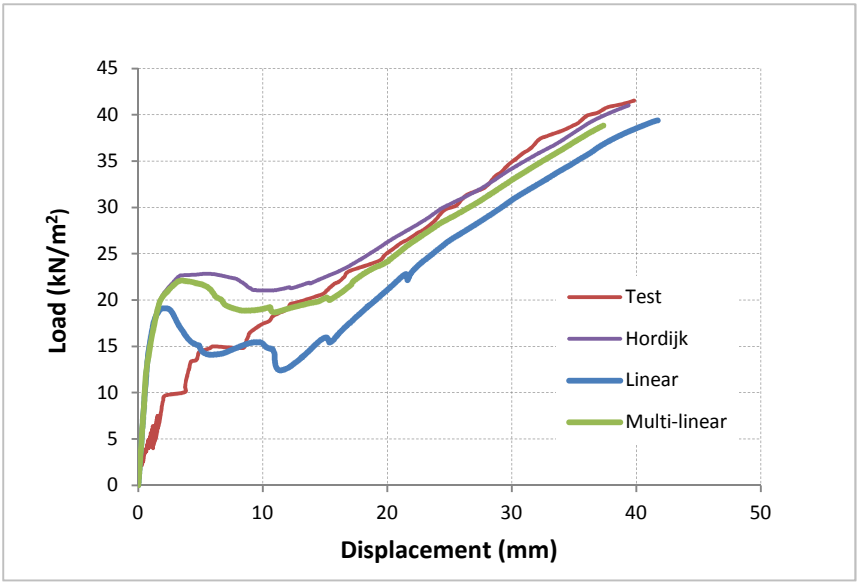

Figure 7-5 Effect of tension softening curve on the slab model at ambient temperature

7.2.2 Analysis of Results of Reinforced Concrete Slabs

Following the sensitivity tests, a mesh with 6X6 elements was used for this model. The lower bound limit of the tensile strength of concrete according to BSEN 1992-1-2 [29] was adopted for all the slabs and the fracture energy was assumed to be 0.065 N/mm according to CEB [165]. Hordijik's branch was adopted for the tension softening behaviour of concrete.

Table 7-3 and Figure 7-6 show the comparison between the test results, the simplified theory model and the ABAQUS damage plasticity model. The results show a good correlation for the load – displacement relationship between the test and the two models up to the failure loads. Also it can be seen that the ratio between the load predicted by the simple model to the test load is close to the ratio between the load predicted by ABAQUS model to the test load.

In the ABAQUS model, the load – displacement relationship predicted at the early stage of the curve is different to the test and the maximum displacement is lower. This is attributed to the fact that the numerical model does not take into account the initial cracks developed by the self – weight of the slab in the test. Hence, the overall stiffness of the slab in the test is smaller than the numerical model.

Table 7-3 The results of modelling the slabs at ambient temperature

Slab Mark	Test load (A) (kN/m^2)	Predicted Load(kN/m^2)		B/A	C/A	Δ_{Test}	Δ_{ABAQUS}
		Simple model (B)	ABAQUS (C)				
G0F1	41.54	40.57	41.00	0.98	0.99	39.82	39.39
G2F1	40.98	38.26	38.90	0.93	0.95	42.50	36.25
G2F3	43.01	39.57	38.40	0.92	0.89	41.59	34.92
G2F5	35.32	38.10	41.10	1.08	1.16	40.66	39.78
G4F1	37.52	39.65	38.90	1.06	1.04	39.25	35.31
G6F1	38.06	38.62	40.10	1.01	1.05	42.39	40.04

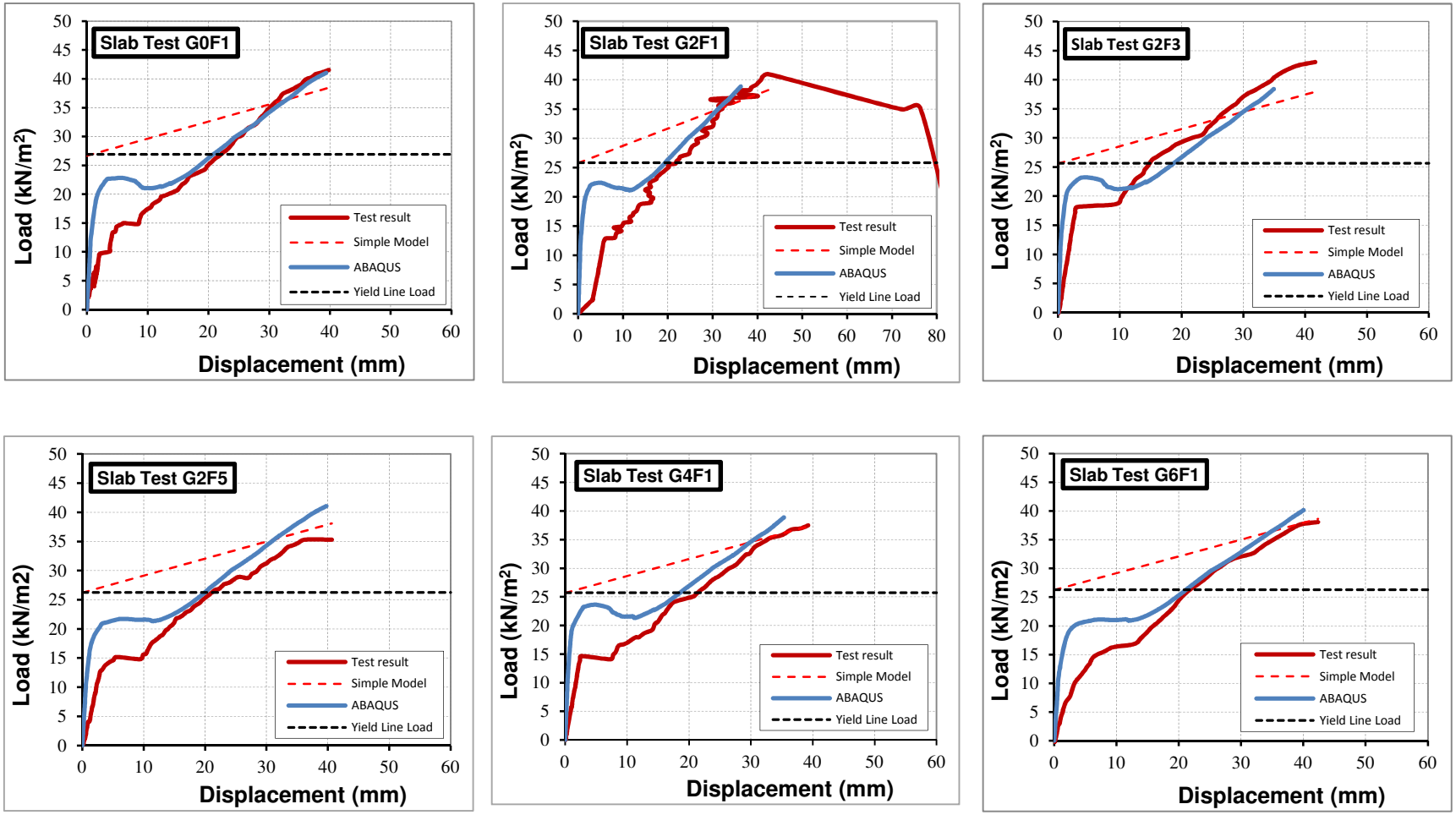

Figure 7-6 The results of modelling the slabs at ambient temperature

7.3 SLABS AT ELEVATED TEMPERATURE

Similar to the slab modelled at ambient temperature, only quarter of the slab was modelled with the same support and loading conditions. The span of the slab was assumed to be 1.1x1.1 m.

Shell elements (S4R) with 4 nodes doubly curved linear reduced integration scheme were adopted in both the thermal model and structural models. Eleven Simpson thickness I.P. were used in both the thermal and structural models in order to provide more accurate results at the reinforcement position.

The measured stress–strain curve for the slab at ambient temperature was used to calculate the stress–strain curves at elevated temperatures, following the reduction factors given in BSEN1992-1-2 [29].

The thermal distribution throughout the slab thickness was predicted first and the output file of this model was used as input data in the structural model.

The reinforcement temperature – vertical displacement relationship predicted from the model was presented, discussed, compared with the simplified method and validated against the slab test results. The in-plane stresses predicted in the ABAQUS model was also presented and discussed in this section.

7.3.1 Sensitivity Analysis of ABAQUS Model

The aim of this section, similar to the slab at ambient temperature, is to investigate the effect of some parameters on the accuracy of the results of modelling the slab at elevated temperature and to choose the one which gives more accurate results, close to the test results. It is also to understand the effect of changing these parameters on the results of the model. These parameters are:-

- Mesh size.
- Tensile strength.
- Fracture energy.

- Tension softening.

Slab G0F1 was taken as an example for the sensitivity tests carried out in this section.

7.3.1.1 Mesh Size

Similar to the slab at ambient temperature four mesh sizes were examined, which were ; M2x2, M4x4, M6x6, and M8x8.

The fracture energy value (0.065 N/mm) and the lower bound limit of the tensile strength were kept constant for all mesh sizes.

Figure 7-7 shows the predicted reinforcement temperature-displacement relationship for slab G0F1. The results show that the maximum temperature at failure for all mesh sizes is approximately the same, however, the curve obtained from using mesh M6x6 converges to that obtained from the test up to the test displacement at failure. Therefore, M6x6 was adopted to model all slabs at elevated temperature.

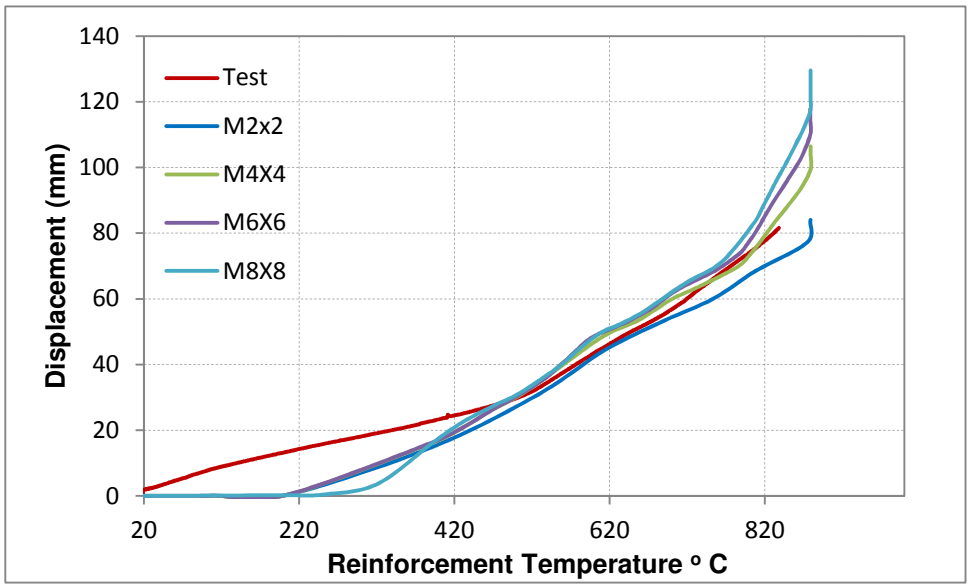

Figure 7-7 Sensitivity of the slab model at elevated temperature to the element size

7.3.1.2 Effect of Tensile Strength

The effect of the value of the tensile strength of concrete is shown in Figure 7-8. The fracture energy value (0.065 N/mm) and M6x6 mesh size were assumed for all models to show the effect of the tensile strength only. The early stage of the curve shows that the predicted displacement is less than the test results for all the values of the tensile strength and the reduction in its magnitude increases with increase in the tensile strength. Again this might be attributed to the fact that the the numerical model did not take into account the initial cracks developed by the self – weight of the slab in the test. The stiffness increases with increasing the tensile strength beyond the lower bound value.

BSEN1992-1-2 [29] assumes zero value for the tensile strength of concrete above 600°C and it was adopted in this model.

Figure **7-8** shows that the reinforcement temperature – displacement curves for different tensile strength value and for the test converge together above 600°C.

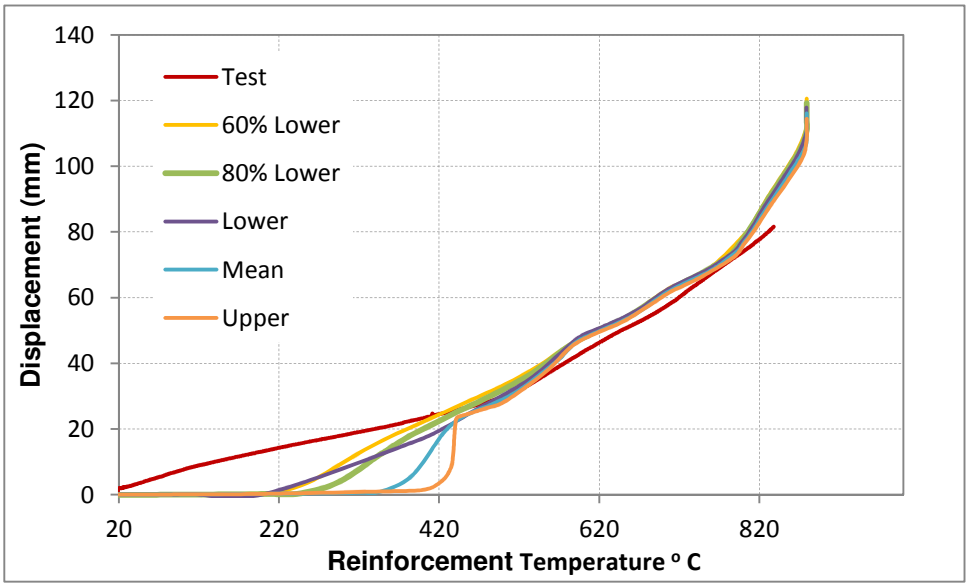

Figure 7-8 Sensitivity of the slab model at elevated temperature to the tensile strength

7.3.1.3 Effect of Fracture Energy

In this test, the lower bound limit of the tensile strength and M6x6 mesh size were assumed for all models. Varying the fracture energy results in no significant effect on the reinforcement temperature – displacement relationship for the slab G0F1 at elevated temperature, as illustrated in Figure 7-9. The fracture energy for all the slabs was taken as 0.065 N/mm.

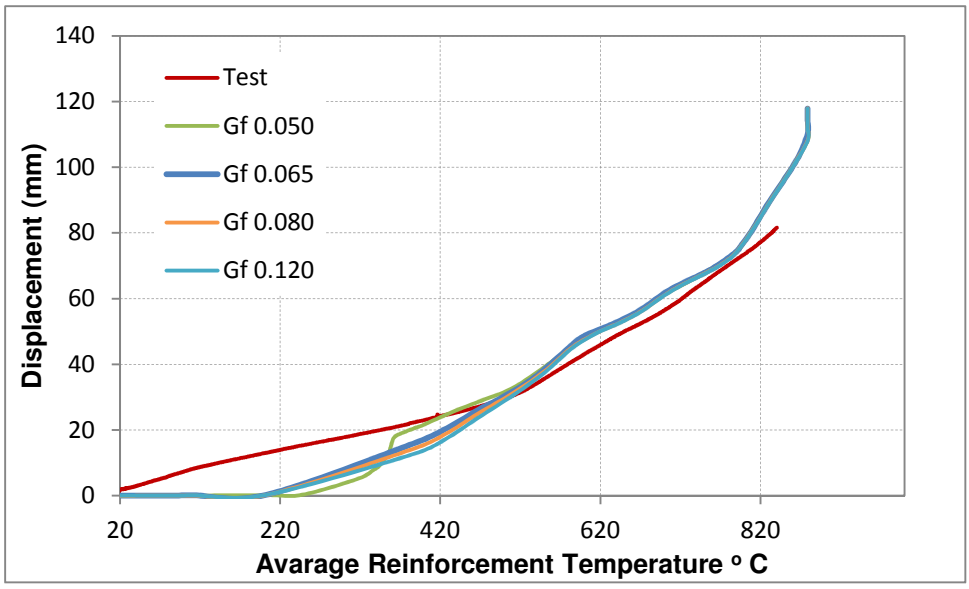

Figure 7-9 Sensitivity of the slab model at elevated temperature to the fracture energy

7.3.1.4 Effect of Tension Softening Curve

Similar to the slab at ambient temperature model, the following approaches were studied to see their effect on modelling the reinforced concrete slab at elevated temperature:-

- Linear Tension Softening.
- Multi-linear Tension Softening.
- Hordijk Nonlinear Tension Softening

Again the results show that Hordijik approach provides more realistic tension softening behaviour than the other two approaches as shown in Figure 7-10. The Hordijik approach was adopted in modelling the slab at both ambient and elevated temperature.

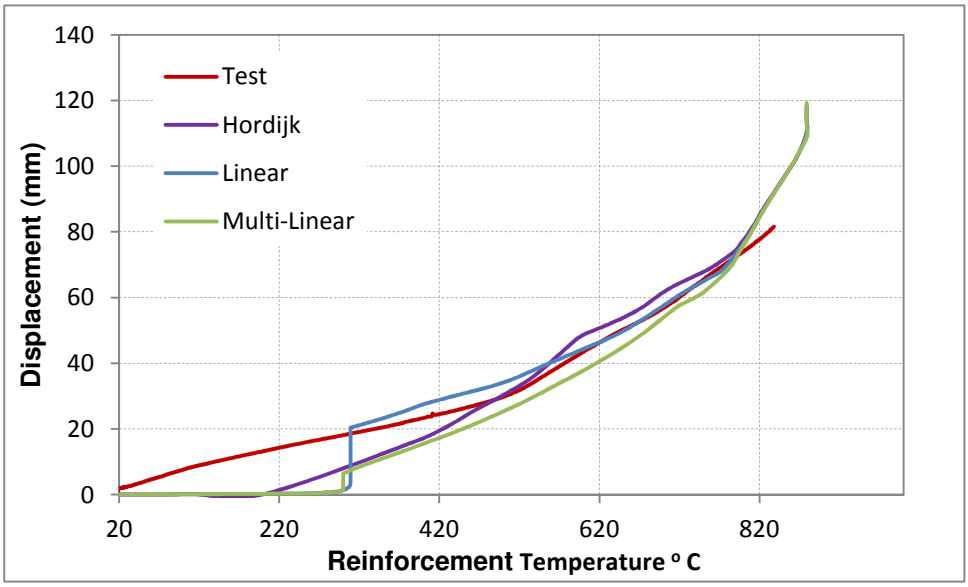

Figure 7-10 Effect of tension softening curve on the slab model at elevated temperature

7.3.2 Thermal Model with ABAQUS

The aim of this model is to predict the temperature distribution through the slab thickness in order to use it as input data in the structural model at elevated temperature. The material properties defined for concrete are its density, thermal conductivity and specific heat. These properties are modelled as temperature-dependent properties according to BSEN1992-1-2. The effect of the reinforcement was not taken into account as its temperature was assumed to be the same as the concrete element superimposed in the same position. The temperature profile for the top surface (unexposed side) and the bottom surface (exposed to fire) of the slab recorded from the test were used as a temperature boundary conditions. The laboratory

temperature of 18℃ was taken as the initial temperature of the slab and 0.8 was the assumed value of the emissivity of the concrete [30].

Once the geometry of the problem, material properties and boundary conditions are set, it can be analysed using a suitable analysis step. In this case, a transient heat transfer step with 8hrs simulated time period was adopted.

The result of interest in this heat transfer analysis is the temperature development through the thickness of the slab. Figure 7-11 shows the temperature distribution in the slab G0F1 at exposed (hot) and unexposed (cold) surfaces and also at the reinforcement (mesh) position that recorded in the test and that obtained from ABAQUS model. It can be seen that ABAQUS with shell elements can provide a good prediction of the temperature distribution through the thickness. The output data files for all the slabs were used in the structural analysis of the slab.

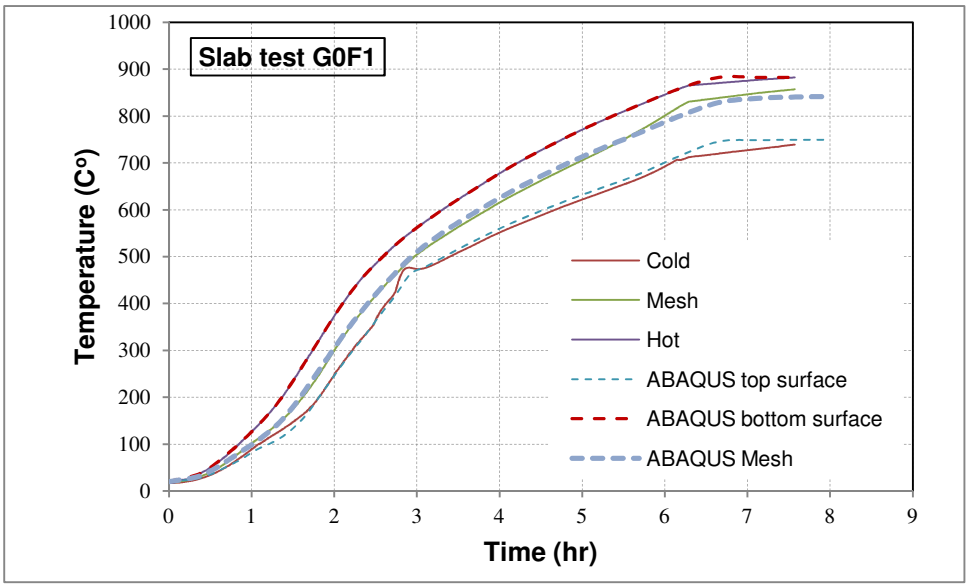

Figure 7-11 Thermal model

7.3.3 Structural Model with ABAQUS

The structural model geometry for the slab at ambient temperature was adopted to model the slab at elevated temperature. As stated before the output file obtained from the thermal model was used as an input data for the temperature distribution through the thickness. The materials mechanical properties such as compressive strength, the thermal expansion, modulus of elasticity and the tensile strength for the reinforcement and the concrete were modelled as temperature dependent properties.

The displacement – reinforcement temperature relationship predicated using the simplified method and ABAQUS finite element program were presented and compared with test results.

The key features of the structural model were as follows:

1- Damage plasticity model was used to model concrete cracking.
2- The STABILIZE algorithm method was adopted as it can predict the nonlinear behaviour of the concrete slab.
3- The reinforcement was assumed to be perfectly bonded to concrete.
4- The crack band width was assumed to be the square root of the area between each integration points.
5- Hordijik's branch was adopted to provide realistic tension softening behaviour of concrete [164].
6- The analysis was terminated once the total step time reached 1.0 or the maximum number of iterations exceeded 1000.

7.3.4 Analysis Results and Discussion

Table 7-4 and Figure 7-12 show the comparison between the test results, the simplified theory model and ABAQUS damage plasticity model for the slabs at elevated temperatures. In the simplified method, the maximum allowable vertical displacement at elevated temperature (Δ_T) was estimated by adding the effects of the thermal curvature (the first term) to the equation proposed by Bailey [142] to calculate the maximum allowable vertical displacement at ambient temperature (Δ_{20}) (the second term) [20] :

$$\Delta_T = \frac{\alpha(T_{Bot} - T_{Top})l^2}{19.2H} + \sqrt{\left(\frac{0.5f_y}{E}\right)\frac{3L^2}{8}}$$ Equation 13

Where α is the coefficient of thermal expansion of concrete, which for normal weight concrete can be taken as 18x10^{-6}, and $(T_{Bot} - T_{Top})$ is the difference between the temperature at the bottom and the top surfaces of the slab and H is the slab thickness.

It can be seen from the results shown in Table 7-4 that this equation gives a conservative prediction for both Δ_{20} and Δ_T, as a result, the simplified method underestimates the temperature at which the reinforcement fracture occurs. According to the test results for this study and the previous study [127] , the displacement at failure at elevated temperature is twice or more the displacement at ambient temperature while the first term adds a small amount to Δ_{20} equation, which already gives conservative prediction to the maximum allowable vertical displacement at ambient temperature, to estimate Δ_T . More numerical work is needed to improve this equation to give more accurate value for the maximum allowable vertical displacement at both conditions

The ABAQUS model gives reasonable predictions for the temperature – displacement relationship, although the predicted displacement at a given temperature at the early stage of the curve is generally lower than that recorded in the test. However, the curve becomes closer to the test curve with increasing the temperature. An explanation for this is was given by Chan [176] who had similar results with a smeared crack model using the DIANA finite element software to model small-scale slabs at elevated temperature. He attributed that to the perfect bond, which is assumed in his model and this study model, between the concrete and the reinforcement. However, the sensitivity test in Section (6.3.4.4) showed that the smeared crack model underestimates the effect of the temperature on the structural behaviour of the slab. The reason for this behaviour in the damage plasticity model maybe due to the reduction factors, given in BSEN1992-1-2[29], which assumes

there is no difference in the compressive strength at temperature ranging between 0 to 200^{o}C which contradicts the test results. Further research is needed to investigate the accuracy of the reduction factors suggested by the EC.

Table 7-4 The results of modelling the slabs at elevated temperature

Slab mark	Δ_{Test} (mm)	T_{Test} (C^o)	Simple model			ABAQUS model				
			Δ_T (mm)	T_{Pred} based on Δ_T (C^o)	T_{pred}/T_{Test}	Δ_T (mm)	T_{Pred} (C^o)	T_{pred}/T_{Test}	T_{Pred} based on Δ_{Test} (C^o)	T_{pred}/T_{Test}
G0F1	85.1	840	34.2	670	0.80	117.9	879.1	1.05	820.3	0.98
G2F1	86.3	844	34.2	670	0.79	117.9	879.1	1.04	826.3	0.98
G2F3	84.2	847	34.2	670	0.79	118.9	879.1	1.04	821.2	0.97
G2F5	92	849	34.2	670	0.79	118.9	879.1	1.04	843.1	0.99
G4F1	110.4	844	34.3	670	0.79	117.8	879.1	1.04	879.1	1.04
G6F1	105.7	847	34.2	670	0.79	118.2	879.1	1.04	867.7	1.03

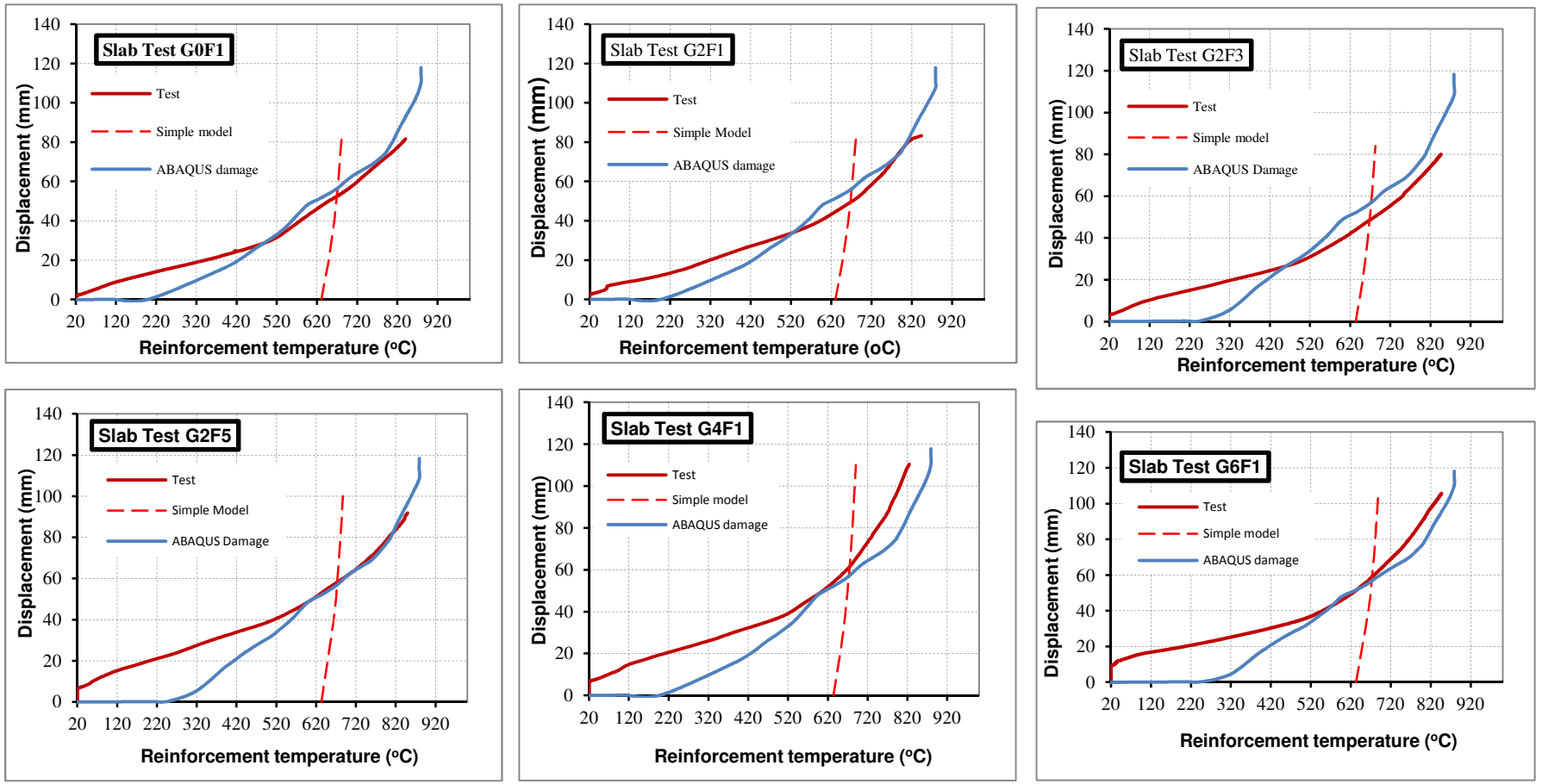

Figure 7-12 The results of modelling the slabs at elevated temperature

7.4 PARAMETRIC STUDY

7.4.1 General

In addition to the parameters stated in Sections (7.2.1) and (7.3.1), the effect of concrete cover depth and load ratio on the behaviour of the reinforced concrete slab at ambient and elevated temperatures were also investigated.

Slab G0F1 was examined for this purpose. Shell elements (S4R) with 4 nodes doubly curved linear reduced integration scheme, and mesh size M6x6 were also adopted in the model. The same material properties that used in modelling the slab at ambient and elevated temperatures were also were used in this section. The Hordijik's branch was also adopted for tension softening behaviour of concrete.

The load – vertical displacement and the reinforcement temperature – vertical displacement relationships predicted from modelling the slab at ambient and elevated temperatures respectively was presented and discussed.

7.4.2 Effect of Concrete Cover Depth

One of the critical parameters in which the designer should take into consideration when designing a reinforced concrete structure is the concrete cover. The concrete cover, which is also called the concrete cover depth, refers to the concrete thickness from the external edge of the reinforcement bar to the outer concrete surface. The concrete cover depth value should meet the design specification, otherwise, it will cause some defects such as surface cracks on building components and steel corrosion, and even reduce the structure strength and durability.

The layer of concrete cover protects the rebar against fire. Since the rebar is near the concrete member surface, it is subjected to a greater temperature increase and its strength is first affected compared with the main body of concrete. It was found that the concrete cover depth has significant influence on the concrete structure ultimate capacity in the presence of fire, However, this influence decreases with an increase in the concrete cover depth [177].

The high concrete cover depth leads to increase in the depth of the flexural tension zone which may lead to larger crack width [178].

BS 8110-1[179] provides tabular data for the minimum concrete cover to reinforcement considering many factors such as: maximum size of aggregate, protection of the steel against corrosion and fire, and spalling.

In this section the effect of different values of the concrete cover was investigated. Figure 7-13 shows that increasing the cover depth up to 10 mm results in a slight decrease in the load carrying capacity for the slab at ambient temperature, however, using 13 mm cover depth results in a significant reduction in the load carrying capacity for a given maximum displacement.

At the same applied load, increasing the concrete cover depth results in an increase in the maximum vertical displacement and temperature at failure for the slab at elevated temperature, as shown in Figure 7-14 and Table 7-5. This means more protection for the rebar against increase in temperature. We can conclude from the results obtained from both models that 10 mm cover depth is a good choice in terms of protecting the rebar with no significant effect in the ultimate load carrying capacity.

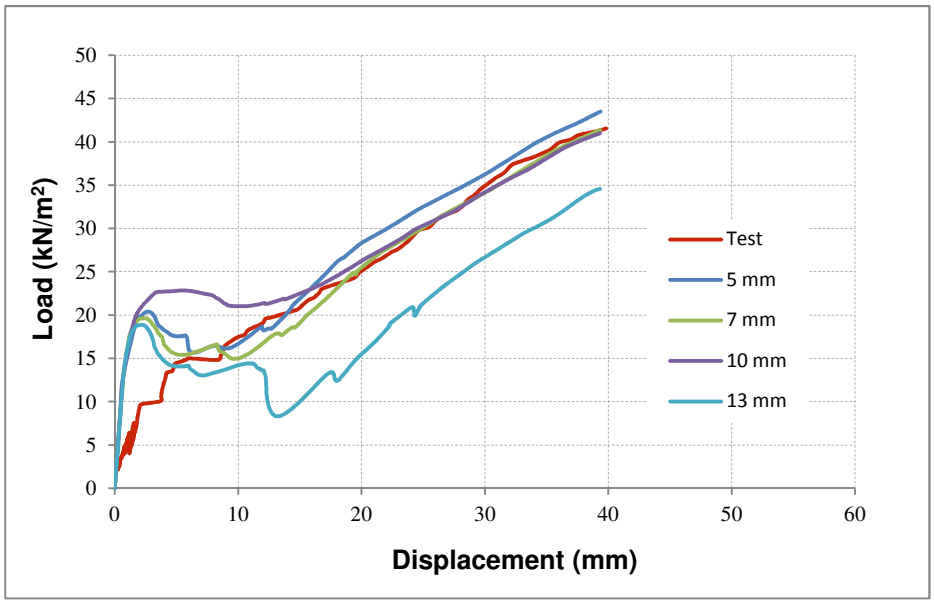

Figure 7-13 Effect of the concrete cover depth (ambient temperature)

Table 7-5 Effect of the concrete cover depth

Concrete cover depth (mm)	5	7	10	13
Temperature (C°)	875	877	879	882
Max. vertical displacement (mm)	113	115	118	121

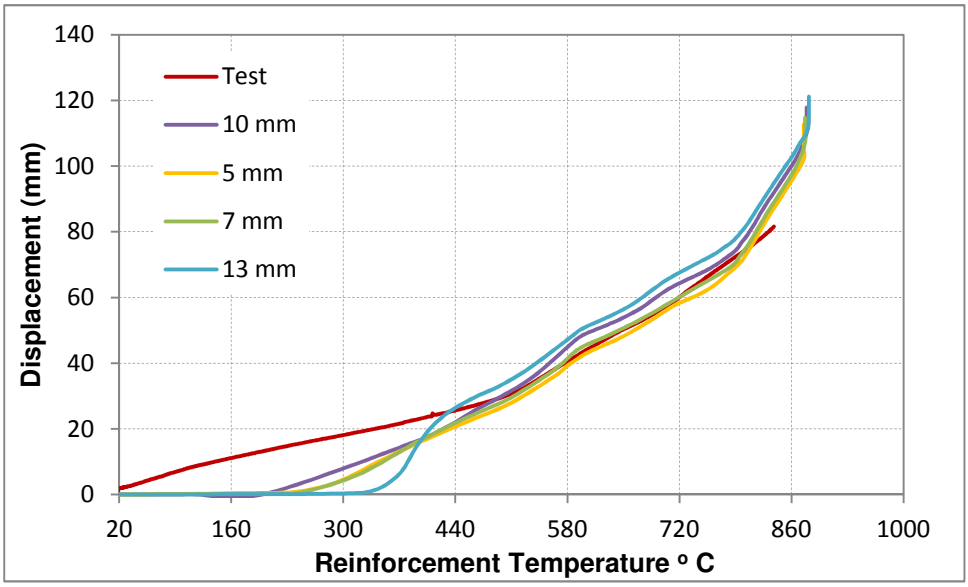

Figure 7-14 Effect of the concrete cover depth (elevated temperature)

7.4.3 Effect of the Load Ratio

The load ratio applied to the slab at the time of the fire could also effect the overall behaviour. As the greater the load applied, the higher the possibility the structure will fail as well as having a lower fire resistance [30].

As expected, at the test maximum displacement, the reinforcement temperature predicted reduced with increasing the load ratio (applied load/yield line load) as shown in Figure 7-15.

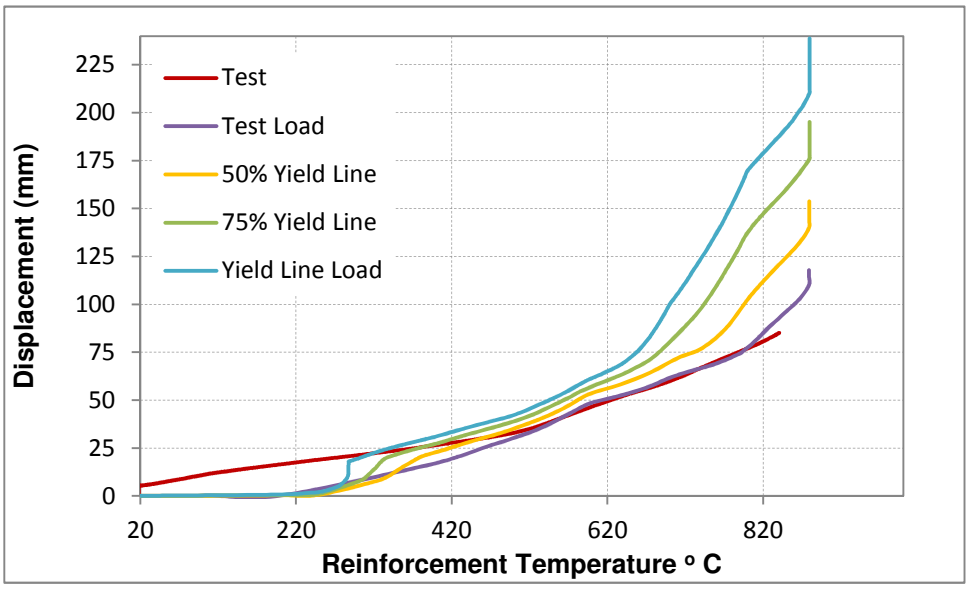

Figure 7-15 Effect of the load ratio

7.5 SUMMARY

The analysis of the small-scale slabs at ambient and elevated temperatures, conducted in this study, was presented in this chapter. Two methods were used for this purpose; the simplified method and the finite element software package ABAQUS.

The results show that the damage plasticity model is more accurate than the smeared crack model, therefore it was adopted in this study.

Sensitivity tests were carried out to ensure more accurate results. These tests have shown that a finite element size of M6X6, the fracture energy value of 0.065 N/mm, the lower bound limit of the tensile strength and the Hordijik approach for tension softening curve is suitable for modelling the slabs in ABAQUS under both ambient and elevated temperatures.

For the slabs at ambient temperature, the results showed a good correlation for the load – displacement relationship between the test and the two models up to the failure loads.
For the slab at elevated temperature, the ABAQUS model gives reasonable prediction for the temperature – displacement relationship while the simplified method gives conservative predictions for the maximum allowable vertical displacement at elevated temperature, as a result, the simplified method underestimates the temperature at which the reinforcement fracture occurs.

The parametric study shows that a 10 mm cover depth is a good choice in terms of protecting the rebar with no significant effect in the ultimate load bearing capacity. Also the study shows that at the test maximum displacement, the reinforcement temperature predicted reduced with increasing the load ratio (applied load/yield line load).

CHAPTER EIGHT

8 CONCLUSION AND FUTURE WORK

8.1 CONCLUSION

From the results obtained in this study it can be concluded that basalt fibre reinforced glass concrete is a good alternative to provide good strength and low thermal conductivity concrete. In addition, it has a good fire resistance and fulfils the requirements for fire protection. It was also found that the current analytical methods need to be developed to give more accurate prediction for the structural behaviour, especially when subjected to fire, of this type of concrete. The conclusions from the results obtained are summarized as follows;

8.1.1 Material Properties

1- The optimum content of glass sand is 20%. At 28 days, there is a 4.23% and 15% enhancement in the compressive strength and the splitting tensile strength respectively.

2- Above 20% glass, a slight reduction (6.6% and 22%) was observed in the compressive strength and the splitting tensile strength when 60% glass was used.

3- Attracting CaO by basalt fibre has a benefit when a higher percentage of glass sand was used to add resistance against the ASR as this reaction will not occur without the availability of this ion.

4- When glass sand and basalt fibre contents increases there was a slight decrease in the amount of heat conducted through the thickness of concrete specimens (a decrease in the thermal conductivity range from 4.35% to 50% at temperature levels between 60oC to 600oC).

5- ABAQUS with heat transfer tests can be used to predict an approximate value for the thermal conductivity. Although this method cannot give accurate values due to different reasons, such as error possibility of the test and assumed specific heat values, this method can be adopted to compare the value of the thermal conductivity of this type of concrete with other concrete instead of heat transfer test results.

8.1.2 Structural Behaviour

The following can be concluded from the results of the small-scale slab tests at ambient and elevated temperature

1. The fracture of the reinforcement is the mode of failure for all the slabs and the fracture was along various yield line patterns at ambient temperature tests and across various yield line patterns at elevated temperature tests.
2. For all slabs there was an increase in the load bearing capacity which highlighted the presence of the membrane action.
3. the increase in glass results in a slight increase (3%) in the enhancement when 20% glass aggregate is used then there is a slight reduction with 40% and 60% glass contents (10% and 11% respectively) compared to the slab with no glass and the same percentage of basalt fibre.For the slabs with 20% glass sand, increasing the volume fraction of basalt fibre to 0.3% (G2F3) results in increasing the enhancement by 9% compared to G2F1 and 12% compared to G0F1.
4. For the elevated temperature test, the enhancement due to membrane action is at least twice higher than that recorded at ambient temperature tests.
5. The results obtained support the recommendation of using the glass aggregate as a partial replacement of the natural sand in concrete with basalt fibre.
6. The temperature differences between the bottom and the top surfaces increases with increasing glass and basalt fibre content (from 126oC for G0F1 to 240oC for G6F1) providing the resistance to the heat transfer.

8.1.3 Simplified and Advanced Analysis

Two numerical methods were adopted to analyze the small-scale slab at ambient and elevated temperatures. The results showed:

1. For the slab at ambient temperature, there was a good correlation for the load – displacement relationship between the test and the two methods up to the failure loads.

2. For the slab at elevated temperature, the ABAQUS model gives reasonable predictions for the temperature – displacement relationship whilst the simplified method gives conservative prediction for the maximum allowable vertical displacement, the simplified method underestimates the temperature at which the reinforcement fracture occurs.
3. The damage plasticity model is more accurate than the smeared crack model to predict the ultimate load and displacement for concrete slab.
4. The results show that the Hordijik approach provides more realistic tension softening behaviour than the Linear Tension Softening and Multi-linear Tension Softening.
5. The parametric study shows that 10 mm cover depth is a good choice in terms of protecting the rebar with no significant effect in the ultimate load bearing capacity.
6. The test maximum displacement, the reinforcement temperature predicted reduced with increasing the load ratio (applied load/yield line load).

8.2 FUTURE WORK

It is possible to use the ABAQUS with the heat transfer test to predict the thermal properties of concrete. However, further work might be needed to improve this method and reduce the number of assumptions.

The effect of the reinforcement ratio is not clear in this study. This needs further research to investigate the effect of the reinforcement ratio on the enhancement due to membrane action for fibre reinforced concrete.

The simplified method is underestimating the temperature at which the reinforcement fracture occurs. More numerical work is needed to improve the equations that have been used to predict the maximum allowable vertical displacement at ambient and elevated temperatures to give more accurate and less conservative value at both conditions.

Further research is also needed to investigate the accuracy of the reduction factors (of concrete strength) suggested by the EC.

REFRENCES

1. WBCSD, *Energy Efficiency In Building Fact And Trend, Summary Report*. 2008, World Business Council For Sustainable Development. p. 42.

2. *Concrete and Fire, The Concrete Centre,ISBN 1-904818-11-0, 2004*

3. Buchanan, A., *Structural design for fire safety*. Vol. 179. 2001: Wiley Chichester, UK.

4. Box, T.E.T. *Thermal Conductivity of Some Common Materials*. Available from: http://www.engineeringtoolbox.com/thermal-conductivity-d_429.html.

5. Park, S., B. Lee, and J. Kim, *Studies on mechanical properties of concrete containing waste glass aggregate.* Cement and Concrete Research, 2004. **34**(12): p. 2181-2189.

6. Petrella, A., Petrella, M. , Boghetich, G. , Petruzzelli, D. , Calabrese, D. , Stefanizzi, P. , De Napoli, D. , Guastamacchia, M., *Recycled waste glass as aggregate for lightweight concrete.* Construction Materials, 2007. **160**(4): p. 165-170.

7. Jin, W., C. Meyer, and S. Baxter, *"Glascrete"—Concrete with Glass Aggregate.* ACI Materials Journal, 2000. **97**(2): p. 208-213.

8. Meyer, R., C, Shimanovich, S, Vilkner, G, *Precast Concrete Wall Panels with Glass Concrete.* Final Report , New York State Energy Research and Development Authority (NYSERDA 4710),Department of Civil Engineering and Engineering Mechanics, Columbia University. , 2002: p. 45.

9. Helmuth, R., Stark, D. , Diamond, S. , Moranville-Regourd, M, *Alkali-silica reactivity: An overview of research.* Contract, 1993. **100**: p. 202.

10. Sabir, B., S. Wild, and J. Bai, *Metakaolin and calcined clays as pozzolans for concrete: a review.* Cement and Concrete Composites, 2001. **23**(6): p. 441-454.

11. Justice, J., Kennison, LH. , Mohr, BJ. , Beckwith, SL. , McCormick, LE. , Wiggins, B. , Zhang, ZZ. , Kurtis, KE. *Comparison of two metakaolins and silica fume used as supplementary cementitious materials*. 2005.

12. Park, S.-B. and B.-C. Lee, *Studies on expansion properties in mortar containing waste glass and fibers.* Cement and Concrete Research, 2004. **34**(7): p. 1145-1152.

13. Deák, T. and T. Czigány, *Chemical composition and mechanical properties of basalt and glass fibers: A comparison.* Textile Research Journal, 2009. **79**(7): p. 645.

14. Lopresto, V., C. Leone, and I. De Iorio, *Mechanical characterization of basalt fibre reinforced plastic.* Composites Part B: Engineering, 2011.

15. Di Ludovico, M., A. Prota, and G. Manfredi, *Concrete Confinement Using Innovative Materials: Basalt Reinforced Mortar (BRM).* CCC2008-Challenges for Civil Construction, Torres Marques et al.(Eds)© FEUP, Porto, 2008: p. 124-125.

16. Ramachandran, B., V. Velpari, and N. Balasubramanian, *Chemical durability studies on basalt fibres.* Journal of Materials Science, 1981. **16**(12): p. 3393-3397.

17. Sim, J., C. Park, and D. Moon, *Characteristics of basalt fiber as a strengthening material for concrete structures.* Composites Part B: Engineering, 2005. **36**(6-7): p. 504-512.

18. Li, W. and J. Xu, *Mechanical properties of basalt fiber reinforced geopolymeric concrete under impact loading.* Materials Science and Engineering: A, 2009. **505**(1-2): p. 178-186.

19. Dias, D. and C. Thaumaturgo, *Fracture toughness of geopolymeric concretes reinforced with basalt fibers.* Cement and Concrete Composites, 2005. **27**(1): p. 49-54.

20. Bailey, C.G. and W.S. Toh, *Behaviour of concrete floor slabs at ambient and elevated temperatures.* Fire Safety Journal, 2007. **42**(6-7): p. 425-436.

21. Neville, A., *Properties of Concrete*, ed. 4th. 1996, New York: John Wiley & Sons Inc. 844.

22. YANG, S., KIM, N, KIM, J, Park, J, *Experimental Measurement of Concrete Thermal Expansion.* Journal of the Eastern Asia Society for Transportation Studies, 2003. **5**: p. 1035-1048.

23. Cruz, C. and M. Gillen, *Thermal expansion of Portland cement paste, mortar and concrete at high temperatures.* Fire and Materials, 1980. **4**(2): p. 66-70.

24. *United States Department of Transportation- Federal Highway Administration "Thermal Coefficient of Portland Cement Concrete".* 2006; Available from: http://www.fhwa.dot.gov/pavement/pccp/thermal.cfm.

25. Walker, S., Bloem, D. L., Mullen, W. G., *Effects of Temperature Changes on Concrete as Influenced by Aggregates.* ACI Material Journal, 1952. **48**(4): p. 661-679.

26. Takeuchi, M., Hiramoto, M. , Kumagai, N. , Yamazaki, N. , Kodaira, A. , Sugiyama, K. *Material Properties of Concrete and Steel Bars at Elevated Temperatures*. 1993.

27. Schneider, U., *Concrete at high temperatures--A general review.* Fire Safety Journal, 1988. **13**(1): p. 55-68.

28. Kodur, V. and M. Sultan, *Effect of temperature on thermal properties of high-strength concrete.* Journal of materials in civil engineering, 2003. **15**(2): p. 101-107.

29. BSEN1992:1-2, *Eurocode 2, Design of Concrete Structures. General Rules - Structural Fire Design*. 2004, British Standards.

30. Ellobody, E. and C.G. Bailey, *Modelling of unbonded post-tensioned concrete slabs under fire conditions.* Fire Safety Journal, 2009. **44**(2): p. 159-167.

31. Bergeson, K., *Thermal expansion of concretes: case study in Iowa.* Journal of materials in civil engineering, 1995. **7**: p. 246.

32. *Building research board,The thermal expansion of concrete. National building studies, Technical paper, No. 7. HMSO, 1950.*

33. Khan, M., *Factors affecting the thermal properties of concrete and applicability of its prediction models.* Building and Environment, 2002. **37**(6): p. 607-614.

34. Franco, A., *An apparatus for the routine measurement of thermal conductivity of materials for building application based on a transient hot-wire method.* Applied Thermal Engineering, 2007. **27**(14-15): p. 2495-2504.

35. Nenad Stepanić, a., Nenad Milošević, *Correction on the Influence of Thermal Contact Resistance in Thermal Conductivity Measurements Using the Guarded Hot Plate Method.* Serbian Journal Of Electrical Engineering, 2009. **6**(3): p. 479-488.

36. Sass, J.H., C. Stone, and R.J. Munroe, *Thermal conductivity determinations on solid rock — a comparison between a steady-state divided-bar apparatus and a commercial transient line-source device.* Journal of Volcanology and Geothermal Research, 1984. **20**(1-2): p. 145-153.

37. Kim, K., Jeon, SE. , Kim, JK. , Yang, S, *An experimental study on thermal conductivity of concrete.* Cement and Concrete Research, 2003. **33**(3): p. 363-371.

38. Choktaweekarn, P., W. Saengsoy, and S. Tangtermsirikul, *A model for predicting thermal conductivity of concrete.* Magazine of Concrete Research, 2009. **61**(4): p. 271-280.

39. Toman, J. and R. Cerny, *Temperature and Moisture Dependence of the Specific Heat of High Performance Concrete.* Acta Politechnica-Czech Technical University in Prague, 2001. **41**(1): p. 5-7.

40. Kim, J., K. Kim, and J. Yang, *Thermal analysis of hydration heat in concrete structures with pipe-cooling system.* Computers & Structures, 2001. **79**(2): p. 163-171.

41. Incropera, F. and D. DeWitt, *Introduction to heat transfer*. 1996: John Wiley & Sons New York.

42. Chan, Y.N., G.F. Peng, and M. Anson, *Residual strength and pore structure of high-strength concrete and normal strength concrete after exposure to high temperatures.* Cement and Concrete Composites, 1999. **21**(1): p. 23-27.

43. Dias, W., G. Khoury, and P. Sullivan, *Mechanical properties of hardened cement paste exposed to temperatures up to 700 C (1292 F).* ACI Materials Journal, 1990. **87**(2).

44. Fletcher, I., Borg, A. , Hitchen, N. , Welch, S., *Performance of concrete in fire: a review of the state of the art, with a case study of the windsor tower fire.* 2006.

45. Schneider, U., *Behaviour of concrete at high temperatures.* RILEM committee, 1985.

46. Xing, Z., Beaucour, A.L. , Hebert, R. , Noumowe, A., Ledesert, B., *Influence of the nature of aggregates on the behaviour of concrete subjected to elevated temperature.* Cement and Concrete Research, 2011. **41**(4): p. 392-402.

47. Anderberg, Y., and Therlandersson, S., , *Stress and deformation characteristics of concrete at high temperatures, Bulletin 55, Division of Structural Mechanics and Concrete Construction, Lund Institute of Technology, Lund, Sweden.* 1976.

48. BSEN1991:1-2, E., *Actions on Structures*. 2002, British Standards.

49. Malhotra, H.L., *Spalling of Concrete in Fires.* Technical Note NO.118, Construction Industrial Research and Information Association (CIRIA), 1984.

50. Khoury, G. and Y. Anderberg, *Concrete spalling review.* Fire Safety Design AB (FSD), Swedish National Road Administration, 2000.

51. Hertz, K.D. and L.S. Sørensen, *Test method for spalling of fire exposed concrete.* Fire Safety Journal, 2005. **40**(5): p. 466-476.

52. Han, C., Hwang, YS. , Yang, SH. , Gowripalan, N, *Performance of spalling resistance of high performance concrete with polypropylene fiber contents and lateral confinement.* Cement and Concrete Research, 2005. **35**(9): p. 1747-1753.

53. Campione, G., N. Miraglia, and M. Papia, *Mechanical properties of steel fibre reinforced lightweight concrete with pumice stone or expanded clay aggregates.* Materials and Structures, 2001. **34**(4): p. 201-210.

54. Hossain, K. *Performance of volcanic pumice concrete with special reference to high rise composite construction*. 1999: Thomas Telford.

55. Demirboa, R., *Effects of expanded perlite aggregate and mineral admixtures on the compressive strength of low-density concretes.* Cement and Concrete Research, 2001. **31**(11): p. 1627-1632.

56. Demirboa, R. and R. Gül, *The effects of expanded perlite aggregate, silica fume and fly ash on the thermal conductivity of lightweight concrete.* Cement and Concrete Research, 2003. **33**(5): p. 723-727.

57. C1113-99, A., *Standard test method for thermal conductivity of refractories by hot wire (platinum resistance thermometer technique*. 2004, American Society for Testing and Materials.

58. Wasserman, R. and A. Bentur, *Effect of lightweight fly ash aggregate microstructure on the strength of concretes.* Cement and Concrete Research, 1997. **27**(4): p. 525-537.

59. Vaysburd, A., *Durability of lightweight concrete bridges in severe environments.* Concrete International, 1996. **18**(7): p. 33-38.

60. Uysal, H. and R. Demirboa, *The effects of different cement dosages, slumps, and pumice aggregate ratios on the thermal conductivity and density of concrete.* Cement and Concrete Research, 2004. **34**(5): p. 845-848.

61. Ünal, O., T. Uygunoglu, and A. Yildiz, *Investigation of properties of low-strength lightweight concrete for thermal insulation.* Building and Environment, 2007. **42**(2): p. 584-590.

62. Saradhi Babu, D., K. Ganesh Babu, and T. Wee, *Properties of lightweight expanded polystyrene aggregate concretes containing fly ash.* Cement and Concrete Research, 2005. **35**(6): p. 1218-1223.

63. Babu, D., K. Ganesh Babu, and W. Tiong-Huan, *Effect of polystyrene aggregate size on strength and moisture migration characteristics of lightweight concrete.* Cement and Concrete Composites, 2006. **28**(6): p. 520-527.

64. Bouvard, D., Chaix, JM. , Dendievel, R. , Fazekas, A. , Létang, JM. , Peix, G. , Quenard, D, *Characterization and simulation of microstructure and properties of EPS lightweight concrete.* Cement and Concrete Research, 2007. **37**(12): p. 1666-1673.

65. Behera, J., Nayak, BD. , Ray, HS. , Sarangi, B, *Light weight concrete with sintered flyash aggregate: A study on partial replacement to normal granite aggregate.* Journal of the Institution of Engineers. India. Civil Engineering Division, 2004. **85**(aout): p. 84-87.

66. Kayali, O., *Fly ash lightweight aggregates in high performance concrete.* Construction and Building Materials, 2008. **22**(12): p. 2393-2399.

67. Demirboga, R., *Influence of mineral admixtures on thermal conductivity and compressive strength of mortar.* Energy and buildings, 2003. **35**(2): p. 189-192.

68. Bilodeau, A. and V.M. Malhotra, *High-volume fly ash system: concrete solution for sustainable development.* ACI Materials Journal, 2000. **97**(1).

69. Demirboga, R., *Thermal conductivity and compressive strength of concrete incorporation with mineral admixtures.* Building and Environment, 2007. **42**(7): p. 2467-2471.

70. Kodur, V. and W. Khaliq, *Effect of Temperature on Thermal Properties of Different Types of High-Strength Concrete.* Journal of materials in civil engineering, 2011. **23**: p. 793.

71. Eldin, N. and A. Senouci, *Measurement and prediction of the strength of rubberized concrete.* Cement and Concrete Composites, 1994. **16**(4): p. 287-298.

72. Topçu, I., *The properties of rubberized concretes.* Cement and Concrete Research, 1995. **25**(2): p. 304-310.

73. Topçu, B., *Assessment of the brittleness index of rubberized concretes.* Cement and Concrete Research, 1997. **27**(2): p. 177-183.

74. Toutanji, H., *The use of rubber tire particles in concrete to replace mineral aggregates.* Cement and Concrete Composites, 1996. **18**(2): p. 135-139.

75. Skripki nas, G., A. Grinys, and B. ernius, *Deformation properties of concrete with rubber waste additives.* Materials Science [Medžiagotyra], 2007. **13**(3): p. 219-223.

76. Khatib, Z. and F. Bayomy, *Rubberized Portland cement concrete.* Journal of materials in civil engineering, 1999. **11**: p. 206.

77. Güneyisi, E., M. Gesoglu, and T. Özturan, *Properties of rubberized concretes containing silica fume.* Cement and Concrete Research, 2004. **34**(12): p. 2309-2317.

78. Sukontasukkul, P., *Use of crumb rubber to improve thermal and sound properties of pre-cast concrete panel.* Construction and Building Materials, 2009. **23**(2): p. 1084-1092.

79. Polley, C., S. Cramer, and V. Rodolfo, *Potential for using waste glass in Portland cement concrete.* Journal of materials in civil engineering, 1998. **10**: p. 210.

80. Topçu, B. and M. Canbaz, *Properties of concrete containing waste glass.* Cement and Concrete Research, 2004. **34**(2): p. 267-274.

81. Meyer, C. and S. Baxter, *Use of Recycled Glass and Fly Ash for Precast Concrete, Final Report 98-18, New York State Energy Research and Development Authority, Albany, NY*. 1998, October.

82. ASTM, C., *1260-05. Standard Test Method for Potential Alkali Reactivity of Aggregates (Mortar-Bar Method).* Section. **4**: p. 676-680.

83. McCoy, W. and A. Caldwell. *New approach to inhibiting alkali-aggregate expansion*. 1951: ACI.

84. Xie, Z., W. Xiang, and Y. Xi, *ASR potentials of glass aggregates in water-glass activated fly ash and portland cement mortars.* Journal of materials in civil engineering, 2003. **15**: p. 67.

85. Diamond, S., *Mechanisms Of Alkali-Silica Reaction, In Alkali-Aggregate Reaction, Proceeding 8th International Conference, Kyoto, pp. 83-94. Sited by Neville (1995)* 1989.

86. Babu, K. and D. Babu, *Behaviour of lightweight expanded polystyrene concrete containing silica fume.* Cement and Concrete Research, 2003. **33**(5): p. 755-762.

87. Curcio, F., B.A. DeAngelis, and S. Pagliolico, *Metakaolin as a pozzolanic microfiller for high-performance mortars.* Cement and Concrete Research, 1998. **28**(6): p. 803-809.

88. Düzgün, O., R. Gül, and A. Aydin, *Effect of steel fibers on the mechanical properties of natural lightweight aggregate concrete.* Materials Letters, 2005. **59**(27): p. 3357-3363.

89. Balaguru, P. and M. Dipsia, *Properties of Fiber Reinforced High-Strength Semi-Lightweight Concrete.* ACI Materials Journal, 1993. **90**(5).

90. Lie, T.T. and V. Kodur, *Thermal properties of fibre-reinforced concrete at elevated temperatures.* 2010.

91. Lie, T. and V. Kodur, *Thermal and mechanical properties of steel-fibre-reinforced concrete at elevated temperatures.* Canadian Journal of Civil Engineering, 1996. **23**(2): p. 511-517.

92. Song, P., S. Hwang, and B. Sheu, *Strength properties of nylon-and polypropylene-fiber-reinforced concretes.* Cement and Concrete Research, 2005. **35**(8): p. 1546-1550.

93. Chen, P. and D. Chung, *Carbon fiber reinforced concrete for smart structures capable of non-destructive flaw detection.* Smart Materials and Structures, 1993. **2**: p. 22.

94. Chung, D., *Cement reinforced with short carbon fibers: a multifunctional material.* Composites Part B: Engineering, 2000. **31**(6-7): p. 511-526.

95. Toutanji, H., El-Korchi, T. , Katz, RN. , Leatherman, GL, *Behaviour of carbon fiber reinforced cement composites in direct tension.* Cement and Concrete Research, 1993. **23**(3): p. 618-626.

96. Mingchao, W., Zuoguang, Z. , Yubin, L. , Li, M. , Sun, Z, *Chemical Durability and Mechanical Properties of Alkali-proof Basalt Fiber and its Reinforced Epoxy Composites.* Journal of Reinforced Plastics and Composites, 2008.

97. Park, S. and B. Lee, *Mechanical properties of carbon-fiber-reinforced polymer-impregnated cement composites.* Cement and Concrete Composites, 1993. **15**(3): p. 153-163.

98. Topçu, B. and M. Canbaz, *Effect of different fibers on the mechanical properties of concrete containing fly ash.* Construction and Building Materials, 2007. **21**(7): p. 1486-1491.

99. Köksal, F., Altun, F. , Yigit, I. , Sahin, Y, *Combined effect of silica fume and steel fiber on the mechanical properties of high strength concretes.* Construction and Building Materials, 2008. **22**(8): p. 1874-1880.

100. Atis, C. and O. Karahan, *Properties of steel fiber reinforced fly ash concrete.* Construction and Building Materials, 2009. **23**(1): p. 392-399.

101. Sari, D. and A. Pasamehmetoglu, *The effects of gradation and admixture on the pumice lightweight aggregate concrete.* Cement and Concrete Research, 2005. **35**(5): p. 936-942.

102. Aruntas, H., Cemalgil, S. , Simsek, O. , Durmus, G. , Erdal, M, *Effects of super plasticizer and curing conditions on properties of concrete with and without fiber.* Materials Letters, 2008. **62**(19): p. 3441-3443.

103. Harmathy, T., *Fire Safety Design and Concrete (Concrete Design and Construction Series).* 1993, Longman Scientific and Technical, London, UK.

104. *BSEN1993:1-2, Eurocode 3, Design of Steel Structures. Part 1.2. General Rules. Structural Fire Engineering. British Standards, London 2005.*

105. Eurocode, C., *3: Design of Steel Structures, Part 1-1;"General Rules and Rules for Buildings".* BS-EN 1993-1-2: 2005.

106. Kirby, B. and R. Preston, *High temperature properties of hot-rolled, structural steels for use in fire engineering design studies.* Fire Safety Journal, 1988. **13**(1): p. 27-37.

107. Johansen, K., *Yield-line theory*. 1962: Cement and Concrete Association.

108. Bailey, C., T. Lennon, and D. Moore, *The behaviour of full-scale steel-framed buildings subjected to compartment fires.* Structural Engineer, 1999. **77**: p. 15-21.

109. Bailey, C. and D. Moore, *The structural behaviour of steel frames with composite floorslabs subject to fire. Pt. 2: design.* Structural Engineer, 2000.

110. Lange, D.J., *Risk and Performance Based Fire Safety Design of Steel and Composite Structures, PhD thesis*. 2009, The University of Edinburgh.

111. Cameron, N. and A. Usmani, *New design method to determine the membrane capacity of laterally restrained composite floor slabs in fire.* Part, 2005. **1**: p. 28–33.

112. Salami, A., *Equation for predicting the strength of fully-clamped two-way reinforced concrete slabs.* Proceedings of the ICE-Structures and Buildings. **104**(1): p. 101-107.

113. Taplin, G. and A. Hon, *Compressive Membrane Action in Bridge Deck Slabs.*

114. Ockleston, A.J., *Load tests on a 3-storey reinforced concrete building in Johannesburg.* The Structural Engineer, 1955. **33**(10): p. 304–322.

115. Powell, D., *The ultimate strength of concrete panels subjected to uniformly distributed loads.* Cambridge University Thesis, 1956.

116. Wood, R., *Plastic and elastic design of slabs and plates: with particular reference to reinforced concrete floor slabs*. 1961: Thames and Hudson, London.

117. Park, R. *Ultimate Strength Of Rectangular Concrete Slabs Under Short-Term Uniform Loading With Edges Restrained Against Lateral Movement*. 1964: Ice Virtual Library.

118. Wang, Y. *Tensile membrane action in slabs and its application to the Cardington fire tests*. 1997: Taylor & Francis.

119. Taylor, R., *A note on a possible basis for a new method of ultimate load design of reinforced concrete slabs.* Magazine of Concrete Research, 1965. **17**(53): p. 183-186.

120. Sawczuk, A. and L. Winnicki, *Plastic behavior of simply supported reinforced concrete plates at moderately large deflections.* International Journal of Solids and Structures, 1965. **1**(1): p. 97-110.

121. Hayes, B., *Allowing for membrane action in the plastic analysis of rectangular reinforced concrete slabs.* Magazine of Concrete Research, 1968. **20**(65): p. 205-212.

122. Bailey, C., D. White, and D. Moore, *The tensile membrane action of unrestrained composite slabs simulated under fire conditions.* Engineering Structures, 2000. **22**(12): p. 1583-1595.

123. Bailey, C., *Membrane action of unrestrained lightly reinforced concrete slabs at large displacements.* Engineering Structures, 2001. **23**(5): p. 470-483.

124. Lim, L., *Membrane action in fire exposed concrete floor systems.* Department of Civil Engineering of the University of Canterbury, Christchurch, 2003.

125. Foster, S., Bailey, CG. , Burgess, IW. , Plank, RJ, *Experimental behaviour of concrete floor slabs at large displacements.* Engineering Structures, 2004. **26**(9): p. 1231-1247.

126. Foster SJ, Burgess IW, and P. RJ, *Experimental behaviour of model-scale concrete floor slabs at large displacement and high temperatures. In: Proc. second international conference on steel and composite structures.* 2004: p. 1268–1282.

127. Bailey, C.G. and W.S. Toh, *Small-scale concrete slab tests at ambient and elevated temperatures.* Engineering Structures, 2007. **29**(10): p. 2775-2791.

128. *BS EN 12350-2:2009 , Testing Fresh Concrete: Slump Test, British Standards. .*

129. *BS EN 12390-3:2002 ,Testing Hardened Concrete Part 3: Compressive Strength of Test Specimens, British Standard. .*

130. *BS EN 12390-6:2000 ,Testing Hardened Concrete Part 6: Tensile Spliting Strength of Test Specimens, British Standard. .*

131. Alhumoud, J., N. Al-Mutairi, and M. Terro, *Recycling crushed glass in concrete mixes.* International Journal of Environment and Waste Management, 2008. **2**(1): p. 111-124.

132. Ismail, Z. and E. AL-Hashmi, *Recycling of waste glass as a partial replacement for fine aggregate in concrete.* Waste Management, 2009. **29**(2): p. 655-659.

133. Kou, S. and C. Poon, *Properties of self-compacting concrete prepared with recycled glass aggregate.* Cement and Concrete Composites, 2009. **31**(2): p. 107-113.

134. *EuroLightCon, LWAC Material Properties State-ofthe-Art, Document BE96-3942/R2, December 1998.*

135. Rabinovich, F., V. Zueva, and L. Makeeva, *Stability of basalt fibers in a medium of hydrating cement.* Glass and ceramics, 2001. **58**(11): p. 431-434.

136. Tasong, W., C. Lynsdale, and J. Cripps, *Aggregate-cement paste interface. II: Influence of aggregate physical properties.* Cement and Concrete Research, 1998. **28**(10): p. 1453-1465.

137. Li, X., *Study on Thermal Resistance of Basalt Filament Yarn.* Advanced Materials Research, 2011. **146**: p. 666-669.

138. Sukontasukkul, P. and C. Chaikaew, *Properties of concrete pedestrian block mixed with crumb rubber.* Construction and Building Materials, 2006. **20**(7): p. 450-457.

139. Kemp, K.O., *Yield of a Square Reinforced Slab on Simple Supports, Allowing for Membrane Forces* The Structural Engineering, 1967. **45**(7): p. 6.

140. BSEN1994-1-2:Eurocode4, *Design of composite steel and concrete structures. Part 1.2 Structural Fire Design*. 2005, European Committee for Standardisation.

141. Newman, G.M., J.T. Robinson, and C.G. Bailey, *Fire Safe Design;A New Approach to Multi-Story Steel-Framed Buildings* in *SCI publication*. 2000. p. 288.

142. Bailey, C.G., *Steel Structures Supporting Composite Floor Slabs: Design for Fire* 2001, BRE digest 462: Watford: The Building Research Establishment.

143. Newman, G.M., J.T. Robinson, and C.G. Bailey, *Fire Safe Design;A New Approach to Multi-Story Steel-Framed Buildings* in *2nd ed. SCI publication*. 2006. p. 288.

144. Bailey, C.G., W.S. Toh, and B.M. Chan, *Simplified and Advanced Analysis of Membrane Action of Concrete Slabs.* ACI Structural Journal, 2008. **105**(1): p. 30-40.

145. Bailey, C.G., *Efficient arrangement of reinforcement for membrane behaviour of composite floor slabs in fire conditions.* Journal of Constructional Steel Research, 2003. **59**(7): p. 931-949.

146. *Dassault Systemes Simula Corp., ABAQUS Standard / Explicit User's Manual*. 2004: Providence, R1, USA.

147. Pepper, D.w. and J.C. Heinrich, *The finite element method: basic concepts and applications*. 1992, Hemisphere Publishing Corporation.

148. KWAK, H.-G. and F.C. FILIPPOU, *Finite Element Analysis of Reinforced Concrete Structures Under Monotonic Loads, Structural Engineering Mechanics and Materials*. 1990. p. Report No.USB/SEMM-90/14, 120 pp.

149. Wang, C., *Introduction to fracture mechanics*. 1996, DSTO Aeronautical and Maritime Research Laboratory. p. 72.

150. Gdoutos, E., *Fracture mechanics: an introduction*. 2005: Kluwer Academic Pub.

151. Bažant, Z. and B. Oh, *Crack band theory for fracture of concrete.* Materials and structures, 1983. **16**(3): p. 155-177.

152. Hillerborg, A., M. Modéer, and P.E. Petersson, *Analysis of crack formation and crack growth in concrete by means of fracture mechanics and finite elements.* Cement and Concrete Research, 1976. **6**(6): p. 773-781.

153. Hillerborg, A., *Application of the fictitious crack model to different types of materials.* International Journal of Fracture, 1991. **51**(2): p. 95-102.

154. Nago, D., Scordelis A.C., *Finite Element Analysis of Reinforced Concrete Beams.* ACI Journal, 1976. **64**(14): p. 152-163.

155. Prasad, M. and C. Krishnamoorthy, *Computational model for discrete crack growth in plain and reinforced concrete.* Computer Methods in Applied Mechanics and Engineering, 2002. **191**(25-26): p. 2699-2725.

156. Huang, Z., Burgess, I., Plank, J., *Modeling Membrane Action of Concrete Slabs in Composite Buildings in Fire. I: Theoretical Development.* Journal of Structural Engineering, 2003. **129**(8): p. 1093-1102.

157. Zhaohui Huang, I.W.B., Roger J. Plank, *Modeling Membrane Action of Concrete Slabs in Composite Buildings in Fire. II: Validations.* Journal of Structural Engineering, 2003. **129**(8): p. 1103-1112.

158. Rots, J.G., *Computational Modeling of Concrete Fracture*. 1988, Delft University of Technology.

159. Oliver, J., *A consistent characteristic length for smeared cracking models.* International Journal for Numerical Methods in Engineering, 1989. **28**(2): p. 461–474.

160. Mosalam, K. and G. Paulino, *Evolutionary characteristic length method for smeared cracking finite element models.* Finite elements in Analysis and Design, 1997. **27**(1): p. 99-108.

161. *Comite Euro-International Du Beton (CEB), RC elements under cyclic loading, state of the art report*. 1996, Thomas Telford, London.

162. Reinhardt, H., J. Blaauwendraad, and J. Jongedijk. *Temperature development in concrete structures taking account of state dependent properties*. 1982.

163. Hordijk, D., *Local approach to fatigue of concrete, PhD thesis, Delft University of Technology, 1991.*

164. Cornelissen, H., D. Hordijk, and H. Reinhardt, *Experimental determination of crack softening characteristics of normalweight and lightweight concrete.* Heron, 1986. **31**(2): p. 45-56.

165. CEB-FIPM, *Thomas Telford Ltd.* London (1993), 1990.

166. Nielsen, C. and N. Biéani *Residual fracture energy of high-performance and normal concrete subject to high temperatures.* Materials and structures, 2003. **36**(8): p. 515-521.

167. Gilbert, R. and R. Warner, *Tension stiffening in reinforced concrete slabs.* Journal of the structural division, 1978. **104**(12): p. 1885-1900.

168. Branson, D. and G. Metz, *Instantaneous and time-dependent deflections of simple and continuous reinforced concrete beams*. 1963: Dept. of Civil Engineering and Auburn Research Foundation, Auburn University.

169. *American Concrete Institute (ACI) , Building Cod Requierments for Structural Concrete, ACI Committee 318, Detroit.* 2005.

170. *CEN: Eurocode 2: Design of Concrete Structures Part I-I: General Rules for Buildings.* 1992.

171. *BS, Structural Use of Concrete Part 2, Code of Practice for Special Circumstances, BS8100.* 1985.

172. Malm, R., *Shear cracks in concrete structures subjected to in-plane stresses.* Trita-BKN. Bulletin, 2006. **88**.

173. Lubliner J.J. , Oliver S.O. , and O. E., *A plastic-damage model for concrete, International Journal of Solids and Structures, 25, 3(1989)229-326.*

174. Flazon, B., Aliabadi, M., *Buckling and postbuckling structures: experimental, analytical and numerical studies*. 2008, Imperial College Press, London. p. 504.

175. *ABAQUS Theory Manual, User Manual and Example Manual, Version 6.8, Providence, RI.* 2009.

176. Chan, B.M., *Membrane Action of Concrete Floor Slabs at Ambient and Elevated Temperatures*. 2008, University of Manchester. p. 286.

177. Shi, X., Tan, T.H. , Tan, K.H. , Guo, Z., *Influence of concrete cover on fire resistance of reinforced concrete flexural members.* Journal of Structural Engineering, 2004. **130**: p. 1225.

178. Makhlouf, H.M. and F.A. Malhas, *The effect of thick concrete cover on the maximum flexural crack width under service load.* ACI Structural Journal, 1996. **93**(3): p. 257-265.

179. BSI, B.S., *8110-1:(1997),"*. Structural use of concrete–Part 1: Code of practice for design and construction.

APPENDIX –A

TYPICAL PROPERTIES of the Thermo-glue

Colour Part A: Blue
Part B: Cream
Viscosity: Paste
Operating
Temperature Range: -40℃ to + 300℃
Tensile Strength: 2200N/cm_2
Deflection Temperature: 100℃
Electric Strength: 11 to 12 kV/mm
Volume Resistivity: 10_{14} to 10_{15} Ohms/cm
Thermal Conductivity: 1.1 W/m.K
Modulus of Elasticity: 2 to 3 GN/m_2
0.29 - 0.435 x 10_6 lbf/in_2
Mix Ratio by Volume: 3 parts A
1 part B
Mix Ratio by Weight: 6.66 parts A
2.32 parts B
Usable Life: 3 to 4 hours
Cure Time: 45 mins @ 100℃
75 mins @ 60℃
8 to 12 hrs @ room temperature - hard
48 hours @ room temperature - full cure
Specific Heat Capacity: 0.5 cal/g/℃ @ 30℃ – resin
0.35 cal/g/℃ @ 30℃ - harden

APPENDIX –B

Splitting Tensile Strength

Table B-1 Splitting tensile Strength test data for three specimens

Mix	S1	S2	S3
G0F0	4.92	4.01	5.01
G0F0.1	4.652	4.745	4.683
G0F0.3	5.274	4.985	5.3
G0F0.5	4.557	4.46	4.21
G2F0	5.37	5.35	5.32
G2F0.1	4.027	4.04	5.561
G2F0.3	4.586	5.16	4.873
G2F0.5	4.384	5.12	4.5
G4F0	4.451	4.5	4.607
G4F0.1	4.794	4.82	4.428
G4F0.3	4.24	4.44	4.165
G4F0.5	3.804	3.747	4.15
G6F0	3.51	3.706	3.68
G6F0.1	4.676	4.084	3.843
G6F0.3	3.509	3.822	4.23
G6F0.5	4.342	4.307	4.278

Statistical Analysis

Anova: Single Factor 0% Glass

SUMMARY

Groups	*Count*	*Sum*	*Average*	*Variance*
Column (0% Fibre)	3	13.94	4.646667	0.306033
Column 2(0.1% fibre)	3	14.08	4.693333	0.002242

ANOVA

Source of Variation	*SS*	*df*	*MS*	*F*	*P-value*	*F crit*
Between Groups	0.003267	1	0.003267	0.021193	0.891295	7.708647
Within Groups	0.616551	4	0.154138			
Total	0.619818	5				

Anova: Single Factor 0% Glass

SUMMARY

Groups	*Count*	*Sum*	*Average*	*Variance*
Column 1(0.1%Fibre)	3	14.08	4.693333	0.002242
Column 2(0.3%Fibre)	3	15.559	5.186333	0.03057

ANOVA

Source of Variation	*SS*	*df*	*MS*	*F*	*P-value*	*F crit*
Between Groups	0.364574	1	0.364574	22.22151	0.009213	7.708647
Within Groups	0.065625	4	0.016406			
Total	0.430199	5				

Anova: Single Factor 0% Glass

SUMMARY

Groups	*Count*	*Sum*	*Average*	*Variance*
Column 1(0.3%Fibre)	3	15.559	5.186333	0.03057
Column 2(0.5%Fibre)	3	13.227	4.409	0.032053

ANOVA

Source of Variation	*SS*	*df*	*MS*	*F*	*P-value*	*F crit*
Between Groups	0.906371	1	0.906371	28.94674	0.005768	7.708647
Within Groups	0.125247	4	0.031312			
Total	1.031617	5				

Anova: Single Factor 0% Glass

SUMMARY

Groups	*Count*	*Sum*	*Average*	*Variance*
Column 1(0%Fubre)	3	13.94	4.646667	0.306033
Column 2(0.3%Fibre)	3	15.559	5.186333	0.03057

ANOVA

Source of Variation	*SS*	*df*	*MS*	*F*	*P-value*	*F crit*
Between Groups	0.43686	1	0.43686	2.595695	0.182445	7.708647
Within Groups	0.673207	4	0.168302			
Total	1.110068	5				

Anova: Single Factor 0% Glass

SUMMARY

Groups	*Count*	*Sum*	*Average*	*Variance*
Column 1(0%Fibre)	3	13.94	4.646667	0.306033
Column 2(0.5%Fibre)	3	13.227	4.409	0.032053

ANOVA

Source of Variation	*SS*	*df*	*MS*	*F*	*P-value*	*F crit*
Between Groups	0.084728	1	0.084728	0.501222	0.518036	7.708647
Within Groups	0.676173	4	0.169043			
Total	0.760901	5				

Anova: Single Factor 0% Glass

SUMMARY

Groups	*Count*	*Sum*	*Average*	*Variance*
Column 1(0.1%Fibre)	3	14.08	4.693333	0.002242
Column 2(0.5%Fibre)	3	13.227	4.409	0.032053

ANOVA

Source of Variation	*SS*	*df*	*MS*	*F*	*P-value*	*F crit*
Between Groups	0.121268	1	0.121268	7.071992	0.05643	7.708647
Within Groups	0.068591	4	0.017148			
Total	0.189859	5				

Anova: Single Factor 0% Glass

SUMMARY

Groups	*Count*	*Sum*	*Average*	*Variance*
Column 1(0%Fibre)	3	13.94	4.646667	0.306033
Column 2(0.1%Fibre)	3	14.08	4.693333	0.002242
Column 3(0.3%Fibre)	3	15.559	5.186333	0.03057
Column 4(0.5%Fibre)	3	13.227	4.409	0.032053

ANOVA

Source of Variation	*SS*	*df*	*MS*	*F*	*P-value*	*F crit*
Between Groups	0.958534	3	0.319511	3.445803	0.071825	4.066181
Within Groups	0.741798	8	0.092725			
Total	1.700332	11				

Anova: Single Factor 20% Glass

SUMMARY

Groups	*Count*	*Sum*	*Average*	*Variance*
Column 1(0%Fibre)	3	16.04	5.346667	0.000633
Column 2(0.1%Fibre)	3	13.628	4.542667	0.777794

ANOVA

Source of Variation	*SS*	*df*	*MS*	*F*	*P-value*	*F crit*
Between Groups	0.969624	1	0.969624	2.491237	0.189623	7.708647
Within Groups	1.556855	4	0.389214			
Total	2.526479	5				

Anova: Single Factor 20% Glass

SUMMARY

Groups	*Count*	*Sum*	*Average*	*Variance*
Column 1(0.1%Fibre)	3	13.628	4.542667	0.777794
Column 2(0.3%Fibre)	3	14.619	4.873	0.082369

ANOVA

Source of Variation	*SS*	*df*	*MS*	*F*	*P-value*	*F crit*
Between Groups	0.16368	1	0.16368	0.380579	0.570676	7.708647
Within Groups	1.720327	4	0.430082			
Total	1.884007	5				

Anova: Single Factor 20% Glass

SUMMARY

Groups	*Count*	*Sum*	*Average*	*Variance*
Column 1(0.3%Fibre)	3	14.619	4.873	0.082369
Column 2(0.5%Fibre)	3	14.004	4.668	0.156592

ANOVA

Source of Variation	*SS*	*df*	*MS*	*F*	*P-value*	*F crit*
Between Groups	0.063038	1	0.063038	0.527597	0.507844	7.708647
Within Groups	0.477922	4	0.119481			
Total	0.54096	5				

Anova: Single Factor 20% Glass

SUMMARY

Groups	*Count*	*Sum*	*Average*	*Variance*
Column 1(0%Fibre)	3	16.04	5.346667	0.000633
Column 2(0.3%Fibre)	3	14.619	4.873	0.082369

ANOVA

Source of Variation	*SS*	*df*	*MS*	*F*	*P-value*	*F crit*
Between Groups	0.33654	1	0.33654	8.109174	0.046506	7.708647
Within Groups	0.166005	4	0.041501			
Total	0.502545	5				

Anova: Single Factor 20% Glass

SUMMARY

Groups	*Count*	*Sum*	*Average*	*Variance*
Column 1(0%Fibre)	3	16.04	5.346667	0.000633
Column 2(0.5%Fibre)	3	14.004	4.668	0.156592

ANOVA

Source of Variation	*SS*	*df*	*MS*	*F*	*P-value*	*F crit*
Between Groups	0.690883	1	0.690883	8.78844	0.041368	7.708647
Within Groups	0.314451	4	0.078613			
Total	1.005333	5				

Anova: Single Factor 20% Glass

SUMMARY

Groups	*Count*	*Sum*	*Average*	*Variance*
Column 1(0.1%Fibre)	3	13.628	4.542667	0.777794
Column 2(0.5%Fibre)	3	14.004	4.668	0.156592

ANOVA

Source of Variation	*SS*	*df*	*MS*	*F*	*P-value*	*F crit*
Between Groups	0.023563	1	0.023563	0.050435	0.833314	7.708647
Within Groups	1.868773	4	0.467193			
Total	1.892335	5				

Anova: Single Factor 20% Glass

SUMMARY

Groups	*Count*	*Sum*	*Average*	*Variance*
Column 1(0%Fibre)	3	16.04	5.346667	0.000633
Column 2(0.1%Fibre)	3	13.628	4.542667	0.777794
Column 3(0.3%Fibre)	3	14.619	4.873	0.082369
Column 4(0.5%Fibre)	3	14.004	4.668	0.156592

ANOVA

Source of Variation	*SS*	*df*	*MS*	*F*	*P-value*	*F crit*
Between Groups	1.123664	3	0.374555	1.472611	0.293491	4.066181
Within Groups	2.034777	8	0.254347			
Total	3.158441	11				

Anova: Single Factor 40% Glass

SUMMARY

Groups	*Count*	*Sum*	*Average*	*Variance*
Column 1(0%Fibre)	3	13.558	4.519333	0.006364
Column 2(0.1%Fibre)	3	14.042	4.680667	0.048049

ANOVA

Source of Variation	*SS*	*df*	*MS*	*F*	*P-value*	*F crit*
Between Groups	0.039043	1	0.039043	1.435032	0.297073	7.708647
Within Groups	0.108827	4	0.027207			
Total	0.14787	5				

Anova: Single Factor 40% Glass

SUMMARY

Groups	*Count*	*Sum*	*Average*	*Variance*
Column 1(0.1%Fibre)	3	14.042	4.680667	0.048049
Column 2(0.3%Fibre)	3	12.845	4.281667	0.020208

ANOVA

Source of Variation	*SS*	*df*	*MS*	*F*	*P-value*	*F crit*
Between Groups	0.238802	1	0.238802	6.99706	0.057268	7.708647
Within Groups	0.136515	4	0.034129			
Total	0.375317	5				

Anova: Single Factor 40% Glass

SUMMARY

Groups	*Count*	*Sum*	*Average*	*Variance*
Column 1(0.3%Fibre)	3	12.845	4.281667	0.020208
Column 2(0.5%Fibre)	3	11.701	3.900333	0.047562

ANOVA

Source of Variation	*SS*	*df*	*MS*	*F*	*P-value*	*F crit*
Between Groups	0.218123	1	0.218123	6.437082	0.064176	7.708647
Within Groups	0.135541	4	0.033885			
Total	0.353664	5				

Anova: Single Factor 40% Glass

SUMMARY

Groups	*Count*	*Sum*	*Average*	*Variance*
Column 1(0%Fibre)	3	13.558	4.519333	0.006364
Column 2(0.3%Fibre)	3	12.845	4.281667	0.020208

ANOVA

Source of Variation	*SS*	*df*	*MS*	*F*	*P-value*	*F crit*
Between Groups	0.084728	1	0.084728	6.377092	0.06499	7.708647
Within Groups	0.053145	4	0.013286			
Total	0.137874	5				

Anova: Single Factor 40% Glass

SUMMARY

Groups	*Count*	*Sum*	*Average*	*Variance*
Column 1(0%Fibre)	3	13.558	4.519333	0.006364
Column 2(0.5%Fibre)	3	11.701	3.900333	0.047562

ANOVA

Source of Variation	*SS*	*df*	*MS*	*F*	*P-value*	*F crit*
Between Groups	0.574742	1	0.574742	21.31567	0.009904	7.708647
Within Groups	0.107853	4	0.026963			
Total	0.682595	5				

Anova: Single Factor 40% Glass

SUMMARY

Groups	*Count*	*Sum*	*Average*	*Variance*
Column 1(0.1%Fibre)	3	14.042	4.680667	0.048049
Column 2(0.5%Fibre)	3	11.701	3.900333	0.047562

ANOVA

Source of Variation	*SS*	*df*	*MS*	*F*	*P-value*	*F crit*
Between Groups	0.91338	1	0.91338	19.10604	0.011958	7.708647
Within Groups	0.191223	4	0.047806			
Total	1.104604	5				

Anova: Single Factor 40% Glass

SUMMARY

Groups	*Count*	*Sum*	*Average*	*Variance*
Column 1(0%Fibre)	3	13.558	4.519333	0.006364
Column 2(0.1%Fibre)	3	14.042	4.680667	0.048049
Column 3(0.3%Fibre)	3	12.845	4.281667	0.020208
Column 4(0.5%Fibre)	3	11.701	3.900333	0.047562

ANOVA

Source of Variation	*SS*	*df*	*MS*	*F*	*P-value*	*F crit*
Between Groups	1.034408	3	0.344803	11.28795	0.00302	4.066181
Within Groups	0.244369	8	0.030546			
Total	1.278777	11				

Anova: Single Factor 60% Glass

SUMMARY

Groups	*Count*	*Sum*	*Average*	*Variance*
Column 1(0%Fibre)	3	10.896	3.632	0.011332
Column 2(0.1%Fibre)	3	12.603	4.201	0.183739

ANOVA

Source of Variation	*SS*	*df*	*MS*	*F*	*P-value*	*F crit*
Between Groups	0.485642	1	0.485642	4.979126	0.089472	7.708647
Within Groups	0.390142	4	0.097536			
Total	0.875784	5				

Anova: Single Factor 60% Glass

SUMMARY

Groups	*Count*	*Sum*	*Average*	*Variance*
Column 1(0.1%Fibre)	3	12.603	4.201	0.183739
Column 2(0.3%Fibre)	3	11.561	3.853667	0.130712

ANOVA

Source of Variation	*SS*	*df*	*MS*	*F*	*P-value*	*F crit*
Between Groups	0.180961	1	0.180961	1.150961	0.343761	7.708647
Within Groups	0.628903	4	0.157226			
Total	0.809863	5				

Anova: Single Factor 60% Glass

SUMMARY

Groups	*Count*	*Sum*	*Average*	*Variance*
Column 1(0.3%Fibre)	3	11.561	3.853667	0.130712
Column 2(0.5%Fibre)	3	12.927	4.309	0.001027

ANOVA

Source of Variation	*SS*	*df*	*MS*	*F*	*P-value*	*F crit*
Between Groups	0.310993	1	0.310993	4.721334	0.095504	7.708647
Within Groups	0.263479	4	0.06587			
Total	0.574471	5				

Anova: Single Factor 60% Glass

SUMMARY

Groups	*Count*	*Sum*	*Average*	*Variance*
Column 1(0%Fibre)	3	10.896	3.632	0.011332
Column 2(0.3%Fibre)	3	11.561	3.853667	0.130712

ANOVA

Source of Variation	*SS*	*df*	*MS*	*F*	*P-value*	*F crit*
Between Groups	0.073704	1	0.073704	1.037763	0.365945	7.708647
Within Groups	0.284089	4	0.071022			
Total	0.357793	5				

Anova: Single Factor 60% Glass

SUMMARY

Groups	*Count*	*Sum*	*Average*	*Variance*
Column 1(0%Fibre)	3	10.896	3.632	0.011332
Column 2(0.5%Fibre)	3	12.927	4.309	0.001027

ANOVA

Source of Variation	*SS*	*df*	*MS*	*F*	*P-value*	*F crit*
Between Groups	0.687494	1	0.687494	111.2539	0.000457	7.708647
Within Groups	0.024718	4	0.00618			
Total	0.712212	5				

Anova: Single Factor 60% Glass

SUMMARY

Groups	*Count*	*Sum*	*Average*	*Variance*
Column 1(0.1%Fibre)	3	12.603	4.201	0.183739
Column 2(0.5%Fibre)	3	12.927	4.309	0.001027

ANOVA

Source of Variation	*SS*	*df*	*MS*	*F*	*P-value*	*F crit*
Between Groups	0.017496	1	0.017496	0.189385	0.68588	7.708647
Within Groups	0.369532	4	0.092383			
Total	0.387028	5				

Anova: Single Factor 60% Glass

SUMMARY

Groups	*Count*	*Sum*	*Average*	*Variance*
Column 1(0%Fibre)	3	10.896	3.632	0.011332
Column 2(0.1%Fibre)	3	12.603	4.201	0.183739
Column 3(0.3%Fibre)	3	11.561	3.853667	0.130712
Column 4(0.5%Fibre)	3	12.927	4.309	0.001027

ANOVA

Source of Variation	*SS*	*df*	*MS*	*F*	*P-value*	*F crit*
Between Groups	0.878144	3	0.292715	3.582687	0.066126	4.066181
Within Groups	0.653621	8	0.081703			
Total	1.531765	11				

Anova: Single Factor 0% Fibre

SUMMARY

Groups	*Count*	*Sum*	*Average*	*Variance*
Column 1(0%Glass)	3	13.94	4.646667	0.306033
Column 2(20%Glass)	3	16.04	5.346667	0.000633

ANOVA

Source of Variation	*SS*	*df*	*MS*	*F*	*P-value*	*F crit*
Between Groups	0.735	1	0.735	4.793478	0.093755	7.708647
Within Groups	0.613333	4	0.153333			
Total	1.348333	5				

Anova: Single Factor 0% Fibre

SUMMARY

Groups	*Count*	*Sum*	*Average*	*Variance*
Column 1(0%Glass)	3	13.94	4.646667	0.306033
Column 2(40%Glass)	3	13.558	4.519333	0.006364

ANOVA

Source of Variation	*SS*	*df*	*MS*	*F*	*P-value*	*F crit*
Between Groups	0.024321	1	0.024321	0.155703	0.713279	7.708647
Within Groups	0.624795	4	0.156199			
Total	0.649116	5				

Anova: Single Factor 0% Fibre

SUMMARY

Groups	*Count*	*Sum*	*Average*	*Variance*
Column 1(0%Glass)	3	13.94	4.646667	0.306033
Column 2(60%Glass)	3	10.896	3.632	0.011332

ANOVA

Source of Variation	*SS*	*df*	*MS*	*F*	*P-value*	*F crit*
Between Groups	1.544323	1	1.544323	9.732145	0.035539	7.708647
Within Groups	0.634731	4	0.158683			
Total	2.179053	5				

Anova: Single Factor 0% Fibre

SUMMARY

Groups	*Count*	*Sum*	*Average*	*Variance*
Column 1(20%Glass)	3	16.04	5.346667	0.000633
Column 2(40%Glass)	3	13.558	4.519333	0.006364

ANOVA

Source of Variation	*SS*	*df*	*MS*	*F*	*P-value*	*F crit*
Between Groups	1.026721	1	1.026721	293.4466	6.81E-05	7.708647
Within Groups	0.013995	4	0.003499			
Total	1.040716	5				

Anova: Single Factor 0% Fibre

SUMMARY

Groups	*Count*	*Sum*	*Average*	*Variance*
Column 1(20%Glass)	3	16.04	5.346667	0.000633
Column 2(60%Glass)	3	10.896	3.632	0.011332

ANOVA

Source of Variation	*SS*	*df*	*MS*	*F*	*P-value*	*F crit*
Between Groups	4.410123	1	4.410123	737.15	1.09E-05	7.708647
Within Groups	0.023931	4	0.005983			
Total	4.434053	5				

Anova: Single Factor 0% Fibre

SUMMARY

Groups	*Count*	*Sum*	*Average*	*Variance*
Column 1(40%Glass)	3	13.558	4.519333	0.006364
Column 2(60%Glass)	3	10.896	3.632	0.011332

ANOVA

Source of Variation	*SS*	*df*	*MS*	*F*	*P-value*	*F crit*
Between Groups	1.181041	1	1.181041	133.4786	0.000321	7.708647
Within Groups	0.035393	4	0.008848			
Total	1.216433	5				

Anova: Single Factor 0% Fibre

SUMMARY

Groups	*Count*	*Sum*	*Average*	*Variance*
Column 1(0%Glass)	3	13.94	4.646667	0.306033
Column 2(20%Glass)	3	16.04	5.346667	0.000633
Column 3(40%Glass)	3	13.558	4.519333	0.006364
Column 4(60%Glass)	3	10.896	3.632	0.011332

ANOVA

Source of Variation	*SS*	*df*	*MS*	*F*	*P-value*	*F crit*
Between Groups	4.460764	3	1.486921	18.33651	0.000606	4.066181
Within Groups	0.648726	8	0.081091			
Total	5.10949	11				

Compressive Strength

Table B-2 Compressive strength test data for three specimens

Mix	7 days			28 days			90days		
	S1	S2	S3	S1	S2	S3	S1	S2	S3
G0F0	35.679	41.163	36.25	62.883	63.1	62.988	71.47	71.659	70.345
G0F0.1	36.817	36.829	35.438	64.569	64.085	64.6	71.625	70.036	69.903
G0F0.3	49.967	46.311	48.592	72.882	71.917	72.9	77.198	79.136	79.436
G0F0.5	41.974	43.148	41.679	54.9	54.179	55.448	60.456	59.353	59.069
G2F0	37.846	37.13	39.287	64.719	64.84	63.573	68.84	70.62	69.9
G2F0.1	42.986	43.077	42.789	66.998	66.947	67.1	66.88	67.66	67.84
G2F0.3	40.672	40.462	41.25	63.786	62.656	62.672	67.281	67.67	66.484
G2F0.5	42.845	42.7	40.982	63.335	63.07	63.42	60.04	64.28	65.27
G4F0	37.177	42.996	40.549	60.555	60.64	59.758	67.059	66.16	66.742
G4F0.1	42.669	43.231	41.967	64.555	64.933	64.854	67.84	68.69	65.57
G4F0.3	38.066	38.139	36.574	54.088	54.875	53.565	61.525	57.841	60.293
G4F0.5	45.154	45.949	43.389	62.567	62.815	62.78	64.09	63.05	61.78
G6F0	36.224	38.031	36.857	58.771	58.179	59.533	64.383	61.425	64.616
G6F0.1	45.342	42.778	44.436	61.24	60.947	60.39	65.23	64.18	64.25
G6F0.3	38.003	33.454	35.429	52.402	54.246	53.413	57.486	57.987	57.85
G6F0.5	45.954	48.5	48.383	62.281	61.127	63.868	64.78	64	66.22

Statistical Analysis

7 Days

Anova: Single Factor 0% Glass

SUMMARY

Groups	*Count*	*Sum*	*Average*	*Variance*
Column 1(0%Fibre)	3	113.092	37.69733	9.089644
Column 2(0.1%Fibre)	3	109.084	36.36133	0.639444

ANOVA

Source of Variation	*SS*	*df*	*MS*	*F*	*P-value*	*F crit*
Between Groups	2.677344	1	2.677344	0.550379	0.499359	7.708647
Within Groups	19.45818	4	4.864544			
Total	22.13552	5				

Anova: Single Factor 0% Glass

SUMMARY

Groups	*Count*	*Sum*	*Average*	*Variance*
Column 1(0.1%Fibre)	3	109.084	36.36133	0.639444
Column 2(0.3%Fibre)	3	144.87	48.29	3.409987

ANOVA

Source of Variation	*SS*	*df*	*MS*	*F*	*P-value*	*F crit*
Between Groups	213.4396	1	213.4396	105.4171	0.000507	7.708647
Within Groups	8.098863	4	2.024716			
Total	221.5385	5				

Anova: Single Factor 0% Glass

SUMMARY

Groups	*Count*	*Sum*	*Average*	*Variance*
Column 1(0.3%Fibre)	3	144.87	48.29	3.409987
Column 2(0.5%Fibre)	3	126.801	42.267	0.603877

ANOVA

Source of Variation	*SS*	*df*	*MS*	*F*	*P-value*	*F crit*
Between Groups	54.41479	1	54.41479	27.11342	0.006485	7.708647
Within Groups	8.027728	4	2.006932			
Total	62.44252	5				

Anova: Single Factor 0% Glass

SUMMARY

Groups	*Count*	*Sum*	*Average*	*Variance*
Column 1(0%Fibre)	3	113.092	37.69733	9.089644
Column 2(0.3%Fibre)	3	144.87	48.29	3.409987

ANOVA

Source of Variation	*SS*	*df*	*MS*	*F*	*P-value*	*F crit*
Between Groups	168.3069	1	168.3069	26.9299	0.006564	7.708647
Within Groups	24.99926	4	6.249816			
Total	193.3061	5				

Anova: Single Factor 0% Glass

SUMMARY

Groups	*Count*	*Sum*	*Average*	*Variance*
Column 1(0%Fibre)	3	113.092	37.69733	9.089644
Column 2(0.5%Fibre)	3	126.801	42.267	0.603877

ANOVA

Source of Variation	*SS*	*df*	*MS*	*F*	*P-value*	*F crit*
Between Groups	31.32278	1	31.32278	6.462622	0.063834	7.708647
Within Groups	19.38704	4	4.846761			
Total	50.70982	5				

Anova: Single Factor 0% Glass

SUMMARY

Groups	*Count*	*Sum*	*Average*	*Variance*
Column 1(0.1%Fibre)	3	109.084	36.36133	0.639444
Column 2(0.5%Fibre)	3	126.801	42.267	0.603877

ANOVA

Source of Variation	*SS*	*df*	*MS*	*F*	*P-value*	*F crit*
Between Groups	52.31535	1	52.31535	84.15419	0.000784	7.708647
Within Groups	2.486643	4	0.621661			
Total	54.80199	5				

Anova: Single Factor 0% Glass

SUMMARY

Groups	*Count*	*Sum*	*Average*	*Variance*
Column 1(0%Fibre)	3	113.092	37.69733	9.089644
Column 2(0.1%Fibre)	3	109.084	36.36133	0.639444
Column 3(0.3%Fibre)	3	144.87	48.29	3.409987
Column 4(0.5%Fibre)	3	126.801	42.267	0.603877

ANOVA

Source of Variation	*SS*	*df*	*MS*	*F*	*P-value*	*F crit*
Between Groups	261.2384	3	87.07946	25.3452	0.000194	4.066181
Within Groups	27.48591	8	3.435738			
Total	288.7243	11				

Anova: Single Factor 20% Glass

SUMMARY

Groups	*Count*	*Sum*	*Average*	*Variance*
Column 1(0%Fibre)	3	114.263	38.08767	1.206964
Column 2(0.1%Fibre)	3	128.852	42.95067	0.021672

ANOVA

Source of Variation	*SS*	*df*	*MS*	*F*	*P-value*	*F crit*
Between Groups	35.47315	1	35.47315	57.74393	0.001609	7.708647
Within Groups	2.457273	4	0.614318			
Total	37.93043	5				

Anova: Single Factor 20% Glass

SUMMARY

Groups	*Count*	*Sum*	*Average*	*Variance*
Column 1(0.1%Fibre)	3	128.852	42.95067	0.021672
Column 2(0.3%Fibre)	3	122.384	40.79467	0.166521

ANOVA

Source of Variation	*SS*	*df*	*MS*	*F*	*P-value*	*F crit*
Between Groups	6.972504	1	6.972504	74.09924	0.001001	7.708647
Within Groups	0.376387	4	0.094097			
Total	7.348891	5				

Anova: Single Factor 20% Glass

SUMMARY

Groups	*Count*	*Sum*	*Average*	*Variance*
Column 1(0.3%FiBre)	3	122.384	40.79467	0.166521
Column 2(0.5%Fibre)	3	126.527	42.17567	1.073886

ANOVA

Source of Variation	*SS*	*df*	*MS*	*F*	*P-value*	*F crit*
Between Groups	2.860742	1	2.860742	4.612583	0.098236	7.708647
Within Groups	2.480815	4	0.620204			
Total	5.341557	5				

Anova: Single Factor 20% Glass

SUMMARY

Groups	*Count*	*Sum*	*Average*	*Variance*
Column 1(0%Fibre)	3	114.263	38.08767	1.206964
Column 2(0.3%Fibre)	3	122.384	40.79467	0.166521

ANOVA

Source of Variation	*SS*	*df*	*MS*	*F*	*P-value*	*F crit*
Between Groups	10.99177	1	10.99177	16.00566	0.016121	7.708647
Within Groups	2.746971	4	0.686743			
Total	13.73874	5				

Anova: Single Factor 20% Glass

SUMMARY

Groups	*Count*	*Sum*	*Average*	*Variance*
Column 1(0%Fibre)	3	114.263	38.08767	1.206964
Column 2(0.5%Fibre)	3	126.527	42.17567	1.073886

ANOVA

Source of Variation	*SS*	*df*	*MS*	*F*	*P-value*	*F crit*
Between Groups	25.06762	1	25.06762	21.98094	0.009389	7.708647
Within Groups	4.561701	4	1.140425			
Total	29.62932	5				

Anova: Single Factor 20% glass

SUMMARY

Groups	*Count*	*Sum*	*Average*	*Variance*
Column 1(0.1%Fibre)	3	128.852	42.95067	0.021672
Column 2(0.5%Fibre)	3	126.527	42.17567	1.073886

ANOVA

Source of Variation	*SS*	*df*	*MS*	*F*	*P-value*	*F crit*
Between Groups	0.900937	1	0.900937	1.644709	0.268957	7.708647
Within Groups	2.191117	4	0.547779			
Total	3.092055	5				

Anova: Single Factor 20% Glass

SUMMARY

Groups	*Count*	*Sum*	*Average*	*Variance*
Column 1(0%Fibre)	3	114.263	38.08767	1.206964
Column 2(0.1%Fibre)	3	128.852	42.95067	0.021672
Column 3(0.3%Fibre)	3	122.384	40.79467	0.166521
Column 4(0.5%Fibre)	3	126.527	42.17567	1.073886

ANOVA

Source of Variation	*SS*	*df*	*MS*	*F*	*P-value*	*F crit*
Between Groups	41.13336	3	13.71112	22.21284	0.000311	4.066181
Within Groups	4.938089	8	0.617261			
Total	46.07145	11				

Anova: Single Factor 40% Glass

SUMMARY

Groups	*Count*	*Sum*	*Average*	*Variance*
Column 1(0%Fibre)	3	120.722	40.24067	8.536492
Column 2(0.1%Fibre)	3	127.867	42.62233	0.401057

ANOVA

Source of Variation	*SS*	*df*	*MS*	*F*	*P-value*	*F crit*
Between Groups	8.508504	1	8.508504	1.90399	0.239743	7.708647
Within Groups	17.8751	4	4.468775			
Total	26.3836	5				

Anova: Single Factor 40% Glass

SUMMARY

Groups	*Count*	*Sum*	*Average*	*Variance*
Column 1(0.1%Fibre)	3	127.867	42.62233	0.401057
Column 2(0.3%Fibre)	3	112.779	37.593	0.780103

ANOVA

Source of Variation	*SS*	*df*	*MS*	*F*	*P-value*	*F crit*
Between Groups	37.94129	1	37.94129	64.2441	0.001314	7.708647
Within Groups	2.362321	4	0.59058			
Total	40.30361	5				

Anova: Single Factor 40% Glass

SUMMARY

Groups	*Count*	*Sum*	*Average*	*Variance*
Column 1(0.3%Fibre)	3	112.779	37.593	0.780103
Column 2(0.5%Fibre)	3	134.492	44.83067	1.716808

ANOVA

Source of Variation	*SS*	*df*	*MS*	*F*	*P-value*	*F crit*
Between Groups	78.57573	1	78.57573	62.93834	0.001367	7.708647
Within Groups	4.993823	4	1.248456			
Total	83.56955	5				

Anova: Single Factor 40% Glass

SUMMARY

Groups	*Count*	*Sum*	*Average*	*Variance*
Column 1(0%Fibre)	3	120.722	40.24067	8.536492
Column 2(0.3%Fibre)	3	112.779	37.593	0.780103

ANOVA

Source of Variation	*SS*	*df*	*MS*	*F*	*P-value*	*F crit*
Between Groups	10.51521	1	10.51521	2.257307	0.207403	7.708647
Within Groups	18.63319	4	4.658298			
Total	29.1484	5				

Anova: Single Factor 40% Glass

SUMMARY

Groups	*Count*	*Sum*	*Average*	*Variance*
Column 1(0%Fibre)	3	120.722	40.24067	8.536492
Column 2(0.5%fibre)	3	134.492	44.83067	1.716808

ANOVA

Source of Variation	*SS*	*df*	*MS*	*F*	*P-value*	*F crit*
Between Groups	31.60215	1	31.60215	6.164288	0.068007	7.708647
Within Groups	20.5066	4	5.12665			
Total	52.10875	5				

Anova: Single Factor 40% Glass

SUMMARY

Groups	*Count*	*Sum*	*Average*	*Variance*
Column 1(0.1%Fibre)	3	127.867	42.62233	0.401057
Column 2(0.5%Fibre)	3	134.492	44.83067	1.716808

ANOVA

Source of Variation	*SS*	*df*	*MS*	*F*	*P-value*	*F crit*
Between Groups	7.315104	1	7.315104	6.907996	0.05829	7.708647
Within Groups	4.235731	4	1.058933			
Total	11.55084	5				

Anova: Single Factor 40% Glass

SUMMARY

Groups	*Count*	*Sum*	*Average*	*Variance*
Column 1(0%Fibre)	3	120.722	40.24067	8.536492
Column 2(0.1%Fibre)	3	127.867	42.62233	0.401057
Column 3(0.3%Fibre)	3	112.779	37.593	0.780103
Column 4(0.5%fibre)	3	134.492	44.83067	1.716808

ANOVA

Source of Variation	*SS*	*df*	*MS*	*F*	*P-value*	*F crit*
Between Groups	87.22899	3	29.07633	10.17147	0.004182	4.066181
Within Groups	22.86892	8	2.858615			
Total	110.0979	11				

Anova: Single Factor 60% Glass

SUMMARY

Groups	*Count*	*Sum*	*Average*	*Variance*
Column 1(0%Fibre)	3	111.112	37.03733	0.840702
Column 2(0.1%Fibre)	3	132.556	44.18533	1.690649

ANOVA

Source of Variation	*SS*	*df*	*MS*	*F*	*P-value*	*F crit*
Between Groups	76.64086	1	76.64086	60.55331	0.001471	7.708647
Within Groups	5.062703	4	1.265676			
Total	81.70356	5				

Anova: Single Factor 60% Glass

SUMMARY

Groups	*Count*	*Sum*	*Average*	*Variance*
Column 1(0.1%Fibre)	3	132.556	44.18533	1.690649
Column 2(0.3%Fibre)	3	106.886	35.62867	5.20325

ANOVA

Source of Variation	*SS*	*df*	*MS*	*F*	*P-value*	*F crit*
Between Groups	109.8248	1	109.8248	31.86145	0.004851	7.708647
Within Groups	13.7878	4	3.44695			
Total	123.6126	5				

Anova: Single Factor 60% Glass

SUMMARY

Groups	*Count*	*Sum*	*Average*	*Variance*
Column 1(0.3%Fibre)	3	106.886	35.62867	5.20325
Column 2(0.5%Fibre)	3	142.837	47.61233	2.065974

ANOVA

Source of Variation	*SS*	*df*	*MS*	*F*	*P-value*	*F crit*
Between Groups	215.4124	1	215.4124	59.26695	0.001532	7.708647
Within Groups	14.53845	4	3.634612			
Total	229.9508	5				

Anova: Single Factor 60% Glass

SUMMARY

Groups	*Count*	*Sum*	*Average*	*Variance*
Column 1(0%Fibre)	3	111.112	37.03733	0.840702
Column 2(0.3%Fibre)	3	106.886	35.62867	5.20325

ANOVA

Source of Variation	*SS*	*df*	*MS*	*F*	*P-value*	*F crit*
Between Groups	2.976513	1	2.976513	0.984956	0.377155	7.708647
Within Groups	12.08791	4	3.021976			
Total	15.06442	5				

Anova: Single Factor 60% Glass

SUMMARY

Groups	*Count*	*Sum*	*Average*	*Variance*
Column 1(0%Fibre)	3	111.112	37.03733	0.840702
Column 2(0.5%fibre)	3	142.837	47.61233	2.065974

ANOVA

Source of Variation	*SS*	*df*	*MS*	*F*	*P-value*	*F crit*
Between Groups	167.7459	1	167.7459	115.4211	0.000426	7.708647
Within Groups	5.813353	4	1.453338			
Total	173.5593	5				

Anova: Single Factor 60% Glass

SUMMARY

Groups	*Count*	*Sum*	*Average*	*Variance*
Column 1(0.1%Fibre)	3	132.556	44.18533	1.690649
Column 2(0.5%Fibre)	3	142.837	47.61233	2.065974

ANOVA

Source of Variation	*SS*	*df*	*MS*	*F*	*P-value*	*F crit*
Between Groups	17.61649	1	17.61649	9.378897	0.037567	7.708647
Within Groups	7.513247	4	1.878312			
Total	25.12974	5				

Anova: Single Factor 60% Glass

SUMMARY

Groups	*Count*	*Sum*	*Average*	*Variance*
Column 1(0%Fibre)	3	111.112	37.03733	0.840702
Column 2(0.1%Fibre)	3	132.556	44.18533	1.690649
Column 3(0.3%Fibre)	3	106.886	35.62867	5.20325
Column 4(0.5%Fibre)	3	142.837	47.61233	2.065974

ANOVA

Source of Variation	*SS*	*df*	*MS*	*F*	*P-value*	*F crit*
Between Groups	295.1085	3	98.3695	40.14846	3.61E-05	4.066181
Within Groups	19.60115	8	2.450144			
Total	314.7097	11				

Anova: Single Factor 0% Fibre

SUMMARY

Groups	*Count*	*Sum*	*Average*	*Variance*
Column 1(0%Glass)	3	113.092	37.69733	9.089644
Column 2(20%Glass)	3	114.263	38.08767	1.206964

ANOVA

Source of Variation	*SS*	*df*	*MS*	*F*	*P-value*	*F crit*
Between Groups	0.22854	1	0.22854	0.044391	0.843425	7.708647
Within Groups	20.59322	4	5.148304			
Total	20.82176	5				

Anova: Single Factor 0% Fibre

SUMMARY

Groups	*Count*	*Sum*	*Average*	*Variance*
Column 1(20%Glass)	3	114.263	38.08767	1.206964
Column 2(40%Glass)	3	120.722	40.24067	8.536492

ANOVA

Source of Variation	*SS*	*df*	*MS*	*F*	*P-value*	*F crit*
Between Groups	6.953114	1	6.953114	1.427238	0.29821	7.708647
Within Groups	19.48691	4	4.871728			
Total	26.44003	5				

Anova: Single Factor 0% Fibre

SUMMARY

Groups	*Count*	*Sum*	*Average*	*Variance*
Column 1(40%Glass)	3	120.722	40.24067	8.536492
Column 2(60%Glass)	3	111.112	37.03733	0.840702

ANOVA

Source of Variation	*SS*	*df*	*MS*	*F*	*P-value*	*F crit*
Between Groups	15.39202	1	15.39202	3.282862	0.144234	7.708647
Within Groups	18.75439	4	4.688597			
Total	34.14641	5				

Anova: Single Factor 0% Fibre

SUMMARY

Groups	*Count*	*Sum*	*Average*	*Variance*
Column 1(0%Glass)	3	113.092	37.69733	9.089644
Column 2(40%Glass)	3	120.722	40.24067	8.536492

ANOVA

Source of Variation	*SS*	*df*	*MS*	*F*	*P-value*	*F crit*
Between Groups	9.702817	1	9.702817	1.100958	0.353268	7.708647
Within Groups	35.25227	4	8.813068			
Total	44.95509	5				

Anova: Single Factor 0% Fibre

SUMMARY

Groups	*Count*	*Sum*	*Average*	*Variance*
Column 1(0%Glass)	3	113.092	37.69733	9.089644
Column 2(60%Glass)	3	111.112	37.03733	0.840702

ANOVA

Source of Variation	*SS*	*df*	*MS*	*F*	*P-value*	*F crit*
Between Groups	0.6534	1	0.6534	0.131597	0.735138	7.708647
Within Groups	19.86069	4	4.965173			
Total	20.51409	5				

Anova: Single Factor 0% Fibre

SUMMARY

Groups	*Count*	*Sum*	*Average*	*Variance*
Column 1(20%Glass)	3	114.263	38.08767	1.206964
Column 2(60%Glass)	3	111.112	37.03733	0.840702

ANOVA

Source of Variation	*SS*	*df*	*MS*	*F*	*P-value*	*F crit*
Between Groups	1.6548	1	1.6548	1.616279	0.272508	7.708647
Within Groups	4.095333	4	1.023833			
Total	5.750134	5				

Anova: Single Factor 0% Fibre

SUMMARY

Groups	*Count*	*Sum*	*Average*	*Variance*
Column 1(0%Glass)	3	113.092	37.69733	9.089644
Column 2(20%Glass)	3	114.263	38.08767	1.206964
Column 3(40%Glass)	3	120.722	40.24067	8.536492
Column 4(60%Glass)	3	111.112	37.03733	0.840702

ANOVA

Source of Variation	*SS*	*df*	*MS*	*F*	*P-value*	*F crit*
Between Groups	17.29234	3	5.764115	1.171937	0.379157	4.066181
Within Groups	39.34761	8	4.918451			
Total	56.63995	11				

28 Days

Anova: Single Factor 0% Glass

SUMMARY

Groups	*Count*	*Sum*	*Average*	*Variance*
Column 1(0%Fibre)	3	188.971	62.99033	0.011776
Column 2(0.1%Fibre)	3	193.254	64.418	0.083407

ANOVA

Source of Variation	*SS*	*df*	*MS*	*F*	*P-value*	*F crit*
Between Groups	3.057348	1	3.057348	64.24125	0.001314	7.708647
Within Groups	0.190367	4	0.047592			
Total	3.247715	5				

Anova: Single Factor 0% Glass

SUMMARY

Groups	*Count*	*Sum*	*Average*	*Variance*
Column 1(0.1%Fibre)	3	193.254	64.418	0.083407
Column 2(0.3%Fibre)	3	217.699	72.56633	0.316306

ANOVA

Source of Variation	*SS*	*df*	*MS*	*F*	*P-value*	*F crit*
Between Groups	99.593	1	99.593	498.3222	2.38E-05	7.708647
Within Groups	0.799427	4	0.199857			
Total	100.3924	5				

Anova: Single Factor 0% Glass

SUMMARY

Groups	*Count*	*Sum*	*Average*	*Variance*
Column 1(0.3%Fibre)	3	217.699	72.56633	0.316306
Column 2(0.5%Fibre)	3	164.527	54.84233	0.405084

ANOVA

Source of Variation	*SS*	*df*	*MS*	*F*	*P-value*	*F crit*
Between Groups	471.2103	1	471.2103	1306.394	3.5E-06	7.708647
Within Groups	1.442781	4	0.360695			
Total	472.653	5				

Anova: Single Factor 0% Glass

SUMMARY

Groups	*Count*	*Sum*	*Average*	*Variance*
Column 1(0%Fibre)	3	188.971	62.99033	0.011776
Column 2(0.3%Fibre)	3	217.699	72.56633	0.316306

ANOVA

Source of Variation	*SS*	*df*	*MS*	*F*	*P-value*	*F crit*
Between Groups	137.5497	1	137.5497	838.5061	8.47E-06	7.708647
Within Groups	0.656165	4	0.164041			
Total	138.2058	5				

Anova: Single Factor 0% Glass

SUMMARY

Groups	*Count*	*Sum*	*Average*	*Variance*
Column 1(0%Fibre)	3	188.971	62.99033	0.011776
Column 2(0.5%Fibre)	3	164.527	54.84233	0.405084

ANOVA

Source of Variation	*SS*	*df*	*MS*	*F*	*P-value*	*F crit*
Between Groups	99.58486	1	99.58486	477.7849	2.59E-05	7.708647
Within Groups	0.833721	4	0.20843			
Total	100.4186	5				

Anova: Single Factor 0% Glass

SUMMARY

Groups	*Count*	*Sum*	*Average*	*Variance*
Column 1(0.1%Fibre)	3	193.254	64.418	0.083407
Column 2(0.5%Fibre)	3	164.527	54.84233	0.405084

ANOVA

Source of Variation	*SS*	*df*	*MS*	*F*	*P-value*	*F crit*
Between Groups	137.5401	1	137.5401	563.1219	1.87E-05	7.708647
Within Groups	0.976983	4	0.244246			
Total	138.5171	5				

Anova: Single Factor 0% Glass

SUMMARY

Groups	*Count*	*Sum*	*Average*	*Variance*
Column 1(0%Fibre)	3	188.971	62.99033	0.011776
Column 2(0.1%Fibre)	3	193.254	64.418	0.083407
Column 3(0.3%Fibre)	3	217.699	72.56633	0.316306
Column 4(0.5%Fibre)	3	164.527	54.84233	0.405084

ANOVA

Source of Variation	*SS*	*df*	*MS*	*F*	*P-value*	*F crit*
Between Groups	474.2676	3	158.0892	774.4023	3.41E-10	4.066181
Within Groups	1.633148	8	0.204144			
Total	475.9008	11				

Anova: Single Factor 20% Glass

SUMMARY

Groups	*Count*	*Sum*	*Average*	*Variance*
Column 1(0%Fibre)	3	193.132	64.37733	0.488874
Column 2(0.1%Fibre)	3	201.045	67.015	0.006069

ANOVA

Source of Variation	*SS*	*df*	*MS*	*F*	*P-value*	*F crit*
Between Groups	10.43593	1	10.43593	42.17019	0.0029	7.708647
Within Groups	0.989887	4	0.247472			
Total	11.42581	5				

Anova: Single Factor 20% Glass

SUMMARY

Groups	*Count*	*Sum*	*Average*	*Variance*
Column 1(0.1%Fibre)	3	201.045	67.015	0.006069
Column 2(0.3%Fibre)	3	189.114	63.038	0.419692

ANOVA

Source of Variation	*SS*	*df*	*MS*	*F*	*P-value*	*F crit*
Between Groups	23.72479	1	23.72479	111.4465	0.000455	7.708647
Within Groups	0.851522	4	0.212881			
Total	24.57632	5				

Anova: Single Factor 20% Glass

SUMMARY

Groups	*Count*	*Sum*	*Average*	*Variance*
Column 1(0.3%Fibre)	3	189.114	63.038	0.419692
Column 2(0.5%Fibre)	3	189.825	63.275	0.033325

ANOVA

Source of Variation	*SS*	*df*	*MS*	*F*	*P-value*	*F crit*
Between Groups	0.084254	1	0.084254	0.371966	0.574882	7.708647
Within Groups	0.906034	4	0.226509			
Total	0.990288	5				

Anova: Single Factor 20% Glass

SUMMARY

Groups	*Count*	*Sum*	*Average*	*Variance*
Column 1(0%Fibre)	3	193.132	64.37733	0.488874
Column 2(0.3%Fibre)	3	189.114	63.038	0.419692

ANOVA

Source of Variation	*SS*	*df*	*MS*	*F*	*P-value*	*F crit*
Between Groups	2.690721	1	2.690721	5.923003	0.071692	7.708647
Within Groups	1.817133	4	0.454283			
Total	4.507853	5				

Anova: Single Factor 20% Glass

SUMMARY

Groups	*Count*	*Sum*	*Average*	*Variance*
Column 1(0%Fibre)	3	193.132	64.37733	0.488874
Column 2(0.5%Fibre)	3	189.825	63.275	0.033325

ANOVA

Source of Variation	*SS*	*df*	*MS*	*F*	*P-value*	*F crit*
Between Groups	1.822708	1	1.822708	6.98089	0.057452	7.708647
Within Groups	1.044399	4	0.2611			
Total	2.867107	5				

Anova: Single Factor 20% Glass

SUMMARY

Groups	*Count*	*Sum*	*Average*	*Variance*
Column 1(0.1%Fibre)	3	201.045	67.015	0.006069
Column 2(0.5%Fibre)	3	189.825	63.275	0.033325

ANOVA

Source of Variation	*SS*	*df*	*MS*	*F*	*P-value*	*F crit*
Between Groups	20.9814	1	20.9814	1065.208	5.25E-06	7.708647
Within Groups	0.078788	4	0.019697			
Total	21.06019	5				

Anova: Single Factor 20% Glass

SUMMARY

Groups	*Count*	*Sum*	*Average*	*Variance*
Column 1(0%Fibre)	3	193.132	64.37733	0.488874
Column 2(0.1%Fibre)	3	201.045	67.015	0.006069
Column 3(0.3%Fibre)	3	189.114	63.038	0.419692
Column 4(0.5%Fibre)	3	189.825	63.275	0.033325

ANOVA

Source of Variation	*SS*	*df*	*MS*	*F*	*P-value*	*F crit*
Between Groups	29.8699	3	9.956634	42.01287	3.05E-05	4.066181
Within Groups	1.895921	8	0.23699			
Total	31.76582	11				

Anova: Single Factor 40% Glass

SUMMARY

Groups	*Count*	*Sum*	*Average*	*Variance*
Column 1(0%Fibre)	3	180.953	60.31767	0.236726
Column 2(0.1%Fibre)	3	194.342	64.78067	0.039754

ANOVA

Source of Variation	*SS*	*df*	*MS*	*F*	*P-value*	*F crit*
Between Groups	29.87755	1	29.87755	216.1276	0.000125	7.708647
Within Groups	0.552961	4	0.13824			
Total	30.43051	5				

Anova: Single Factor 40% Glass

SUMMARY

Groups	*Count*	*Sum*	*Average*	*Variance*
Column 1(0.1%Fibre)	3	194.342	64.78067	0.039754
Column 2(0.3%Fibre)	3	162.528	54.176	0.434833

ANOVA

Source of Variation	*SS*	*df*	*MS*	*F*	*P-value*	*F crit*
Between Groups	168.6884	1	168.6884	710.8847	1.18E-05	7.708647
Within Groups	0.949175	4	0.237294			
Total	169.6376	5				

Anova: Single Factor 40% Glass

SUMMARY

Groups	*Count*	*Sum*	*Average*	*Variance*
Column 1(0.3%Fibre)	3	162.528	54.176	0.434833
Column 2(0.5%Fibre)	3	188.162	62.72067	0.018016

ANOVA

Source of Variation	*SS*	*df*	*MS*	*F*	*P-value*	*F crit*
Between Groups	109.517	1	109.517	483.6796	2.53E-05	7.708647
Within Groups	0.905699	4	0.226425			
Total	110.4227	5				

Anova: Single Factor 40% Glass

SUMMARY

Groups	*Count*	*Sum*	*Average*	*Variance*
Column 1(0%fibre)	3	180.953	60.31767	0.236726
Column 2(0.3%Fibre)	3	162.528	54.176	0.434833

ANOVA

Source of Variation	*SS*	*df*	*MS*	*F*	*P-value*	*F crit*
Between Groups	56.5801	1	56.5801	168.5037	0.000203	7.708647
Within Groups	1.343119	4	0.33578			
Total	57.92322	5				

Anova: Single Factor 40% Glass

SUMMARY

Groups	*Count*	*Sum*	*Average*	*Variance*
Column 1(0%Fibre)	3	180.953	60.31767	0.236726
Column 2(0.5%Fibre)	3	188.162	62.72067	0.018016

ANOVA

Source of Variation	*SS*	*df*	*MS*	*F*	*P-value*	*F crit*
Between Groups	8.661613	1	8.661613	68.00285	0.001179	7.708647
Within Groups	0.509485	4	0.127371			
Total	9.171099	5				

Anova: Single Factor 40% Glass

SUMMARY

Groups	*Count*	*Sum*	*Average*	*Variance*
Column 1(0.1%Fibre)	3	194.342	64.78067	0.039754
Column 2(0.5%Fibre)	3	188.162	62.72067	0.018016

ANOVA

Source of Variation	*SS*	*df*	*MS*	*F*	*P-value*	*F crit*
Between Groups	6.3654	1	6.3654	220.3679	0.00012	7.708647
Within Groups	0.115541	4	0.028885			
Total	6.480941	5				

Anova: Single Factor 40% Glass

SUMMARY

Groups	*Count*	*Sum*	*Average*	*Variance*
Column 1(0%Fibre)	3	180.953	60.31767	0.236726
Column 2(0.1%Fibre)	3	194.342	64.78067	0.039754
Column 3(0.3%Fibre)	3	162.528	54.176	0.434833
Column 4(0.5%fibre)	3	188.162	62.72067	0.018016

ANOVA

Source of Variation	*SS*	*df*	*MS*	*F*	*P-value*	*F crit*
Between Groups	189.845	3	63.28168	347.0675	8.29E-09	4.066181
Within Groups	1.45866	8	0.182333			
Total	191.3037	11				

Anova: Single Factor 60% Glass

SUMMARY

Groups	*Count*	*Sum*	*Average*	*Variance*
Column 1(0%Fibre)	3	176.483	58.82767	0.460737
Column 2(0.1%Fibre)	3	182.577	60.859	0.186433

ANOVA

Source of Variation	*SS*	*df*	*MS*	*F*	*P-value*	*F crit*
Between Groups	6.189473	1	6.189473	19.1278	0.011935	7.708647
Within Groups	1.294341	4	0.323585			
Total	7.483813	5				

Anova: Single Factor 60% Glass

SUMMARY

Groups	*Count*	*Sum*	*Average*	*Variance*
Column 1(0.1%Fibre)	3	182.577	60.859	0.186433
Column 2(0.3%Fibre)	3	160.061	53.35367	0.852724

ANOVA

Source of Variation	*SS*	*df*	*MS*	*F*	*P-value*	*F crit*
Between Groups	84.49504	1	84.49504	162.6222	0.000218	7.708647
Within Groups	2.078315	4	0.519579			
Total	86.57336	5				

Anova: Single Factor 60% Glass

SUMMARY

Groups	*Count*	*Sum*	*Average*	*Variance*
Column 1(0.3%Fibre)	3	160.061	53.35367	0.852724
Column 2(0.5%Fibre)	3	187.276	62.42533	1.893894

ANOVA

Source of Variation	*SS*	*df*	*MS*	*F*	*P-value*	*F crit*
Between Groups	123.4427	1	123.4427	89.88704	0.000691	7.708647
Within Groups	5.493237	4	1.373309			
Total	128.9359	5				

Anova: Single Factor 60% Glass

SUMMARY

Groups	*Count*	*Sum*	*Average*	*Variance*
Column 1(0%Fibre)	3	176.483	58.82767	0.460737
Column 2(0.3%Fibre)	3	160.061	53.35367	0.852724

ANOVA

Source of Variation	*SS*	*df*	*MS*	*F*	*P-value*	*F crit*
Between Groups	44.94701	1	44.94701	68.44054	0.001165	7.708647
Within Groups	2.626923	4	0.656731			
Total	47.57394	5				

Anova: Single Factor 60% Glass

SUMMARY

Groups	*Count*	*Sum*	*Average*	*Variance*
Column 1(0%Fibre)	3	176.483	58.82767	0.460737
Column 2(0.5%Fibre)	3	187.276	62.42533	1.893894

ANOVA

Source of Variation	*SS*	*df*	*MS*	*F*	*P-value*	*F crit*
Between Groups	19.41481	1	19.41481	16.49074	0.015338	7.708647
Within Groups	4.709263	4	1.177316			
Total	24.12407	5				

Anova: Single Factor 60% Glass

SUMMARY

Groups	*Count*	*Sum*	*Average*	*Variance*
Column 1(0.1%Fibre)	3	182.577	60.859	0.186433
Column 2(0.5%fibre)	3	187.276	62.42533	1.893894

ANOVA

Source of Variation	*SS*	*df*	*MS*	*F*	*P-value*	*F crit*
Between Groups	3.6801	1	3.6801	3.538001	0.133134	7.708647
Within Groups	4.160655	4	1.040164			
Total	7.840755	5				

Anova: Single Factor 60% Glass

SUMMARY

Groups	*Count*	*Sum*	*Average*	*Variance*
Column 1(0%Fibre)	3	176.483	58.82767	0.460737
Column 2(0.1%Fibre)	3	182.577	60.859	0.186433
Column 3(0.3%Fibre)	3	160.061	53.35367	0.852724
Column 4(0.5%Fibre)	3	187.276	62.42533	1.893894

ANOVA

Source of Variation	*SS*	*df*	*MS*	*F*	*P-value*	*F crit*
Between Groups	141.0846	3	47.02819	55.42854	1.07E-05	4.066181
Within Groups	6.787578	8	0.848447			
Total	147.8721	11				

Anova: Single Factor 0% Fibre

SUMMARY

Groups	*Count*	*Sum*	*Average*	*Variance*
Column 1(0%Glass)	3	188.971	62.99033	0.011776
Column 2(20%glass)	3	193.132	64.37733	0.488874

ANOVA

Source of Variation	*SS*	*df*	*MS*	*F*	*P-value*	*F crit*
Between Groups	2.885653	1	2.885653	11.52761	0.027397	7.708647
Within Groups	1.001301	4	0.250325			
Total	3.886955	5				

Anova: Single Factor 0% Fibre

SUMMARY

Groups	*Count*	*Sum*	*Average*	*Variance*
Column 1(20%Glass)	3	193.132	64.37733	0.488874
Column 2(40%Glass)	3	180.953	60.31767	0.236726

ANOVA

Source of Variation	*SS*	*df*	*MS*	*F*	*P-value*	*F crit*
Between Groups	24.72134	1	24.72134	68.14035	0.001175	7.708647
Within Groups	1.451201	4	0.3628			
Total	26.17254	5				

Anova: Single Factor 0% Fibre

SUMMARY

Groups	*Count*	*Sum*	*Average*	*Variance*
Column 1(40%Glass)	3	180.953	60.31767	0.236726
Column 2(60%Glass)	3	176.483	58.82767	0.460737

ANOVA

Source of Variation	*SS*	*df*	*MS*	*F*	*P-value*	*F crit*
Between Groups	3.33015	1	3.33015	9.549315	0.036567	7.708647
Within Groups	1.394927	4	0.348732			
Total	4.725077	5				

Anova: Single Factor 0% Fibre

SUMMARY

Groups	*Count*	*Sum*	*Average*	*Variance*
Column 1(0%Glass)	3	188.971	62.99033	0.011776
Column 2(40%Glass)	3	180.953	60.31767	0.236726

ANOVA

Source of Variation	*SS*	*df*	*MS*	*F*	*P-value*	*F crit*
Between Groups	10.71472	1	10.71472	86.23425	0.000748	7.708647
Within Groups	0.497005	4	0.124251			
Total	11.21173	5				

Anova: Single Factor 0% Fibre

SUMMARY

Groups	*Count*	*Sum*	*Average*	*Variance*
Column 1(0%Glass)	3	188.971	62.99033	0.011776
Column 2(60%Glass)	3	176.483	58.82767	0.460737

ANOVA

Source of Variation	*SS*	*df*	*MS*	*F*	*P-value*	*F crit*
Between Groups	25.99169	1	25.99169	110.0146	0.000467	7.708647
Within Groups	0.945027	4	0.236257			
Total	26.93672	5				

Anova: Single Factor 0% Fibre

SUMMARY

Groups	*Count*	*Sum*	*Average*	*Variance*
Column 1(20%Glass)	3	193.132	64.37733	0.488874
Column 2(60%Glass)	3	176.483	58.82767	0.460737

ANOVA

Source of Variation	*SS*	*df*	*MS*	*F*	*P-value*	*F crit*
Between Groups	46.1982	1	46.1982	97.29914	0.000593	7.708647
Within Groups	1.899223	4	0.474806			
Total	48.09742	5				

Anova: Single Factor 0% Fibre

SUMMARY

Groups	*Count*	*Sum*	*Average*	*Variance*
Column 1(0%Glass)	3	188.971	62.99033	0.011776
Column 2(20%Glass)	3	193.132	64.37733	0.488874
Column 3(40%Glass)	3	180.953	60.31767	0.236726
Column 4(60%Glass)	3	176.483	58.82767	0.460737

ANOVA

Source of Variation	*SS*	*df*	*MS*	*F*	*P-value*	*F crit*
Between Groups	56.92088	3	18.97363	63.34496	6.45E-06	4.066181
Within Groups	2.396229	8	0.299529			
Total	59.31711	11				

90 Days

Anova: Single Factor 0% Glass

SUMMARY

Groups	*Count*	*Sum*	*Average*	*Variance*
Column 1(0%Fibre)	3	213.474	71.158	0.504657
Column 2(0.1%Fibre)	3	211.564	70.52133	0.917982

ANOVA

Source of Variation	*SS*	*df*	*MS*	*F*	*P-value*	*F crit*
Between Groups	0.608017	1	0.608017	0.854773	0.407532	7.708647
Within Groups	2.845279	4	0.71132			
Total	3.453295	5				

Anova: Single Factor 0% Glass

SUMMARY

Groups	*Count*	*Sum*	*Average*	*Variance*
Column 1(0.1%Fibre)	3	211.564	70.52133	0.917982
Column 2(0.3%Fibre)	3	235.77	78.59	1.475748

ANOVA

Source of Variation	*SS*	*df*	*MS*	*F*	*P-value*	*F crit*
Between Groups	97.65507	1	97.65507	81.59238	0.000832	7.708647
Within Groups	4.787461	4	1.196865			
Total	102.4425	5				

Anova: Single Factor 0% Glass

SUMMARY

Groups	*Count*	*Sum*	*Average*	*Variance*
Column 1(0.3%Fibre)	3	235.77	78.59	1.475748
Column 2(0.5%Fibre)	3	178.878	59.626	0.536839

ANOVA

Source of Variation	*SS*	*df*	*MS*	*F*	*P-value*	*F crit*
Between Groups	539.4499	1	539.4499	536.0761	2.06E-05	7.708647
Within Groups	4.025174	4	1.006294			
Total	543.4751	5				

Anova: Single Factor 0% Glass

SUMMARY

Groups	*Count*	*Sum*	*Average*	*Variance*
Column 1(0%Fibre)	3	213.474	71.158	0.504657
Column 2(0.3%Fibre)	3	235.77	78.59	1.475748

ANOVA

Source of Variation	*SS*	*df*	*MS*	*F*	*P-value*	*F crit*
Between Groups	82.85194	1	82.85194	83.67171	0.000793	7.708647
Within Groups	3.96081	4	0.990203			
Total	86.81275	5				

Anova: Single Factor 0% Glass

SUMMARY

Groups	*Count*	*Sum*	*Average*	*Variance*
Column 1(0%Fibre)	3	213.474	71.158	0.504657
Column 2(0.5%Fibre)	3	178.878	59.626	0.536839

ANOVA

Source of Variation	*SS*	*df*	*MS*	*F*	*P-value*	*F crit*
Between Groups	199.4805	1	199.4805	383.0654	4.02E-05	7.708647
Within Groups	2.082992	4	0.520748			
Total	201.5635	5				

Anova: Single Factor 0% Glass

SUMMARY

Groups	*Count*	*Sum*	*Average*	*Variance*
Column 1(0.1%Fibre)	3	211.564	70.52133	0.917982
Column 2(0.5%Fibre)	3	178.878	59.626	0.536839

ANOVA

Source of Variation	*SS*	*df*	*MS*	*F*	*P-value*	*F crit*
Between Groups	178.0624	1	178.0624	244.7894	9.75E-05	7.708647
Within Groups	2.909643	4	0.727411			
Total	180.9721	5				

Anova: Single Factor 0% Glass

SUMMARY

Groups	*Count*	*Sum*	*Average*	*Variance*
Column 1(0%Fibre)	3	213.474	71.158	0.504657
Column 2(0.1%Fibre)	3	211.564	70.52133	0.917982
Column 3(0.3%Fibre)	3	235.77	78.59	1.475748
Column 4(0.5%Fibre)	3	178.878	59.626	0.536839

ANOVA

Source of Variation	*SS*	*df*	*MS*	*F*	*P-value*	*F crit*
Between Groups	549.054	3	183.018	213.1073	5.71E-08	4.066181
Within Groups	6.870453	8	0.858807			
Total	555.9244	11				

Anova: Single Factor 20% Glass

SUMMARY

Groups	*Count*	*Sum*	*Average*	*Variance*
Column 1(0%Fibre)	3	209.36	69.78667	0.801733
Column 2(0.1%Fibre)	3	202.38	67.46	0.2604

ANOVA

Source of Variation	*SS*	*df*	*MS*	*F*	*P-value*	*F crit*
Between Groups	8.120067	1	8.120067	15.29011	0.01739	7.708647
Within Groups	2.124267	4	0.531067			
Total	10.24433	5				

Anova: Single Factor 20% Glass

SUMMARY

Groups	*Count*	*Sum*	*Average*	*Variance*
Column 1(0.1%Fibre)	3	202.38	67.46	0.2604
Column 2(0.3%Fibre)	3	201.435	67.145	0.365521

ANOVA

Source of Variation	*SS*	*df*	*MS*	*F*	*P-value*	*F crit*
Between Groups	0.148837	1	0.148837	0.475579	0.528354	7.708647
Within Groups	1.251842	4	0.312961			
Total	1.40068	5				

Anova: Single Factor 20% Glass

SUMMARY

Groups	*Count*	*Sum*	*Average*	*Variance*
Column 1(0.3%Fibre)	3	201.435	67.145	0.365521
Column 2(0.5%Fibre)	3	189.59	63.19667	7.718433

ANOVA

Source of Variation	*SS*	*df*	*MS*	*F*	*P-value*	*F crit*
Between Groups	23.384	1	23.384	5.785289	0.073933	7.708647
Within Groups	16.16791	4	4.041977			
Total	39.55191	5				

Anova: Single Factor 20% Glass

SUMMARY

Groups	*Count*	*Sum*	*Average*	*Variance*
Column 1(0%Fibre)	3	209.36	69.78667	0.801733
Column 2(0.3%Fibre)	3	201.435	67.145	0.365521

ANOVA

Source of Variation	*SS*	*df*	*MS*	*F*	*P-value*	*F crit*
Between Groups	10.4676	1	10.4676	17.93543	0.013316	7.708647
Within Groups	2.334509	4	0.583627			
Total	12.80211	5				

Anova: Single Factor 20% Glass

SUMMARY

Groups	*Count*	*Sum*	*Average*	*Variance*
Column 1(0%Fibre)	3	209.36	69.78667	0.801733
Column 2(0.5%Fibre)	3	189.59	63.19667	7.718433

ANOVA

Source of Variation	*SS*	*df*	*MS*	*F*	*P-value*	*F crit*
Between Groups	65.14215	1	65.14215	15.29129	0.017388	7.708647
Within Groups	17.04033	4	4.260083			
Total	82.18248	5				

Anova: Single Factor 20% Glass

SUMMARY

Groups	*Count*	*Sum*	*Average*	*Variance*
Column 1(0.1%Fibre)	3	202.38	67.46	0.2604
Column 2(0.5%Fibre)	3	189.59	63.19667	7.718433

ANOVA

Source of Variation	*SS*	*df*	*MS*	*F*	*P-value*	*F crit*
Between Groups	27.26402	1	27.26402	6.834086	0.059158	7.708647
Within Groups	15.95767	4	3.989417			
Total	43.22168	5				

Anova: Single Factor 20% Glass

SUMMARY

Groups	*Count*	*Sum*	*Average*	*Variance*
Column 1(0%Fibre)	3	209.36	69.78667	0.801733
Column 2(0.1%Fibre)	3	202.38	67.46	0.2604
Column 3(0.3%fibre)	3	201.435	67.145	0.365521
Column 4(0.5%Fibre)	3	189.59	63.19667	7.718433

ANOVA

Source of Variation	*SS*	*df*	*MS*	*F*	*P-value*	*F crit*
Between Groups	67.26334	3	22.42111	9.805772	0.004681	4.066181
Within Groups	18.29218	8	2.286522			
Total	85.55551	11				

Anova: Single Factor 40% Glass

SUMMARY

Groups	*Count*	*Sum*	*Average*	*Variance*
Column 1(0%Fibre)	3	199.961	66.65367	0.207902
Column 2(0.1%Fibre)	3	202.1	67.36667	2.601633

ANOVA

Source of Variation	*SS*	*df*	*MS*	*F*	*P-value*	*F crit*
Between Groups	0.762553	1	0.762553	0.542832	0.502138	7.708647
Within Groups	5.619071	4	1.404768			
Total	6.381625	5				

Anova: Single Factor 40% glass

SUMMARY

Groups	*Count*	*Sum*	*Average*	*Variance*
Column 1(0.1%Fibre)	3	202.1	67.36667	2.601633
Column 2(0.3%Fibre)	3	179.659	59.88633	3.516997

ANOVA

Source of Variation	*SS*	*df*	*MS*	*F*	*P-value*	*F crit*
Between Groups	83.93308	1	83.93308	27.43525	0.006349	7.708647
Within Groups	12.23726	4	3.059315			
Total	96.17034	5				

Anova: Single Factor 40% Glass

SUMMARY

Groups	*Count*	*Sum*	*Average*	*Variance*
Column 1(0.3%Fibre)	3	179.659	59.88633	3.516997
Column 2(0.5%Fibre)	3	188.92	62.97333	1.338433

ANOVA

Source of Variation	*SS*	*df*	*MS*	*F*	*P-value*	*F crit*
Between Groups	14.29435	1	14.29435	5.887986	0.072252	7.708647
Within Groups	9.710861	4	2.427715			
Total	24.00521	5				

Anova: Single Factor 40% Glass

SUMMARY

Groups	*Count*	*Sum*	*Average*	*Variance*
Column 1(0%Fibre)	3	199.961	66.65367	0.207902
Column 2(0.3%Fibre)	3	179.659	59.88633	3.516997

ANOVA

Source of Variation	*SS*	*df*	*MS*	*F*	*P-value*	*F crit*
Between Groups	68.6952	1	68.6952	36.88432	0.003713	7.708647
Within Groups	7.449799	4	1.86245			
Total	76.145	5				

Anova: Single Factor 40% Glass

SUMMARY

Groups	*Count*	*Sum*	*Average*	*Variance*
Column 1(0%Fibre)	3	199.961	66.65367	0.207902
Column 2(0.5%Fibre)	3	188.92	62.97333	1.338433

ANOVA

Source of Variation	*SS*	*df*	*MS*	*F*	*P-value*	*F crit*
Between Groups	20.31728	1	20.31728	26.27797	0.006857	7.708647
Within Groups	3.092671	4	0.773168			
Total	23.40995	5				

Anova: Single Factor 40% Glass

SUMMARY

Groups	*Count*	*Sum*	*Average*	*Variance*
Column 1(0.1%Fibre)	3	202.1	67.36667	2.601633
Column 2(0.5%Fibre)	3	188.92	62.97333	1.338433

ANOVA

Source of Variation	*SS*	*df*	*MS*	*F*	*P-value*	*F crit*
Between Groups	28.95207	1	28.95207	14.69623	0.018561	7.708647
Within Groups	7.880133	4	1.970033			
Total	36.8322	5				

Anova: Single Factor 40% Glass

SUMMARY

Groups	*Count*	*Sum*	*Average*	*Variance*
Column 1(0%Fibre)	3	199.961	66.65367	0.207902
Column 2(0.1%Fibre)	3	202.1	67.36667	2.601633
Column 3(0.3%Fibre)	3	179.659	59.88633	3.516997
Column 4(0.5%Fibre)	3	188.92	62.97333	1.338433

ANOVA

Source of Variation	*SS*	*df*	*MS*	*F*	*P-value*	*F crit*
Between Groups	108.4773	3	36.15909	18.8698	0.000549	4.066181
Within Groups	15.32993	8	1.916242			
Total	123.8072	11				

Anova: Single Factor 60% Glass

SUMMARY

Groups	*Count*	*Sum*	*Average*	*Variance*
Column 1(0%Fibre)	3	190.424	63.47467	3.164422
Column 2(0.1%Fibre)	3	193.66	64.55333	0.344633

ANOVA

Source of Variation	*SS*	*df*	*MS*	*F*	*P-value*	*F crit*
Between Groups	1.745283	1	1.745283	0.994731	0.375035	7.708647
Within Groups	7.018111	4	1.754528			
Total	8.763394	5				

Anova: Single Factor 60% Glass

SUMMARY

Groups	*Count*	*Sum*	*Average*	*Variance*
Column 1(0.1%Fibre)	3	193.66	64.55333	0.344633
Column 2(0.3%Fibre)	3	173.323	57.77433	0.067044

ANOVA

Source of Variation	*SS*	*df*	*MS*	*F*	*P-value*	*F crit*
Between Groups	68.93226	1	68.93226	334.8846	5.25E-05	7.708647
Within Groups	0.823355	4	0.205839			
Total	69.75562	5				

Anova: Single Factor 60% Glass

SUMMARY

Groups	*Count*	*Sum*	*Average*	*Variance*
Column 1(0.3%Fibre)	3	173.323	57.77433	0.067044
Column 2(0.5%Fibre)	3	195	65	1.2684

ANOVA

Source of Variation	*SS*	*df*	*MS*	*F*	*P-value*	*F crit*
Between Groups	78.31539	1	78.31539	117.2874	0.000412	7.708647
Within Groups	2.670889	4	0.667722			
Total	80.98628	5				

Anova: Single Factor 60% Glass

SUMMARY

Groups	*Count*	*Sum*	*Average*	*Variance*
Column 1(0%Fibre)	3	190.424	63.47467	3.164422
Column 2(0.3%Fibre)	3	173.323	57.77433	0.067044

ANOVA

Source of Variation	*SS*	*df*	*MS*	*F*	*P-value*	*F crit*
Between Groups	48.7407	1	48.7407	30.1663	0.005355	7.708647
Within Groups	6.462933	4	1.615733			
Total	55.20363	5				

Anova: Single Factor 60% Glass

SUMMARY

Groups	*Count*	*Sum*	*Average*	*Variance*
Column 1(0%Fibre)	3	190.424	63.47467	3.164422
Column 2(0.5%Fibre)	3	195	65	1.2684

ANOVA

Source of Variation	*SS*	*df*	*MS*	*F*	*P-value*	*F crit*
Between Groups	3.489963	1	3.489963	1.574601	0.277855	7.708647
Within Groups	8.865645	4	2.216411			
Total	12.35561	5				

Anova: Single Factor 60% Glass

SUMMARY

Groups	*Count*	*Sum*	*Average*	*Variance*
Column 1(0.1%Fibre)	3	193.66	64.55333	0.344633
Column 2(0.5%Fibre)	3	195	65	1.2684

ANOVA

Source of Variation	*SS*	*df*	*MS*	*F*	*P-value*	*F crit*
Between Groups	0.299267	1	0.299267	0.371061	0.575328	7.708647
Within Groups	3.226067	4	0.806517			
Total	3.525333	5				

Anova: Single Factor 60% Glass

SUMMARY

Groups	*Count*	*Sum*	*Average*	*Variance*
Column 1(0%Fibre)	3	190.424	63.47467	3.164422
Column 2(0.1%Fibre)	3	193.66	64.55333	0.344633
Column 3(0.3%Fibre)	3	173.323	57.77433	0.067044
Column 4(0.5%Fibre)	3	195	65	1.2684

ANOVA

Source of Variation	*SS*	*df*	*MS*	*F*	*P-value*	*F crit*
Between Groups	100.7614	3	33.58714	27.73219	0.000141	4.066181
Within Groups	9.689	8	1.211125			
Total	110.4504	11				

Anova: Single Factor 0% Fibre

SUMMARY

Groups	*Count*	*Sum*	*Average*	*Variance*
Column 1(0%Glass)	3	213.474	71.158	0.504657
Column 2(20%Glass)	3	209.36	69.78667	0.801733

ANOVA

Source of Variation	*SS*	*df*	*MS*	*F*	*P-value*	*F crit*
Between Groups	2.820833	1	2.820833	4.318514	0.106251	7.708647
Within Groups	2.612781	4	0.653195			
Total	5.433613	5				

Anova: Single Factor 0% Fibre

SUMMARY

Groups	*Count*	*Sum*	*Average*	*Variance*
Column 1(20%Glass)	3	209.36	69.78667	0.801733
Column 2(40%Glass)	3	199.961	66.65367	0.207902

ANOVA

Source of Variation	*SS*	*df*	*MS*	*F*	*P-value*	*F crit*
Between Groups	14.72353	1	14.72353	29.16603	0.00569	7.708647
Within Groups	2.019271	4	0.504818			
Total	16.7428	5				

Anova: Single Factor 0% Fibre

SUMMARY

Groups	*Count*	*Sum*	*Average*	*Variance*
Column 1(40%Glass)	3	199.961	66.65367	0.207902
Column 2(60%Glass)	3	190.424	63.47467	3.164422

ANOVA

Source of Variation	*SS*	*df*	*MS*	*F*	*P-value*	*F crit*
Between Groups	15.15906	1	15.15906	8.990274	0.040006	7.708647
Within Groups	6.744649	4	1.686162			
Total	21.90371	5				

Anova: Single Factor 0% Fibre

SUMMARY

Groups	*Count*	*Sum*	*Average*	*Variance*
Column 1(0%Glass)	3	213.474	71.158	0.504657
Column 2(40%Glass)	3	199.961	66.65367	0.207902

ANOVA

Source of Variation	*SS*	*df*	*MS*	*F*	*P-value*	*F crit*
Between Groups	30.43353	1	30.43353	85.42033	0.000762	7.708647
Within Groups	1.425119	4	0.35628			
Total	31.85865	5				

Anova: Single Factor 0% Fibre

SUMMARY

Groups	*Count*	*Sum*	*Average*	*Variance*
Column 1(0%Glass)	3	213.474	71.158	0.504657
Column 2(60%Glass)	3	190.424	63.47467	3.164422

ANOVA

Source of Variation	*SS*	*df*	*MS*	*F*	*P-value*	*F crit*
Between Groups	88.55042	1	88.55042	48.26847	0.002255	7.708647
Within Groups	7.338159	4	1.83454			
Total	95.88858	5				

Anova: Single Factor 0% Fibre

SUMMARY

Groups	*Count*	*Sum*	*Average*	*Variance*
Column 1(20%Glass)	3	209.36	69.78667	0.801733
Column 2(60%Glass)	3	190.424	63.47467	3.164422

ANOVA

Source of Variation	*SS*	*df*	*MS*	*F*	*P-value*	*F crit*
Between Groups	59.76202	1	59.76202	30.13599	0.005365	7.708647
Within Groups	7.932311	4	1.983078			
Total	67.69433	5				

Anova: Single Factor 0% Fibre

SUMMARY

Groups	*Count*	*Sum*	*Average*	*Variance*
Column 1(0%Glass)	3	213.474	71.158	0.504657
Column 2(20%Glass)	3	209.36	69.78667	0.801733
Column 3(40%Glass)	3	199.961	66.65367	0.207902
Column 4(60%Glass)	3	190.424	63.47467	3.164422

ANOVA

Source of Variation	*SS*	*df*	*MS*	*F*	*P-value*	*F crit*
Between Groups	105.7247	3	35.24156	30.12927	0.000104	4.066181
Within Groups	9.35743	8	1.169679			
Total	115.0821	11				

APPENDIX –C

Material properties

Concrete

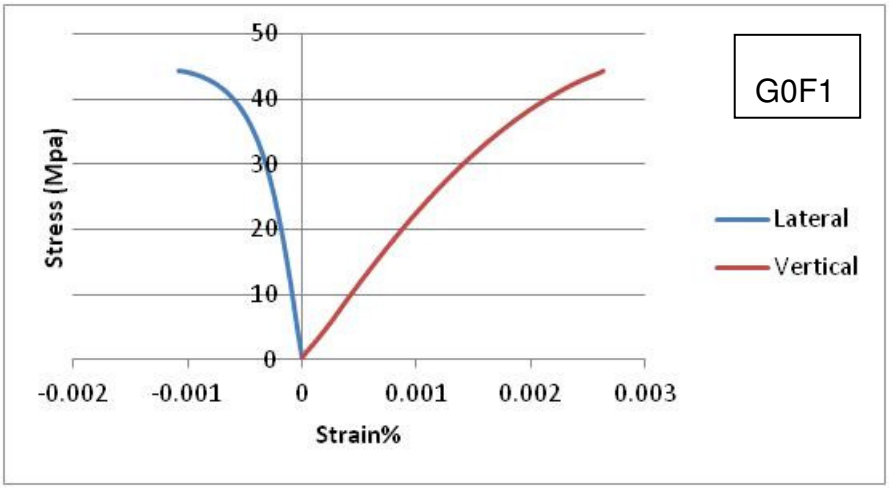

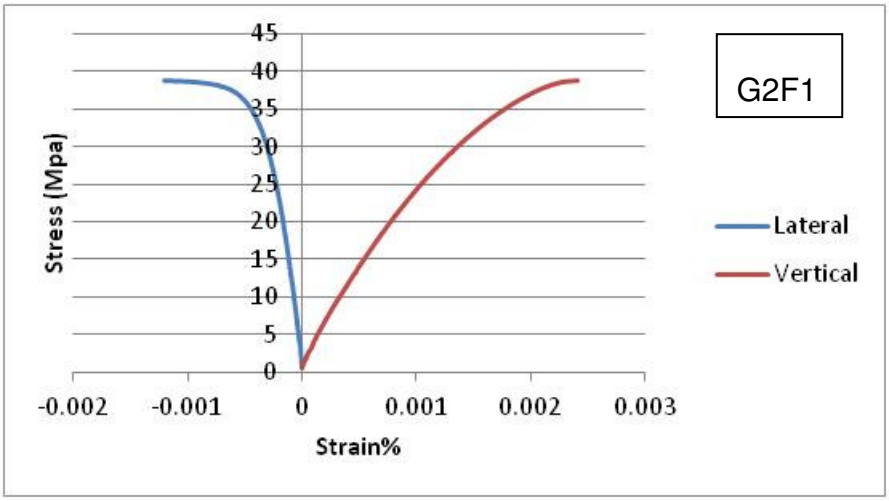

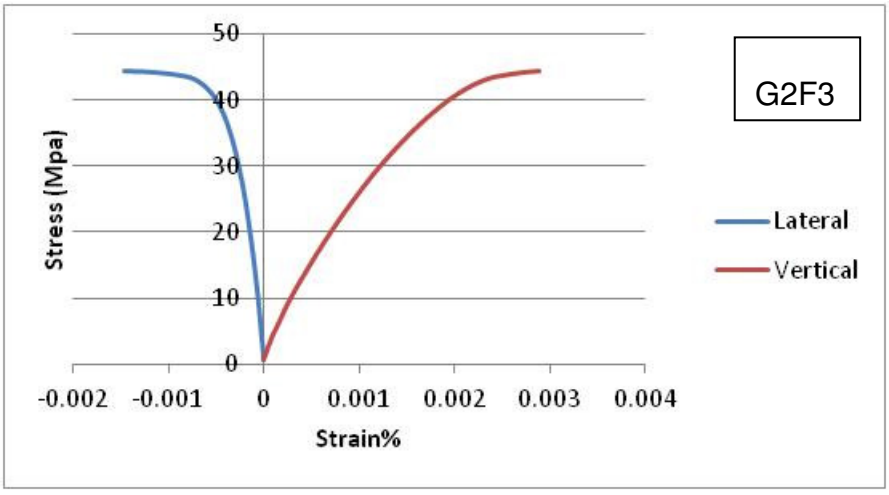

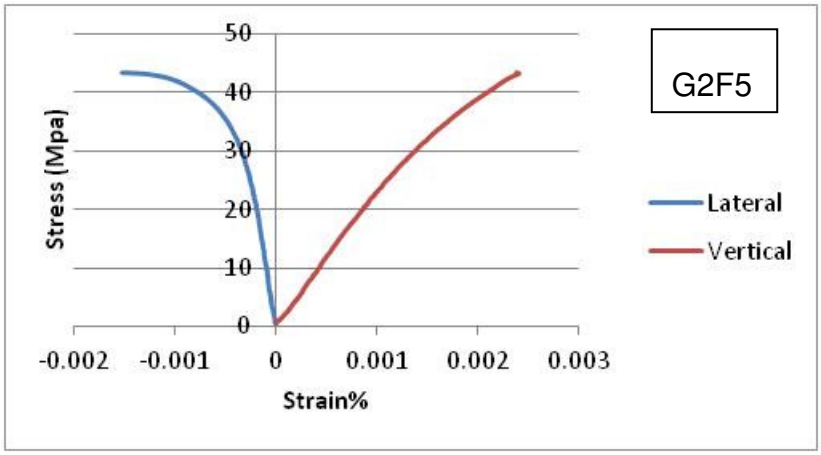

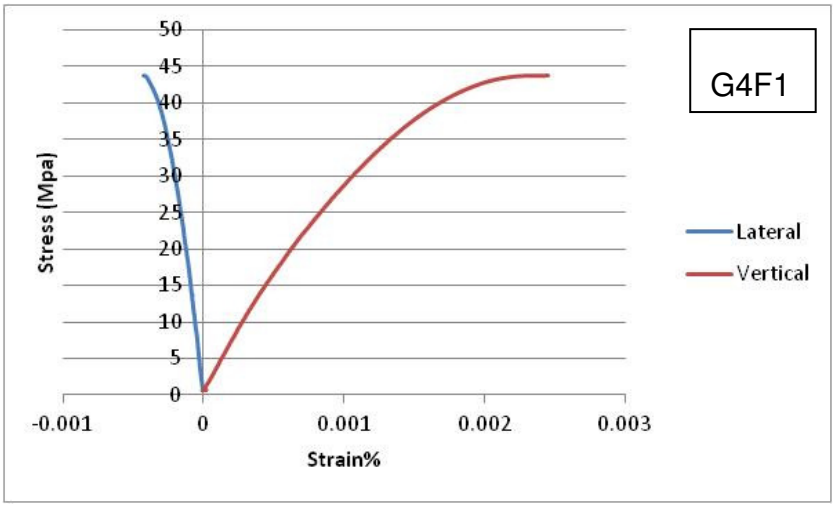

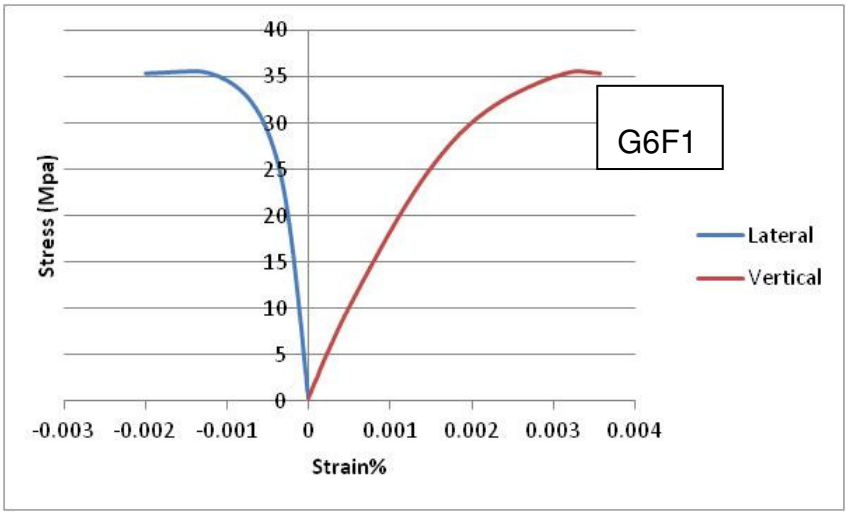

Figure C-1 Concrete material properties

Steel

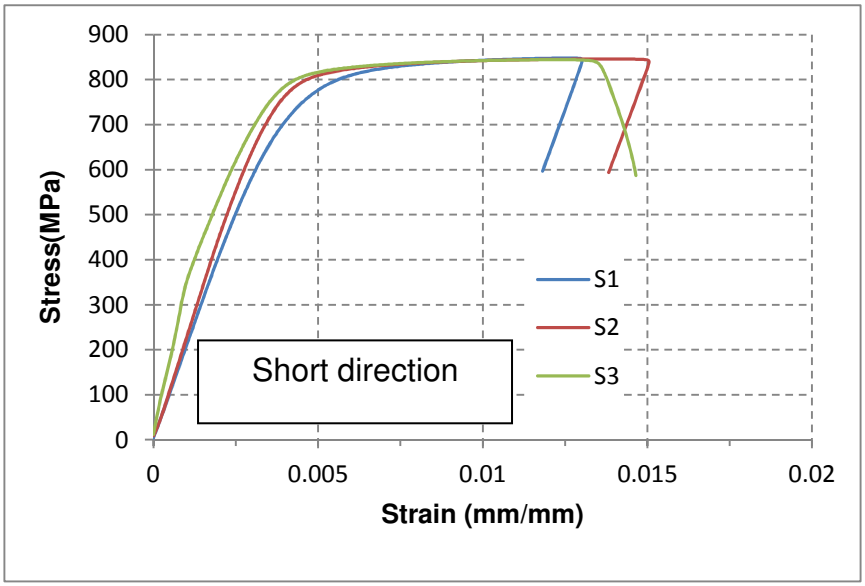

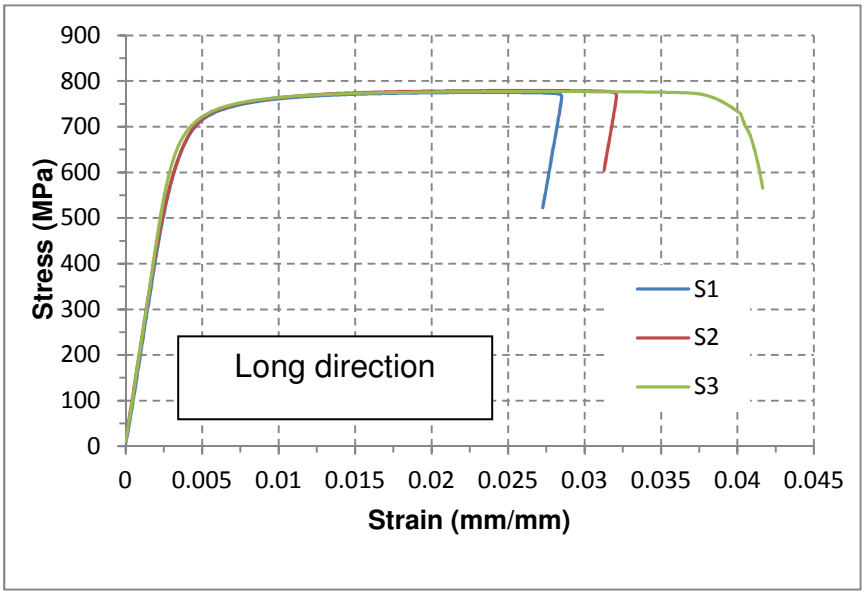

Figure C-2 Steel material properties

APPENDIX –D

The input file for slab G0F1 at ambient temperature

*Heading

** Job name: G0F1 Model name: G0F1

** Generated by: Abaqus/CAE 6.10-1

*Preprint, echo=NO, model=NO, history=NO, contact=NO

**

** PARTS

**

*Part, name=Part-1

*Node

1, 0., 0., 0.

2, 91.6666641, 0., 0.

3, 183.333328, 0., 0.

4, 275., 0., 0.

5, 366.666656, 0., 0.

6, 458.333344, 0., 0.

7, 550., 0., 0.

8, 0., 91.6666641, 0.

9, 91.6666641, 91.6666641, 0.

10, 183.333328, 91.6666641, 0.

11, 275., 91.6666641, 0.

12, 366.666656, 91.6666641, 0.

13, 458.333344, 91.6666641, 0.

14, 550., 91.6666641, 0.

15, 0., 183.333328, 0.

16, 91.6666641, 183.333328, 0.

17, 183.333328, 183.333328, 0.

18, 275., 183.333328, 0.

19, 366.666656, 183.333328, 0.

20, 458.333344, 183.333328, 0.

21, 550., 183.333328, 0.
22, 0., 275., 0.
23, 91.6666641, 275., 0.
24, 183.333328, 275., 0.
25, 275., 275., 0.
26, 366.666656, 275., 0.
27, 458.333344, 275., 0.
28, 550., 275., 0.
29, 0., 366.666656, 0.
30, 91.6666641, 366.666656, 0.
31, 183.333328, 366.666656, 0.
32, 275., 366.666656, 0.
33, 366.666656, 366.666656, 0.
34, 458.333344, 366.666656, 0.
35, 550., 366.666656, 0.
36, 0., 458.333344, 0.
37, 91.6666641, 458.333344, 0.
38, 183.333328, 458.333344, 0.
39, 275., 458.333344, 0.
40, 366.666656, 458.333344, 0.
41, 458.333344, 458.333344, 0.
42, 550., 458.333344, 0.
43, 0., 550., 0.
44, 91.6666641, 550., 0.
45, 183.333328, 550., 0.
46, 275., 550., 0.
47, 366.666656, 550., 0.
48, 458.333344, 550., 0.
49, 550., 550., 0.
*Element, type=S4R
1, 1, 2, 9, 8
2, 2, 3, 10, 9

3, 3, 4, 11, 10

4, 4, 5, 12, 11

5, 5, 6, 13, 12

6, 6, 7, 14, 13

7, 8, 9, 16, 15

8, 9, 10, 17, 16

9, 10, 11, 18, 17

10, 11, 12, 19, 18

11, 12, 13, 20, 19

12, 13, 14, 21, 20

13, 15, 16, 23, 22

14, 16, 17, 24, 23

15, 17, 18, 25, 24

16, 18, 19, 26, 25

17, 19, 20, 27, 26

18, 20, 21, 28, 27

19, 22, 23, 30, 29

20, 23, 24, 31, 30

21, 24, 25, 32, 31

22, 25, 26, 33, 32

23, 26, 27, 34, 33

24, 27, 28, 35, 34

25, 29, 30, 37, 36

26, 30, 31, 38, 37

27, 31, 32, 39, 38

28, 32, 33, 40, 39

29, 33, 34, 41, 40

30, 34, 35, 42, 41

31, 36, 37, 44, 43

32, 37, 38, 45, 44

33, 38, 39, 46, 45

34, 39, 40, 47, 46

35, 40, 41, 48, 47

36, 41, 42, 49, 48

*Nset, nset=_PickedSet4, internal, generate

1, 49, 1

*Elset, elset=_PickedSet4, internal, generate

1, 36, 1

** Section: concrete

*Shell Section, elset=_PickedSet4, material=concrete

35., 9

*Rebar Layer

x, 4.35, 50., -3.975, steel, 0., 1

y, 4.35, 50., -3.975, steel, 90., 1

*End Part

**

**

** ASSEMBLY

**

*Assembly, name=Assembly

**

*Instance, name=Part-1-1, part=Part-1

*End Instance

**

*Nset, nset=_PickedSet5, internal, instance=Part-1-1, generate

7, 49, 7

*Elset, elset=_PickedSet5, internal, instance=Part-1-1, generate

6, 36, 6

*Nset, nset=_PickedSet6, internal, instance=Part-1-1, generate

43, 49, 1

*Elset, elset=_PickedSet6, internal, instance=Part-1-1, generate

31, 36, 1

*Nset, nset=_PickedSet7, internal, instance=Part-1-1

1, 2, 3, 4, 5, 6, 7, 8, 15, 22, 29, 36, 43

```
*Elset, elset=_PickedSet7, internal, instance=Part-1-1
  1,  2,  3,  4,  5,  6,  7, 13, 19, 25, 31
*Elset, elset=__PickedSurf4_SPOS, internal, instance=Part-1-1, generate
  1,  36,   1
*Surface, type=ELEMENT, name=_PickedSurf4, internal
__PickedSurf4_SPOS, SPOS
*End Assembly
**
** MATERIALS
**
*Material, name=concrete
*Density
 2.4e-06,
*Elastic
 25482.1, 0.213
*Concrete Damaged Plasticity
20.,  0.1, 1.16,  0.8,   0.
*Concrete Compression Hardening
 10.2565,          0.
 44.5096, 0.000836592
*Concrete Tension Stiffening
 2.2,      0.
  0., 0.00329
*Material, name=steel
*Density
 7.8e-06,
*Elastic
215000., 0.15
*Plastic
688.,0.
** ----------------------------------------------------------------
**
```

```
** STEP: Step-1
**
*Step, name=Step-1, nlgeom=YES, inc=1000
*Static, stabilize=0.0002, allsdtol=0.05, continue=NO
0.001, 1., 1e-15, 0.2
**
** BOUNDARY CONDITIONS
**
** Name: support Type: Displacement/Rotation
*Boundary
_PickedSet7, 3, 3
** Name: x sym Type: Symmetry/Antisymmetry/Encastre
*Boundary
_PickedSet5, XSYMM
** Name: y sym Type: Symmetry/Antisymmetry/Encastre
*Boundary
_PickedSet6, YSYMM
**
** LOADS
**
** Name: Load-1   Type: Pressure
*Dsload
_PickedSurf4, P, 0.0415
**
** OUTPUT REQUESTS
**
*Restart, write, frequency=0
**
** FIELD OUTPUT: F-Output-1
**
*Output, field, variable=PRESELECT
**
```

** HISTORY OUTPUT: H-Output-1

**

*Output, history, variable=PRESELECT

*End Step

The input file for slab G0F1 at elevated temperature

*Heading

** Job name: G0F1 Model name: G0F1

** Generated by: Abaqus/CAE 6.10-1

*Preprint, echo=NO, model=NO, history=NO, contact=NO

**

** PARTS

**

*Part, name=Part-1

*Node

1, 0., 0., 0.

2, 0.0916666687, 0., 0.

3, 0.183333337, 0., 0.

4, 0.275000006, 0., 0.

5, 0.366666675, 0., 0.

6, 0.458333343, 0., 0.

7, 0.550000012, 0., 0.

8, 0., 0.0916666687, 0.

9, 0.0916666687, 0.0916666687, 0.

10, 0.183333337, 0.0916666687, 0.

11, 0.275000006, 0.0916666687, 0.

12, 0.366666675, 0.0916666687, 0.

13, 0.458333343, 0.0916666687, 0.

14, 0.550000012, 0.0916666687, 0.

15, 0., 0.183333337, 0.

16, 0.0916666687, 0.183333337, 0.

17, 0.183333337, 0.183333337, 0.

18, 0.275000006, 0.183333337, 0.

19, 0.366666675, 0.183333337, 0.

20, 0.458333343, 0.183333337, 0.

21, 0.550000012, 0.183333337, 0.

22, 0., 0.275000006, 0.

23, 0.0916666687, 0.275000006, 0.

24, 0.183333337, 0.275000006, 0.

25, 0.275000006, 0.275000006, 0.

26, 0.366666675, 0.275000006, 0.

27, 0.458333343, 0.275000006, 0.

28, 0.550000012, 0.275000006, 0.

29, 0., 0.366666675, 0.

30, 0.0916666687, 0.366666675, 0.

31, 0.183333337, 0.366666675, 0.

32, 0.275000006, 0.366666675, 0.

33, 0.366666675, 0.366666675, 0.

34, 0.458333343, 0.366666675, 0.

35, 0.550000012, 0.366666675, 0.

36, 0., 0.458333343, 0.

37, 0.0916666687, 0.458333343, 0.

38, 0.183333337, 0.458333343, 0.

39, 0.275000006, 0.458333343, 0.

40, 0.366666675, 0.458333343, 0.

41, 0.458333343, 0.458333343, 0.

42, 0.550000012, 0.458333343, 0.

43, 0., 0.550000012, 0.

44, 0.0916666687, 0.550000012, 0.

45, 0.183333337, 0.550000012, 0.

46, 0.275000006, 0.550000012, 0.

47, 0.366666675, 0.550000012, 0.

48, 0.458333343, 0.550000012, 0.

```
    49,  0.550000012,  0.550000012,          0.
*Element, type=S4R
 1,  1,  2,  9,  8
 2,  2,  3, 10,  9
 3,  3,  4, 11, 10
 4,  4,  5, 12, 11
 5,  5,  6, 13, 12
 6,  6,  7, 14, 13
 7,  8,  9, 16, 15
 8,  9, 10, 17, 16
 9, 10, 11, 18, 17
10, 11, 12, 19, 18
11, 12, 13, 20, 19
12, 13, 14, 21, 20
13, 15, 16, 23, 22
14, 16, 17, 24, 23
15, 17, 18, 25, 24
16, 18, 19, 26, 25
17, 19, 20, 27, 26
18, 20, 21, 28, 27
19, 22, 23, 30, 29
20, 23, 24, 31, 30
21, 24, 25, 32, 31
22, 25, 26, 33, 32
23, 26, 27, 34, 33
24, 27, 28, 35, 34
25, 29, 30, 37, 36
26, 30, 31, 38, 37
27, 31, 32, 39, 38
28, 32, 33, 40, 39
29, 33, 34, 41, 40
30, 34, 35, 42, 41
```

31, 36, 37, 44, 43

32, 37, 38, 45, 44

33, 38, 39, 46, 45

34, 39, 40, 47, 46

35, 40, 41, 48, 47

36, 41, 42, 49, 48

*Nset, nset=_PickedSet2, internal, generate

 1, 49,   1

*Elset, elset=_PickedSet2, internal, generate

 1, 36,   1

** Section: concrete

*Shell Section, elset=_PickedSet2, material=concrete

0.035, 11

*Rebar Layer

x, 4.337e-06, 0.05, -0.003975, steel, 0., 1

y, 4.337e-06, 0.05, -0.003975, steel, 90., 1

*End Part

**

**

** ASSEMBLY

**

*Assembly, name=Assembly

**

*Instance, name=Part-1-1, part=Part-1

*End Instance

**

*Nset, nset=_PickedSet20, internal, instance=Part-1-1

 1, 2, 3, 4, 5, 6, 7, 8, 15, 22, 29, 36, 43

*Elset, elset=_PickedSet20, internal, instance=Part-1-1

 1, 2, 3, 4, 5, 6, 7, 13, 19, 25, 31

*Nset, nset=_PickedSet21, internal, instance=Part-1-1, generate

 7, 49,   7

```
*Elset, elset=_PickedSet21, internal, instance=Part-1-1, generate
 6,  36,   6
*Nset, nset=_PickedSet22, internal, instance=Part-1-1, generate
 43,  49,   1
*Elset, elset=_PickedSet22, internal, instance=Part-1-1, generate
 31,  36,   1
*Nset, nset=_PickedSet23, internal, instance=Part-1-1, generate
 1,  49,   1
*Elset, elset=_PickedSet23, internal, instance=Part-1-1, generate
 1,  36,   1
*Nset, nset=_PickedSet26, internal, instance=Part-1-1, generate
 1,  49,   1
*Elset, elset=_PickedSet26, internal, instance=Part-1-1, generate
 1,  36,   1
*Elset, elset=__PickedSurf19_SPOS, internal, instance=Part-1-1, generate
 1,  36,   1
*Surface, type=ELEMENT, name=_PickedSurf19, internal
__PickedSurf19_SPOS, SPOS
*End Assembly
**
** MATERIALS
**
*Material, name=concrete
*Density
2400.,
*Elastic
 2.65326e+10,  0.2,  20.
 1.65829e+10,  0.2, 100.
 1.14572e+10,  0.2, 200.
  8.0545e+09,  0.2, 300.
  4.9749e+09,  0.2, 400.
  2.6533e+09,  0.2, 500.
```

1.194e+09, 0.2, 600.

7.96e+08, 0.2, 700.

3.98e+08, 0.2, 800.

2.123e+08, 0.2, 900.

1.061e+08, 0.2,1000.

*Expansion, zero=18.

8.1e-06, 20.

8.1e-06, 805.

0., 900.

0.,1000.

*Concrete Damaged Plasticity

20., 0.1, 1.16, 0.664, 0.

*Concrete Compression Hardening

1.32669e+07, 0., , 20.

1.71652e+07, 0.00065, , 20.

2.09685e+07, 0.0008, , 20.

2.46322e+07, 0.00095, , 20.

2.81069e+07, 0.0011, , 20.

3.13412e+07, 0.00125, , 20.

3.42855e+07, 0.0014, , 20.

3.68954e+07, 0.00155, , 20.

3.91353e+07, 0.0017, , 20.

4.09808e+07, 0.00185, , 20.

4.24204e+07, 0.002, , 20.

4.34558e+07, 0.00215, , 20.

4.41014e+07, 0.0023, , 20.

4.44e+07, 0.0025, , 20.

0., 0.02, , 20.

1.32669e+07, 0., , 100.

1.71652e+07, 0.00104, , 100.

2.09685e+07, 0.00128, , 100.

2.46322e+07, 0.00152, , 100.

2.81069e+07, 0.00176, , 100.

3.13412e+07, 0.002, , 100.

3.42855e+07, 0.00224, , 100.

3.68954e+07, 0.00248, , 100.

3.91353e+07, 0.00272, , 100.

4.09808e+07, 0.00296, , 100.

4.24204e+07, 0.0032, , 100.

4.34558e+07, 0.00344, , 100.

4.41014e+07, 0.00368, , 100.

4.44e+07, 0.004, , 100.

0., 0.0225, , 100.

1.28689e+07, 0., , 200.

1.66502e+07, 0.00143, , 200.

2.03394e+07, 0.00176, , 200.

2.38932e+07, 0.00209, , 200.

2.72637e+07, 0.00242, , 200.

3.04009e+07, 0.00275, , 200.

3.32569e+07, 0.00308, , 200.

3.57885e+07, 0.00341, , 200.

3.79612e+07, 0.00374, , 200.

3.97514e+07, 0.00407, , 200.

4.11478e+07, 0.0044, , 200.

4.21522e+07, 0.00473, , 200.

4.27783e+07, 0.00506, , 200.

4.3068e+07, 0.0055, , 200.

0., 0.025, , 200.

1.20729e+07, 0., , 300.

1.56203e+07, 0.00182, , 300.

1.90813e+07, 0.00224, , 300.

2.24153e+07, 0.00266, , 300.

2.55773e+07, 0.00308, , 300.

2.85205e+07, 0.0035, , 300.

3.11998e+07, 0.00392, , 300.

3.35748e+07, 0.00434, , 300.

3.56131e+07, 0.00476, , 300.

3.72925e+07, 0.00518, , 300.

3.86025e+07, 0.0056, , 300.

3.95448e+07, 0.00602, , 300.

4.01323e+07, 0.00644, , 300.

4.0404e+07, 0.007, , 300.

0., 0.0275, , 300.

1.12769e+07, 0., , 400.

1.45904e+07, 0.0026, , 400.

1.78232e+07, 0.0032, , 400.

2.09374e+07, 0.0038, , 400.

2.38908e+07, 0.0044, , 400.

2.664e+07, 0.005, , 400.

2.91426e+07, 0.0056, , 400.

3.13611e+07, 0.0062, , 400.

3.3265e+07, 0.0068, , 400.

3.48337e+07, 0.0074, , 400.

3.60573e+07, 0.008, , 400.

3.69375e+07, 0.0086, , 400.

3.74862e+07, 0.0092, , 400.

3.774e+07, 0.01, , 400.

0., 0.03, , 400.

9.81753e+06, 0., , 500.

1.27022e+07, 0.0039, , 500.

1.55167e+07, 0.0048, , 500.

1.82278e+07, 0.0057, , 500.

2.07991e+07, 0.0066, , 500.

2.31925e+07, 0.0075, , 500.

2.53712e+07, 0.0084, , 500.

2.73026e+07, 0.0093, , 500.

2.89601e+07, 0.0102, , 500.

3.03258e+07, 0.0111, , 500.

3.13911e+07, 0.012, , 500.

3.21573e+07, 0.0129, , 500.

3.2635e+07, 0.0138, , 500.

3.2856e+07, 0.015, , 500.

0., 0.025, , 500.

7.96016e+06, 0., , 600.

1.02991e+07, 0.0065, , 600.

1.25811e+07, 0.008, , 600.

1.47793e+07, 0.0095, , 600.

1.68641e+07, 0.011, , 600.

1.88047e+07, 0.0125, , 600.

2.05713e+07, 0.014, , 600.

2.21372e+07, 0.0155, , 600.

2.34812e+07, 0.017, , 600.

2.45885e+07, 0.0185, , 600.

2.54522e+07, 0.02, , 600.

2.60735e+07, 0.0215, , 600.

2.64608e+07, 0.023, , 600.

2.664e+07, 0.025, , 600.

0., 0.035, , 600.

5.70478e+06, 0., , 700.

7.38102e+06, 0.0065, , 700.

9.01643e+06, 0.008, , 700.

1.05918e+07, 0.0095, , 700.

1.2086e+07, 0.011, , 700.

1.34767e+07, 0.0125, , 700.

1.47427e+07, 0.014, , 700.

1.5865e+07, 0.0155, , 700.

1.68282e+07, 0.017, , 700.

1.76217e+07, 0.0185, , 700.

1.82408e+07, 0.02, , 700.

1.8686e+07, 0.0215, , 700.

1.89636e+07, 0.023, , 700.

1.9092e+07, 0.025, , 700.

0., 0.0375, , 700.

3.58207e+06, 0., , 800.

4.63459e+06, 0.0065, , 800.

5.66148e+06, 0.008, , 800.

6.65069e+06, 0.0095, , 800.

7.58886e+06, 0.011, , 800.

8.46212e+06, 0.0125, , 800.

9.25707e+06, 0.014, , 800.

9.96176e+06, 0.0155, , 800.

1.05665e+07, 0.017, , 800.

1.10648e+07, 0.0185, , 800.

1.14535e+07, 0.02, , 800.

1.17331e+07, 0.0215, , 800.

1.19074e+07, 0.023, , 800.

1.1988e+07, 0.025, , 800.

0., 0.04, , 800.

1.99004e+06, 0., , 900.

2.57477e+06, 0.0065, , 900.

3.14527e+06, 0.008, , 900.

3.69483e+06, 0.0095, , 900.

4.21603e+06, 0.011, , 900.

4.70118e+06, 0.0125, , 900.

5.14282e+06, 0.014, , 900.

5.53431e+06, 0.0155, , 900.

5.8703e+06, 0.017, , 900.

6.14712e+06, 0.0185, , 900.

6.36306e+06, 0.02, , 900.

6.51837e+06, 0.0215, , 900.

6.61521e+06, 0.023, , 900.

6.66e+06, 0.025, , 900.

0., 0.0425, , 900.

796016., 0., , 1000.

1.02991e+06, 0.0065, , 1000.

1.25811e+06, 0.008, , 1000.

1.47793e+06, 0.0095, , 1000.

1.68641e+06, 0.011, , 1000.

1.88047e+06, 0.0125, , 1000.

2.05713e+06, 0.014, , 1000.

2.21372e+06, 0.0155, , 1000.

2.34812e+06, 0.017, , 1000.

2.45885e+06, 0.0185, , 1000.

2.54522e+06, 0.02, , 1000.

2.60735e+06, 0.0215, , 1000.

2.64608e+06, 0.023, , 1000.

2.664e+06, 0.025, , 1000.

0., 0.045, , 1000.

*Concrete Tension Stiffening

2.26e+06, 0., , 20.

0., 0.00322291, , 20.

2.26e+06, 0., , 100.

0., 0.00322291, , 100.

1.808e+06, 0., , 200.

0., 0.00402864, , 200.

1.356e+06, 0., , 300.

0., 0.00537152, , 300.

904000., 0., , 400.

0., 0.00805728, , 400.

452000., 0., , 500.

0., 0.0161146, , 500.

0., 0., , 600.

```
      0.,        0., ,       700.
      0.,        0., ,       800.
      0.,        0., ,       900.
      0.,        0., ,      1000.
*Material, name=steel
*Density
7850.,
*Elastic
   2.1e+11, 0.15,  20.
   2.1e+11, 0.15, 100.
  1.89e+11, 0.15, 200.
  1.68e+11, 0.15, 300.
  1.47e+11, 0.15, 400.
  1.26e+11, 0.15, 500.
  2.73e+10, 0.15, 700.
  1.89e+10, 0.15, 800.
 1.4175e+10, 0.15, 900.
  9.45e+09, 0.15,1000.
*Expansion
 1.6e-05,
*Plastic
  6.88e+08,   0.,  20.
  6.88e+08,   0., 300.
  6.88e+08,   0., 400.
 5.3664e+08,   0., 500.
 3.2336e+08,   0., 600.
 1.5824e+08,   0., 700.
  7.568e+07,   0., 800.
  2.752e+07,   0.,1000.
**
** PREDEFINED FIELDS
**
```

```
** Name: Predefined Field-1   Type: Temperature
*Initial Conditions, type=TEMPERATURE
_PickedSet26, 18.
** ----------------------------------------------------------------
**
** STEP: Step-1
**
*Step, name=Step-1, nlgeom=YES, inc=10000
*Static, stabilize=0.0002, allsdtol=0.05, continue=NO
0.001, 1., 1e-25, 0.2
**
** BOUNDARY CONDITIONS
**
** Name: support Type: Displacement/Rotation
*Boundary
_PickedSet20, 3, 3
** Name: x sym Type: Symmetry/Antisymmetry/Encastre
*Boundary
_PickedSet21, XSYMM
** Name: y sym Type: Symmetry/Antisymmetry/Encastre
*Boundary
_PickedSet22, YSYMM
**
** LOADS
**
** Name: Load-1   Type: Pressure
*Dsload
_PickedSurf19, P, 8440.
**
** PREDEFINED FIELDS
**
** Name: Predefined Field-2   Type: Temperature
```

```
*Temperature, file=C:/Work/Thermal/G0F1/G0F1.odb, bstep=1, binc=1, interpolate
**
** OUTPUT REQUESTS
**
*Restart, write, frequency=0
**
** FIELD OUTPUT: F-Output-1
**
*Output, field
*Node Output
CF, NT, RF, U
*Element Output, directions=YES
LE, PE, PEEQ, PEMAG, S, TEMP
*Element Output, rebar, directions=YES
LE, PE, PEEQ, PEMAG, S, TEMP
*Contact Output
CDISP, CSTRESS
**
** HISTORY OUTPUT: H-Output-1
**
*Output, history
*Energy Output
*End Step
```